UNIVERSITÉ DU QUÉBEC À TROIS-RIVIÈRES

HYBRIDATION PASSIVE DE LA PILE À COMBUSTIBLE ET SUPERCONDENSATEUR POUR LES VÉHICULES ÉLECTRIQUES

THÈSE PRÉSENTÉE
COMME EXIGENCE PARTIELLE DU

DU DOCTORAT EN GÉNIE ÉLECTRIQUE

PAR
ALVARO OMAR MACIAS FERNANDEZ

FÉVRIER 2023

UNIVERSITÉ DU QUÉBEC À TROIS-RIVIÈRES

DOCTORAT EN GÉNIE ÉLECTRIQUE (PH.D.)

Direction de recherche :

Loïc Boulon	Directeur de recherche
João Pedro F. Trovão	Codirecteur de recherche

Jury d'évaluation

Alben Cardenas	Président UQTR
Marie-Cécile Péra	Évaluatrice externe, Université de Franche-Comté
Luiz Lopes	Évaluateur externe, Concordia
Loïc Boulon	Directeur de recherche
João Pedro F. Trovão	Codirecteur de recherche

Thèse soutenue le 26-01-2023

Abstract

Fuel cell hybrid electric vehicles (FCHEV) are receiving more attention from academia and industries due to their long-term benefits, such as zero-local emissions, high autonomy, and fast refueling time. However, recreational vehicles represent a new challenge in power supply systems since they are constrained to limited dimensions, dynamic requested power, and long-range trips. Therefore, the design stage becomes crucial to reduce their mass and increase their fuel economy, benefiting future more affordable vehicles. In this respect, the selection of the fuel cell (FC), energy storage system (ESS) technology, component size, and power splitting strategy needs to be improved. The formulation of this problem is represented as correlation between energy management strategy (EMS) and sizing. Due to the fact the performance of an EMS depends on the system size because this size will define the operating range and the possible combination of the system states. An appropriate component sizing declines the overall ownership cost of a FCHEV while maintaining the expected performance. Driven by this motivation, this thesis firstly devises a thorough literature review concerning the electric topology configurations and choices of the ESS. This literature study revealed that most existing papers focus on a single topology without a fair comparison with the other possible options. Moreover, it suggests that the hybridization of a FC with a supercapacitor (SC) is more advantageous than a battery to provide rapid current peaks; SC has a higher specific power, longer lifespan, and better resilience to different operating temperatures. Therefore, an even-handed benchmark analysis was carried out to study the advantages and disadvantages of three FC-SC configurations (active, semi-active, and passive) under the developed system model of a three-wheel electric recreational vehicle (Spyder). In addition, a two-step nested method was formulated to optimize the component size with a genetic algorithm in the outer loop and the power distribution with dynamic programming in the inner loop. It should be mentioned that the multi-objective cost function and optimization method used can be applied to any hybrid system that integrates two power sources. As a result, it is retained that a passive hybrid architecture in which the FC stack is connected to a secondary ESS without a power electronic system fits better for the studied

recreational vehicle. In this respect, although SC presents notable results, it suffers from a low energy density and a high self-discharge that can lead to high-power peak requests from the FC. The last stage of the work focused on evaluating the integration of a lithium-ion capacitor (LIC) in a FCHEV instead of a SC. This choice is driven by the high-power, high-energy density, and stable voltage properties of the LIC's new technology. The results demonstrated that a passive topology could supply the requested power along different FC stages of life with self-management and a compacted structure. This opens up new possibilities of power system configurations for electric vehicles.

Acknowledgments

First, I would like to thank my director, Professor Loïc Boulon, for his constructive comments and valuable guidance over my different stages of research. I am grateful to him for all the support during my postgraduate studies. I want to thank my co-director, Professor João Pedro F. Trovão, for the constant inspiration and valuable pieces of advice. He provided me with the tools that I needed to choose the right direction. I also thank Mitacs, RQEI, FRQNT and UQTR Foundation for the financial support.

I am grateful to Professors Pascal Venet and Ali Sari, for their encouragement and practical advice during my internship at Ampère Lab in Lyon. I also want to thank to all my colleagues at the Hydrogen Research Institute for the nice working environment and all the good times shared.

Thanks to my friends during my studies at Trois-Rivières, for all the trips, and outdoor activities during the summer and winter. Special thanks to my friend Mohsen Kandi for his constant support and guidance during my postgraduate studies. I could not have imagined having a better friend and colleague.

I would like to thank my partners Jonathan and Mario at Moduly for their support and opportunity for this new stage of entrepreneurship in my life.

Last but not the least; I would like to thank my family: my parents, Maria del Carmen and Lorenzo; and Elena for all their constant support.

Contents

List of Tables

List of Figures

Chapter 1 - Introduction

1.1 Motivation

The electrification of the transport sector has become part of the agenda of several countries to mitigate its dependency to the fossil fuels, because this sector is one of the main contributors to the greenhouse gases emissions (37% as reported by the IEA) and other pollutants [1]. In this regard, researchers and manufacturers have been working on the development of hybrid electric vehicles (HEVs), battery electric vehicles (BEVs), and fuel cell vehicles (FCVs) [2]. The HEV generates less pollution than the conventional vehicle, due to the integrated electric technologies, but still presents a dependency on fossil fuels. On the other hand, the BEVs are powered just by the internal batteries resulting on a zero-local emission vehicle. However, it has a long recharging time and limited driving range. And finally the FC vehicle, which offers a solution with interesting advantages at the long term: zero-local emission, high level of driving autonomy, and fast refueling time [3]. Nevertheless, in the short term this technology faces a high acquisition cost and slow dynamic response [4]. To approach these concerns, it has been proved that the hybridization of the fuel cell (FC) system with an energy storage system (ESS), such as battery, supercapacitor (SC) or Lithium-Ion Capacitor (LIC) can results in cheaper, more resilient, and efficient system. In addition, this hybridization also permitted the system to store the regenerative energy of the braking mechanism, provide the high dynamic power of vehicular applications and handle cold start conditions [5]. In such hybrid system, known as fuel cell hybrid electric

vehicle (FCHEV), the FC will supply the low-frequency requested power while the ESS takes care of the high-frequency variations [6]. In the literature, some works have already reviewed the characteristics of coupling a FC and an ESS in vehicular applications [7-11]. Though, most studies utilize the same size of the components for active and passive configurations while a customized size is required for each of them to exploit their individual strengths and to have a fair comparison.

To date, hydrogen technology use in the automotive sector has been limited as the necessary infrastructure has not been sufficiently developed. However, their commercialization is beginning to take off, having currently more than 50,000 vehicles on the road globally. Different vehicle manufacturers have concentrated their efforts on passenger light-duty vehicles, which accounted for three-quarters of the market, buses with 15% and 10% the rest of the vehicles. Some of the commercial FC vehicles that have already been manufacturer and tested in real-world road conditions are Toyota Mirai, Hyundai Tucson, and 2014 Honda FCX Clarity [12, 13].

Following the objective of reducing the environmental impact of the transport sector, this thesis work focuses on recreational vehicles, which represent a new challenge in terms of power supply systems compared to the current light-duty electric vehicles. These types of vehicles need to heed the limited dimension requirements while assuring the high requested power, aggressive dynamics, and long-range trips. Therefore, integrating a FC system as power supply will reduce their mass, refueling/charging time and extend their range compared to a pure battery configuration. But to reach more affordable vehicles special attention is required at the design stage, that involves the selection of the FC and ESS technology, size components and definition of the energy management strategy (EMS) [14].

In this regard, few researchers in Toyota and Suzuki company have already started working on FC recreational vehicles, yet, no commercial vehicle production can be found [15, 16]. This offers new commercial opportunities for the automotive sector, for example in Quebec, Canada where this study is conducted, it is in an ideal building ground for electric and smart transportation. This relies on the competitive advantages linked to the low-cost and abundant renewable electric energy production, availability of strategic mineral deposit resources, research knowledge on new vehicle technologies and wide range of climate conditions for testing and demonstration purposes. In the manufacturing point of view, it is observed that Canada is currently the thirteen-largest auto-producing nation in the world with a total revenue of more than 77 billion dollars as reported by the national statical office of Canada.

1.2 Positioning of the thesis

The objective of the thesis is a continuation of the work of the Canada Research Chair in "Energy Sources for the Vehicles of the Future" team of the Hydrogen Research Institute (IRH) of Université du Québec à Trois-Rivières (UQTR) on the fuel cell hybrid electric vehicles (FCHEV). This research project is a joint program between the UQTR and University of Sherbrooke under the supervision of Prof. Loïc Boulon and Prof. João Trovão, who has a Canada Research Chair in "Energy Sources for the Vehicles of the Future" and "Efficient Electric Vehicles with Hybridized Energy Storage Systems", respectively. This work proposes a novel hybrid powertrain for an electric vehicle called Spyder, a three-wheel pure battery electric vehicle used essentially for leisure purposes. The electric motorcycle studied in this thesis work is an experimental test bench in e-TESC laboratory at the University of Sherbrooke.

Previous to this work, several works conducted at the IRH have focused on the energy management of FCHEV and the integration of SC as a secondary ESS. Let us quote, for example, the theses of R. Silvia (2016), which focuses on providing a solution for the limited lifetime of Proton Exchange Membrane Fuel Cell (PEMFC) by implementing a prognostic and health management architecture and proposing a passive hybridization of the PEMFC with SC [17]. In C Dépature (2017) thesis, a control structure based on Energetic Macroscopic Representation (EMR) and the Backstepping method have reached a stable inversion-based control for an FC/SC vehicle [18]. The work of K. Ettihir (2017) focuses on an optimal adaptive EMS based on the online identification of FC parameters to seek the maximum efficiency and power of the FC that allows reducing hydrogen consumption while preserving the fuel cell during its functioning [19]. From a different perspective, A. Akrem (2018) work proposed an adaptative FC strategy for the cold start below frizzing conditions. The thesis of M. Kandidayeni (2020) presents a deeper study on the simultaneous systemic management of the FC energetic performance based on a multi-input model and an online identification method considering its operating conditions and impact of aging [20].

Regarding the positioning of this thesis work inside the e-TESC laboratory at the University of Sherbrooke, several theses utilized the three-wheel electric vehicle Spyder as the case study. The first work was presented by M. Boisvert (2015) in his Ph.D. thesis, where an original strategy has been proposed, which consists of controlling the braked wheel's slip according to the vehicle's speed to maximize the energy recovery on a three-wheeled electric vehicle [21]. Following a similar research path, J. Nadeau (2017) presented a Ph.D. thesis where a non-linear predictive control maximizes the regenerative braking torque with the collaborative use of the electro-hydraulic braking system of an electric-powered three-

wheeled recreational vehicle while respecting the braking setpoint [22]. The objective of N. Bảo-Huy (2019) thesis work was to develop a real-time optimization-based EMS for an electric vehicle and a parallel hybrid battery-SC configuration with the EMR method [23]. With the same approach of the EMR method, H. Chadi (2019) implemented a Hardware-In-the-Loop method for a small-scale test bed to perform real-time simulations to validate different electric vehicle topologies, EMS, and new power electronics topologies [24].

Following the research trend of both laboratories, this thesis proposes a passive coupling hybridization method to connect an FC stack to an SC without power electronics for the three-wheel electric vehicle Spyder. In this respect, firstly, a comparison of active, semi-active, and passive configurations for different common scenarios in vehicular applications were performed with the EMR method. Secondly, a Hardware-In-the-Loop method is implemented for a small-scale testbench of the Spyder vehicle with an FC-SC hybrid configuration. Thirdly, a novel FC-LIC configuration proof of concept was tested under a simulated environment using an experimental-based semi-empirical model.

1.3 Literature review

This section summarizes the current state-of-the-art concerning the fuel cell hybrid power supply systems for vehicular applications. In this respect, a literature review from 2015 to 2022 (January) reveals that the number of works related to fuel cell vehicles has been growing over the years, as shown in Figure 1.1. The total of work found by Scopus research engine motor was 2168, with the keywords: hydrogen, fuel cell, electric vehicle, energy management strategy, hybrid vehicle and PEMFC. These works can be group based on their publication year: 247 documents correspond to 2015, 228 to 2016, 260 to 2017, 279 to 2018, 296 to 2019, 396 to 2020, and 462 to 2021.

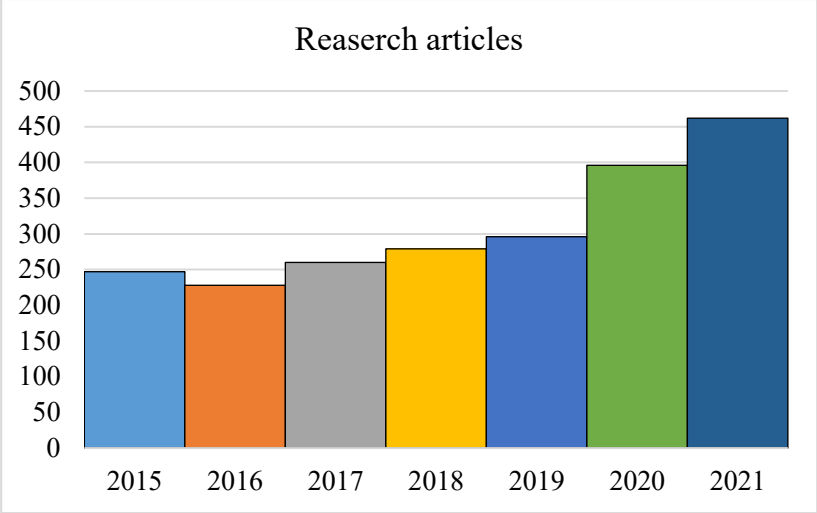

Figure 1.1 Related published research articles

A bibliometric analysis has been utilized to analyze the researcher behavior, publications trends, and visibility using representation methods in VOSviewer software [25-27]. The map shown in Figure 1.2 is known as a co-occurrence cluster map, where all the terms that present an occurrence of at least three times in the article index keywords are represented by an individual node. It should be noted that the map was limited to 50 nodes, and the searching keywords, such as fuel cell, fuel cell vehicle, and hydrogen, were omitted from the representation. The node's size depends on the number of articles containing the term, and the distance between them depends on the co-occur tendance. In addition, the terms are colored based on their occurrence and connections.

Besides the mentioned keywords, Figure 1.2 shows that the most used element is ESS (324 times), followed by GHG (369 times), and then EMS (279 times). The presented analysis shows that the main motivation of the researchers is GHG emissions, followed by renewable energies. It is observed that the batteries cluster (purple) is between the EMS (dark blue), ESS (brown), and PEMFC (green) nodes, meaning that they are the main secondary

storage system for hybrid vehicles. Also, it is shown that there is a new growing research trend in performance analysis (light blue), cost function (orange), and optimization methods (dark blue).

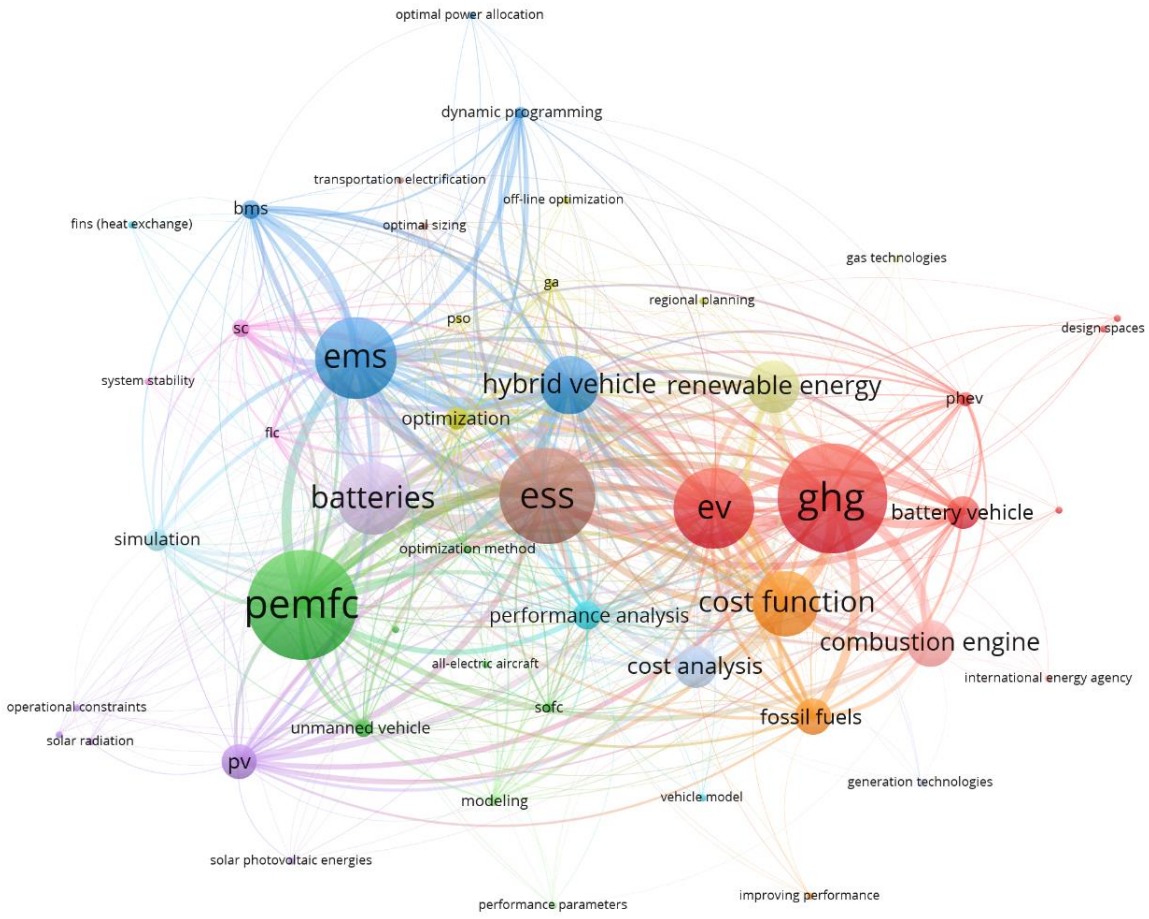

Figure 1.2 Keyword co-occurrence cluster similarity map for research articles

Due to the diversity of research focuses, a more specific literature review is presented in the following sub-sections. First, the advantages and disadvantages of each topology and the current situation are discussed. Then, in a second sub-section, the most relevant power source sizing and power split methods, which significantly influence the performance and cost of the vehicle power system, are analyzed.

1.3.1 Fuel cell hybrid power supply system

The power supply of a FCHEV is a coupling of a FC with an ESS as the secondary power source to overcome some of their drawbacks. The topologies discussed in different works in the literature can be classified into six categories [7-11], as shown in Figure 1.3 [10]. The full-active architectures, T1 and T2, are characterized by connecting all the power sources to the DC bus through a DC-DC converter, while semi-active structures, T3, T4, and T5, have at least one of the sources connected directly to the DC bus. Contrary to the active connections, the passive configuration shown in T6 directly connects the FC and ESS to the DC bus.

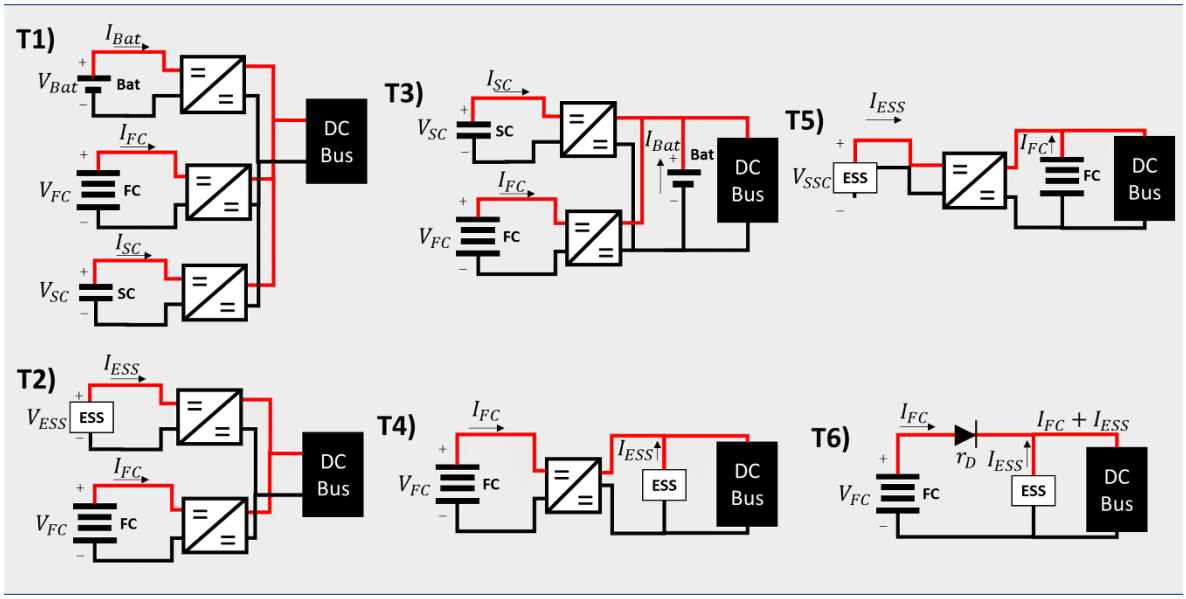

Figure 1.3 Topologies of a FCHEV

The main strength of an active connection is its flexibility to adjust the power split between the FC stack and the ESS through the formulation of an EMS, which has made it the regular choice for enhancing the lifetime of the system [28]. In this respect, the full-active topology has been applied more in high-duty applications such as tramways, hybrid buses,

ships, and excavators [29-32]. In these applications, the voltage at the DC bus should be stable and within a specific range because the three-phase motor inverter and the auxiliary systems are usually coupled directly to the DC bus. However, strict control on the DC converter is required in the full-active structure to reach a stable voltage level during the high-pulse power profiles. The semi-active has been extensively used because the passive component absorbs the surplus energy in the bus, facilitating the power split control over the FC. This architecture has been use by different light-duty vehicle manufacturers for example in the Toyota Mirai, Honda Clarity, among others [33]. On the other hand, passive coupling benefits from a simple implementation, self-management, low asset cost and light system [34, 35]. However, just some works outside this thesis works have proposed the passive configuration for vehicle applications [34-44]. From the viewpoint of passenger vehicles layout constraints, the topologies T1 and T3 are discarded from the study due to their heavyweight and high volume, which are not a limitation in high-duty vehicles with more space to place the components.

Based on the reported results, FCs have attracted much interest in the automotive industry during the past few decades due to their high efficiency, zero-local carbon emissions, and modular design. However, the DC/DC boost converter used for FCHEV must improve the following characteristics in order to increase EMS reliability and efficiency as well as fuel cell lifespan: low input current ripple, high voltage gain ratio, high efficiency, high compactness, and high redundancy [45]. Therefore DC-DC converter plays a crucial role in multiple sources of power supply system at the DC bus. Due to this, the topology selection represents more challenges in choosing the best fit for the specific energy storage technology and applications. In [46], a comprehensive study on the design rules of multi-input

converters, their architectures, merits, and demerits for various applications is detailed. In [47], a DC-DC boost converter with a wide input range and high voltage gain is proposed to act as the required power interface, which reduces voltage stress across the power devices and operates with an acceptable conversion efficiency. In [48], a dual-droop coefficient to expand DC bus signaling and droop control is presented for an SC-battery hybrid energy storage system. The suggested droop constant allows the SC to participate in power-sharing in the steady state and a lower variation in the battery current.

In [11], a comparative study of active and passive hybrid topologies for a FC-battery vehicle indicates that passive topology has a superior performance for the application in which the requested power does not contain high fluctuations. However, as the requested power starts having high pulses, the FC stack operation is shifted to a lower efficiency region. Another study compares the active and passive topology, respectively coupled with a battery pack and SC, as the complementary power source in a FCHEV [7]. This study shows that using an active topology with a battery result in noticeable power changes in the FC stack compared to the passive configuration of FC and SC. The use of SCs as the ESS stems from the fact that they are more prevalent than a battery pack to cope with the erratic behavior in a passive FCHEV. The passive topology with SC makes the drawn power from the FC smoother and leads to higher energy efficiency and a longer lifetime of the FC. In addition, SC benefits from high power density, high efficiency (in high voltage region), fast charge, wide temperature window, and excellent recyclability [49]. Given the reviewed papers, some efforts have already been made concerning active and passive topologies in vehicular applications. However, so far, these configurations have not been benchmarked comprehensively. In addition to common concerns regarding the cost, hydrogen

consumption, lifetime of the system, lightness, and compactness are also necessary considerations in recreational vehicle design.

Based on the mentioned works, the battery and the supercapacitor (SC) have been broadly employed in the literature and industry as secondary ESS for vehicular applications [50]. The most common rechargeable battery used in vehicles is the lithium-ion battery because of its high energy density and efficiency. However, its main disadvantages are the low power density, the reduced life cycle, and the long charging time. Regarding the SC, it is the most suitable device to provide rapid peaks of current due to the fast formation of the electric double layer at the interface between the electrodes and the electrolyte. Furthermore, the SC has a higher specific power, a longer lifespan, and better resilience to different operation temperatures than the batteries. Nevertheless, SCs suffer from a low energy density and a high self-discharge, which can generate a high-power peak request if both systems do not have the same electric potential. A novel hybrid capacitor that shows promising results in other electric systems, such as electric buses, tramways, renewable energies, spacecraft, and grid connection, is the Lithium-Ion Capacitor (LIC) [51]. The LIC is composed of a SC positive electrode (activated carbon), a battery kind negative electrode (carbon material pre-doped with lithium), and an electrolyte containing a lithium salt [52]. This hybrid structure yields a higher energy density than a SC while conserving its high-power density and long lifetime. The main electric characteristic of the above-mentioned ESSs is illustrated in Figure 1.4 [53, 54].

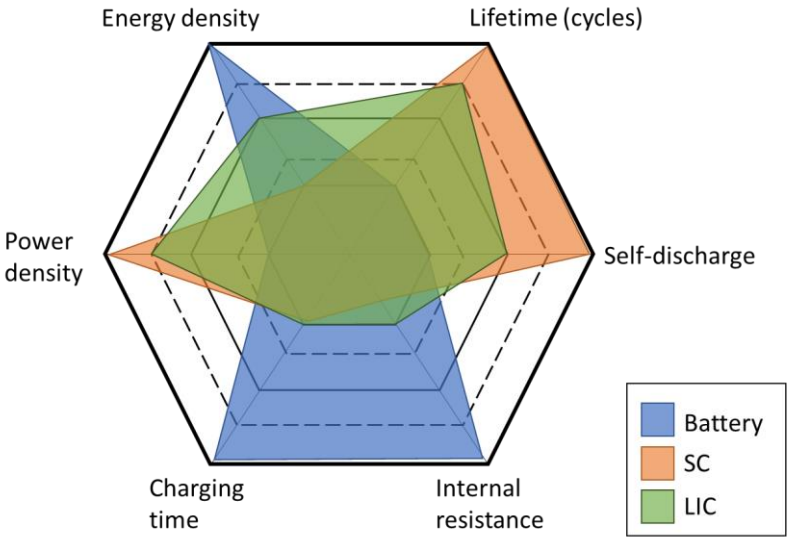

Figure 1.4 Comparison of ESSs in a radar chart

SC is a great ESS candidate to be integrated in a FCHEV for recreational applications based on the mentioned characteristics. For which the common concerns in previous works, using the full-active topology, are to compensate for the slow dynamic of the FC stack, minimize the hydrogen consumption, and increase the efficiency while taking care of the vehicle's lifetime [55-57]. Regarding semi-active FC-SC topology, the SC is directly connected to the DC bus, and the FC is interfaced with a unidirectional converter. The SC supplies and passively absorb the peak power. In [58], the FC is regulated by an EMS based on game theory, which considers the controller and the future driving condition to reduce hydrogen consumption and avoid unnecessary on-off cycles. Concerning the passive configuration, the Nissan company was the first to propose this type of configuration in 2005 by connecting a SC in parallel to each cell of the FC stack [44]. The attained experimental outcomes show that passive topology avoids negative voltage has self-protection in sudden power fluctuations, and improves the energetic performance as patented by Nissan company [59, 60]. In [40], a passive architecture connects a 9.5-kW proton exchange membrane FC

(PEMFC) to a SC bank. This configuration has decreased the dynamic load, idling time, and rapid load changes in the FC without using a DC-DC converter. In addition, it benefits from the lack of any DC-DC converter saving of weight, cost, and energy losses linked with an extra level of power conversion. This kind of architecture is independent of an EMS and has self-management due to the characteristics (different impedance) of the components. Therefore, some authors refer to it as "natural energy management" [59, 61]. The FC stack supplies the main component of the requested traction power following a smoother path since the ESS functions as a low-pass filter. However, if both systems do not have the same electric potential, this can lead to higher power ripples at the FC side and consequently increase the degradation rate of the stack. In [61], the presented principles are experimentally validated using a current pulse load to simulate the FC/SC passive configuration and study the degradation effect.

Recently, some efforts have been made in the initial voltage conditions of the FC/SC passive configuration, mainly focusing on the SC pre-charging and the passive system operation. Because the SC voltage decrease between 5% to 15% within the first 48h, due to the auto-discharge phenomenon [62]. This voltage mismatch between the SC and the FC open-circuit voltage will cause a high inrush current, leading to the FC membrane's degradation. One of the most common methods to overcome this drawback is presented by Wu et al., which uses a pre-charging fixed resistor to charge the SC below the FC open-circuit voltage (OCV). However, this method increases the startup time of the power supply system [40, 63]. An alternative approach to limit the instantaneous high input current without a resistor is made by controlling the H_2 flow into the FC. It has been proved in a single membrane FC that it is possible to set and operate the FC voltage below the threshold

recommended by the manufacturer while the SC is being charged to converge with the FC voltage [64]. One last alternative is to replace the commonly used electrostatic double-layer capacitors (EDLC) with the LIC mentioned above due to its stabler operational voltage. LIC cell operates in a voltage range of 2V and 3.8V, compared to SC cell that operates between 0V and its rated voltage (between 2.7V and 3V). This technology has already been tested in other applications improving the system performance, lifetime, and efficiency. However, the FC-LIC configuration has never been integrated, neither tested into a FCHEV for recreational applications. From the mentioned methods, the most straightforward and compact is using a pre-charging resistor to limit the FC current. In [63], a three-criteria SC sizing method, storage capacity, maximum voltage, and FC operating current dynamics are combined with a pre-charging strategy (a more detailed explanation is given in the Appendix C section). Experimental results reveal that there is a reduction in the FC degradation and improvement in the global system. The SCs support the FC to meet the requirements of the load while guarantying the system stability and less stress over the FC system.

Several EMSs are proposed for distributing the power between the FC stack and the ESS. However, special attention needs to be paid to the selection of the EMS and sizing method to avoid misleading conclusions. This is due to the intrinsic correlation between energy management and sizing problems. In fact, the performance of an EMS depends on the system size because this size will define the operating range and the possible combination of the system states [65]. An appropriate component sizing declines the overall ownership cost of a FCHEV while maintaining the expected performance. The use of an EMS is also necessary since the involved power/energy sources have different energetic characteristics in this hybrid powertrain. Still, most of the FCHEV works only analyze one specific topology and/or

do not use the best system size. Next section will deep dive into the sizing and power split methods for the vehicle hybrid systems.

1.3.1 Sizing and power split methods

As shown in Figure 1.2, EMS is one of the most frequent keywords in the research articles nowadays. In [27], a bibliometric analysis of the management strategies identifies the main research trends for electric vehicles. From this, it is observed that 21% of the strategies focus on increasing vehicle efficiency, followed by 17.8% on fuel economy or hydrogen consumption strategies, and 6.29% concentrate on performance optimization and emission reduction. However, to reach an optimal performance of the power supply system, it is required to take into account the intrinsic relationship of the EMS and sizing methods. Therefore, at first, a comprehensive survey on the existing component sizing methods and EMS is necessary.

Respecting the component sizing methods, they are defined as the mechanism to select the required dimensions of the power supply components to operate the system thoroughly. The sizing methods are mainly categorized into three different subtypes: experience-based, equivalent calculation-based, and optimization-based [65]. On the one hand, the most common sizing methods are designed based on the engineer's expertise or simple calculations to meet the vehicle requirements. On the other hand, optimization-based visualize this problem as a plant-controller with a multi-objective function to be minimized. The optimization-based can be classified based on their structure into sequential, iterative, two-steps, and simultaneous. Sequential is a fast method because it optimizes the component sizing, and then a predefined EMS is utilized. The iterative method improves the component sizing and EMS separately without compromising the system performance until the previous

optimization converges. The two-steps method can reach an optimal global result by employing a heavy computational process. The outer loop optimizes the plant's component sizing, and the inner loop optimizes the coordination of the selected plant. Lastly, the simultaneous method optimizes the EMS and sizing in a single global search optimization loop. However, the integration of both sub-problems might not have a convex solution, and the mathematical complexity increases. Based on the characteristics mentioned above, the preferable methods in the literature are; sequential [66-68] and two-step methods [55, 69-73].

The EMS is in charge of distributing the power across the power sources of the system in order to minimize fuel consumption and maximize the system lifespan. However, because of the effects of aging and various environmental and operational circumstances, the energy properties of the FCHEV electrochemical devices changes. Therefore, direct measurement of internal parameters to monitor the FC degradation in real-time applications is challenging. In this respect, several works perform an indirect estimation with mathematical model approaches, mainly grouped in white-box, black-box, and grey-box methods [74]. In [75], it is explained that the FC degradation is usually estimated with a semi-empirical model that considers the voltage drop at the stack level and extrapolates it by the number of cells. Another approach is the prognostic and health management methods that can anticipate failures and take preventive measurements to extend the lifespan of the systems. In [76], a data-driven relative power-loss rate health indicator identifies the real power by monitoring the current and voltage that are furnished into a double-input echo state network structure prognostic algorithm. The FC power decay can be calculated also as a sum of effect from the

different load conditions based on the empirical coefficients of a percentage FC performance degradation [77, 78].

Regarding the power-split strategy or EMS, they coordinate the energy sources and ESS to meet the requested power while respecting the system constraints. As a result, the EMS strongly influences the fuel economy and degradation of the vehicle. However, these strategies are only applicable to active topologies; semi-active and full-active. They are categorized into two main groups: rule-based and optimization-based [28, 75]. The rule-based strategy is a set of policies formulated by an expert opinion, and optimization-based are formulated with an objective cost function to maximize or minimize. This last group is divided into real-time and global optimization strategies. Real-time optimization strategies are preferred for real-world applications because they solve the optimization problem by defining an instantaneous cost function updated through time. On the contrary, global optimization strategies need to know in advance the complete driving cycle information. Nevertheless, these techniques are helpful to extract the maximum potential or optimal global solution. Hence, global optimization is a convenient method for benchmark analysis. That can be classified based on their objective: minimizing consumption, maximizing consumer satisfaction, reducing costs, and improving vehicle performance.

Based on the aforementioned methods and strategies, a literature review of some research works that implement sequential or two-step sizing approach is shown next. In [66], a hysteresis-based EMS and an alternative approach based on pinch analysis principles are employed to size the ESS and FC for a FCHEV. Different combination sizes of the components are categorized in terms of feasible and infeasible regions based on the energy storage required capacity. In [67], a multi-objective genetic algorithm (GA) technique is used

to solve the optimum sizing of a FCHEV problem that minimizes fuel consumption and acceleration performance. In [79], a real-time operating cost minimization EMS of a FC-battery based hybrid electric vehicle is performed via model predictive control, assisted by the forecasted speed and dynamic programming to determine the optimal power splitting over a moving time horizon. In [68], a non-dominated sorting genetic algorithm II (NDSGA-II) and a rule-based EMS are implemented to optimize the hydrogen consumption and component sizing of a FC-SC-battery power system. A model predictive control (MPC) and a sizing method based on a power source map indicate that the size of FC has a significant influence on hydrogen consumption [55]. The optimal based MPC considers hydrogen consumption, SC state of charge (SOC), and FC degradation to predict and compensate the power coordination of a FC-SC system. A multi-objective optimal model predictive control and power source sizing map are studied in [69]. An adaptative weight method based on a fuzzy logic controller is utilized to reduce the complexity and non-linearity of the problem into a single-objective function. This method shows a good control performance, low fuel consumption, long battery lifetime, and good use-cost economy. In [80], a two-step methodology that combines the Particle Swarm Optimization (PSO) technique and the rapid Pontryagin's Minimum Principle (PMP) optimal control algorithm to simultaneously tune the energy management and component sizing. The external loop (PSO) defines the architecture size according to the constraints and criteria, and the inner loop (PMP) optimizes the cost function of the defined powertrain. Finally, in [70-73], dynamic programming (DP) and Pareto front are used in a two-step manner. DP is employed to solve the non-linear multi-objective cost function EMS problem of FCHEV, and the Pareto front is used to determine the best combination of sizes to achieve the lowest cost. However, the main drawback of

Pareto front analysis is the high calculation time because this method evaluates all the possible combinations.

Concerning the investigated papers, it can be inferred that the employment of sizing procedures needs more attention with a specific view into the power splitting strategy to obtain the optimal global size. Therefore, it is necessary to analyze the cost of different sizes with optimal-based EMS, such as a two-step method that reaches the global minimum and is mainly used as a reference to benchmark new EMS and sizing methodologies. Moreover, the few papers regarding optimization-based sizing methods are just implemented to one specific FC hybrid configuration.

1.4 Objectives and contributions

Concerning the investigated works, some attempts have already been made regarding designing FCHEV, in which the focus was on the development of EMS and sizing methods for a specific hybrid configuration, compared to the presented thesis work in which several electric configurations are evaluated. In addition, such couplings have never been used for recreational electric vehicles, which is an originality of this thesis work. The studied electric vehicle Can-Am Spyder from Bombardier Recreational Products (BRP) is shown in Figure 1.5. These types of vehicles are typically exposed to high dynamics and need to be light and compact. Given these characteristics, the sizing of the components becomes a critical stage that directly influences the vehicle's performance, cost, and dimensions.

Figure 1.5 Can-Am Spyder electric vehicle

As pointed out earlier, the choice of the ESS is an important task that is closely linked to the FC behavior and degradation rate of the components. In this respect, the conditions affecting FC performance and lifespan are load changing cycles, start-stop cycles, low-power load, and high-power load [78]. Although, most of the commercial vehicles use a battery as the secondary energy source, a coupling of FC with a SC is more prevalent since the SC characteristics are more suitable for coping with the intermittent behavior of a recreational FCHEV. In other words, the SC will operate as a low-pass filter that leaves the main components of the requested power to the FC system. Furthermore, the SC makes the drawn power from the FC smoother, reducing the high-power load changes and keep running the FC for a longer time, leading to higher energy efficiency and a longer lifetime of the FC. In addition, SC benefits from a high power density, high efficiency (in high voltage region), fast

charge, wide operating temperature range, and excellent recyclability [49]. Although the mentioned benefits of SC, this thesis work presents an original study of a hybrid FC-LIC power supply system for the mentioned electric motorcycle.

In this respect, this thesis aims to investigate the applicability of a hybrid FC configuration for recreational vehicles. To fill the gaps which are brought into attention, three main objectives are set.

1. To define an optimal component sizing method that integrates the energy management and a multi-objective cost function.
2. Based on the previous optimal sizing method to comprehensively compare the performance of three customized FC-SC hybrid energy system configurations: full-active, semi-active, and passive.
3. To evaluate the suitability of using LIC instead of SC as the second power supply next to the FC in a passive configuration.

As such, the contributions of this thesis will be:

1. Develop a FC-SC hybrid power supply system model for a three-wheel electric recreational vehicle that integrates the hydrogen consumption and FC degradation phenomena. Compared to the existing studies that use a battery pack to power up a recreational vehicle, this work is the first in its class to propose the use of FC as a power supply system. Furthermore, this hybrid system can reduce the CO2 emissions compared to an internal combustion engine system and increase the range compared to a battery pack system.
2. Design of a two-step optimization methodology to determine the optimal system component size. There is a variety of sizing methods for hybrid systems in the

literature, but the more suitable ones for a benchmark study are the optimal-based sequential and two-step methods. However, these methods tend to use a real-time or simple cost function to coordinate the power splitting of the system while reducing the processing time. In this respect, the objective function of the proposed method considers a trip cost composed of the hydrogen consumption, FC degradation, and operational cost of the ESS and DC converters. Moreover, it reduces the computational time and solves the non-linearity of the multi-objective cost function by using a new unified solution method for DP and GA. This methodology applies to any hybrid electric vehicle in which a FC is coupled with a secondary ESS.

3. Implementation of a FC-SC passive architecture as the energy power supply system of an electric vehicle. The passive architecture for a hybrid power supply system has not been widely studied by the researchers focusing on vehicular applications because of its self-management characteristic and lack of control over the component performance. However, this configuration is lighter, more compact, and simpler to integrate compared to the other hybrid architectures. Moreover, this system can furnish the irregular requested power while taking care of the components due to SC's low pass filtering function and the high-energy supply role of FC.
4. Integration of LIC as the second power supply system in a FC passive configuration. LIC is a new ESS that has never been used in hybrid FC systems. However, it guarantees a smooth FC operation thanks to its high energy and power density. Furthermore, this coupling removes the necessity of a pre-charging system as needed for the SC. In this sense, from the passive coupling

side, the system will benefit from self-management and a compressed structure. Moreover, from the LIC properties side, the LIC has a stable voltage level as the lithium batteries and a low degradation rate similar to the SC.

1.5 Methodology

A six-step methodology has been followed to complete this thesis. The first step is to review the literature to provide state-of-the-art information about the proposed topic. In this regard, the recent works related to the FC hybrid vehicles are studied and grouped in power supply and energy storage systems, sizing methods, and power split strategies. From which it can be highlighted the gap on hybrid architecture comparisons of electric vehicles, this has given place to the developed benchmark study in this thesis work.

In this respect, to perform the mentioned analysis, the second step of this work deals with developing a model of the complete power train and power supply systems of the studied vehicle. This model is designed based on experimental data in MATLAB/™Simulink environment to study the system performance. Regarding the DC/DC converters it has been use an equivalent model based on commercial converters, that has a lower performance and bigger size compared to new state-of-art architectures. In order to improve the accuracy of the FC performance during long driving cycles a FC degradation model has been included. The FC degradation model includes the FC power drop coefficients of the major causes; high and low power operation, start-stop cycles, fast-dynamic loads, and natural decay. Compared to real-vehicle test, a simulator provides a time saving, safe environment, cost-effective procedure, and repeatability conditions for testing high-power electronic systems before a hardware implementation [81].

Following that, the third step of this project uses the virtual environment in place to define an optimal sizing method that brings a fair performance comparison of the hybrid systems. The proposed approach is based on utilizing a metaheuristic optimization algorithm and an optimal power flow sharing between the sources to satisfy the requested power while declining the fuel consumption and enhancing the system lifetime.

In addition to hydrogen consumption that is a common concern, the system's cost and lifetime are considered in a multi-objective cost function for which a sensitivity analysis is performed as the fourth step. It should be highlighted, that the prices of the technologies used in this thesis vary a lot and the choices of configuration, sizing and energy management are highly dependent on these prices. Therefore, perform a sensitivity analysis provides an insight into the influence of input parameter's uncertainties for the price fluctuation on the economic benefits and performance of the system.

Considering the discussed configurations, some attempts have already been made to couple FC and an ESS in vehicular applications. However, there is a lack of a coupling configuration benchmark study for hybrid vehicles, which gives place to this thesis's fifth step. It compares the vehicle performance under two standard driving cycles and one real-world condition of three optimal size architectures, namely full-active, semi-active, and passive.

The last step of this work deals with a compatibility study on the integration of LIC and FC in a passive hybrid configuration. The choice of this new component for a passive coupling with the FC resides in its electric properties, such as high power and energy density. A review of semi-empirical models that can represent the different electric behavior phases of the LIC, is carried out to study the viability of this new configuration in a virtual

environment. In addition, based on experimental data, the selected model is tuned and validated. The performance of the system is evaluated in terms of FC degradation and hydrogen consumption in three different stages of life.

1.6 Thesis outline

The rest of this document is organized as follows. Chapter 2 investigates the optimal sizing method for hybrid vehicles with an emphasis on sensitivity analysis. Chapter 3 provides a benchmark study of fuel cell-supercapacitor topologies on a three-wheel electric vehicle model design. Chapter 4 presents a new perspective of passive hybridization of Lithium-ion capacitors with a fuel cell system. Finally, the conclusion is given with some suggestions for future steps concerning this work in Chapter 5. Appendix B presents an initial comparison of passive and active fuel cell-supercapacitor coupling for a three-wheel electric vehicle. Appendix C describes a three-criteria SC sizing method combined with a pre-charging strategy for the SC.

Chapter 2 - Two-step optimal sizing method for fuel cell hybrid electric vehicles

2.1 Introduction

The presented fuel cell hybrid structures from the previous chapter illustrated that this integration of power sources handles dynamic power demands and recovers the regenerative energy from the braking system. However, proper component sizing and EMS are required to provide the requested traction power efficiently. The importance of such a design resides in their intrinsic correlation, in which the performance of the sizing influences the outcome of the EMS and vice versa. In the current literature, EMS and sizing have been mainly treated separately, and just some papers have considered these two problems as a coupled optimization problem. In addition, the definition of a suitable cost function plays an essential role in the optimization stage of a system design. However, due to the presence of several objectives (technical, economic, environmental, and socio-political) makes the definition of a suitable cost function vital. Hence, the use of a multi-objective cost function (MOCF), based on an economic point of view, has been widely practiced in the literature [82, 83]. A MOCF attempts to reach a compromise among the defined goals using a weighted sum approach [84]. However, these weights are normally specified based on the prices of components which are variable owing to different policies and technological advancement [85].

In this respect, this chapter aims at proposing a two-step optimization method with a nested structure to obtain a system-level optimal solution by making a trade-off between components size and system performance. For which genetic algorithm (GA) defines a near-

optimal dimensioning and dynamic programming (DP) finds the optimal power split by using a MOCF, which reaches a compromise between the capital and operating cost of the system. These weights describe the importance of the objective function and are usually defined based on each component's prices that vary due to different policies and technology maturity. Therefore, a sensitivity analysis is also conducted to study the impact of different price ranges on the overall operational cost. This will provide an insight into the influence of input parameter's uncertainties on the economic benefits.

The process system dimension and sensitivity analysis are explained by presenting an article entitled "Effects of Price Range Variation on Optimal Sizing and Energy Management Performance of a Hybrid Fuel Cell Vehicle". The utilized methodology and the summary of the results are discussed first. Afterward, the paper is presented.

2.1 Article 1: Effects of Price Range Variation on Optimal Sizing and Energy Management Performance of a Hybrid Fuel Cell Vehicle

Authors: Alvaro Macias, Mohsen Kandidayeni, Loïc Boulon, João P. Trovão

Journal: IEEE Transactions on Energy Conversion

Publication date: 31 January 2023

DOI: 10.1109/TEC.2023.3240723

2.1.1 Methodology

This article comprehensively reviews the works that adopt a system-level optimization perspective that can be classified into four categories: sequential, alternating, simultaneous, and nested methods. For which their main characteristics are summarized in the radar chart

of Figure 2.1 [65, 86]. This figure shows that the nested structure reaches the global optima by making a trade-off between component sizing and EMS. Also, it has a simple implementation and intermediate mathematical complexity. These features verify the frequent use of this method in the literature.

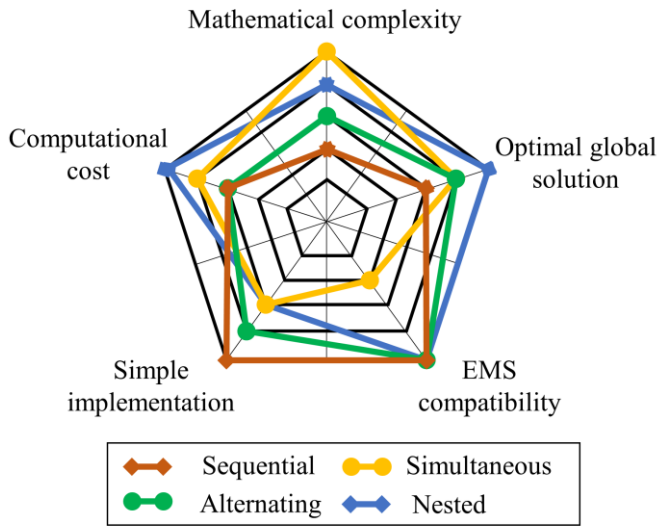

Figure 2.1 Comparison of component sizing structures

Therefore, the investigation of the coupled sizing and energy management problem has been the origin of the following studies. First, the studied e-TESC-3W vehicle platform from the University of Sherbrooke is modeled using the energetic macroscopic representation (EMR) formalism [87]. This method organizes and shows all the element's interactions graphically of complex multiphysics system models. Subsequently, a two-nested optimization loops method is explained. In which, the first (outer) loop uses GA to minimize the cost function by finding the right decision variables (size of powertrain components). The second (inner) one employs DP to optimally distribute the power using the obtained sizes in the first loop.

Nevertheless, this method requires the definition of a suitable cost function as multiple criteria. In the literature, there is a lack of insight regarding the interaction between component price variation and the FCHEV performance. Sensitivity analysis (SA) is one of the best tools to clarify such interactions and has been successfully utilized in other research and development areas [88]. SA can be mainly divided into local and global approaches, as shown in classification. Figure. Local SA techniques probe the effect of small perturbations around one point while the global ones consider a wider variation range of the inputs and analyze their influence over the whole feature space [89]. In the context of this work, Morris or elementary effect (EE) method is one of the screening techniques suitable for the systemic analysis of FCHEVs, mainly due to its ability to cope with complex systems (multiple criteria) with a low computational complexity.

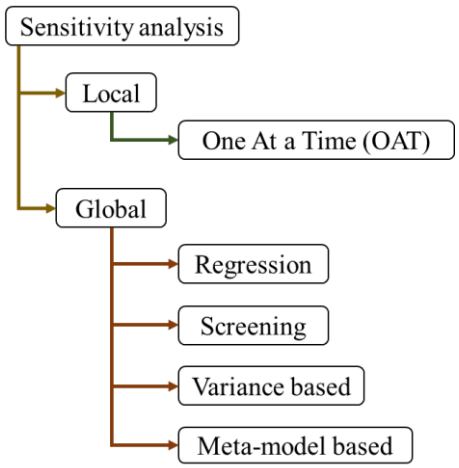

Figure 2.2 Sensitivity analysis methods classification.

In this regard, the performance of the presented Can-Am Spyder electric vehicle is examined in two phases: simulation and experimental. In the simulation phase, a multi-objective cost function is used to determine the best dimension of the powertrain components with the help of the two-step nested optimization. The utilized MOCF in this study has four

elements: FC degradation, hydrogen consumption, operational cost of SC, and operational cost of DC-DC converter. This multi-objective function is compared with two single-objective ones to realize their operational differences. Subsequently, the SA is performed since each element of the multi-objective cost function is influenced by its range of price. Lastly, in the experiment phase, a hardware-in-the-loop (HIL) setup is utilized to examine the multi-objective cost function with a real FC stack. For which, sequential quadratic programming (SQP) method is used as an EMS to split the requested power between the FC and the SC, due to its ease implementation and good performance. SQP is an iterative technique that solves non-linear optimization problems, reaching optimal/sub-optimal results using a quadratic programming subproblem [90].

2.1.2 Outcomes

As the first attempt, the MOCF is compared with two single-objective ones (hydrogen minimization: $H_{2,min} = \int W_{H_2} dt$ and FC degradation minimization: $FC_{deg,min} = \int \Delta_{FC} dt$), which represent the optimal limits of hydrogen and FC power degradation minimization. In this regard, the extreme component prices are considered for the MOCF to evaluate the influence of the minimum and maximum prices over the size of the components. Regarding the single-objective cost functions, the inclusion of prices does not have any effect on their performance as they pursue only one objective. Figure 2.3 shows the optimization surfaces (hydrogen consumption, and FC degradation) and pareto frontiers formed by the mentioned cost functions under the World Motorcycle Test Cycle (WMTC) driving cycle. The single points in each plot signify the GA population evaluated during the two-step optimization, and the markers locate the best result coordinate in each case. From these plots, it can be observed that the presented case is a nontrivial multi-objective optimization problem, where

the components of the MOCF are in conflict, and none of them can be improved in value without declining some of the other objective values. However, MOCF reaches a balance between both single objectives. Also, both MOCFs component prices converges to a pareto optimal point in the same optimal system size that could mislead to conclude that the prices don't affect the system size.

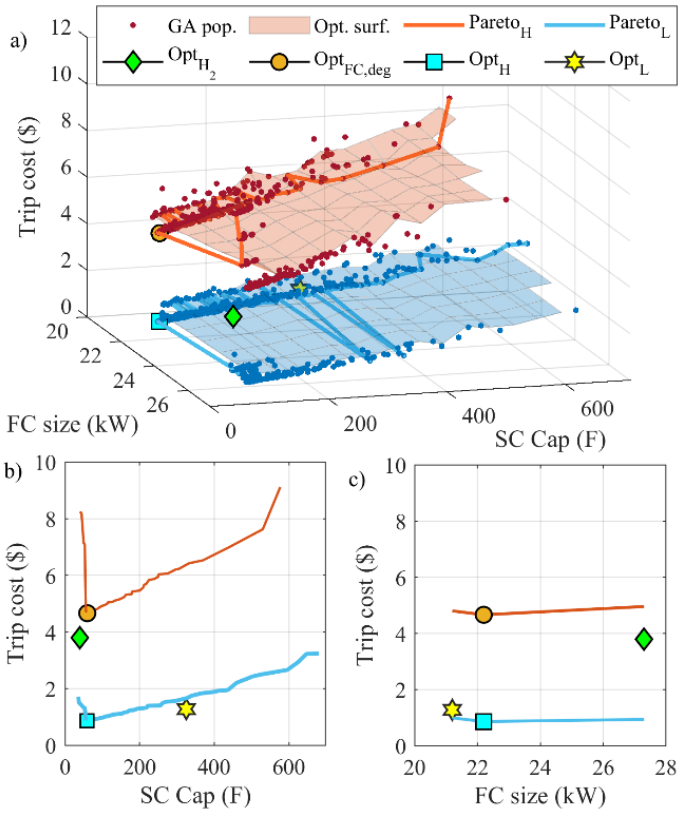

Figure 2.3 Electric Spyder performance under WMTC driving cycle through two-step optimization method, a) multi-objective, Pareto frontier based on b) SC size and c) FC size

These results show that further analysis is required to comprehend the effect and interaction of price variation on the sizing and operational cost. The results of the EEs sensitivity analysis of the component's prices under the World Motorcycle Test Cycle (WMTC) and road-test driving cycles are shown in Figure 2.4.

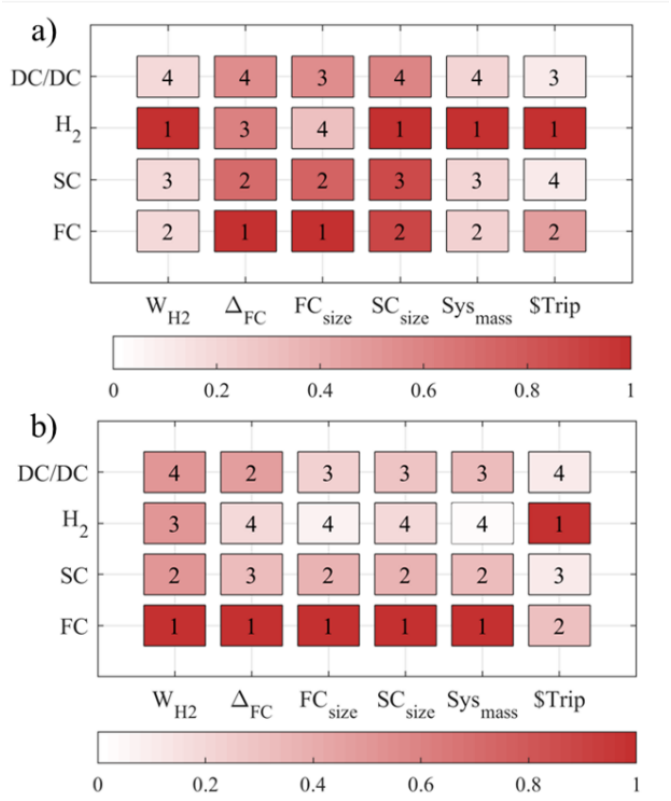

Figure 2.4 Elementary effects of component price variation on system performance under (a) WMTC and (b) on-road driving cycle

The rank of each parameter is in the center of the sub-square, which is defined using the mean of the absolute EEs values of the component prices concerning the system performance in terms of hydrogen consumption (W_{H_2}), FC system degradation (Δ_{FC}), FC size ($P_{FC,max}$), SC size (c_{sc}), system mass (m_{pow_sys}), and total trip cost ($\$Trip$). It can be seen from this figure that the hydrogen and FC prices are the most influential parameters in both cases. In other words, it means that a slight variation of this parameter will have a significant effect on the behavior of the power splitting and sizing.

In the experiment phase, the online SQP based EMS is implemented for the multi-objective cost function under different set of weights for an on-road driving cycle. This test is deployed in a HIL setup, where the SC is a mathematical model, and the FC system is the

real component. The FC output power in the HIL test bench is scaled up after the DC-DC converter to satisfy the demanded power. The EMS has been coded in LabVIEW environment and implemented in the real-time module of Compact-RIO by means of the block "Constrained Nonlinear Optimization virtual instrument VI". The system size, trip cost, total hydrogen consumption, and FC degradation of the tree baseline cases are compared against two optimal size and presented in Table 2-1.

Table 2-1 Multi-objective cost functions performance comparison

Cost function weights	Trips cost	H2 cons.	FC deg.
Highest price$_{baseline\ size}$	\$8.091	6.72 gr	%0.0039
FC cheap$_{baseline\ size}$	\$7.065	6.73 gr	%0.0040
H2 cheap$_{baseline\ size}$	\$5.008	6.63 gr	%0.0055
FC cheap$_{optimal\ size}$	\$6.668	6.65 gr	%0.0040
H2 cheap$_{optimal\ size}$	\$4.809	6.62 gr	%0.0055

The obtained results show that changing the price weights in a MOCF can result in more degradation and fuel consumption while using the same size. However, finding an optimal size for each price change on the MOCF can enhance the performance of the FCHEV up to 6 %. This research demonstrates the impact of basic variation on FCHEV, which might help guide the automobile industry's future development and market strategy. In future works, it should be evaluated the influence of the FC and ESS degradation on the performance of the vehicle.

Effects of Price Range Variation on Optimal Sizing and Energy Management Performance of a Hybrid Fuel Cell Vehicle

Alvaro Macias, *Student Member, IEEE*, Mohsen Kandidayeni, *Student Member, IEEE*, Loïc Boulon, *Senior Member, IEEE*, João P. Trovão, *Senior Member, IEEE*

***Abstract*-- The usage of multi-objective cost functions (MOCFs) in sizing and energy management strategy (EMS) of fuel cell hybrid electric vehicles (FCHEVs) has expanded due to the participation of multiple technological and economic disciplines. To better understand the impact of price fluctuation on the component size and EMS of an FCHEV, this article proposed a sensitivity analysis methodology. First, a two-step optimization approach that considers hydrogen consumption, system degradation, and trip cost is used to minimize a MOCF of the Can-Am Spyder electric motorcycle simulator. Then, an effect analysis is carried out for the cost-optimal results under two driving profiles to understand the link between cost variation and system performance. These simulations indicate that each might result in different system sizes and EMS compromise. After that, an online optimization EMS based on sequential quadratic programming is used on a reduced-scale hardware-in-the-loop configuration to evaluate the simulation results with varied weights. Experimental results indicate that when an adequate size is used for each pair of weights, the EMS results in a 6 % decrease in the trip cost.**

***Index Terms*— Electric vehicles, fuel cells, genetic algorithms, multi-objective programming, optimal control**

NOMENCLATURES

DP	Dynamic programming
EE	Elementary effects
EMR	Energetic macroscopic representation
EMS	Energy management strategy
FC	Fuel cell
FCHEV	Fuel cell hybrid electric vehicle
GA	Genetic algorithm
HIL	Hardware-in-the-loop
MOCF	Multi-objective cost function
SA	Sensitivity analysis
SC	Supercapacitor
SQP	Sequential quadratic programming
WMTC	World motorcycle test cycle

I. INTRODUCTION

A fuel cell hybrid electric vehicle (FCHEV) is composed of a proton exchange membrane fuel cell (FC), as the principal power source, and a battery and/or supercapacitor (SC), as the energy storage system [1]. This hybrid structure can supply the dynamic power demand, absorb the regenerative braking energy, and handle cold start issues provided that proper component sizing and energy management strategy (EMS) are designed [2]. An appropriate component sizing declines the overall ownership cost of a FCHEV while maintaining the expected performance. In [3], it is shown that determining the optimal battery and SC capacity according to the recuperation potential and FC dynamics can lead to small-sized battery and more stable FC operation. The use of an EMS is also necessary since the involved power/energy sources have different energetic characteristics in this hybrid powertrain. This strategy is supposed to distribute the power flow between the sources with the aim of minimizing the hydrogen consumption and maximizing the lifetime of the components. The presence of several objectives (technical, economic, environmental, and socio-political) in the design of a proper sizing and EMS makes the definition of a suitable cost function vital. Hence, the use of a multi-objective cost function (MOCF), based on an economic and system dimensions point of view, has been practiced in [4, 5]. A MOCF attempts to reach a compromise among the defined goals using the given importance or weights to each of the objectives. In [6], an economic comparison of a multi-objective hierarchical EMS against single objective ones is presented. The results shows that an equivalent consumption minimization strategy will regulate the FC to work in the optimal efficiency region, while the MOCF controls the output current of the FC to achieve an optimal balance between the FC degradation and hydrogen consumption. In [7], an economic assessment of a convex multicriteria optimization approach is implemented in a FC

This work was supported in part by the Fonds de Recherche du Québec Nature et Technologies (FRQNT) (283370 & 284914), Réseau Québécois sur l'Énergie Intelligente (3rd cycle and postdoctoral scholarships), Natural Sciences and Engineering Research Council of Canada (NSERC) (Grant RGPIN-2018-06527 and RGPIN-2017-05924) and Canada Research Chairs program (Grant 950-230863 and 950-230672).

Alvaro Macias and Loïc Boulon are with the Hydrogen Research Institute, Department of Electrical and Computer Engineering, *Université du Québec à Trois-Rivières*, QC G8Z4M3, Canada (email: alvaro.omar.macias.fernandez@uqtr.ca, loic.boulon@uqtr.ca).

Mohsen Kandidayeni is with Department of Electrical Engineering and Computer Engineering, *Université de Sherbrooke*, Sherbrooke, QC, J1K 2R1, Canada, and also with the Hydrogen Research Institute, Department of Electrical and Computer Engineering, *Université du Québec à Trois-Rivières*, QC G8Z4M3, Canada (e-mail: Mohsen.Kandidayeni@USherbrooke.ca).

João P. F. Trovão is with the Department of Electrical Engineering and Computer Engineering, *Université de Sherbrooke*, Sherbrooke, QC, J1K 2R1, Canada, and also with Polytechnic of Coimbra (IPC-ISEC) and INESC Coimbra, Portugal (e-mail: Joao.Trovao@USherbrooke.ca).

hybrid bus. The resulted pareto plots show that a balance between the FC lifetime and hydrogen consumption is necessary to reach the maximum benefits of the hybrid powertrains. In [8], a multi-objective design exploration shows that the FC size has a considerable effect on the overall vehicle performance and system degradation. However, these weights are normally specified based on the prices of components which are variable owing to different policies and technological advancement [9]. In this regard, sensitivity analysis (SA) has been successfully utilized in other research areas to clarify such interactions. The SA approaches can be mainly divided into two groups of local and global [10]. Local SA techniques investigate the effect of small perturbations around one point while the global ones consider a wider variation range of the inputs and analyze their influence over the whole feature space [11]. The performed SA approaches in the area of FCHEVs have mainly focused on the one-at-a-time method to identify the parameters or strategies that lead to the best result. In [12], a convex programming problem is formulated to optimize the power distribution and sizing of a plug-in FC urban logistics vehicle. In order to define the battery and FC sizes which in turn minimize the energy and power sources cost, a one-at-a-time SA is done based on different driving cycles and hydrogen prices. However, the authors have mainly focused on the performance of the EMS without paying attention to the real influence of the component prices. In [13], a multi-objective optimal problem, considering the decay of an electrochemical surface area model, fuel consumption and battery degradation, is developed using different weight factors. The obtained results show that assigning different factors to the FC degradation can change its operating function from a load-following to a more constant profile, which dramatically affects its lifetime. However as underlined in the article, future changes in the cost or degradation rates may yield different results. In [14], a sizing approach is implemented for FC electrified heavy-duty trucks and tested under different cost scenarios by defining total cost of ownership. The obtained results suggest that a FC powertrain will be more attractive than a pure battery one in 10 years according to current projections for the cost of FC system, battery pack, fuel storage, hydrogen, and electricity. In [15], a SA is performed for different initial battery SOC and energy prices to assess the effect of a multi-scheme EMS for a driven passenger ship. Another example is given in [16], where the influence of the modeling parameters on the dynamical performance of PEMFC is investigated. This study shows that the most sensitive parameters can mislead the polarization curve estimation from the real behavior.

So far, several methods have been proposed for determining the most appropriate combination of component sizes based on the hydrogen consumption, FC degradation or MOCFs. However, these works do not ponder the effect of weight variations on the cost function. Therefore, this paper proposed a methodology to scrutinize the impact of component price variation on the sizing and energy management of a FCHEV. The Morris or elementary effects (EE) method is used in this work due to its low computational within the feasible parameter space; the performance of this screening technique has already been validated in other engineering problems [17]. This global SA is suitable for the systemic analysis of FCHEVs, mainly due to its ability to cope with complex systems (multiple criteria) with a low computational complexity compared with variance-based methods. However, special attention needs to be paid to selecting the EMS and sizing method to avoid misleading conclusions. In fact, the performance of an EMS depends on the system size because this size will define the operating range and the possible combination of the system states [18]. Therefore, in this work, a two-step optimization method with a nested structure is utilized to reach the global optima and remove any influence on the EMS or system size results during the SA. The nested or bi-level method is one of the most used methods to solve this coupled optimization problem in recently published papers since it reaches a system-level optimal solution by making a tradeoff between the two problems [19, 20]. This work employs genetic algorithm (GA) and dynamic programming (DP) to reach near-optimal sizing and optimal power splitting, respectively, in a multi-objective system-level optimization. Several simulations and experiments are carried out to verify the outcomes of this study.

The rest of the paper is organized as follows. First, the followed methodology is discussed in Section II. Then, the obtained results are discussed in Section III. Finally, the conclusion is given in Section IV.

II. Methodology

In this work, the vehicle under study is the Can-Am Spyder electric motorcycle, which has an electric motor (permanent magnet synchronous: 28 kW, 96 V) directly linked to the rear wheel. It is utilized as an experimental test bench in e-TESC laboratory at the University of Sherbrooke [21]. In this manuscript, the performance of this electric motorcycle is evaluated for a FC-SC semi-active architecture. To do so, a simulation stage and an experimental stage validation are considered. In the simulation stage, an experimental based vehicle, FC and SC models are utilized to develop a coupled sizing and EMS problem and conduct a SA on the price variation of the power supply system. Consequently, in the experimental stage, a reduced-scale hardware-in-the-loop (HIL) set-up is utilized to evaluate with a real-time EMS the sizing achieved in the simulation stage. Hereinafter, the modeling procedure of each stage is briefly explained.

A. Studied vehicle - powertrain model and simulation

FCHEVs are multi-physical systems that can be conveniently represented by energy-flow modeling approaches, such as energetic macroscopic representation (EMR). EMR uses causal graphic descriptions to show how energy is converted and exchanged in multi-energy domain systems. It has basic coupling elements that correspond to the multi-energy components and control elements that allow inversed model-based control loops to be deduced. Different colors and blocks reflect the interactions in the subsystems differently in EMR's graphical elements. Energy source, accumulation, conversion, and distribution are the four key elements employed in EMR to emphasize the system's energetic properties. The formalism of

This article has been accepted for publication in IEEE Transactions on Energy Conversion. This is the author's version which has not been fully edited and content may change prior to final publication. Citation information: DOI 10.1109/TEC.2023.3240723

EMR was initially presented in [22] and used in several other papers for FCHEVs [23]. Fig. 1 presents the forces acting on the vehicle alongside its moving direction (Fig. 1a) and the utilized FC-SC semi-active powertrain configuration (Fig. 1b). The vehicle dynamics and forces, shown in Fig. 1a, are divided into the mechanical transmission, chassis and environment interaction, shown in Fig. 1b. This was calculated using Newton's laws, as:

$$\frac{dV_{EV}}{dt} = \frac{(F_{tr} - F_{env})}{m_{eq} \sin\theta} \quad (1)$$

$$F_{tr} = (G_{gb}/r) T_{em} \eta_{gb}^{\beta} \quad (2)$$

$$F_{env} = F_{roll} + F_{grade} + F_{air} \quad (3)$$

$$F_{roll} = mg\mu_{fr} \cos\theta \quad (4)$$

$$F_{air} = 0.5 \rho_{air} A_{aero} C_d {V_{EV}}^2 \quad (5)$$

$$F_{grade} = mg \sin\theta \quad (6)$$

$$\Omega_m = (G_{gb}/r) V_{EV} \quad (7)$$

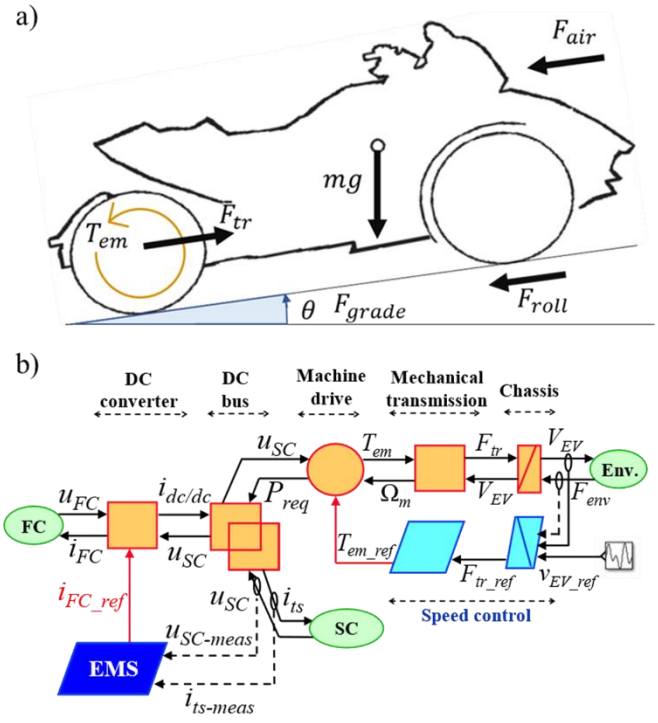

Fig. 1 The studied vehicle, a) Can-Am Spyder electric motorcycle, and b) powertrain configuration modeling using EMR.

where V_{EV} is the vehicle velocity, F_{tr} is the traction force, F_{env} is the vehicle traction force resistance, m is the vehicle mass, G_{gb} is the gearbox transmission ratio, r is the wheel radius, T_{em} is the electric machine torque, η_{gb} is the gearbox transmission efficiency, g is the gravitational acceleration, ρ_{air} is the air density, β is 1 in traction mode and -1 in braking mode, and Ω_m is the rotor rotation speed. It is worth mentioning that the vehicle mass includes an approximation of the mass of the chassis, passenger, powertrain and the energy sources. The mass of the energy/power sources are calculated based on the number of cells for the FC and SC arrangement [24].

The requested power (P_{req}), represented with a multi-physic conversion element, is calculated based on the torque and drive efficiency (η_m) that considers the inverter and motor efficiency by:

$$P_{req} = T_{em} \Omega_m \eta_{\mathrm{m}}^{\beta} \quad (8)$$

The relationship of P_{req}, effective FC power ($P_{FC,bus}$), and SC power (P_{SC}) observed in the DC bus can be defined by:

$$P_{req} = P_{FC,bus} + P_{SC} \quad (9)$$

The FC stack performance is modeled by an electrochemical model proposed by Amphlett et al., [25] which was successfully implemented with experimental data in several papers [26]. In this work, the FCvelocity-9SSL from Ballard Power Systems has been chosen as the main power supply system due to the different available sizes, from 3.8 kW to 27.3 kW. The cell voltage (u_{FC}) of a proton exchange membrane type FC is approximated as (10-14):

$$u_{FC} = N_{FC}(E_{Nernst} + u_{act} + u_{ohmic} + u_{con}) \quad (10)$$

$$E_{Nernst} = 1.229 - 0.85 \times 10^{-3}(T_{FC} - 298.15) + 4.3085 \times 10^{-5} T_{FC}[\ln(p_{H2}) + 0.5 \ln(p_{O2})] \quad (11)$$

$$\begin{cases} u_{act} = \xi_1 + \xi_2 T_{FC} + \xi_3 T_{FC} ln(CO_2) + \xi_4 T_{FC} ln(i_{FC}) \\ C_{O_2}^{*} = \frac{P_{O2}}{5.08 \times 10^6 \, exp(-498/T_{FC})} \end{cases} \quad (12)$$

$$u_{ohmic} = -i_{FC} R_{internal} = -i_{FC}(\zeta_1 + \zeta_2 T_{FC} + \zeta_3 i_{FC}) \quad (13)$$

$$u_{con} = \alpha ln(1 - i_{FC}/i_{FC,max}) \quad (14)$$

where u_{FC} is calculated with the number of cells (N_{FC}), the reversible voltage (E_{Nernst}), and the irreversible voltage losses composed of the activation loss (u_{act}), ohmic loss (u_{ohmic}), and concentration loss (u_{con}). The voltage components are in function of the operating current (i_{FC}), stack temperature (T_{FC}), hydrogen partial pressure (p_{H2}), oxygen partial pressure (p_{O2}), activation empirical coefficients (ξ_n), oxygen concentration ($C_{O_2}^{*}$), internal resistor ($R_{internal}$) defined by the three parametric coefficients ζ_n (n = 1 … 3), a semi-empirical parameter related to the diffusion mechanism (α), and the maximum current ($i_{FC,max}$). More information about each of these parameters can be found in [20].

The effective power of the FC system in the DC bus is calculated by using the efficiency ratio (η_{DC-DC}) of the DC-DC converter and the consumed power by the auxiliaries; composed of the fan cooling system (P_{fan}) and the power of the compressor (P_{comp}), as follow:

$$P_{FC,bus} = (i_{FC} \cdot u_{FC}) \eta_{DC-DC} - P_{comp} - P_{fan} \quad (21)$$

Moreover, the hydrogen flow (W_{H_2}) is approximated based on a linear function of the requested FC current as follow:

$$W_{H_2} = 0.00696 \, i_{FC} \, N_{FC} \quad (18)$$

A classical RC model represents the SC energy block due to the ease of calculation and a good approximation of the system behavior [27]. The electrical behavior is calculated as:

$$u_{SC}(t) = u_c(0) + \frac{1}{C_{SC}} \int i_{SC} dt - i_{SC} R_{SC} \quad (19)$$

where the SC voltage ($u_{SC}(t)$) is a function of the initial open-circuit voltage ($u_c(0)$) and the current across the SC (i_{SC}). The values of equivalent capacitance (C_{SC}), and the equivalent resistor of the SC (R_{SC}) are reported in the Maxwell Technologies manufacturer datasheet. The remaining energy in the SC is estimated by the formula of Coulomb counting, where $SOC_{SC}(0)$ represents the initial level of charge, and Q_{max} is the maximum capacity [28].

$$SOC_{SC}(t) = SOC_{SC}(0) + \int \frac{i_{SC}\, dt}{Q_{max}} \quad (20)$$

B. Hardware-in-the-loop set-up

Compared to real-vehicle tests, HIL is an attested, cost-effective procedure for designing an EMS. Moreover, the repeatability of the same case studies is a real plus to HIL simulation against on-road test facilities [29]. The developed HIL set-up for evaluating the performance of the vehicle model using different online EMSs is presented in Fig. 2. This HIL test bench is exactly based on the explained vehicle model in Fig. 1, in which the FC model has been replaced with an open cathode proton exchange membrane FC H-500 from Horizon company.

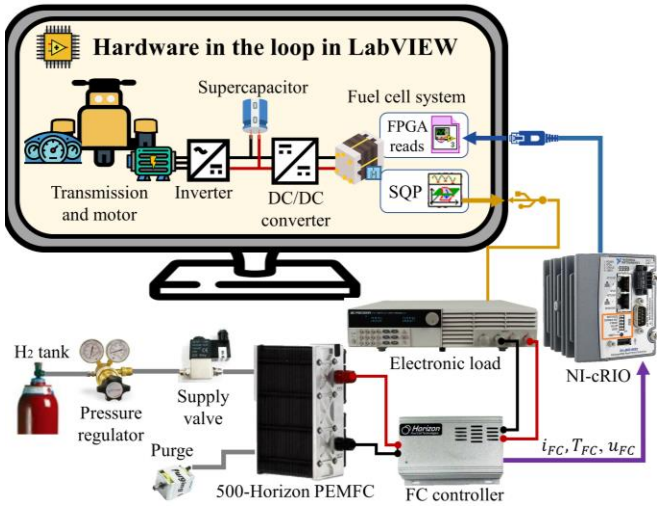

Fig. 2 The developed HIL set-up for evaluating the vehicle performance.

The FC controller handles the affixed axial fan, hydrogen valve, and purge valve. The axial fan has a dual role of cooling down the stack temperature and providing the required oxygen for the reactions. The information between the CompactRIO and the PC is transferred by an Ethernet connection with a rate of 10 Hz. A DC Electronic Load (8514 BK Precision) is employed to demand the imposed load profile by the DC-DC converter from the FC stack.

C. Nested optimization method

The utilized optimization method has two nested loops. The first (outer) one uses GA to minimize the cost function by finding the right decision variables (size of powertrain components). The second (inner) employs DP to optimally distribute the power using the obtained sizes in the first loop.

GA is appropriate for optimization problems in which the cost function is nonlinear, discontinuous, nondifferentiable, or stochastic. Two important components of the GA are the decision variables and the cost function. The decision variables in the sizing problem of this work are limited to the number of cells forming the FC stack (N_{FC}), the capacitance of a single SC ($C_{SC,u}$), the number of SC connected in series ($N_{SC,s}$), and the number of SC series banks in parallel ($N_{SC,p}$). GA is expected to minimize the following MOCF by tuning the mentioned variables. The trip cost is in terms of USD and comprises the costs of fuel consumption and wear of the system. The FC portion is linked to the system degradation, which is considered as the percentage of reduction in the maximum power. A dynamic operation of the FC significantly affects its durability and performance by corroding its key components resulting in the degradation of platinum catalyst and increment of the mass transfer resistance [30]. The SC and DC-DC converter, however, are predicted to last for thousands of cycles under typical circumstances [31]. Hence, their costs are only correlated with the trip time to increase their impact on the optimization process.

$$\$Trip = \$FC_{sys}\Delta_{FC} + \$H_2 \int W_{H_2} \mathrm{dt} + \$SC\Delta_{trip} + \$DC_{conv}\Delta_{trip} \quad (22)$$

where the trip cost ($\$Trip$) in USD is composed of the FC system degradation cost ($\$FC_{sys}$: FC system cost based on its maximum power, Δ_{FC}: FC power degradation), the hydrogen consumption cost ($\$H_2$: Hydrogen cost per kilogram, W_{H_2}: hydrogen flow in SLPM), SC operational cost ($\$SC$: SC cost based on the total capacity, Δ_{trip}: trip time), and DC-DC converter operational cost ($\$DC_{conv}$: DC-DC converter cost based on the FC maximum power). However, the direct measurement of some internal parameters to monitor the FC/SC degradation are very challenging in real-time applications. In this respect, an indirect estimation can be done with mathematical models approaches, mainly group in white-box, black-box, and grey-box methods [32]. In [33], it is explained that the FC degradation is normally estimated with a semi-empirical model that consider the voltage drop at the stack level and extrapolate it by the number of cells. A similar approach has been done in [8, 34], where a stochastic dynamic programming strategy quantifies the FC degradation rates in terms of volts to compare different sizes in a common ground. In order to have a direct comparison of FC degradation between different FC sizes, it has been opted to translate the percentage of FC degradation to its equivalent in power decay caused by degradation. In the presented work, the power decay (Δ_{FC}) is calculated as a sum of effect from the different load conditions based on the empirical coefficients of a percentage FC performance degradation [35, 36].

$$\Delta_{FC} = P_{FC,max}(k_1 t_1 + k_2 n_1 + k_3 n_2 + k_4 t_2 + k_5 t_3) \quad (23)$$

where $P_{FC,max}$ is the FC maximum power, k_1 ($0.00126\,\%/h$) is the degradation rate due to low-power operation (less than 5 % of FC maximum power), k_2 ($0.00196\,\%/cycle$) is the degradation rate of one on/off cycle,

k_3 (5.93×10^{-5} $\%/cycle$) is the degradation rate of transient load changes, k_4 is the degradation rate of high-power operation (more than 90 % of FC maximum power), and k_5 (0.002 $\%/h$) is the natural performance decay rate. t_1, t_2, and t_3 are the operation time in low-power, high-power, and FC on conditions respectively while n_1 is the number of on/off cycles and n_2 is the number of transient load changes [33]. According to the US Department of Energy (DOE), FC end of life (EOL) is defined as a 10 % decline in the maximum power with an operational objective of 5000 hours [37]. However, the SC and power components are expected to last around thousands of cycles in normal conditions [31]. Therefore, their cost is linked to the above-defined trip time (Δ_{trip}) to increase their importance in the optimization process, which is the total time divided by the operational objective of 5000 hours. It should be noted that the price of the system cost components ($\$FC_{sys}$, $\$H_2$, $\$SC$, and $\$DC_{conv}$) is variable in the market.

The decision variables used for the optimization problem are defined as discrete values based on the commercial capacitance of Maxwell SC and the size of the Ballard FC. This work focuses on the FCvelocity-9SSL model in which the number of cells defines the maximum power N_{FC}. Table I shows the search space formed by the decision variable ranges. Regarding the GA, the available function in the Optimization Tool of MATLAB is utilized while considering the following setting: Population size 200, maximum generations 200, Elite count 10, Selection function: "selectionstochunif", and Crossover fraction: 0.8.

TABLE I DISCRETE DECISION VARIABLES RANGE

Variable	Search space
N_{FC}	[55,71,75,80,90,110,115,135]
$C_{SC,u}$	[100,150,310,325,350,360,450,650,1200,1500,2000,3000,340]
$N_{SC,s}$	$\in Z \geq 1, \leq 60$
$N_{SC,p}$	$\in Z \geq 1, \leq 60$

The FCHEV model is a nonlinear state-space model which DP can solve as one of the most well-known optimal control methods for nonlinear, time-variant, constrained, discrete-time models. DP solves an optimization problem by breaking it down into simpler subproblems assuming that the optimal solution to the overall problem is achieved by calculating the optimal solution to its subproblems. In this work, a DP function introduced in [38, 39] is used, which has been proposed for optimal energy management of FCHEVs. This method works based on calculating the boundary range of the state variable, dividing the state variables space into four operational modes, determining the minimum cost of each grid point forward, and calculating the minimum optimal control decision sequence backward. By doing so, this method shows less computational time and better calculation accuracy. The state-space for the current variable in this work is divided with a grid size of 0.5 A and the SOC space is divided with a grid size of 0.05 %. Using this DP function, the unified state-space equation of the vehicle under study can be described by the following four states:

$$\begin{cases} SOC_{SC}(k+1) = SOC_{SC}(k) + \int \frac{i_{SC}(k)\,dk}{Q_{max}} \\ u_{SC}(k+1) = u_c(k) + \frac{1}{C_{SC}} \int i_{SC}(k)dk - i_{SC}(k)R_{SC} \\ P_{FC,s}(k+1) = u_{FC}(k) * i_{FC}(k) \\ M(k+1) = \psi\left(P_{FC,s}, i_{FC}, k\right) \end{cases} \quad (24)$$

where SOC_{SC} is the SC SOC, u_{SC} is the SC voltage, $P_{FC,s}$ is the FC power, and M is the operational work mode. The considered control variable is the FC current (i_{FC}) whose optimal trajectory is given by DP. It should be noted DP uses the defined cost function in (22) to solve this optimization problem. The defined work mode is a function of the control variable (FC current) and the FC power which is a state variable. Definition of the work mode results in the reduction of the computational burden by avoiding the extra calculation for the infeasible areas.

To ensure that the system operates in the desired conditions, some limitations need to be imposed on the state and control variables as:

$$\begin{cases} 50\ \% \leq SOC_{SC} \leq 90\ \% \\ 0A\ \leq i_{FC} \leq 300\ A \\ -300\ A \leq i_{SC} \leq 300\ A \\ 80\ V \leq u_{DC} \leq 120\ V \\ -0.1\ P_{FC,max} \leq \Delta P_{FC} \leq 0.1\ P_{FC,max} \end{cases} \quad (25)$$

where SOC_{SC} range is selected based on the requirements of the installed electric motor on Spyder vehicle. Since SC SOC has a direct relationship with voltage, the minimum and maximum ranges have been defined by considering the input voltage range of the motor driver (80 V – 120 V) in the optimization process. The current limits are based on the manufacturer's manual, the u_{DC} range is defined based on the motor driver operating voltage, and the ΔP_{FC} is the slew rate of the FC power given by:

$$\Delta P_{FC} = P_{FC}(k) - P_{FC}(k-1) \quad (26)$$

D. Sensitivity Analysis

SA studies how uncertainty in the input parameters of a model affects the output response, identify the parameters with a significant influence on the model output and their interaction level. The literature review shows that the EE method is a good representation of the total sensitivity index because it evaluates the influence and interaction effect of each independent input parameter [11]. The calculation of the EE starts by discretizing the input variable space Ω of the model $y = f(\boldsymbol{X})$ in p levels. $\boldsymbol{X}$ represents the independent input parameters $X_i, i = 1, \ldots, k$ with k dimensions. The EE of the ith parameter is defined as:

$$E_i = \frac{[f(X_1, X_2, \ldots, X_i + \Delta, \ldots, X_k) - f(X_1, X_2, \ldots, X_k)]}{\Delta} \quad (27)$$

where $\Delta = p/[2(p-1)]$ is the sampling step between $\{0,1\}$ that assures an equal probability of the p samples. It is recommended to set an even value for p. The number of points in the input space to evaluate is $(k+1)$ because a based value $\boldsymbol{X}^*$is included, which is defined as the initial coordinate to generate all the trajectory points. Therefore, the EE is calculated by two consecutive sets of input variables whose relative

distance in the coordinate X_i is Δ.

From the calculated EE, two sensitivity indices can be obtained:

$$\mu_i^* = \frac{1}{r}\sum_{j=1}^{r}\left|E_i^j\right| \quad (28)$$

where r denotes the number of trajectories with a recommended value between $\{4,10\}$, μ_i^* is the mean of the absolute values that represents the influence of the variable on the output.

In order to improve the scanning of the input domain, the trajectories need to be spread in all the variable space Ω. In this sense, the design of trajectories can be done randomly, as follow:

$$B^* = \left(J_{k+1,1}X^* + (\Delta/2)\left[\left(2B - J_{k+1,k}\right)D^* + J_{k+1,k}\right]\right)P^* \quad (29)$$

where $\boldsymbol{X}^*$ is the base vector randomly selected, B is a lower triangular matrix of ones whose dimension is $(k+1)\times k$, $J_{k+1,k}$ is a $(k+1)\times k$ matrix of 1's, D^* is a k-dimensional diagonal matrix in which each element is either $+1$ or -1 with equal probability, P^* is a k-by-k random permutation matrix of zeros in which each row contains one element equal to 1, and no two columns have 1's in the same position. P^* gives the order in which factors are moved and P^* sets whether the factors will increase or decrease their value along the trajectory. Moreover, the scanning can be improved by maximizing the distance between the trajectories, which is calculated in this way:

$$d_{ml} = \sum_{i=1}^{k+1}\sum_{j=1}^{k+1}\sqrt{\sum_{z=1}^{k}\left[X_z^{(i)}(m) - X_z^{(j)}(l)\right]^2} \quad (30)$$

where d_{ml} is the sum of the geometrical distance between all the pairs of points of two different trajectories m and l.

III. Results and Discussion

In this section, several scenarios through two phases of simulation and experiments are considered to examine the performance of the presented Can-Am Spyder electric vehicle. In the simulation phase, the introduced MOCF is used to determine the right dimension of the powertrain components with the help of the two-step nested optimization. Since each element of the MOCF is influenced by a range of prices, a SA using the explained EE method is performed. Lastly, in the experiment phase, the HIL set-up is utilized to carry out an experimental test with the aim of examining the influence of a component price on a MOCF with an online EMS

A. Numerical simulation

In the numerical simulation stage, the introduced MOCF is first compared with two single-objective ones to realize their operational differences. Subsequently, the SA is performed. As mentioned earlier, the price of hydrogen, FC, and energy storage are the factors that can affect the system dimensions and operation strategy. In addition, these parameters vary depending on the retail, acquisition volume, and technology readiness level. Therefore, different existing prices in the literature are collected, as reported in Table II, to investigate the influence of the price range variation over the component sizing process [9, 40].

TABLE II COST RANGE OF THE POWERTRAIN COMPONENTS

Variable	Range
$\$FC_{Sys}$	40 \$/kW to 210 \$/kW
$\$H_2$	2 \$/kg to 15 \$/kg
$\$SC$	15 \$/Wh to 30 \$/Wh
$\$DC_{con}$	50 \$/kW to 150\$/kW

To perform the numerical simulation, the standard World Motorcycle Test Cycle (WMTC) and an on-road driving test are utilized, as shown in Fig. 3

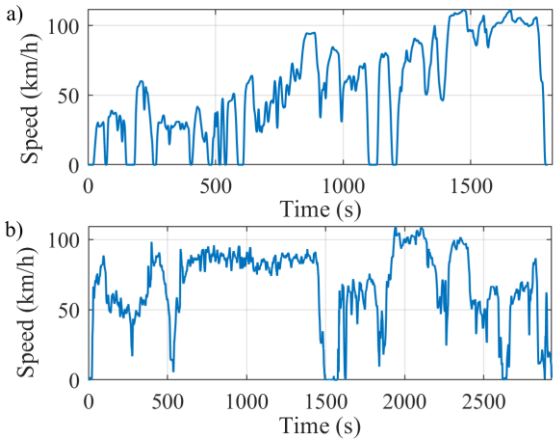

Fig. 3 Utilized driving profiles: (a) WMTC cycle, (b) on-road test.

WMTC represents daily motorcycle driving cycles in Europe, Japan, and the USA [41]. The real on-road driving test is about 49 minutes, reaching a top speed of 110 km/h. The vehicle operates mainly in the high-speed region in this driving profile. The average calculation time of the DP optimization step is 247 s for the WMTC profile, and for the on-road driving cycle is 342 s.

1) Cost function comparison

The utilized MOCF (22) in this study has four elements: FC degradation (23), hydrogen consumption (18), the operational cost of SC, and the operational cost of the DC-DC converter that are related to the (Δ_{trip}) trip time. The MOFC tries to reach a compromise among the objectives using a weighted sum approach [20]. Therefore, the price of each element defines the importance of each objective in terms of \$USD. In the first attempt, the MOCF is compared with two single-objective ones (hydrogen minimization: $H_{2,min} = \int W_{H_2}dt$ and FC degradation minimization: $FC_{deg,min} = \int \Delta_{FC}dt$), which represent the optimal limits of hydrogen and FC degradation minimization. In this regard, the extreme component prices, minimum and maximum from Table II, are considered for the MOCF. The maximum prices correspond to the actual component cost, and the minimum prices represent the objective values in the mid-term. In this way, the influence of the minimum and maximum prices over the size of the components will be appreciated. Regarding the single-objective cost functions, the inclusion of prices does not affect their performance as they pursue only one objective. Fig. 4 shows the optimization surfaces and pareto frontiers formed by different cost functions under WMTC driving cycle. This figure

This article has been accepted for publication in IEEE Transactions on Energy Conversion. This is the author's version which has not been fully edited and content may change prior to final publication. Citation information: DOI 10.1109/TEC.2023.3240723

represents trip cost (22) as the MOCF, and two single-objective: hydrogen consumption (18), and FC degradation (23). Fig. 4a shows the optimization surfaces of the MOCF with the extreme component prices, highest in orange at the top and lowest in blue at the bottom. The single points in each plot signify the GA population evaluated during the two-step optimization. Moreover, the surfaces show the pareto frontier with a continuous line, and the markers locate the best result coordinate in each case. The orange circle marker shows the minimum possible answer using the MOCF with the highest prices of the elements. The blue square marker presents the minimum result for the case of MOCF with the lowest prices for the elements. The single-objective functions were evaluated with the lowest component price and represented with a yellow hexagram marker for the best result obtained by the FC degradation minimization cost function, and the green diamond marker indicates the minimum result achieved by the hydrogen minimization cost function. From the next two subplots, Fig. 4b and Fig. 4c, it can be observed that although both MOCFs have different component prices, their pareto frontier converges to a pareto optimal point in the same optimal system size.

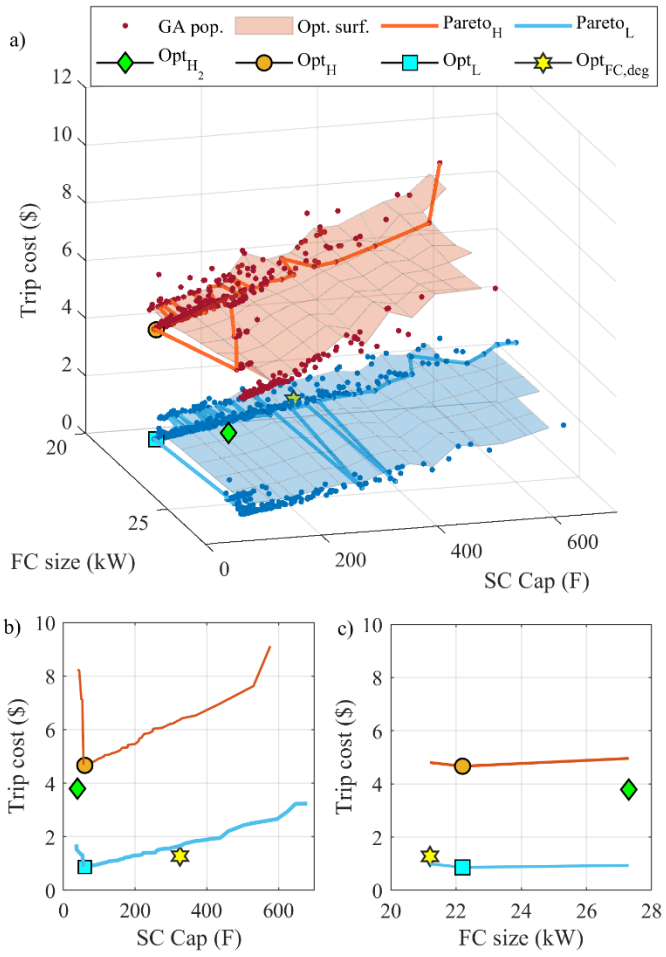

Fig. 4 Electric Spyder performance under WMTC driving cycle through two-step optimization method, a) multi-objective, b) Pareto frontier based on SC size and c) Pareto frontier based on FC size

This result shows that further analysis is required to comprehend the effect and interaction of price variation on the sizing and operational cost. Therefore, a more detail analysis of the MOCF is presented next in Fig. 5 where special attention is paid on the hydrogen consumption and FC degradation component.

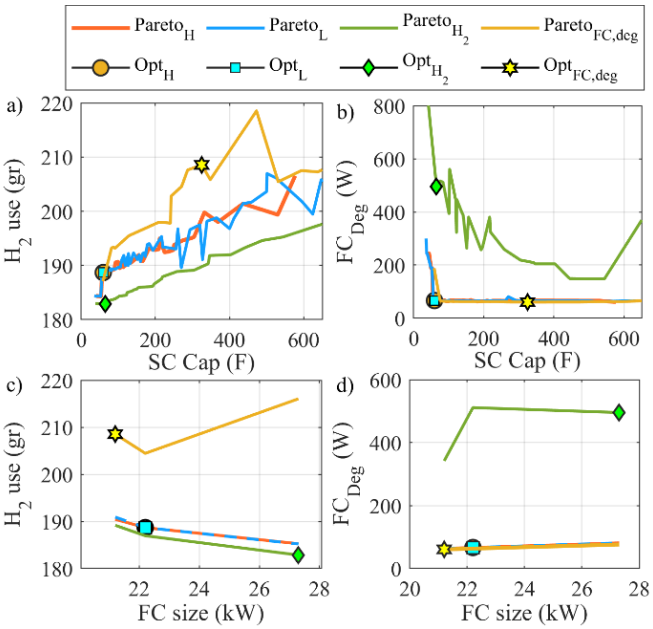

Fig. 5 Single-objective perspective of MOCF under WMTC driving cycle, a) hydrogen use vs SC size, b) FC deg. vs SC size, c) hydrogen use vs FC size and, d) FC deg vs FC size

The performance of the cost functions in terms of hydrogen consumption based on the SC and FC size are shown in Fig. 5a and Fig. 5c in terms of FC degradation and in terms of FC degradation in Fig. 5b and Fig. 5d. At first glance it is observed that the presented case is a nontrivial multi-objective optimization problem, where no single solution exists that simultaneously optimizes each single objective. This means that the components of the MOCF are in conflict, and none of them can be improved in value without declining some of the other objective values. From these plots, it can be observed that the single objective cost functions converge to the optimal solutions in their corresponded spaces while giving low-performance results in the other aspects. However, the optimal solutions obtained by the MOCF are near to the minimum results in both cases. To better interpret the performance of the explained cost functions in Fig. 4 and Fig. 5, the optimal results of each cost function are summarized in Table III. In addition, three MOCF with different components cost are included to highlight the influence of different set of weight in the cost function calculation. The extreme MOCF presents an increment of 3 % in terms of hydrogen consumption and 8% in terms of FC degradation, compared to the optimal results obtained by $H_{2,min}$ and $FC_{deg,min}$ cost functions, respectively. In addition, to reach a balance between both objectives, Table III shows that hydrogen minimization strategy will opt to use the highest FC size since the maximum efficiency power point will be higher, contrary to the FC degradation minimization that selects a smaller size to reduce the power decay caused by degradation. It should be noted that the FC degradation function has the biggest SC size because the bigger the filter the less the

This article has been accepted for publication in IEEE Transactions on Energy Conversion. This is the author's version which has not been fully edited and content may change prior to final publication. Citation information: DOI 10.1109/TEC.2023.3240723

degradation in the FC. At this point the obtained sizes and prices for the two price scenarios of MOCFs are similar. These results could mislead to conclude that the prices don't affect the system size, for this reason three weight sets with a minimum cost in one of the components is included in the Table III. When one of the components has a low cost, the system tends to operate as a single cost function, e.g., the MOCF with a low FC price has similar fuel performance as the $H_{2,min}$ function, which represents the optimal consumption. The MOCF is able to reach a balance although the weights are in the high or low extremes.

TABLE III COST FUNCTIONS COMPARISON UNDER WMTC DRIVING CYCLE

Cost function	H2 cons.	FC deg.	FC size	SC size (S-series and P-Parallel)
$H_{2,min}$	182.85 gr	496.8 W (0.0182 %)	27.3 kW	65.38 F (52S1P)
$FC_{deg,min}$	208.54 gr	61.5 W (0.0029 %)	21.2 kW	325 F (59S59P)
MOCF (lowest prices)	188.69 gr	66.6 W (0.003 %)	22.2 kW	59.6 F (49S9P)
MOCF (highest prices)	188.68 gr	66.6 W (0.003 %)	22.2 kW	59.6 F (49S9P)
MOCF (H2 cheap)	191.40 gr	63.6 W (0.003 %)	21.2 kW	122.7 F (48S19P)
MOCF (FC cheap)	185.16 gr	81.9 W (0.003 %)	27.3 kW	65 F (50S10P)
MOCF (SC cheap)	190.93 gr	63.6 W (0.003 %)	21.2 kW	103.3 F (16S48P)

From a wider perspective, a deeper analysis on the ratio of the FC and hydrogen price shows that the highest and lowest prices have similar weighting ratio. Under the low-cost conditions, the ratio of the hydrogen cost (2 $/kg) to FC cost (40 $/kW) is 1:20, while in the high-price conditions, the ratio of hydrogen cost (15 $/kg) to FC cost (210 $/kW) is 1:14. In case of the lowest prices scenario, the hydrogen cost is $0.377 and the FC degradation cost is $0.266, and in case of the highest cost scenario, the prices are $2.83 and $1.39, respectively. Based on the obtained trip cost, the ratio of the hydrogen to the FC degradation is 1.4:1 for the lowest price and 2:1 for the highest price. Under the tested driving cycle, it can be observed that although the FC has a higher ratio than the hydrogen, the hydrogen has a more considerable impact on the trip cost. Moreover, this analysis presents a very interesting perspective regarding the impact on the technology development and maturity where both technologies could reach similar trip cost influence at one instant.

Regarding the on-road driving cycle, sizing outcomes of two single-objective and three price sets (highest price, H2 cheap, and FC cheap) are analyzed and summarized in Table IV. The single objective functions set the baseline reference of the FC degradation and hydrogen consumption. The highest price shows the optimal dimension of the components for the highest reported prices in Table II. H2 cheap represents the optimal sizes using the highest prices for H_2, SC, and DC_{con}, and the lowest price for FC_{Sys}. FC cheap illustrates the optimal dimensions for the highest prices of FC_{Sys}, SC, and DC_{con}, and the lowest price of H_2. In fact, H2 cheap, and FC cheap cases simulate the situation in which one technology becomes cheaper faster than the others. From Table IV, when merely one weight is in the lowest extreme, the power distribution tends to exploit its corresponding resource more (consume more hydrogen or degrade more the FC). These outcomes show that a SA is required to check each component's price change effect on the sizing and operating cost of the whole system. Since the technology evolution might not be at the same rate for all the components, they will take different values.

TABLE IV MULTI-OBJECTIVE COST FUNCTIONS COMPARISON UNDER ON-ROAD DRIVING CYCLE

MOCF	H2 cons.	FC deg.	FC size	SC size (S-series and P-Parallel)
$H_{2,min}$	337.38 gr	513.2 W (0.0188 %)	27.3 kW	75.5 F (45S1P)
$FC_{deg,min}$	398.16 gr	62.28 W (0.0036 %)	17.3 kW	364 F (50S28P)
MOCF (highest prices)	348.69 gr	76.3 W (0.0036 %)	21.2 kW	85.8 F (53S14P)
MOCF (highest prices)	347.25 gr	76.3 W (0.0036 %)	21.2 kW	88 F (48S13P)
MOCF (H2 cheap)	347.56 gr	76.3 W (0.0036 %)	21.2 kW	94.8 F (48S14P)
MOCF (FC cheap)	343.71 gr	124.3 W (0.0056 %)	22.2 kW	63.5 F (46S9P)
MOCF (SC cheap)	347.56 gr	76.3 W (0.0036 %)	21.2 kW	94.7 F (48S14P)

2) Sensitivity analysis

To clarify the effect of the price variation on the component sizing, the results of the EEs SA under WMTC and road-test driving cycles are discussed in this section. Fig. 6 presents the rank of each parameter in the center of the sub-square. The rank is defined using the mean of the absolute EEs values of the component prices. In this regard, the system performance in terms of hydrogen consumption (W_{H_2}), FC system degradation (Δ_{FC}), FC size ($P_{FC,max}$), SC size (C_{SC}), System mass (m_{pow_sys}), and total trip cost ($\$Trip$) is considered. From Fig. 6, the hydrogen and FC prices are the most influential parameters that almost overwhelm all other factors in both cases. In other words, a slight variation of these two parameters will have a considerable effect on the outputs. From the presented results in Fig. 6a, hydrogen is the most important parameter, and FC is the second most important one in the case of fuel efficiency for the WMTC driving cycle. This follows the results presented in Table III, where a low price of hydrogen generates an increment of 5 % in the fuel consumption. Moreover, the EE shows that the hydrogen price has a strong influence at defining the sizes of FC and SC. This point is also well represented in Table III, where it is shown that a low price in the FC will push the algorithm to choose the biggest FC size. Fig. 6b represents the obtained results regarding the SA under the road-test driving cycle. From this figure, the influence of the FC system cost increased compared to the WMTC driving cycle. The long-time operation reduces the percentage of fuel difference between the extreme cost function shown in Table IV, this means there is a change of importance due to the high speed and duration of the profile. However, it is observed that in both cases the hydrogen cost is the most influential parameter in term of trip cost.

This article has been accepted for publication in IEEE Transactions on Energy Conversion. This is the author's version which has not been fully edited and content may change prior to final publication. Citation information: DOI 10.1109/TEC.2023.3240723

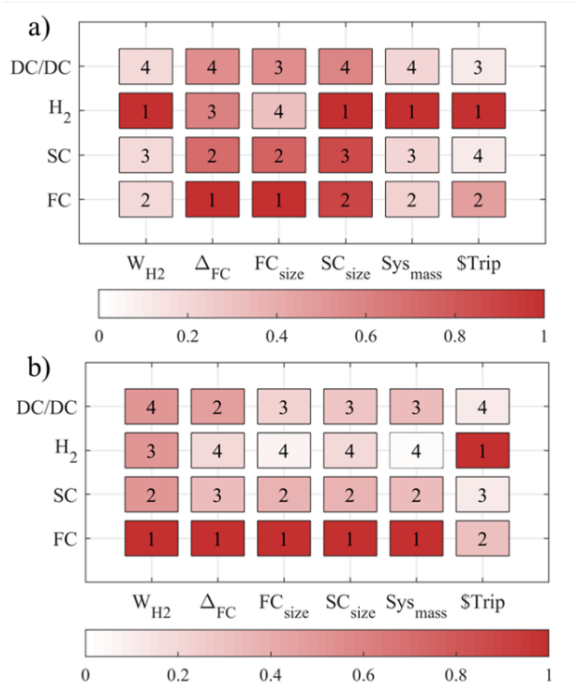

Fig. 6 Elementary effects of component price variation on system performance under (a) WMTC and (b) on-road driving cycle

B. Experimental test

Finally, the effect of component price variation is investigated using a HIL by comparing the performance of an EMS for three sets of weight and their corresponding optimal sizes obtained by the numerical simulation. The utilized EMS is based on online sequential quadratic programming (SQP) and the sizes are based on the reported values in Table IV. This test is deployed in a HIL setup, previously explained in Fig. 2. In this setup, the SC is a mathematical model, and the FC system is the real component. The FC output power in the HIL test bench is scaled up after the DC-DC converter to satisfy the demanded power. The EMS has been coded in LabVIEW environment and implemented in the real-time module of Compact-RIO by means of the block "Constrained Nonlinear Optimization virtual instrument VI". Hereinafter, the implemented strategy is explained first. Subsequently, the obtained results are widely discussed.

1) Real-time instantaneous optimization

The energy management problem in a FCHEV is in principle a nonlinear optimization problem. It can be solved by SQP, which has gained optimal/sub-optimal results for a wide range of engineering problems, such as EMSs [42]. SQP is an iterative technique that solves nonlinear optimization problems by a QP subproblem at a given estimated solution. The application of SQP to the proposed multi-objective EMS at each step is considered in the following form:

$$Min: \quad \$Trip_j = \$FC_{sys}\,\Delta_{FC,j} + \$H_2\,W_{H_2,j} \quad j = 0, 1, 2 \ldots \quad (31)$$

Subject to:

$$\begin{cases} 50\,\% \le SOC_{SC,j} \le 90\,\% \\ 0\,A \le i_{FC,j} \le 42\,A \\ -300\,A \le i_{SC,j} \le 300\,A \\ -0.1P_{FC,max} \le \Delta P_{FC,j} \le 0.1P_{FC,max} \end{cases} \quad (32)$$

The terms $\$SC\,\Delta_{trip,j}$ and $\$DC_{conv}\,\Delta_{trip,j}$, presented in the optimal optimization cost function in (22), are excluded for the online implementation. This is because they are the operational cost of SC and DC-DC converter and are calculated based on the driving profile time. If the vehicle is running, $\$SC\,\Delta_{trip,j}$ and $\$DC_{conv}\,\Delta_{trip,j}$ can be calculated and added to the total trip cost without participating in the optimization process. In the formulated problem, the optimization process is done for the defined MOCF (22).

2) Results

As presented in Table IV, the optimal sizes of components while using the MOCF with the highest price weights (FC_{Sys}: 210 $\frac{\$}{\text{kW}}$, H_2: 15 $\frac{\$}{\text{kg}}$, SC: 30 $\frac{\$}{\text{Wh}}$, DC_{con}: $\frac{150\$}{\text{kW}}$) are 21.2 kW for FC and 85.8 F for SC. In this section, these sizes are considered as the baseline. Then, using these baseline sizes, the online EMS based on SQP is employed to minimize the previously defined MOCF (31) for different cases:

1) "Highest price$_{baseline\ size}$": It uses the highest reported prices of the components in Table II with the baseline size, as shown in Table IV (FC: 21.2 kW, SC: 85.8 F).
2) "FC cheap$_{baseline\ size}$": It utilizes the highest prices for H_2, SC, and DC_{con}, and the lowest price for FC_{Sys} with the baseline sizes. This case study denotes an extreme price drop solely on the FC system.
3) "H2 cheap$_{baseline\ size}$": It employs the highest prices for FC_{Sys}, SC, and DC_{con}, and the lowest price for H_2 with the baseline sizes. In practice, this case study shows an extreme price drop down the hydrogen.
4) "FC cheap$_{optimal\ size}$": It uses the same prices as FC cheap$_{baseline\ size}$ but with the optimal sizes reported in Table IV (FC: 22.2 kW, SC: 63.5 F).
5) "H2 cheap$_{optimal\ size}$": It utilizes the same prices as H2 cheap$_{baseline\ size}$ but with the optimal sizes reported in Table IV (FC: 21.2 kW, SC: 94.8 F).

Fig. 7 shows a zoom on two time periods (from 1300 s to 1800 s and from 2300 s to 2800 s) of the drawn current from the FC system (i_{FC}) by the online EMS (Fig. 7a), the complete FC current profile (Fig. 7b), SOC variation of the SC (SOC_{SC}) (Fig. 7c), and the distribution of the i_{FC} (Fig. 7d) under Highest price$_{baseline\ size}$, FC cheap$_{baseline\ size}$, and H2 cheap$_{baseline\ size}$ cases.

This article has been accepted for publication in IEEE Transactions on Energy Conversion. This is the author's version which has not been fully edited and content may change prior to final publication. Citation information: DOI 10.1109/TEC.2023.3240723

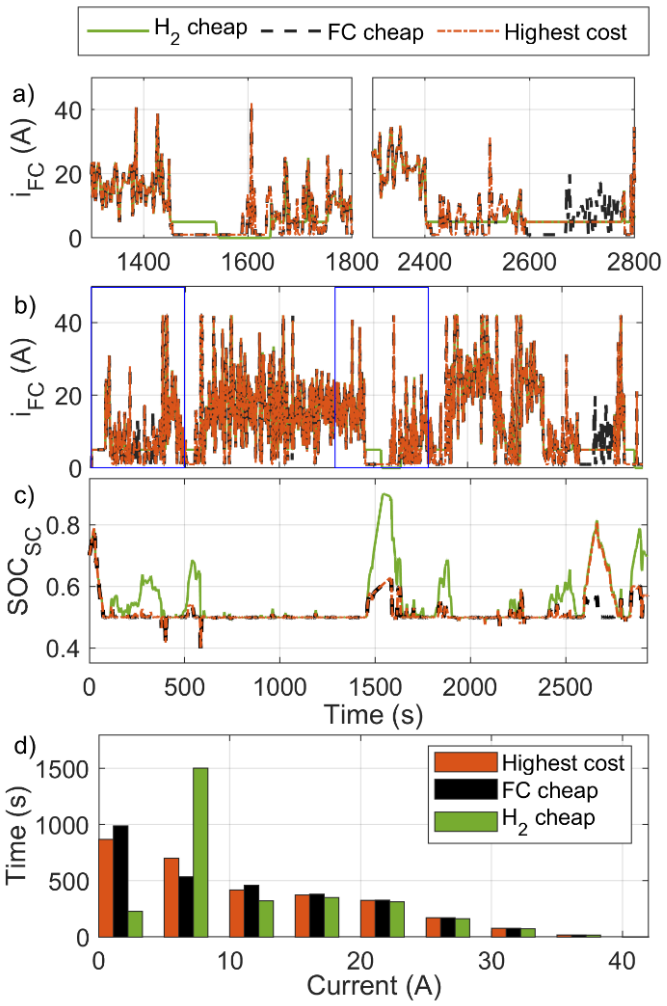

Fig. 7 HIL measurements during the on-road test, (a) a zoom on applied FC current from 1300 s to 1800 s range and 2300 s to 2800 s range, (b) the complete FC profile (c) SC SOC, (d) FC current distribution

As is seen in Fig. 7d, the H2 cheap$_{baseline\ size}$ case tends to avoid operating the FC in the low power region (k_1) most of the time. However, it has to turn off the FC at around 1544 s, as shown in Fig. 7a, since the SC has reached the maximum SOC level (90 %), as shown in Fig. 7c. FC cheap$_{baseline\ size}$ case leads to the minimum power operation, as is seen after 2570 s in Fig. 7a. Contrary to the mentioned cases, the highest price case balances the FC degradation and hydrogen consumption by sustaining the SC charge around 50 % and switching to the low degradation region when the requested power is below the minimum, as observed in Fig. 7a around 2570 s. In this condition, SC absorbs this extra energy. The FC degradation distribution of each case is presented in Fig. 8. This representation corroborates that H2 cheap$_{baseline\ size}$ case minimizes the degradation due to low power operation at the cost of doubling the on/off cycle degradation (k_2).

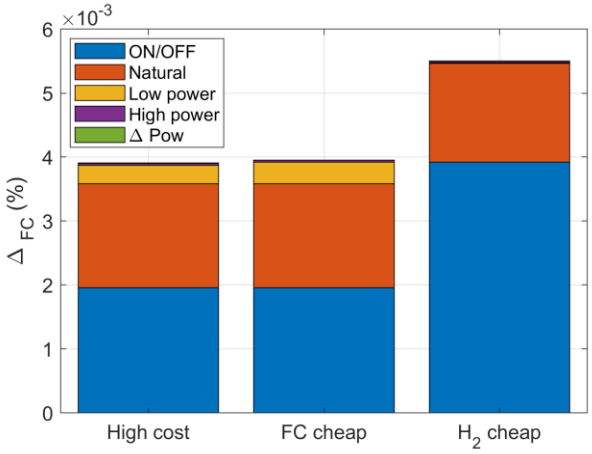

Fig. 8 FC degradation for each set of weights.

The system size, trip cost, total hydrogen consumption, and FC degradation of the five above-discussed cases are presented in Table V. The trip cost of each pair is comparable because they use the same component prices. From this table, the higher capacity of SC size in FC cheap$_{optimal\ size}$ has led to less hydrogen consumption than FC cheap$_{baseline\ size}$. Moreover, H2 cheap$_{optimal\ size}$ has resulted in a lower trip compared to H2 cheap$_{baseline\ size}$ while having the same percentage of degradation. In fact, the lower system capacity in the latter has led to lower trip cost. It should be noted that the experimental case uses a H-500 low-power FC from Horizon which has a different polarization curve compared to the FCvelocity-9SSL from Ballard Power Systems. However, the optimized sizes obtained in previous section are still relevant. In the FC cheap case, the FC operates as a power following with a higher power FC, and in hydrogen cheap case, the FC operates with a more constant trend due to the higher SC low-pass filter effect.

TABLE V MULTI-OBJECTIVE COST FUNCTIONS COMPARISON

Cost function weights	Trips cost	H2 cons.	FC deg.
Highest price$_{baseline\ size}$	$8.091	6.72 gr	0.0039 %
FC cheap$_{baseline\ size}$	$7.065	6.73 gr	0.0040 %
H2 cheap$_{baseline\ size}$	$5.008	6.63 gr	0.0055 %
FC cheap$_{optimal\ size}$	$6.668	6.65 gr	0.0040 %
H2 cheap$_{optimal\ size}$	$4.809	6.62 gr	0.0055 %

IV. CONCLUSIONS

This paper puts forward a SA to investigate the impact of price variation on the component sizing and energy management of a FCHEV. Since sizing and energy management problems have interdependencies, a two-step optimization method with a nested structure is utilized in this paper. The studied MOCF, composed of hydrogen cost, FC degradation cost, and operational costs of SC and DC-DC converter, is defined to optimize the trip cost. However, the performance of the MOCF relies on the defined weights that are based on the price range of the components. Therefore, this article puts forward a methodology for a SA to clarify the influence of the price range fluctuation over the sizing and total cost of the system. Therefore, this paper proposed a methodology to scrutinize the impact of component price

variation on the sizing and energy management of a FCHEV. The Morris or elementary effects (EE) method is used in this work due to its low computational within So, to analyze the results of this work, two phases of numerical simulation and experiments are considered. In the simulation phase, considering the use of the two-step optimization (GA for sizing and DP for power distribution) in the SA, it is realized that the FC and hydrogen prices are the dominant factors in sizing and the total price of the system. Hence, special attention needs to be paid to selecting those prices to avoid negative impacts on the sizing and EMS performance. It should be noted that the implemented methodology to study the SA and the two-step sizing optimization can be implemented in other engineering problems. In the experimental phase, the performance of an online EMS is investigated with the defined MOCF but with different price weights and sizes. To do so, a reduced-scale HIL set-up is used to deploy the strategy. The obtained results show that changing the price weights in a MOCF can result in more degradation and fuel consumption while using the same size. However, finding an optimal size for each price change on the MOCF can enhance the performance of the FCHEV up to 6 % in terms of the trip cost. This research demonstrates the impact of basic variation on FCHEV, which might help guide the automobile industry's future development and market strategy. Moreover, the presented sizing methodology could be implemented at early design phases to appropriately size the propulsion system of any electric vehicle as a function of actual or forecasted cost parameters. In future works, the developed SA methodology could be implemented to analyze the influence of external variables such as driving cycle average speed, maximum speed, ambient temperature, and FC temperature, on the fuel consumption and total trip cost. In addition, a more detailed study on the variation of the mass of the vehicle powertrain as well as different energy source combinations is required to provide an optimal power-source size map. Furthermore, future work could focus on increasing the FCHEV model accuracy in terms of hydrogen consumption and system degradation. Finally, the computing time could be reduced by implementing more recent optimization-based sizing methods.

VARIABLES

$\$DC_{conv}$	DC converter cost
$\$FC_{sys}$	FC system cost
$\$H_2$	Hydrogen cost
$\$SC$	SC cost
$\$Trip$	Trip cost
Δ_{FC}	FC degradation percentage
ΔP_{FC}	FC slew rate
Δ_{trip}	Normalized trip time
Ω_m	Rotor rotation speed
A_{aero}	Vehicle front area
B^*	Random trajectory
$C^*_{O_2}$	Oxygen concentration
$C_{SC,u}$	Single SC capacitance
C_{SC}	SC equivalent capacitance
C_d	Typical aerodynamic drag coefficient
D^*	k-dimensional diagonal matrix
E_{Nernst}	Reversible voltage
E_i	Elementary effect of the ith parameter
F_{env}	Vehicle traction force resistance
F_{tr}	Traction force
G_{gb}	Gearbox transmission ratio
H_{FC}	Heat transfer coefficient
M_{O_2}	Oxygen molar mass
N_{FC}	Number of cells
$N_{SC,p}$	SC parallel branches
$N_{SC,s}$	SC connected in series
P^*	k-by-k random permutation matrix
$P_{FC,bus}$	Effective FC power in the DC bus
$P_{FC,max}$	FC maximum power
$P_{FC,sys}$	Fuel cell system power
P_{FC}	Fuel cell power
P_{SC}	Supercapacitor power
P_{comp}	Compressor power
P_{fan}	Fan electric power
P_{req}	Requested power
Q_{heat}	Residual energy
Q_{conv}	Heat dissipated due to convection
Q_{max}	SC maximum capacity
R_D	Equivalent diode resistance
R_{SC}	SC equivalent resistor
$R_{internal}$	Internal PEMFC resistor
SOC_{SC}	SC level of charge
T_{FC}	PEMFC stack temperature
T_{amb}	Ambient temperature
$T_{em,r}$	Reference torque
T_{em}	Electric machine torque
V_{EV}	Vehicle velocity
W_{H_2}	Consumed hydrogen flow
X^*	Base vector randomly selected
X_i	Independent input parameters
d_{ml}	Geometrical distance between all pairs of points
$i_{FC,max}$	Maximum FC current
i_{SC}	SC current
k_i	Semi-empirical FC degradation coefficient
t_i	Operational time
u_{DC}	DC bus voltage
u_{FC}	Cell voltage of a proton exchange membrane
u_{SC}	Supercapacitor voltage
u_{act}	Activation loss
u_c	Capacitance element OCV
u_{con}	Concentration loss
u_{ohmic}	Ohmic loss
ζ_n	Semi-empirical PEMFC resistor parameters
η_{FC}	System efficiency
η_{comp}	Compressor efficiency
η_{gb}	Gearbox transmission efficiency
η_m	Torque and drive efficiency
μ_{fr}	Typical rolling resistance coefficient
μ_i^*	Influence of the variable on the output

ξ_n	Semi-empirical activation coefficients
ρ_{air}	Air density
B	Lower triangular matrix of ones
F	Faraday constant
g	Gravitational acceleration
m	Vehicle mass
r	Wheel radius
x	DP state variable
α	Semi-empirical diffusion mechanism parameter
β	Discrete braking mode value
γ	Specific heat ratio of the air
λ	Oxygen excess ratio constant

V. References

[1] F. Nadeem, S. M. S. Hussain, P. K. Tiwari, A. K. Goswami, and T. S. Ustun, "Comparative Review of Energy Storage Systems, Their Roles, and Impacts on Future Power Systems," *IEEE Access,* vol. 7, pp. 4555-4585, 2019.

[2] M. A. Hannan, M. M. Hoque, A. Mohamed, and A. Ayob, "Review of energy storage systems for electric vehicle applications: Issues and challenges," *Renewable and Sustainable Energy Reviews,* vol. 69, pp. 771-789, 2017.

[3] S. C. Konradt and H. Rottengruber, "Determination of the optimal battery capacity of a PEM fuel cell vehicle taking into account recuperation and supercapacitors," *Automotive and Engine Technology,* vol. 6, pp. 181-189, 2021/12/01 2021.

[4] M. N. Boukoberine, T. Donateo, and M. Benbouzid, "Optimized Energy Management Strategy for Hybrid Fuel Cell Powered Drones in Persistent Missions using Real Flight Test Data," *IEEE Transactions on Energy Conversion,* pp. 1-1, 2022.

[5] Y. Zhou, A. Ravey, and M.-C. Péra, "Real-time cost-minimization power-allocating strategy via model predictive control for fuel cell hybrid electric vehicles," *Energy Conversion and Management,* vol. 229, p. 113721, 2021/02/01/ 2021.

[6] Y. Liu, J. Li, Z. Chen, D. Qin, and Y. Zhang, "Research on a multi-objective hierarchical prediction energy management strategy for range extended fuel cell vehicles," *Journal of Power Sources,* vol. 429, pp. 55-66, 2019/07/31/ 2019.

[7] X. Hu, J. Jiang, B. Egardt, and D. Cao, "Advanced Power-Source Integration in Hybrid Electric Vehicles: Multicriteria Optimization Approach," *IEEE Transactions on Industrial Electronics,* vol. 62, pp. 7847-7858, 2015.

[8] T. Fletcher and K. Ebrahimi, "The Effect of Fuel Cell and Battery Size on Efficiency and Cell Lifetime for an L7e Fuel Cell Hybrid Vehicle," *Energies,* vol. 13, p. 5889, 2020.

[9] G. Morrison, J. Stevens, and F. Joseck, "Relative economic competitiveness of light-duty battery electric and fuel cell electric vehicles," *Transportation Research Part C: Emerging Technologies,* vol. 87, pp. 183-196, 2018/02/01/ 2018.

[10] A. Saltelli, K. Aleksankina, W. Becker, P. Fennell, F. Ferretti, N. Holst*, et al.*, "Why so many published sensitivity analyses are false: A systematic review of sensitivity analysis practices," *Environmental Modelling & Software,* vol. 114, pp. 29-39, 2019/04/01/ 2019.

[11] A. Saltelli, M. Ratto, T. Andres, F. Campolongo, J. Cariboni, D. Gatelli*, et al.*, *Global sensitivity analysis: the primer*: John Wiley & Sons, 2008.

[12] X. Wu, X. Hu, X. Yin, L. Li, Z. Zeng, and V. Pickert, "Convex programming energy management and components sizing of a plug-in fuel cell urban logistics vehicle," *Journal of Power Sources,* vol. 423, pp. 358-366, 2019/05/31/ 2019.

[13] Y. Wang, S. J. Moura, S. G. Advani, and A. K. Prasad, "Power management system for a fuel cell/battery hybrid vehicle incorporating fuel cell and battery degradation," *International Journal of Hydrogen Energy,* vol. 44, pp. 8479-8492, 2019/03/29/ 2019.

[14] P. G. Anselma and G. Belingardi, "Fuel cell electrified propulsion systems for long-haul heavy-duty trucks: present and future cost-oriented sizing," *Applied Energy,* vol. 321, p. 119354, 2022/09/01/ 2022.

[15] A. M. Bassam, A. B. Phillips, S. R. Turnock, and P. A. Wilson, "Development of a multi-scheme energy management strategy for a hybrid fuel cell driven passenger ship," *International Journal of Hydrogen Energy,* vol. 42, pp. 623-635, 2017/01/05/ 2017.

[16] J. M. Correa, F. A. Farret, V. A. Popov, and M. G. Simoes, "Sensitivity analysis of the modeling parameters used in Simulation of proton exchange membrane fuel cells," *IEEE Transactions on Energy Conversion,* vol. 20, pp. 211-218, 2005.

[17] E. Borgonovo and E. Plischke, "Sensitivity analysis: A review of recent advances," *European Journal of Operational Research,* vol. 248, pp. 869-887, 2016/02/01/ 2016.

[18] Y. Huang, H. Wang, A. Khajepour, B. Li, J. Ji, K. Zhao*, et al.*, "A review of power management strategies and component sizing methods for hybrid vehicles," *Renewable and Sustainable Energy Reviews,* vol. 96, pp. 132-144, 2018/11/01/ 2018.

[19] N. Leahey and J. Bauman, "A Fast Plant-Controller Optimization Process for Mild Hybrid Vehicles," *IEEE Transactions on Transportation Electrification,* vol. 5, pp. 444-455, 2019.

[20] A. Macias, M. Kandidayeni, L. Boulon, and J. P. Trovão, "Fuel cell-supercapacitor topologies benchmark for a three-wheel electric vehicle powertrain," *Energy,* vol. 224, p. 120234, 2021/06/01/ 2021.

[21] J. P. F. Trovão, M. Roux, M. É, and M. R. Dubois, "Energy- and Power-Split Management of Dual Energy Storage System for a Three-Wheel Electric Vehicle," *IEEE Transactions on Vehicular Technology,* vol. 66, pp. 5540-5550, 2017.

[22] A. Bouscayrol, J.-P. Hautier, and B. Lemaire-Semail, "Graphic Formalisms for the Control of Multi-Physical Energetic Systems: COG and EMR," in *Systemic Design Methodologies for Electrical Energy Systems*, I. a. Wiley, Ed., ed, 2012, pp. 89-124.

[23] G. Lopez Lopez, R. Schacht Rodriguez, V. M. Alvarado, J. F. Gomez-Aguilar, J. E. Mota, and C. Sandoval, "Hybrid PEMFC-supercapacitor system: Modeling and energy management in energetic macroscopic representation," *Applied Energy,* vol. 205, pp. 1478-1494, 2017.

[24] J. P. Trovao, M. R. Dubois, M. Roux, E. Menard, and A. Desrochers, "Battery and SuperCapacitor Hybridization for a Pure Electric Three-Wheel Roadster," in *2015 IEEE Vehicle Power and Propulsion Conference (VPPC)*, 2015, pp. 1-6.

[25] R. F. Mann, J. C. Amphlett, M. A. I. Hooper, H. M. Jensen, B. A. Peppley, and P. R. Roberge, "Development and application of a generalised steady-state electrochemical model for a PEM fuel cell," *Journal of Power Sources,* vol. 86, pp. 173-180, 2000/03/01/ 2000.

[26] M. Kandidayeni, H. Chaoui, L. Boulon, S. Kelouwani, and J. P. F. Trovão, "Online System Identification of a Fuel Cell Stack With Guaranteed Stability for Energy Management Applications," *IEEE Transactions on Energy Conversion,* vol. 36, pp. 2714-2723, 2021.

[27] C. Wang, H. He, Y. Zhang, and H. Mu, "A comparative study on the applicability of ultracapacitor models for electric vehicles under different temperatures," *Applied Energy,* vol. 196, pp. 268-278, 2017/06/15/ 2017.

[28] J. Wang, L. Zhang, J. Mao, J. Zhou, and D. Xu, "Fractional Order Equivalent Circuit Model and SOC Estimation of Supercapacitors for Use in HESS," *IEEE Access,* vol. 7, pp. 52565-52572, 2019.

[29] A. Biswas and A. Emadi, "Energy Management Systems for Electrified Powertrains: State-of-the-Art Review and Future Trends," *IEEE Transactions on Vehicular Technology,* vol. 68, pp. 6453-6467, 2019.

[30] K. Wang, N. Li, Y. Yang, S. Ke, Z. Zhang, M. Dou*, et al.*, "Effect of load-cycling amplitude on performance degradation for proton exchange membrane fuel cell," *Chinese Chemical Letters,* 2021/02/23/ 2021.

[31] S. Galla, A. Szewczyk, J. Smulko, and P. Przygocki, "Methods of Assessing Degradation of Supercapacitors by Using Various Measurement Techniques," *Applied Sciences,* vol. 9, 2019.

[32] M. Kandidayeni, J. P. Trovão, M. Soleymani, and L. Boulon, "Towards health-aware energy management strategies in fuel cell hybrid electric vehicles: A review," *International Journal of Hydrogen Energy,* vol. 47, pp. 10021-10043, 2022/02/26/ 2022.

[33] M. Yue, S. Jemei, R. Gouriveau, and N. Zerhouni, "Review on health-conscious energy management strategies for fuel cell hybrid electric vehicles: Degradation models and strategies," *International Journal of Hydrogen Energy,* vol. 44, pp. 6844-6861, 2019/02/18/ 2019.

[34] T. Fletcher, R. Thring, and M. Watkinson, "An Energy Management Strategy to concurrently optimise fuel consumption & PEM fuel cell lifetime in a hybrid vehicle," *International Journal of Hydrogen Energy,* vol. 41, pp. 21503-21515, 2016.

[35] H. Chen, P. Pei, and M. Song, "Lifetime prediction and the economic lifetime of Proton Exchange Membrane fuel cells," *Applied Energy,* vol. 142, pp. 154-163, 2015/03/15/ 2015.

[36] K. Song, H. Chen, P. Wen, T. Zhang, B. Zhang, and T. Zhang, "A comprehensive evaluation framework to evaluate energy management strategies of fuel cell electric vehicles," *Electrochimica Acta,* vol. 292, pp. 960-973, 2018/12/01/ 2018.

[37] U. S. D. o. Energy, "Fuel Cells," vol. Multi-Year Research, Development, and Demonstration Plan, 2017.

[38] W. Zhou, L. Yang, Y. Cai, and T. Ying, "Dynamic programming for new energy vehicles based on their work modes Part II: Fuel cell electric vehicles," *Journal of Power Sources,* vol. 407, pp. 92-104, 2018/12/15/ 2018.

[39] W. Zhou, L. Yang, Y. Cai, and T. Ying, "Dynamic programming for New Energy Vehicles based on their work modes part I: Electric Vehicles and Hybrid Electric Vehicles," *Journal of Power Sources,* vol. 406, pp. 151-166, 2018/12/01/ 2018.

[40] K. Reddi, A. Elgowainy, N. Rustagi, and E. Gupta, "Impact of hydrogen refueling configurations and market parameters on the refueling cost of hydrogen," *International Journal of Hydrogen Energy,* vol. 42, pp. 21855-21865, 2017/08/24/ 2017.

[41] E. G. Giakoumis, "Motorcycles," in *Driving and Engine Cycles*, E. G. Giakoumis, Ed., ed Cham: Springer International Publishing, 2017, pp. 167-191.

[42] N. Andrei, "Sequential Quadratic Programming (SQP)," in *Continuous Nonlinear Optimization for Engineering Applications in GAMS Technology*, N. Andrei, Ed., ed Cham: Springer International Publishing, 2017, pp. 269-288.

Alvaro Macias F. (Member, IEEE) was born in Mexico City, in 1992. He received the B.S. degree in Mechatronics engineering from Tec de Monterrey, Guadalajara, Mexico, in 2015, the M.S. degree in electrical engineering in 2018 and the Ph.D. degree in electrical engineering in 2023, from *Université du Québec à Trois-Rivières* (UQTR), QC, Canada. He is currently a Post-Doctoral Researcher with the Moduly company in collaboration with the Hydrogen Research Institute, UQTR. He has been actively involved in the research of energy management strategies for fuel cell systems, passive and active system configuration, energy storage systems and fuel cell modeling. His research interest includes energy-related topics, such as hybrid electric vehicles, fuel cell systems, energy management strategies, modeling, and control. Moreover, he has been a recipient of several awards/honors during his educational path, such as the Doctoral Scholarship from the *Fonds de recherche du Québec–Nature et technologies* (FRQNT), the scholarship for 3rd cycle from *Réseau Québécois sur l'Energie Intelligente* (RQEI) and the Post-Doctoral Scholarship from Mitacs with the Accelerate Entrepreneur program.

Mohsen Kandidayeni (Member, IEEE) was born in Tehran, Iran, in 1989. He received the B.S. degree in mechanical engineering in 2011, the master's degree (Hons.) in mechatronics from Arak University, Iran, in 2014, and the Ph.D. degree (Hons.) in electrical engineering from the University of Quebec at Trois-Rivières (UQTR), QC, Canada, in 2020. His educational journey has spanned through different paths. In 2016, he joined the Hydrogen Research Institute, UQTR. He is currently a Post-Doctoral Researcher with the electric-Transport, Energy Storage and Conversion Lab (e-TESC), *Université de Sherbrooke*, and a Research Assistant with the Hydrogen Research Institute, UQTR. He has been actively involved in conducting research through authoring, coauthoring, and reviewing several articles in different prestigious scientific journals and also participating in various international conferences. His research interest includes energy-related topics, such as hybrid electric vehicles, fuel cell systems, energy management, multiphysics systems, modeling, and control. Moreover, he has been a recipient of several awards/honors during his educational path, such as the Doctoral Scholarship from the *Fonds de recherche du Québec–Nature et technologies* (FRQNT), the Post-Doctoral Scholarship from FRQNT, the Excellence Student Grant from UQTR, and the Third Prize in Energy Research Challenge from the Quebec Ministry of Energy and Natural Resources.

Loïc Boulon (Senior Member, IEEE) received the master's degree in electrical and automatic control engineering from the University of Lille, France, in 2006, and the Ph.D. degree in electrical engineering from the University of Franche-Comté, France. Since 2010, he has been a Professor with UQTR, where he has been a Full Professor since 2016. Since 2019, he has been the Deputy Director of the Hydrogen Research Institute. His work deals with modeling, control, and energy management of multiphysics systems. He has published more than 120 scientific articles in peer-reviewed international journals and international conferences, and given over 35 invited conferences all over the word. His research interests include hybrid electric vehicles and energy and power sources, such as fuel cell systems, batteries, and ultracapacitors. In 2015, he was the General Chair of the IEEE-Vehicular Power and Propulsion Conference in Montréal, QC, Canada. He is also the VP of Motor Vehicles of the IEEE Vehicular Technology Society and the Founder of the International Summer School on Energetic Efficiency of Connected Vehicles and the IEEE VTS Motor Vehicle Challenge. He is also the holder of the Canada research chair position of energy sources for the vehicles of the future

João Pedro F. Trovão (Senior Member, IEEE) received the M.Sc. and Ph.D. degrees in electrical engineering from the University of Coimbra, Coimbra, Portugal, in 2004 and 2013, respectively. From 2000 to 2014, he was a Teaching Assistant and an Assistant Professor with the Polytechnic Institute of Coimbra—Coimbra Institute of Engineering (IPC—ISEC), Portugal. Since 2014, he has been a Professor with the Department of Electrical Engineering and Computer Engineering, University of Sherbrooke, Sherbrooke, QC, Canada, where he currently holds the Canadian research chair position in efficient electric vehicles with the Hybridized Energy Storage Systems. He is also the Founding Member and the Director of the electric-Transport, Energy Storage and Conversion (e-TESC) Lab, University of Sherbrooke. He is the author/coauthor of over 175 journal articles and conference papers. His research interests cover the areas of electric vehicles, hybridized energy storage systems, energy management, and rotating electrical machines. He was the General Chair of the 2018 IEEE Vehicle Power and Propulsion Conference, Chicago, IL, USA. He was a Guest Editor for the Special Issue of *IET Electrical Systems in Transportation* on energy storage and electric power sub-systems for advanced vehicles and the Special Issue of IEEE TRANSACTIONS ON VEHICULAR TECHNOLOGY on electric powertrains for future vehicles and on advanced vehicle power propulsion systems. He is also a Senior Editor of the automotive electronics topic of the *IEEE Vehicular Technology Magazine*.

Chapter 3 - Benchmark of hybrid fuel cell topologies for electric vehicles

3.1 Introduction

Based on the presented literature review in Chapter 1, the hybrid FC system with an energy storage system (ESS), such as battery or supercapacitor (SC), has been successfully implemented in automotive applications to overcome the fast load dynamics, store the regenerative energy, enhance the FC lifetime, and increase the fuel economy. However, in the literature it can be found that most of the works concentrate their efforts on just one electric configuration, sizing methods, or energy management strategies. In this respect, the presented two-step sizing method and multi-objective cost function from previous chapter are used to compare three FC-SC optimal hybrid energy system configurations, namely: full-active, semi-active and passive, for a recreational vehicle case study. Because a customized size is required for each of them to exploit their strengths and have a fair comparison. In addition to common concerns regarding the cost, hydrogen consumption and lifetime of the system, lightness and compactness are also necessary considerations in the design of this sort of vehicle.

The electric vehicle topologies benchmark process is explained by presenting an article entitled "Fuel cell-supercapacitor topologies benchmark for a three-wheel electric vehicle powertrain". The utilized methodology and the summary of the results are discussed first. Afterwards, the paper is presented.

It should be noted that an article entitled "Passive and Active Coupling Comparison of Fuel Cell and Supercapacitor for a Three-Wheel Electric Vehicle" is added in Appendix B.

This article presents a first attempt of evaluating the performances of passive and active configurations and has not been placed in this section to keep this chapter coherent and concise.

3.1 Article 2: Fuel cell-supercapacitor topologies benchmark for a three-wheel electric vehicle powertrain

Authors: Alvaro Macias, Mohsen Kandidayeni, Loïc Boulon, João P. Trovão

Journal: Energy, The International Journal, Elsevier

Publication date: 1 June 2021

DOI: https://doi.org/10.1016/j.energy.2021.120234

3.1.1 Methodology

This chapter first reviews the characteristics, advantages, and disadvantages of three FC-SC hybrid electric configurations: full-active, semi-active and passive. As a first stage, a SWOT analysis is performed, as shown in Figure 3.1, to recognize the most suitable configuration for the hybrid FC recreational vehicle. The SWOT analysis is commonly used to analyse and position an organization/system resources and environment in four regions: Strengths, Weaknesses, Opportunities and Threats [91]. From Figure 3.1, it is observed that the active configurations benefit from a better control of the power sources that result on a lower hydrogen consumption and degradation rate. On the other hand, the passive configuration presents the lower mass and energy conversion losses. In this respect, the presented chapter aims to evaluate the hybrid configurations to define the most advantageous solution for recreational vehicles in terms of system performance.

		Helpful	Harmful
Internal origin		Strengths	Weakness
	Full-active	• Complete system control • Lowest fuel consumption	• Complicated control system • Highest capital cost
	Semi-active	• Good system management • No unnecessary on-off cycles	• Heavy and voluminous systems • Higher fuel consumption
		• Low-pass filter operation	• The ESS will degrade faster
	Passive	• Low mass and volume requirements	• No control over current distribution
External origin		Opportunities	Threats
	Full-active	• Stable DC bus voltage level	• Converter deals with high current peaks
	Semi-active	• Large variety of EMS • Coupling small component size with converter	• The possible fault of the system caused by the converter
		• High industrial acceptance	• The DC bus voltage range will shrink while the ESS degrades
	Passive	• Low electric losses conversion	• The initial voltage of the ESS should be in the range

Figure 3.1 SWOT analysis of hybrid configurations

By identifying these factors, it is possible to recognize its core benefits for a decision-making, planning and building strategies. Then, a case study simulator is developed, in which an experimental based model for each component of the Can-Am Spyder electric vehicle are used. Subsequently, the optimal size of each topology is determined by the two-step optimization approach, as shown in the flowchart in Figure 3.2. This approach is based on the optimized sizing of power sources, employing a metaheuristic optimization algorithm, and an optimal EMS. In this work, the standard World Motorcycle Test Cycle (WMTC) is utilized for the optimal sizing procedure. This decision resides in the variety of traffic conditions that compound WMTC profile; urban traffic, slow country-road, and fast country-roads of daily motorcycle driving behavior from Europe, Japan, and the USA [92]. Finally, the best-achieved size of each architecture is compared in terms of capital cost, system

weight, and trip cost. The trip cost is composed of hydrogen consumption, FC degradation and an equivalent usage cost for the SC and converter.

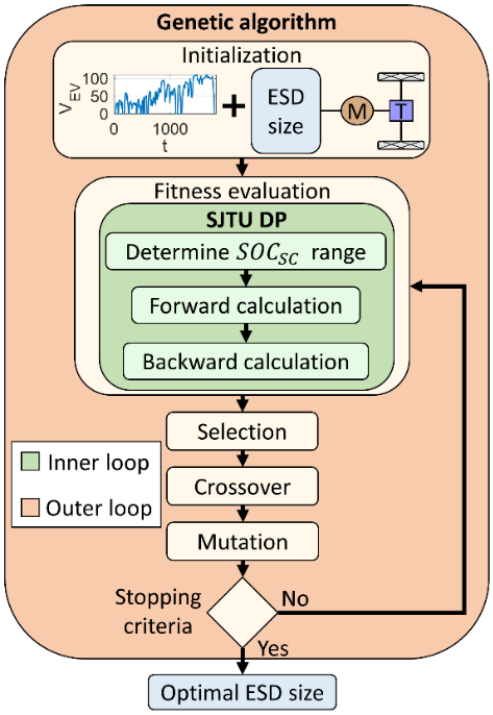

Figure 3.2 The framework of the two-step optimization for sizing and EMS

3.1.2 Outcomes

The numerical studies have been tested via MATLAB. The calculation time depends on the utilized PC hardware (Processor = Core i5, 2.30 GHz, RAM = 8.00 GB). The results of the optimization process are summarized in Table 3-1, where the FC and SC size, mass and cost are reported. The system mass and volume are approximate based on the datasheets, and the capital cost is based on the target values proposed by the US Department of Energy (DoE).

Table 3-1 Obtained results by the two-step optimization method

Configuration	$C_{SC,u}$	$R_{SC,u}$	Q_{max}	$N_{SC,s}$	$N_{SC,p}$	$P_{FC,max}$	System mass	Capital cost
Full-active	310 F	2.2 mΩ	202 Wh	43	15	22.2 kW	77.9 kg	$ 6424
Semi-active	310 F	2.2 mΩ	230 Wh	49	15	22.2 kW	72.3 kg	$ 5598
Passive	450 F	2.8 mΩ	241 Wh	59	9	27.3 kW	59.3 kg	$ 4721

It can be observed that the full-active configuration is the one with the smallest capacitance value, followed by the semi-active. And the passive configuration is the one with the biggest FC size and higher SC capacity. On the other hand, passive configuration, which does not use any DC-DC converters, benefits from a light mass and low volume. In addition, the reported capital cost of the system is lower in the passive configuration compare against the other architectures. The detailed trip cost of the best fitness function for WMTC profile and a real driving cycle are presented in Figure 3.3. Since the results of component sizing have a strong dependency on the selected driving cycle, they are evaluated with a real driving profile. It is observed that the passive configuration has achieved the lowest value in terms of trip cost compared to other configurations for. This superior performance of the passive configuration is achieved mainly due to not using a DC-DC converter. This reduces the cost and energy losses and generates a lower hydrogen consumption. However, full-active, and semi-active operate the FC in a way to minimize its degradation.

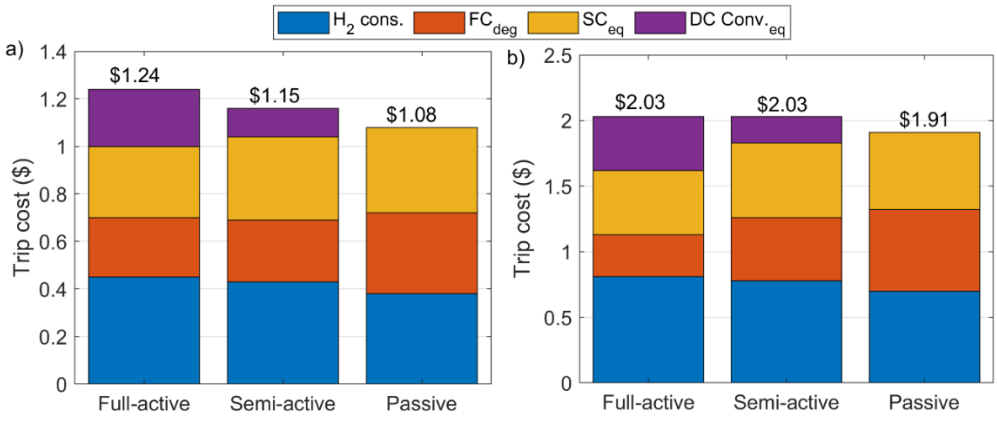

Figure 3.3 Breakdown of the trip cost, a) WMTC, b) real driving profile

Energy 224 (2021) 120234

Contents lists available at ScienceDirect

Energy

journal homepage: www.elsevier.com/locate/energy

Fuel cell-supercapacitor topologies benchmark for a three-wheel electric vehicle powertrain

A. Macias [a, b, d, *], M. Kandidayeni [a, b, d], L. Boulon [a, b], J.P. Trovão [c, d]

[a] Université Du Québec à Trois-Rivières, Trois-Rivières, QC, Canada
[b] Institut de Recherche sur L'Hydrogène, UQTR, Trois-Rivières, QC, Canada
[c] Université de Sherbrooke, Sherbrooke, QC, Canada
[d] e-TESC Laboratory, University of Sherbrooke, Sherbrooke, QC, Canada

ARTICLE INFO

Article history:
Received 13 July 2020
Received in revised form
4 January 2021
Accepted 24 February 2021
Available online 27 February 2021

Keywords:
Components sizing
Energy management
Passive configuration
PEMFC
Two-step optimization
Ultracapacitor

ABSTRACT

This paper compares three optimal hybrid energy system configurations, namely full-active, semi-active and passive, for the particular purpose of assessing the viability of utilizing the passive architecture in a three-wheel electric vehicle composed of a fuel cell (FC) and a supercapacitor. In this respect, the characteristics of these configurations are investigated through three steps. Firstly, the mathematical model of each component is developed by employing experimental data. Subsequently, the optimal size of each topology is determined by a two-step optimization approach. This approach is based on the optimized sizing of power sources, employing a metaheuristic optimization algorithm, and optimal power flow sharing between the sources with the aim of satisfying the requested power while declining the fuel consumption and enhancing the system's lifetime. Finally, the best-achieved size of each architecture is compared in terms of trip cost, capital cost, and the system weight. The obtained results show that passive topology can reduce the trip cost by 14.8% and 6.4% compared to full-active and semi-active ones, respectively. However, the active architecture results in less degradation in the FC compared to the other two topologies. Furthermore, a validation phase is done under a real driving profile and the results are further discussed.

1. Introduction

The transportation sector is one of the main contributors to the emission of greenhouse gases owing to its dependency on fossil fuels [1,2]. However, green vehicles and fuels are creating the necessary bases to decarbonize this sector while enhancing utilities to consumers and the broader economy [3]. The cleaner solutions are based on the electrification of the powertrain through mild/full/plug-in hybrid electric vehicle (HEV), battery electric vehicle (BEV), and fuel cell electric vehicle (FCEV) technologies [4]. Among these solutions, FCEV is one of the most promising due to zero-local emissions, long driving range, and fast refueling [5]. In the short term, fuel cell (FC) technology will be expensive due to the high capital cost of the refilling stations, tanks, and FC systems [6]. However, the FC cost is expected to become competitive with the internal combustion engine (ICE) by 2025, according to the performed study in Ref. [7]. One of the weaknesses of the FC systems is nonetheless their sensitivity to the abrupt load fluctuations which are common in vehicular application [8]. These rapid changes, which can be due to vehicle acceleration, lead to a marked decline in oxygen concentration and consequently a sharp power drop in the FC system [9,10]. Consequently, they are unfavorable for the lifetime of the FC stack as they cause a reduction in the mass activity and an increment on the internal electrical resistance [11,12]. To address these concerns, the hybridization of the FC system with an energy storage system (ESS), such as battery or supercapacitor (SC) has been broadly practiced [13]. This hybridization not only resolves the discussed issues, but also offers the ability to capture regenerative braking energy (since FC stack cannot absorb the energy), increase fuel economy, and deliver a more flexible operating strategy. Various architectures for hybridizing a FC system have been developed in the literature. These architectures fit into two categories of active and passive [14]. Active configuration is denoted by the association of the power source to the DC bus through a DC-DC converter. It is divided into two groups of semi-active, where

* Corresponding author. Université du Québec à Trois-Rivières, Trois-Rivières, QC, Canada.
E-mail address: alvaro.omar.macias.fernandez@uqtr.ca (A. Macias).

https://doi.org/10.1016/j.energy.2021.120234
0360-5442/

only one of the sources is interfaced by a converter, and full-active, where each of the sources has their own converters. Active topology is a common choice in the literature as it has the flexibility to actively control the power split between the FC stack and the ESS and enhance the lifetime of the system. This topology has been applied more in high-duty applications, such as tramway, hybrid bus, ships, and excavators [15–18]. In these applications, the voltage at the DC bus should be stable and within a specific range as the motor drive and the auxiliary systems are usually coupled directly to the DC bus. In the semi-active category, the FC is normally connected to the DC bus via a DC/DC converter while the ESS is directly connected there. This configuration is extensively used because the passive component absorbs the surplus energy in the bus, which facilitates the power split control over the FC. Its main application is in light-duty vehicles, such as Toyota Mirai, Honda Clarity, among others [19]. Regarding the passive configuration, all the components are directly connected to the DC bus in a parallel manner. Compared to the previous topologies, it benefits from a structure with fewer components and simpler implementation.

Concerning the power split, in active topologies they are typically performed through the formulation of an energy management strategy (EMS) [20,21]. In this respect, some works tend to operate the FC in a maximum efficiency region in order to improve the system performance and efficiency [22–24]. While an active configuration offers a well-defined power split among the sources, some studies have proposed the employment of passive architectures since they can decline the complexity, cost, and weight of the vehicle [25,26]. Passive topology is highly straightforward and has a self-management due to the characteristics (different impedance) of the sources. In other words, it does not require an EMS to perform the power distribution between the sources [27]. However, this can lead to the presence of high power ripples at the FC side and consequently increase the degradation rate of the stack.

In [28], a comparison of active and passive hybrid topologies for a FC-battery vehicle indicates that as long as the requested power does not contain high fluctuations, the passive topology has a superior performance. However, as the requested power starts having high-pulses, the FC stack operation is shifted to the low-efficiency regions. The active and passive topology selection between a SC and a battery pack, as the complementary power source in a FC hybrid electric vehicle (FCHEV), has been studied in Ref. [29]. This study shows that the use of an active topology with a battery results in noticeable power changes in the FC stack compared to the passive configuration of FC and SC. The use of a SC as the ESS stems from the fact that the passive coupling of a FC stack with a SC bank is more prevalent than a battery pack since the SC characteristics are more suitable for coping with the intermittency of behavior in a FCHEV with such a configuration. The passive topology with SC makes the drawn power from the FC smoother and leads to a higher energetic efficiency and longer lifetime of the FC. In addition, SC benefits from a high power density, high efficiency (in high voltage region), fast charge, wide operating temperature range, and excellent recyclability [30]. Regarding the FC-SC active configurations, several EMSs are proposed for distributing the power between the FC stack and the SC bank. The common concerns in all these works, using the full-active topology, are to compensate for the slow dynamic of the FC stack, minimize the hydrogen consumption, and increase the efficiency while taking care of the lifetime of the vehicle [31–33]. In Refs. [34,35], two state machine controls based on equivalent consumption minimization for FC-SC full-active configuration are implemented to power up a tramway. Both methods identify the optimum FC operating range, and the optimization of the power distribution based on different situations at each timestep. In Ref. [36], a semi-active FC-SC topology is utilized in which the SC is directly connected to the DC bus and the FC is interfaced with a unidirectional converter. The SC supplies and passively absorbs the peak power, and the FC is regulated by an EMS based on game theory, which considers the controller and the future driving condition to reduce hydrogen consumption and avoid unnecessary on-off cycles. In Refs. [37,38], the principal objective is the passive hybridization of a SC to a single FC. The attained experimental outcomes show that the passive topology avoids negative voltage, has self-protection in sudden power fluctuations, and improves the energetic performance as patented by NISSAN company [39]. In Ref. [40], a 9.5-kW proton exchange membrane FC (PEMFC) is connected to a SC bank by a passive architecture. This configuration has decreased the dynamic load, idling time, and rapid load changes in the FC without using a DC-DC converter.

Based on the previously discussed articles, a SWOT analysis is performed to recognize the most suitable configuration for a hybrid FC recreational vehicle. In this respect, the internal origin factors are the ones that are part of the architecture, and the external origin factors are the ones that cannot be directly controlled. This decision-making tool, shown in Fig. 1, is represented in a matrix of four quadrants; Strengths, Weakness, Opportunities, and Threats. The strengths are the characteristics that pin out each configuration, the weaknesses are the inherent disadvantages, the opportunities are the elements in the environment that can give value to the configuration, and the threats are external circumstances that can cause problems for implementing a configuration [41].

After taking into consideration the previous literature study, the first hypothesis regarding the recreational vehicle case study of this work is that passive configuration is a suitable candidate solution. It stems from the fact that recreational vehicles are limited in terms of mass and volume. Moreover, these vehicles present more erratic and aggressive speed profiles. Under such a basis, a passive configuration is a more compact power supply system with the self-coordination of each component. The second hypothesis is that the configurations with an active coupling will have a longer operational time, because they avoid operating in high degradation conditions. The third hypothesis is the use of SC as an ESS. This is due to its resilience and high-power density. In this sense, the SC operates as a low-pass filter that leaves the main components of the requested power to the FC system to supply. In this respect, this work aims to investigate the applicability of hybrid passive FC configuration for a recreational vehicle.

In view of the reviewed papers, some efforts have already been made concerning the use of active and passive FC-SC topologies in vehicular applications. However, so far, these configurations have not been benchmarked comprehensively. Most studies utilize the same size of FC-SC for active and passive configurations while a customized size is required for each of them to exploit their strengths and have a fair comparison. In addition to common concerns regarding the cost, hydrogen consumption, lifetime of the system, lightness, and compactness are also necessary considerations in the design of this sort of vehicle. In order to bridge the mentioned gaps and validate the hypothesis, this article presents a benchmark study of three FC-SC hybrid energy system configurations, namely full-active, semi-active, and passive. The main objective of this article is to comprehensively weigh up the pros and cons of each customized configuration, in terms of hydrogen consumption, FC degradation, and system weight. In order to reach a fair comparison, an optimal EMS based on dynamic programming (DP) is used because the sizing and the power split methods are intrinsically related to the performance and cost of the power supply system. The rest of this paper is organized as follows. In section 2, the modeling of the vehicle powertrain along with the SC and FC is presented using some semi-empirical equations. Section 3 deals with the component sizing by using genetic algorithm (GA)

		Helpful	Harmful
Internal origin		Strengths	Weakness
	Full-active	• Complete system control • Lowest fuel consumption	• Complicated control system • Highest capital cost
	Semi-active	• Good system management • No unnecessary on-off cycles	• Heavy and voluminous systems • Higher fuel consumption
		• Low-pass filter operation	• The ESS will degrade faster
	Passive	• Low mass and volume requirements	• No control over current distribution
External origin		Opportunities	Threats
	Full-active	• Stable DC bus voltage level	• Converter deals with high current peaks
	Semi-active	• Large variety of EMS • Coupling small component size with converter	• The possible fault of the system caused by the converter
		• High industrial acceptance	• The DC bus voltage range will shrink while the ESS degrades
	Passive	• Low electric losses conversion	• The initial voltage of the ESS should be in the range

Fig. 1. SWOT analysis of hybrid configurations.

while applying DP to do the power split for the active topologies. Section 4 represents a rigorous comparison of the developed topologies under a standard and a real on-road driving profile. Finally, the conclusion is given in section 5.

2. Hybrid electric vehicle modeling

The investigated vehicle in this manuscript (e-TESC-3W platform) is a three-wheel pure electric vehicle specifically employed for recreational purposes, presented in Fig. 2(a). These types of vehicles are normally exposed to high dynamics and need to be light and compact. Given these characteristics, the sizing of the components becomes a critical stage that directly influences the performance, cost, and dimensions of the vehicle. The performed study in Ref. [42] shows that a FCHEV can have a similar weight to the commercially available motorcycles which are propelled by an ICE. Moreover, its tank-to-wheel consumed energy is less than an ICE.

The studied e-TESC-3W platform comprises a permanent magnet synchronous motor (28 kW and 96 V) directly connected to the rear wheel and utilized as an experimental test rig in e-TESC laboratory at the University of Sherbrooke [43–45]. The motor speed is regulated with a three-phase power inverter that converts the direct current in the bus to alternate current. The main characteristics of this vehicle are summarized in Table 1 and explained thoroughly in Ref. [44].

The focus of this work is to compare the performance of this platform for active, semi-active, and passive topologies of FC-SC. Hereinafter, the modeling process of active and passive configurations are discussed with the help of energetic macroscopic representation (EMR). EMR is a graphical formalism of complex multiphysics systems that shows the energetic properties of the elements and their interactions [46]. In addition, a control loop can be easily deduced based on an inversion of the system model.

2.1. Traction system

The traction system of this vehicle is represented using a static model (efficiency map lookup table) of the electric machine and power electronics. This model is composed of different forces and Newton's second law of motion. Fig. 2(b) shows the EMR of the traction system, in which the driving cycle is the reference variable of the control loop, and the torque of the electric motor is the control action [43]. The power source devices are represented as source elements, in which the requested current of the traction system is the input and the voltage on the DC bus is the output. The vehicle modeling is represented by the following equations (1)–(8):where F_{tr} is the traction force, F_{env} is the vehicle traction force resistance, m_{eq} is the vehicle mass, G_{gb} is the gearbox transmission ratio, r is the wheel radius, T_{em} is the electric machine torque, η_{gb} is the gearbox transmission efficiency, ρ_{air} is the air density (1.2 kg/m^3), β is a discrete value that takes the value of -1 when the vehicle is in braking mode otherwise it is 1, and Ω_m is the rotor rotation speed. It is assumed that the reference torque $T_{em,r}$ is the same as the measured one. Where the employs coefficient, rolling resistance μ_{fr} and aerodynamic drag C_d, are typical values. The vehicle's mathematical model has been validated with an on-road driving test carried out in the e-TESC laboratory [45], which is considered adequate for the benchmark analysis purpose of this paper.

Therefore, the necessary current of the electric motor to achieve the reference torque $T_{em,r}$ is then calculated by:

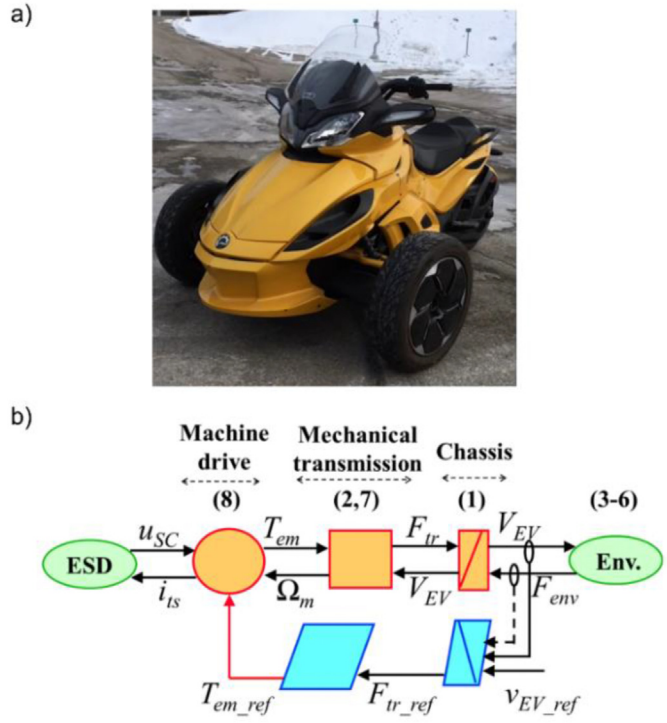

Fig. 2. e-TESC 3W electric vehicle platform, a) picture and, b) the traction system model.

$$\frac{dV_{EV}}{dt} = \frac{(F_{tr} - F_{env})}{m_{eq}} \tag{1}$$

$$F_{tr} = \left(G_{gb} \,/\, r\right) T_{em} \eta_{gb}^{\beta} \tag{2}$$

$$F_{env} = F_{roll} + F_{grade} + F_{air} \tag{3}$$

$$F_{roll} = m_{eq} g \mu_{fr} \cos\theta \tag{4}$$

$$F_{air} = 0.5 \rho_{air} A_{aero} C_d {V_{EV}}^2 \tag{5}$$

$$F_{grade} = m_{eq} g \sin\theta \tag{6}$$

$$\Omega_m = \left(G_{gb} \,/\, r\right) V_{EV} \tag{7}$$

Table 1
Vehicle specifications.

Variable	Symbol	Value	Units
Vehicle mass (w/o power source)	m_{eq}	350	kg
Typical rolling resistance coefficient	μ_{fr}	0.02	–
Typical aerodynamic drag coefficient	C_d	0.75	–
Vehicle front area	A_{aero}	1.25	m2
Wheel radius	r	0.305	m
Belt transmission drive ratio	G_{gb}	5.033 (30:151)	–
Belt transmission drive efficiency	η_{gb}	95	%
Maximum vehicle speed	$V_{EV,max}$	140	km/h-1
Operating motor driver voltage	u_{DC}	80–120	V

$$i_{ts} = \left(T_{em} \Omega_m \eta_m^{\beta}\right) / u_{DC} \tag{8}$$

where u_{DC} is the voltage on the DC bus, and η_m is the drive efficiency that considers the inverter and motor efficiency. This voltage corresponds to the voltage of the SC in the passive and semi-active configurations. In the full-active configuration, it corresponds to the nominal voltage of the motor, which is the interconnection of the two DC-DC converters.

2.2. Fuel cell system

The FC system is represented by an electrochemical based PEMFC model proposed by Amphlett et al. studied in several works [47,48]. This model represents the performance of the FC by a function that includes the reversible potential, which is the maximum possible voltage of the FC, and the irreversible voltage losses. Moreover, this data-driven model has a low computational cost and a good interpolation an extrapolation approximation [49]. The selected FC system for this work is the FCvelocity-9SSL from Ballard Power Systems, whose size varies from 3.8 kW to 27.3 kW [50]. The PEMFC voltage (u_{FC}) is approximated by the following equations 9–13:

$$u_{FC} = N_{FC}(E_{Nernst} + u_{act} + u_{ohmic} + u_{con}) \tag{9}$$

$$E_{Nernst} = 1.229 - 0.85 \times 10^{-3}(T_{FC} - 298.15) + 4.3085 \times 10^{-5} T_{FC}[\ln(p_{H2}) + 0.5\ln(p_{O2})] \tag{10}$$

$$\begin{cases} u_{act} = \xi_1 + \xi_2 T_{FC} + \xi_3 T_{FC} ln(CO_2) + \xi_4 T_{FC} ln(i_{FC}) \\ C_{O_2}^{*} = \dfrac{P_{O2}}{5.08 \times 10^6 \exp(-498/T_{FC})} \end{cases} \tag{11}$$

$$u_{ohmic} = -i_{FC} R_{internal} = -i_{FC}(\zeta_1 + \zeta_2 T_{FC} + \zeta_3 i_{FC}) \tag{12}$$

$$u_{con} = \alpha ln(1 - i_{FC} \,/\, i_{FC,max}) \tag{13}$$

where N_{FC} is the number of cells, E_{Nernst} is the reversible voltage, u_{act} is the activation loss, u_{ohmic} is the ohmic loss, u_{con} is the concentration loss, T_{FC} is the stack temperature, p_{H2} is the hydrogen partial pressure, p_{O2} is the oxygen partial pressure, ξ_n (n = 1 … 4) is the empirical coefficients, $C_{O_2}^{*}$ is the oxygen concentration, i_{FC} is the FC operating current, $R_{internal}$ is the internal resistor defined by the three parametric coefficients ζ_n (n = 1 … 3), α is a semi-empirical parameter related to the diffusion mechanism ($0.3 \leq \alpha \leq 1.8$), and $i_{FC,max}$ is the maximum current. The Amphlett voltage model is compared with the single cell voltage values reported in the Ballard datasheet, shown in Fig. 3(a). The polarization curve represents the FC voltage output for a given current load.

The oxygen partial pressure is approximated as 21% of the cathode pressure since it is the percentage of oxygen in the air flowing to the cathode. Regarding the hydrogen partial pressure, it is approximated as 99% of the anode pressure. The cathode pressure is calculated by (14) in terms of current since the airflow mainly depends on the current. This equation has been introduced in Ref. [51], as fitted to experimental data under different current levels, and the anode inlet pressure p_{an} has been maintained at 0.2 bar above the cathode pressure p_{ca}. This is to reduce the nitrogen crossover, enhance the cell stability, and evacuate the hydrogen in form of water through the cathode in case of an internal leak.

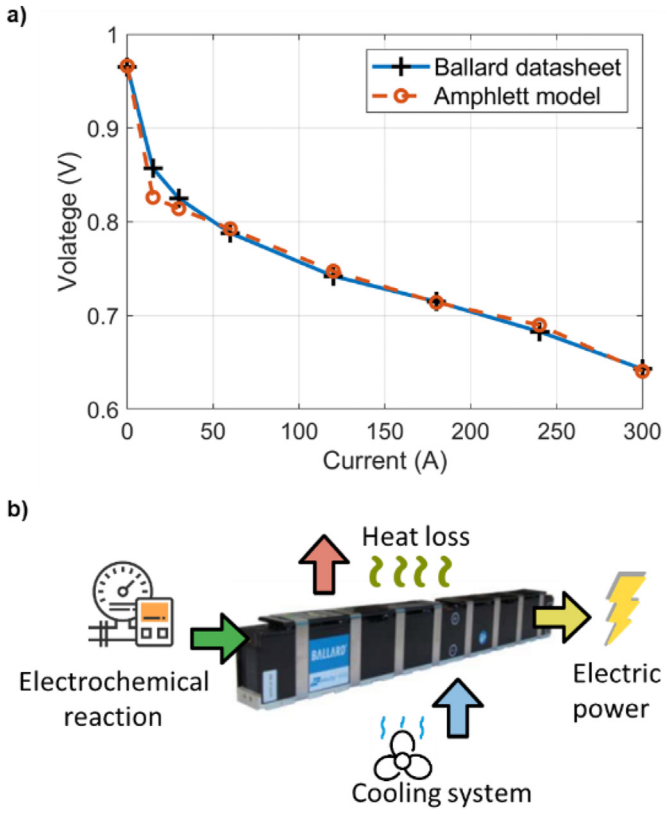

Fig. 3. Studied FC stack from Ballard Power Systems, a) FC voltage model comparison for a single cell, b) energy balance representation.

$$p_{ca} = a_1 + a_2 i_{FC} + a_3 {i_{FC}}^2 + a_4 {i_{FC}}^3 \tag{14}$$

The thermal behavior of the FC is described by using the law of conservation of energy, as shown in the Fig. 3(b). The energy balance for describing the temperature dynamic of the FC system is explained in Ref. [52], by considering only the heat dissipated by the liquid cooling system.

$$Q_{heat} = N_{FC} i_{FC} (1.254 - u_{FC}) \tag{15}$$

$$Q_{conv} = H_{FC} (T_{FC} - T_{amb}) \tag{16}$$

$$\frac{dT_{FC}}{dt} = \frac{Q_{heat} - Q_{conv}}{MC_{FC}} \tag{17}$$

where the generated heat in the FC Q_{heat} is the residual energy of the ideal potential minus the real potential, H_{FC} is the heat transfer coefficient under free convection defined experimentally in Ref. [53], the heat transfer coefficient is calculated by k_{t1} and k_{t2} which are empirical coefficients obtained experimentally in Ref. [52], T_{amb} is the ambient temperature, T_{FC} is the stack temperature, Q_{conv} is the heat dissipated due to convection, and MC_{FC} is the thermal capacity of the FC. After considering all the losses from the auxiliary systems, the power of the FC system is calculated as follow:

$$P_{FC,aux} = P_{comp} + P_{fan} \tag{18}$$

$$P_{comp} = \frac{1}{\eta_{comp}} W_{air} c_p T_{amb} \left(\frac{p_{ca}}{p_{amb}}^{\gamma - 1/\gamma} - 1 \right) \tag{19}$$

$$P_{FC} = u_{FC} i_{FC} \tag{20}$$

$$W_{air} = \lambda W_{O_2} / x_{O_2} \tag{21}$$

$$W_{O_2} = M_{O_2} N_{FC} i_{FC} / 2F \tag{22}$$

$$P_{FC,sys} = P_{FC} - P_{FC,aux} \tag{23a}$$

where $P_{FC,aux}$ is composed of the cooling system losses which are the fan power (P_{fan}) that is considered constant (200W) and the power of the compressor P_{comp}. The efficiency of the compressor η_{comp} is estimated as 70% [54], W_{air} represents the rate of the consumed air, c_p is the specific heat capacity of air (1005 J/kg), p_{amb} is the ambient pressure, γ is the specific heat ratio of the air (1.4), λ is the oxygen excess ratio constant (2), W_{O_2} is the rate of oxygen consumed through the cathode, x_{O_2} is the ideal oxygen mass fraction in the air (23.3%), M_{O_2} is the oxygen molar mass (32 gr/mol), and F is the Faraday constant. Finally, the $P_{FC,sys}$ is the power of the FC system after the auxiliary losses.

The efficiency of the system is calculated considering the consumed energy by the liquid and air-cooling system.

$$\eta_{FC} = (i_{FC,sys} u_{FC}) \,/\, (W_{H_2} \times HHV) \tag{23b}$$

$$W_{H_2} = 0.00696 i_{FC} N_{FC} \tag{24}$$

where HHV is the hydrogen high heating value [55], and W_{H_2} is the hydrogen flow consumed in terms of the current across the FC.

2.3. Supercapacitor and DC-DC converter

The SC is represented by an equivalent circuit model that corresponds to the electrical Faradic reaction that occurred in the electrode surface. In Ref. [56], a comparative study of five equivalent circuit models is performed under different operational temperatures. Based on the reported error and ease of implementation, a classical RC model has been selected. The electrical behavior is calculated as follow:

$$u_{SC}(t) = u_c(0) + \frac{1}{C_{SC}} \int i_{SC} dt - i_{SC} R_{SC} \tag{25}$$

where $u_c(0)$ is the initial open-circuit voltage (OCV) of the capacitance element, i_{SC} is the current across the SC, C_{SC} is the equivalent capacitance value of the SC, and R_{SC} is the equivalent resistor value of the SC. The utilized SC of this work is based on Maxwell Technologies, and the equivalent capacitance and resistor for each model are provided in the manufacturer datasheet [57]. The validation of this equivalent circuit model has already been done in previous papers [58].

The remaining energy in the SC is estimated by the formula of Coulomb counting [59].

$$SOC_{SC}(t) = SOC_{SC}(0) + \int \frac{i_{SC}\, dt}{Q_{max}} \tag{26}$$

where $SOC_{SC}(0)$ represents the initial level of charge, and Q_{max} is the maximum available capacity.

For the active coupling, a DC-DC converter is required to boost

the voltage level of the FC or the SC. This is a common technique used in commercial vehicles, such as Toyota Mirai [60]. In the developed simulator, the DC-DC converter is considered as an efficiency ratio, which is multiplied by the power of the active device [61]. In the case of the FC system, its effective power in the DC bus is calculated as follow:

$$P_{FC,bus} = P_{FC,sys} * DC_{eff} \tag{27a}$$

3. Problem definition and two-level optimization

In the literature, different types of FC hybrid architectures are proposed based on the selected application [62]. The hybrid configurations studied in this work are full-active, semi-active, and passive, as shown in Fig. 4. Fig. 4(a) represents the full-active configuration. In this structure, the FC and SC are connected to the DC bus via a DC-DC converter. This configuration benefits from a flexible power control between the FC and SC, and a more stable voltage level in the DC bus. However, to provide the demanded power, complicated and strict control techniques are required. Fig. 4(b) is the semi-active configuration, in which the FC is connected through a DC-DC converter to the DC bus and the SC is directly connected. In this configuration, the SC voltage represents the DC bus voltage, so the EMS must regulate the level of charge of the SC. The last structure, passive configuration, is shown in Fig. 4(c). In this topology, FC and SC are directly connected to the DC bus. To avoid reverse current inside the FC, a diode is placed in series with it. This configuration does not require an EMS, and the power splitting depends on the natural behavior of each component. Most of the performed studies on this structure have concentrated on the sizing method because it is the principal factor that influences the performance of the system. The FC current is always positive and is defined as follows:

$$i_{FC} = \frac{u_{FC} - u_{SC}}{R_D} \tag{27b}$$

where R_D is the equivalent diode resistance. It can be implied from the passive structure that the voltage of the FC tends to have the same level as the SC voltage, and the requested current is equal to the sum of FC and SC currents.

In the case of full-active and semi-active configurations, a two-step optimization method is used to define the best system size and power split [63,64]. The simultaneous optimization-based energy management and component sizing methods have been successfully implemented in previous works [65,66]. This is a plant/controller iterative optimization that consists of two nested optimization loops. The first step optimizes the cost function by searching the plant variables that are the set of parameters for the system size. The second step is in charge of the optimization of the controller design for each proposed plant [67]. As shown in Fig. 5, the first step is a metaheuristic method used to define the FC and SC

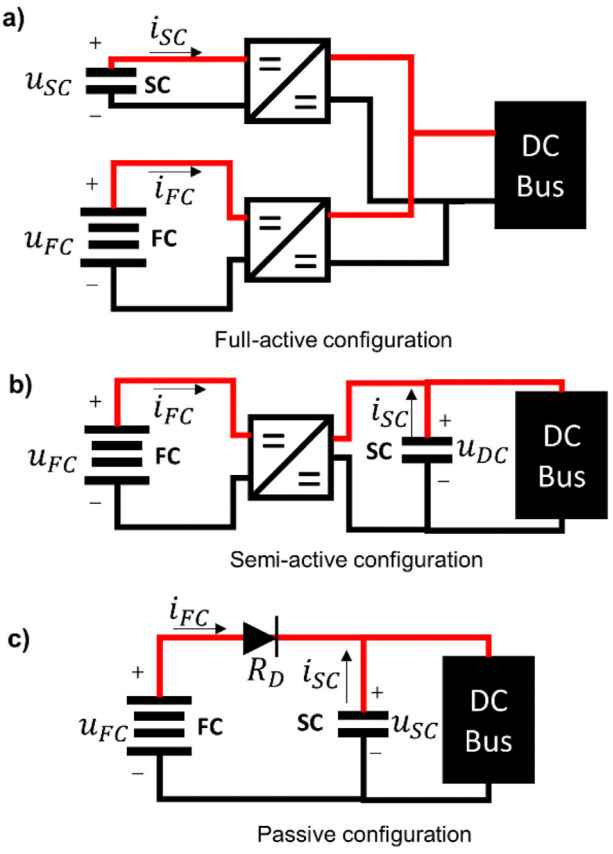

Fig. 4. Studied configurations, a) full-active, b) semi-active, and c) passive.

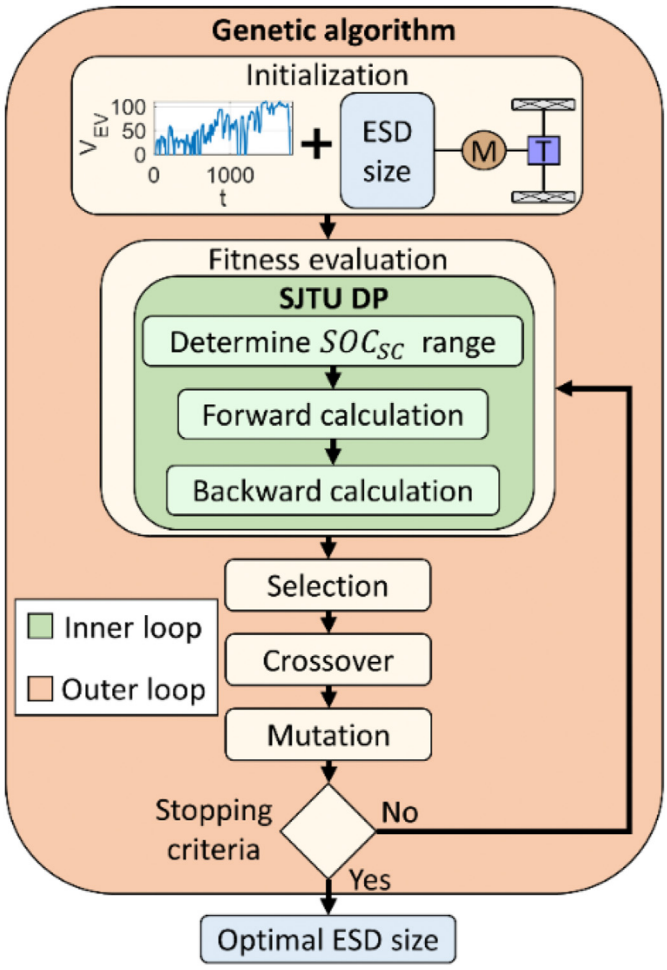

Fig. 5. The framework of the two-step optimization for sizing and EMS.

Table 2
System cost breakdown.

Component	Cost	Variable	Ref.
FC system	40 $\$/kW_{net}$	$\$FC_{sys}$	[74]
SC	15 \$/Wh	$\$SC$	[75]
DC-DC converter	50 $\$/kW$	$\$DC_{conv}$	[76]
Hydrogen	2.3 $\$/kgH_2$	$\$H_2$	[77]

Table 3
Coefficients of FC performance degradation.

Variable	Coefficient
k_1	0.00126 (%/h)
k_2	0.00196 (%/cycle)
k_3	5.93×10^{-5} (%/cycle)
k_4	0.00147 (%/h)
k_5	0.002 (%/h)

sizes. The second step is an inner loop, where DP splits the power between the components while minimizing a cost function. In the passive configuration, only the metaheuristic method is applied since there is no control over the sources.

3.1. System cost and durability

Although cost is a major obstacle for the commercialization of fuel-cell vehicles, most of the existing EMSs have only focused on the minimization of the hydrogen consumption [68,69]. Only a few papers have tried to maximize the overall FC system efficiency while extending its lifetime and avoiding harmful FC conditions [65,70–72]. In this respect, in this work, a multi-objective optimization problem is utilized to minimize hydrogen consumption as well as the system degradation. This problem is solved by using a weighted-sum approach, in which the importance of each objective is defined by a cost factor [73]. In the market, the price of the components varies based on the number of units to buy and manufacturer. For this reason, the standard price proposed by the US Department of Energy (DoE) is used in this work and summarized in Table 2.

The trip cost is in terms of USD and is composed of the consumed hydrogen and a fraction of the system cost. The FC cost is linked to the system degradation, which is considered as the percentage of reduction in the maximum power. The US DoE has defined the FC end of life (EOL) as a 10% drop in the maximum power, and an operational objective of 5000 h [74]. However, the SC and DC-DC converter in normal conditions have an expected lifetime in terms of thousands of cycles [78]. To increase the importance of the SC and DC-DC converter in the optimization process, their costs are linked to the trip time. The proposed trip cost used in the optimization process is calculated as follow:

Table 4
Optimization parameters and constrains of DP method.

Parameter	Min	Max
i_{FC}	0 A	300 A
i_{SC}	−300 A	300 A
SOC_{SC}	50%	90%
u_{DC}	80 V	120 V
$\Delta P_{FC,min}$	$-0.1P_{FC,max}$	$0.1P_{FC,max}$

Table 5
The range of the targeted parameters for optimization.

Variable	Bounded range
N_{FC}	[55,71,75,80,90,110,115,135]
$C_{SC,u}$	[100,150,310,325,350,360,450,650,1200,1500,2000,3000,3400]
$N_{SC,s}$	$\in Z \geq 1, \leq 60$
$N_{SC,p}$	$\in Z \geq 1, \leq 60$

$$\$Trip = \$FC_{sys}\Delta_{FC} + \$H_2 \int W_{H_2} \mathrm{dt} + \$SC\Delta_{trip} + \$DC_{conv}\Delta_{trip} \tag{28}$$

where Δ_{FC} represents the percentage of degradation in the FC system along the trip, the total consumed hydrogen is calculated by the integration of the hydrogen flow (W_{H_2}), and Δ_{trip} is the trip time divided by the operational objective of 5000 h.

The major causes of degradation in a FC system are the high and low power, the start-stop cycles, the fast-dynamic loads, and the natural decay [79]. Table 3 summarizes the empirical coefficients of FC performance degradation in terms of percentage [80].

The percentage of FC degradation is calculated as the sum of FC degradation under each condition.

$$\Delta_{FC} = k_1 t_1 + k_2 n_1 + k_3 n_2 + k_4 t_2 + k_5 t_{FC_{ON}} \tag{29}$$

where k_1 is the low power coefficient (less than 5% of maximum power), k_2 represents one start-stop coefficient, k_3 is the fast-dynamics coefficient (absolute value of power variations larger than 10% of maximum power), k_4 is the high power coefficient (more than 90% of maximum power), k_5 is the natural decay rate (the time that FC is under operation), t_i $(1, 2, FC_{ON})$ are the operational time in their corresponding conditions. In addition, system constrains are implemented to guarantee that the system works within the defined operating conditions.

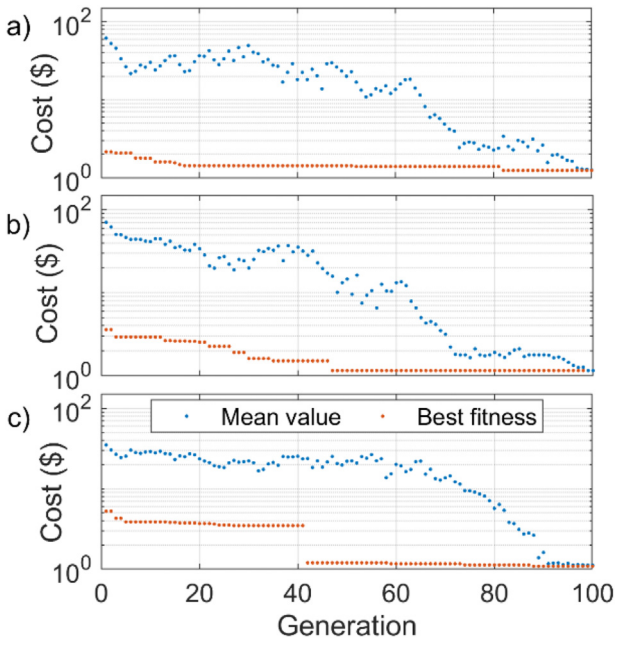

Fig. 6. Fitness function minimization trend for: a) full-active, b) semi-active, and c) passive configurations.

Table 6
Obtained results by the two-step optimization method.

Configuration	$C_{SC,u}$	$R_{SC,u}$	Q_{max}	$N_{SC,s}$	$N_{SC,p}$	$P_{FC,max}$	System mass	Capital cost
Full-active	310 F	2.2 mΩ	202 Wh	43	15	22.2 kW	77.9 kg	$ 6424.00
Semi-active	310 F	2.2 mΩ	230 Wh	49	15	22.2 kW	72.3 kg	$ 5598.00
Passive	450 F	2.8 mΩ	241 Wh	59	9	27.3 kW	59.3 kg	$ 4721.00

3.2. Dynamic programming

The new unified DP model and its solution method (SJTU DP), proposed in Refs. [81,82], is implemented in this work to do the energy management of the full-active and semi-active configurations. This method solves the main four problems of DP, namely the dimension disaster, standardization, Markov problem, and interpolation leakage. The main characteristics of this method are the state-space model with four state variables, the multi-objective cost function formulation, the dimension reduction calculation method, and the forward-backward calculation sequence. Compared with Basic DP and Level-Set DP, the utilized method shows less computational time and better calculation accuracy.

The unified state-space equation of DP model for full-active and semi-active configurations is represented by four states.

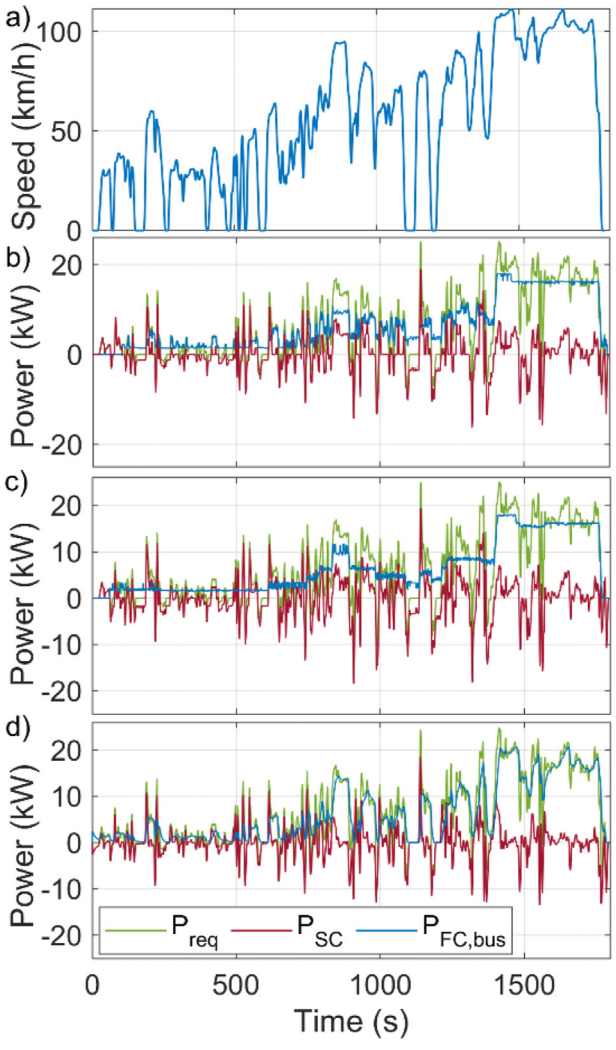

Fig. 7. Power split of WMTC profile by the two-step optimization method, a) utilized WMTC driving cycle, b) full-active, c) semi-active, d) passive configuration.

$$\begin{cases} SOC_{SC}(k+1) = SOC_{SC}(k) + \int \dfrac{i_{SC}(k)\,dk}{Q_{max}} \\ u_{SC}(k+1) = u_c(k) + \dfrac{1}{C_{SC}} \int i_{SC}(k)dk - i_{SC}(k)R_{SC} \\ P_{FC,s}(k+1) = u_{FC}(k)^{*} i_{FC}(k) \\ M(k+1) = \psi(P_{FC,s}, FC_s, k) \end{cases} \tag{30}$$

where the state variable vector is $x = [SOC_{SC}, u_{SC}, P_{FC,s}, M]$, $P_{FC,s}$ represents the power of the FC as a state variable while i_{FC} is the current of the FC as a control variable. In addition, an operational work mode M is included in the states to reduce the extra calculation that will end in infeasible conditions. This work mode is defined by the function $\psi(P_{FC,s}, FC_s, k)$ that creates a relationship between the work mode, the control variable, and the FC state FC_s. The work mode can take four discrete values: SC mode (SCM), Start mode (SM), Normal work mode (NWM), Shutdown mode (SDM). The SCM is defined as the stage when the FC is off and all the requested power is supplied by the SC. SM represents the turning on the procedure of the FC until the FC reaches the minimum idle current level ($i_{FC,idle}$). During the NWM, the requested power is supplied by both FC and SC, which are active, and OM is the turn-off procedure of the FC. The system can change from one mode to another by respecting a fixed order (SCM-SM-NWM-SDM-SCM). That means the FC cannot switch-off while it is starting up. By doing so, the number of unnecessary turn-on cycles is reduced.

In order to assure that the system operates in the desired conditions, some limitations need to be satisfied. They are represented by the following constraints.

$$\begin{cases} SOC_{SC,min} \le SOC_{SC} \le SOC_{SC,max} \\ i_{FC,min} \le i_{FC} \le i_{FC,max} \\ i_{SC,min} \le i_{SC} \le i_{SC,max} \\ u_{DC,min} \le u_{DC} \le u_{DC,max} \\ \Delta P_{FC,min} \le \Delta P_{FC} \le \Delta P_{FC,max} \end{cases} \tag{31}$$

where the SOC_{SC} range is selected based on typical values found in the literature, the current limits are established by the manufacturer, the u_{DC} range is determined based on the motor driver operating voltage, and the ΔP_{FC} is the slew rate of the FC power and can be calculated by:

$$\Delta P_{FC} = P_{FC}(k) - P_{FC,s}(k) \tag{32}$$

The main objective of DP is to minimize the trip cost specified in (28) by finding the right FC current while respecting the constraints in (31). The trip cost equation is a function that only depends on the

Table 7
Breakdown of the trip cost for WMTC profile.

Configuration	H_2 cons.	FC deg.	SC cost	Conv. cost	$Trip
Full-active	$ 0.45	$ 0.25	$ 0.30	$ 0.24	$ 1.24
Semi-active	$ 0.43	$ 0.26	$ 0.35	$ 0.12	$ 1.15
Passive	$ 0.38	$ 0.34	$ 0.36	–	$ 1.08

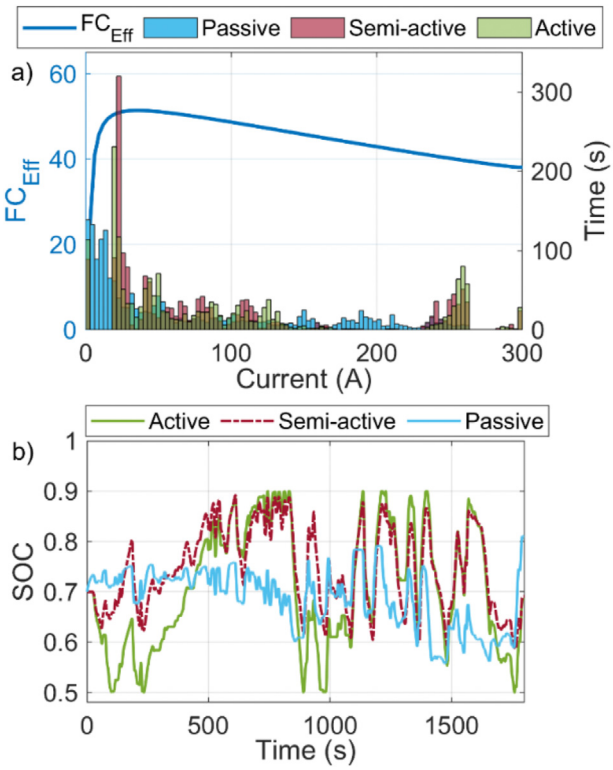

Fig. 8. WMTC test results; a) Current distribution comparison and FC efficiency curve, and b) SOC evolution of the three FC-SC configurations.

current state and the control variable at that step k_{th}. This proves that the DP model fulfills the requirement of the Markov characteristics of DP. The SJTU DP solution method consists mainly in three steps: first, calculating the boundary range of the state variable with the maximum and minimum power for each k_{th} step. Secondly, a forward calculation to determine the minimum cost of each grid point while respecting the constraints. Lastly, defining the optimal control sequence backward.

Table 4 summarizes the constraints utilized in this work in order to warranty that the proposed plants will meet the system requirements. Moreover, these parameters have been selected to reduce the degradation, and maximize the performance of the power sources [83–87].

3.3. Metaheuristic sizing

The optimization of the sizing process in hybrid systems implies non-monotonic effects on objectives and constraints to be reached, while it tries not to get trapped in local optimums [88]. As shown in Fig. 5, GA is implemented to define the optimal size of the power sources in a way to minimize the trip cost. GA is a derivative-free metaheuristic method capable of solving the non-linear constrained optimization problem of the energy system component design. GA is inspired by the process of natural selection described in Darwin's theory of evolution. This optimization technique operates by encoding potential solutions as simple chromosome-like data structures and then applies genetic operators to those structures, such as mutation, crossover, and survival of the fittest. Over many iterations, its population of chromosomes evolves toward better solutions. The algorithm typically terminates when the diversity of its population reaches a predetermined minimum, or a maximum number of iterations [89].

The parameters to be optimized by GA in this work are defined as $x = [N_{FC}, C_{SC,u}, N_{SC,s}, N_{SC,p}]$ where x is the optimized vector, N_{FC} represents the number of cells of the FC stack, $C_{SC,u}$ is the capacitance of a single SC, $N_{SC,s}$ indicates the number of SC connected in series, and $N_{SC,p}$ specifies the number of parallel series banks of SC. The number of generations is set to 100, the population size is 150, the elite count is 10, and the crossover fraction is 0.8. These settings cause GA to use a larger population, to expect the best solution to be close in the initial random population, and to keep searching in the design space until its best member fitness changes by a small amount.

The targeted parameters for optimization by GA are defined as discrete values based on the commercial capacitance of Maxwell SC and the size of the Ballard FC [50,57]. Table 5 summarizes the optimization space of the plant.

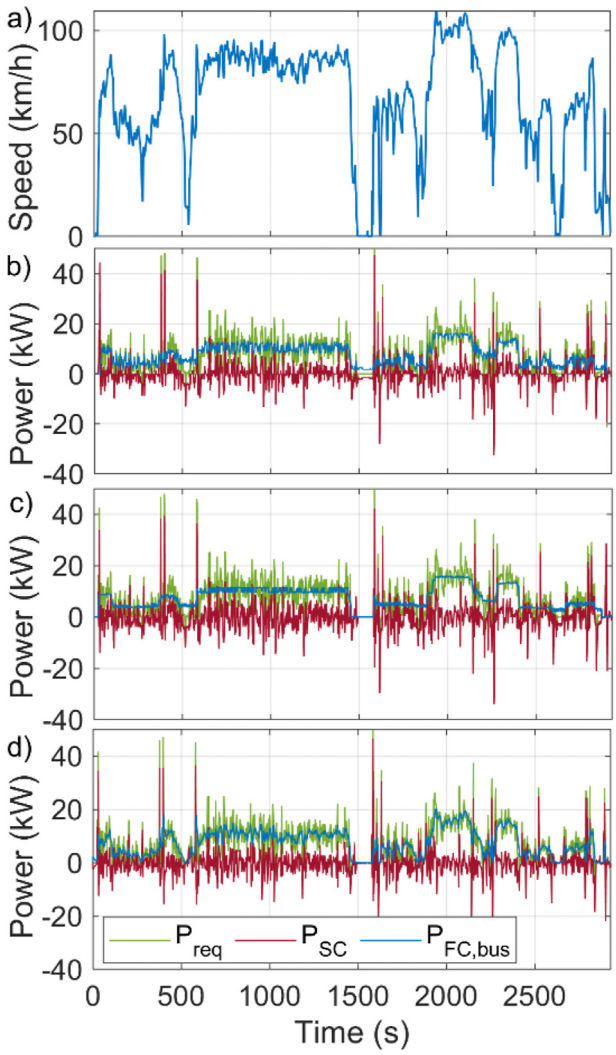

Fig. 9. Power split for the real driving cycle by the optimal size; a) on-road driving cycle b) full-active, c) semi-active, d) passive configuration.

Table 8
Breakdown of the trip cost for real driving profile.

Configuration	H_2 cons.	FC deg.	SC cost	Conv. cost	$/Trip
Full-active	$ 0.81	$ 0.32	$ 0.49	$ 0.41	$ 2.03
Semi-active	$ 0.78	$ 0.48	$ 0.57	$ 0.20	$ 2.03
Passive	$ 0.70	$ 0.62	$ 0.59	–	$ 1.91

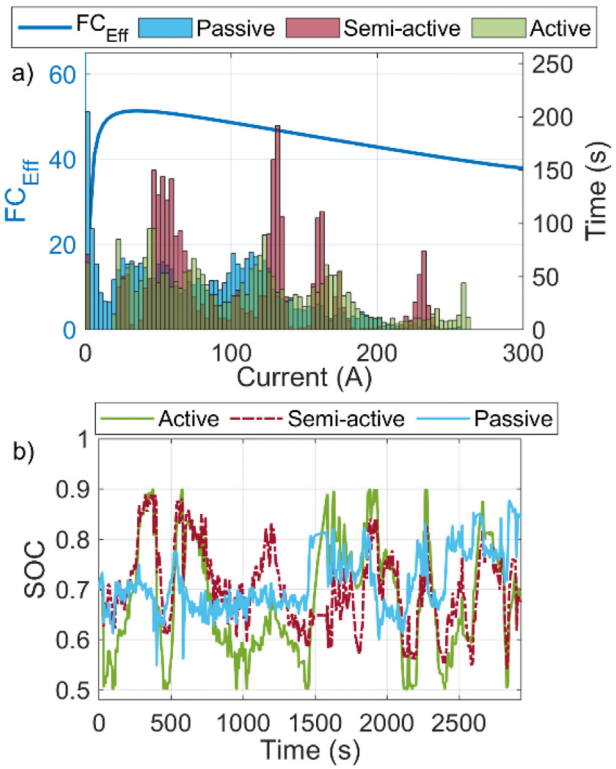

Fig. 10. Real driving cycle test results; a) current distribution comparison and FC efficiency curve, and b) SOC evolution of the three FC-SC configurations.

4. Results analysis

In this work, the standard World Motorcycle Test Cycle (WMTC) is utilized for the optimal sizing procedure. WMTC represents the collection and analysis of daily motorcycle driving behavior in Europe, Japan, and the USA [90]. It is composed of three regimes: urban traffic, slow country-road, and fast country-roads. The fitness function convergence trend of the optimal based sizing method for the three FC-SC configurations is shown in Fig. 6. The trend of mean value alteration represents all different sizes that fulfil the system requirement, and the combination with the lowest cost function value of each population is recorded in the best fitness curve. The minimization trend of the best fitness value has become almost stable after 20 iterations in the full-active, and after 50 iterations in semi-active and passive configurations. Moreover, the mean value trend converges for all the configurations at the end, showing that the best fitness value is the global/near-global optimal result.

The results of the optimization process are summarized in Table 6, where the FC and SC size, mass and cost are reported. It should be noted that the system mass and volume are obtained from the datasheets and it shows an approximated value of the power supply system. The full-active configuration is the one with the smallest capacitance value, followed by the semi-active. The passive configuration is the one with the biggest FC size and higher SC capacity. On the other hand, passive configuration, which does not use any DC-DC converters, benefits from a light mass and low volume.

The requested power (P_{req}), the effective power of the FC system in the DC bus ($P_{FC,bus}$), and the power in the SC (P_{SC}) for the FC-SC configurations are shown in Fig. 7. As shown in Fig. 7(a), the first part of the WMTC profile starts with a cold start and consists of eight micro-trips with a maximum speed of 60 km/h. The second part contains two micro-trips with a maximum speed of 95 km/h. The third part is one micro-trip with the top speed at 110 km/h. As presented in Fig. 7(c), semi-active configuration operates the FC in more stable steps, but the SC manages to absorb all the power peaks. Therefore, the regulation of active configuration reduces those peaks and makes the operation possible with a smaller number of SCs. Also, it is observed that semi-active and full-active configurations operate in SCM around 50 s in the beginning. Regarding the passive configuration shown in Fig. 5(d), the SC works as a low pass filter, and the FC follows the low frequency and main components of the requested power. In addition, it is observed that the FC voltage tends to follow the SC voltage level, as described in equation (27), until it reaches its OCV.

The results of the best fitness function are presented in Table 7. According to Table 7, the passive configuration has achieved the lowest value in terms of trip cost compared to other configurations. However, full-active, and semi-active operate the FC in a way to minimize its degradation. This superior performance of the passive configuration is achieved mainly due to not using a DC-DC converter. This reduces the cost and energy losses and generates a lower hydrogen consumption.

The current distribution analysis in Fig. 8(a) shows how the full-active and semi-active configurations tend to operate more in the maximum efficiency point. Meanwhile, the current of the passive configuration is distributed over the whole range. Fig. 8(b) illustrates the SOC_{SC} evolution along with the driving profile. In the passive configuration, the SOC is more stable due to self-management which determines the FC current as opposed to other configurations that operate in a wider range.

The results of component sizing have a strong dependency on the selected driving cycle. In this respect, the optimal size of each configuration is evaluated with a real driving profile. Real driving patterns differ significantly from standard cycles. These profiles might operate in a specific speed range and may not be suitable for design purposes [91]. The real on-road driving cycle presented in Fig. 9(a) has a maximum speed of 110 km/h and a duration of 49 min. During this driving profile, the vehicle operates mostly in the high-speed region. Fig. 9 shows the power split after using the real driving cycle. The FC power for all the configuration tends to operate with the same trend due to the high level of the requested power. Looking at Fig. 9(c), the FC operates more stably in the semi-active configuration. As mentioned earlier, FC normally works in a more distributed way and avoids unnecessary on-off cycles (SDM-SCM-SM modes) as is seen in the second 1452 of active configuration.

The breakdown of the trip cost obtained from the optimal size for the real driving profile is shown in Table 8. According to this table, the passive configuration has reached the lowest value in terms of trip cost although it has the most expensive FC cost. As

Table 9
Breakdown of the trip cost for the long test profile.

Configuration	Eq. range	H_2 cons.	Fuel Econ.	Capital cost	Total cost	Cost per km
Full-active	98088 km	$ 1598	141.1 km/kg	$ 6424	$ 8022	$ 0.082
Semi-active	94315 km	$ 1468	147.7 km/kg	$ 5598	$ 7066	$ 0.075
Passive	88692 km	$ 1220	167.2 km/kg	$ 4721	$ 5941	$ 0.067

previously discussed, the main advantage of the passive configuration reside in the absence of the DC-DC converter.

The current distribution study presented in Fig. 10(a) shows that the operation of full-active and passive configurations covers most of the FC operating current region while the semi-active configuration has mainly three peaks. The SOC evolution of SC is shown in Fig. 10(b). The full-active configuration can operate in the complete range compared to the other cases because the DC bus voltage value is not related to the SC SOC.

In order to study the impact of FC degradation, the WMTC profile has been continuously repeated until the FC reaches the EOL. Table 9 summarizes the total travel distance, the total cost of the consumed hydrogen, fuel economy, capital cost of the power supply system, and the equivalent cost per km. It is shown that the full-active configuration has the longest range, reaching 4% more than semi-active and 10% more than passive configuration. This is due to better management of the FC system that makes it run for a longer time. However, passive configuration has less efficiency losses in the electric conversion that result in an improvement on the fuel economy. Moreover, active configuration is the most expensive in terms of cost per km that is mainly attributed to the high capital cost. The full-active is 20% more expensive than passive, and semi-active is 11% more expensive than passive.

5. Conclusions

This paper investigates the performance of three optimized FC-SC configurations, namely: full-active, semi-active, and passive. In this regard, a standard driving cycle is utilized to define the size of the power sources by using a two-step optimization method. A trip cost is defined as the fitness function, which is composed of the FC degradation, consumed hydrogen, and a fraction of the capital cost of the SC and DC-DC converter. Subsequently, the obtained optimal size from the standard driving profile is evaluated based on a real driving profile of the e-TESC 3W electric vehicle. The performed analyses indicate that the trip cost of the proposed passive connection is 14.8% less than the full-active configuration and 6.4% less than the semi-active configuration for the standard driving profile of WMTC. In the case of the real driving cycle, the passive configuration presents 6.3% less cost than the other configurations. It is worth reminding that the passive configuration has a more expensive cost in terms of FC degradation compared to other case studies. However, this cost is compensated by other aspects, such as lower hydrogen consumption and DC-DC converter related prices. In conclusion, based on the presented benchmark study and simulation test, the passive configuration seems to be the most suitable power source for the Spyder recreational vehicle. As this work has highlighted the potential of the passive topology in a vehicular application, the implementation of this topology on a real test bench should be practiced in future studies.

Declaration of competing interest

The authors declare that they have no known competing financial interests or personal relationships that could have appeared to influence the work reported in this paper.

Acknowledgments

This work was supported in part by the Fonds de Recherche du Québec Nature et Technologies (283370 & 284914), Réseau Québécois sur l'Énergie Intelligente (3rd cycle and postdoctoral scholarships), Grant 950−230863 and 950−230672 from Canada Research Chairs Program, and in part by Grant RGPIN-2018-06527 and RGPIN-2017-05924 from the Natural Sciences and Engineering Research Council of Canada.

Nomenclatures

Abbreviations

BEV	Battery electric vehicle
DC	Direct current
DoE	US Department of Energy
DP	Dynamic programming
EMR	Energetic macroscopic representation
EMS	Energy management strategy
EOL	End of life
ESS	Energy storage system
FC	Fuel cell
FCEV	Fuel cell electric vehicle
FCHEV	Fuel cell hybrid electric vehicle
GA	Genetic algorithm
HEV	Hybrid electric vehicle
ICE	Internal combustion engine
NWM	Normal work mode
OCV	Open circuit voltage
PEMFC	Proton exchange membrane fuel cell
SC	Supercapacitor
SCM	Supercapacitor mode
SDM	Shutdown mode
SM	Start mode
WMTC	World Motorcycle Test Cycle

Variables

$\$DC_{conv}$	DC converter cost
$\$FC_{sys}$	FC system cost
$\$H_2$	Hydrogen cost
$\$SC$	SC cost
$\$Trip$	Trip cost
Δ_{FC}	FC degradation percentage
ΔP_{FC}	FC slew rate
Δ_{trip}	Normalized trip time
Ω_m	Rotor rotation speed
A_{aero}	Vehicle front area
$C^*_{O_2}$	Oxygen concentration
$C_{SC,u}$	Single SC capacitance
C_{SC}	SC equivalent capacitance
C_d	Typical aerodynamic drag coefficient
E_{Nernst}	Reversible voltage
F_{env}	Vehicle traction force resistance
F_{tr}	Traction force
G_{gb}	Belt transmission drive ratio
H_{FC}	Heat transfer coefficient
M_{O_2}	Oxygen molar mass
N_{FC}	Number of cell FC stacks
$N_{SC,p}$	SC parallel branches
$N_{SC,s}$	SC connected in series
P_{comp}	Compressor power
P_{fan}	Fan electric power
P_{FC}	Fuel cell power
$P_{FC,sys}$	Fuel cell system power
$P_{FC,bus}$	Effective FC power in the DC bus
P_{SC}	Supercapacitor power
P_{req}	Requested power
Q_{heat}	Residual energy
Q_{conv}	Heat dissipated due to convection

Q_{max}	SC maximum capacity
R_D	Equivalent diode resistance
R_{SC}	SC equivalent resistor
$R_{internal}$	Internal PEMFC resistor
SOC_{SC}	SC level of charge
T_{FC}	PEMFC stack temperature
T_{amb}	Ambient temperature
$T_{em,r}$	Reference torque
T_{em}	Electric machine torque
$V_{EV,max}$	Maximum vehicle speed
W_{H_2}	Consumed hydrogen flow
W_{O_2}	Oxygen consumed rate
W_{air}	Consumed air rate
c_p	Specific heat capacity of air
$i_{FC,max}$	Maximum PEMFC current
i_{SC}	SC current
i_{ts}	Traction system current
k_i	FC degradation coefficient
k_{ti}	Empirical coefficients
m_{eq}	Vehicle mass
p_{H2}	Hydrogen partial pressure
p_{O2}	Oxygen partial pressure
p_{amb}	Ambient pressure
p_{an}	Anode inlet pressure
p_{ca}	Cathode pressure
t_i	Operational time
u_{DC}	DC bus voltage
u_{FC}	PEMFC voltage
u_{SC}	Supercapacitor voltage
u_{act}	Activation loss
u_c	Capacitance element OCV
u_{con}	Concentration loss
u_{ohmic}	Ohmic loss
x_{O_2}	Ideal oxygen mass fraction in the air
ζ_n	Semi-empirical PEMFC resistor parameters
η_{FC}	System efficiency
η_{comp}	Compressor efficiency
η_{gb}	Belt transmission drive efficiency
η_m	motor efficiency
μ_{fr}	Typical rolling resistance coefficient
ξ_n	Semi-empirical activation coefficients
ρ_{air}	Air density
F	Faraday constant
HHV	Hydrogen high heating value
M	DP system work mode
MC_{FC}	Thermal capacity of the FC
r	Wheel radius
x	DP state variable
α	Semi-empirical diffusion mechanism parameter
β	Discrete braking mode value
γ	Specific heat ratio of the air
λ	Oxygen excess ratio constant

Credit author statement

Alvaro Macias: Conceptualization, Software, Writing – original draft. Mohsen Kandidayeni: Methodology, Writing – original draft, Validation. Loïc Boulon: Supervision, Writing – review & editing, Funding acquisition. João F. Trovão: Supervision, Writing – review & editing, Resources

References

[1] Wu Y, Zhang L. Can the development of electric vehicles reduce the emission of air pollutants and greenhouse gases in developing countries? Transport Res Transport Environ 2017;51:129–45. 2017/03/01/.

[2] Méjean A, Guivarch C, Lefèvre J, Hamdi-Cherif M. The transition in energy demand sectors to limit global warming to 1.5 °C. Energy Efficiency February 01 2019;12:441–62.

[3] Campíñez-Romero S, Colmenar-Santos A, Pérez-Molina C, Mur-Pérez F. A hydrogen refuelling stations infrastructure deployment for cities supported on fuel cell taxi roll-out. Energy 2018;148:1018–31. 2018/04/01/.

[4] Li Z, Khajepour A, Song J. A comprehensive review of the key technologies for pure electric vehicles. Energy 2019;182:824–39. 2019/09/01/.

[5] Sokolov A, Saritas O, Meissner D. Global market creation for fuel cell electric vehicles. In: Meissner D, Gokhberg L, Saritas O, editors. Emerging technologies for economic development. Cham: Springer International Publishing; 2019. p. 131–52.

[6] Wang Y, Seo B, Wang B, Zamel N, Jiao K, Adroher XC. Fundamentals, materials, and machine Learning of Polymer Electrolyte membrane fuel cell technology. Energy and AI; 2020. p. 100014. 2020/06/29/.

[7] Ruffini E, Wei M. Future costs of fuel cell electric vehicles in California using a learning rate approach. Energy 2018;150:329–41. 2018/05/01/.

[8] Wang G, Huang F, Yu Y, Wen S, Tu Z. Degradation behavior of a proton exchange membrane fuel cell stack under dynamic cycles between idling and rated condition. Int J Hydrogen Energy 2018;43:4471–81. 2018/03/01/.

[9] Wang J. System integration, durability and reliability of fuel cells: challenges and solutions. Appl Energy 2017;189:460–79. 2017/03/01/.

[10] Bodner M, Schenk A, Salaberger D, Rami M, Hochenauer C, Hacker V. Air starvation induced degradation in polymer electrolyte fuel cells. Fuel Cell 2017;17:18–26.

[11] Chen H, Zhao X, Zhang T, Pei P. The reactant starvation of the proton exchange membrane fuel cells for vehicular applications: a review. Energy Convers Manag 2019;182:282–98. 2019/02/15/.

[12] Liu H, Chen J, Hissel D, Lu J, Hou M, Shao Z. Prognostics methods and degradation indexes of proton exchange membrane fuel cells: a review. Renew Sustain Energy Rev 2020;123:109721. 2020/05/01/.

[13] Hannan MA, Hoque MM, Mohamed A, Ayob A. Review of energy storage systems for electric vehicle applications: issues and challenges. Renew Sustain Energy Rev 2017;69:771–89.

[14] Das HS, Tan CW, Yatim AHM. Fuel cell hybrid electric vehicles: a review on power conditioning units and topologies. Renew Sustain Energy Rev 2017;76:268–91.

[15] Han Y, Li Q, Wang T, Chen W, Ma L. Multisource coordination energy management strategy based on SOC consensus for a PEMFC–battery–supercapacitor hybrid tramway. IEEE Trans Veh Technol 2018;67:296–305.

[16] Cheng S, Xu L, Wu K, Fang C, Hu J, Li J, et al. Optimal warm-up control strategy of the PEMFC system on a city bus aimed at improving efficiency. Int J Hydrogen Energy 2017;42:11632–43. 2017/04/20/.

[17] Wu P, Partridge J, Bucknall R. Cost-effective reinforcement learning energy management for plug-in hybrid fuel cell and battery ships. Appl Energy 2020;275:115258. 2020/10/01/.

[18] Truong HV, Dao HV, Do TC, Ho CM, To XD, Dang TD, et al. Mapping fuzzy energy management strategy for PEM fuel cell–battery–supercapacitor hybrid excavator. Energies 2020;13.

[19] Lohse-Busch H, Stutenberg K, Duoba M, Liu X, Elgowainy A, Wang M, et al. Automotive fuel cell stack and system efficiency and fuel consumption based on vehicle testing on a chassis dynamometer at minus 18 °C to positive 35 °C temperatures. Int J Hydrogen Energy 2020;45:861–72. 2020/01/01/.

[20] Yue M, Jemei S, Gouriveau R, Zerhouni N. Review on health-conscious energy management strategies for fuel cell hybrid electric vehicles: degradation models and strategies. Int J Hydrogen Energy 2019;44:6844–61. 2019/02/18/.

[21] Wang Y, Sun Z, Li X, Yang X, Chen Z. A comparative study of power allocation strategies used in fuel cell and ultracapacitor hybrid systems. Energy 2019;189:116142. 2019/12/15/.

[22] Liu Y, Liu J, Zhang Y, Wu Y, Chen Z, Ye M. Rule learning based energy management strategy of fuel cell hybrid vehicles considering multi-objective optimization. Energy 2020;207:118212. 2020/09/15/.

[23] Kandidayeni M, Fernandez AOM, Khalatbarisoltani A, Boulon L, Kelouwani S, Chaoui H. An online energy management strategy for a fuel cell/battery vehicle considering the driving pattern and performance drift impacts. IEEE Trans Veh Technol 2019;68:11427–38.

[24] Zhou Y, Li H, Ravey A, Péra M-C. An integrated predictive energy management for light-duty range-extended plug-in fuel cell electric vehicle. J Power Sources 2020;451:227780. 2020/03/01/.

[25] Silva RE, Harel F, Jemeï S, Gouriveau R, Hissel D, Boulon L, et al. Proton exchange membrane fuel cell operation and degradation in short-circuit. Fuel Cell 2014;14:894–905.

[26] Arora D, Bonnet C, Mukherjee M, Raël S, Lapicque F. Direct hybridization of PEMFC and supercapacitors: effect of excess hydrogen on a single cell fuel cell durability and its feasibility on fuel cell stack. Electrochim Acta 2019;310:

213–20. 2019/07/01/.
[27] Gérardin K, Raël S, Bonnet C, Arora D, Lapicque F. Direct coupling of PEM fuel cell to supercapacitors for higher durability and better energy management. Fuel Cell 2018;18:315–25.
[28] Samsun RC, Krupp C, Baltzer S, Gnörich B, Peters R, Stolten D. A battery-fuel cell hybrid auxiliary power unit for trucks: analysis of direct and indirect hybrid configurations. Energy Convers Manag 2016;127:312–23.
[29] Xun Q, Liu Y, Holmberg E. A comparative study of fuel cell electric vehicles hybridization with battery or supercapacitor. Automation and Motion. International Symposium on power Electronics, electrical drives. SPEEDAM); 2018. p. 389–94. 2018.
[30] Zhang L, Hu X, Wang Z, Sun F, Dorrell DG. A review of supercapacitor modeling, estimation, and applications: a control/management perspective. Renew Sustain Energy Rev 2018;81:1868–78.
[31] Koubaa R, Bacha S, Smaoui M, Lotfi k. Robust optimization based energy management of a fuel cell/ultra-capacitor hybrid electric vehicle under uncertainty. Energy 2020:117530. 2020/04/11/.
[32] Zhang R, Tao J, Zhou H. Fuzzy optimal energy management for fuel cell and supercapacitor systems using neural network based driving pattern recognition. IEEE Trans Fuzzy Syst 2019;27:45–57.
[33] Li T, Huang L, Liu H. Energy management and economic analysis for a fuel cell supercapacitor excavator. Energy 2019;172:840–51. 2019/04/01/.
[34] Li Q, Su B, Pu Y, Han Y, Wang T, Yin L, et al. A state machine control based on equivalent consumption minimization for fuel cell/supercapacitor hybrid tramway. IEEE Transactions on Transportation Electrification 2019;5:552–64.
[35] Yan Y, Li Q, Chen W, Su B, Liu J, Ma L. Optimal energy management and control in multimode equivalent energy consumption of fuel cell/supercapacitor of hybrid electric tram. IEEE Trans Ind Electron 2019;66:6065–76.
[36] Sun Z, Wang Y, Chen Z, Li X. Min-max game based energy management strategy for fuel cell/supercapacitor hybrid electric vehicles. Appl Energy 2020;267:115086. 2020/06/01/.
[37] Turpin C, Van Laethem D, Morin B, Rallières O, Roboam X, Verdu O, et al. Modelling and analysis of an original direct hybridization of fuel cells and ultracapacitors. Math Comput Simulat 2017;131:76–87.
[38] Ait Hammou Taleb S, Brown D, Dillet J, Guillemet P, Mainka J, Crosnier O, et al. Direct hybridization of polymer exchange membrane surface fuel cell with small aqueous supercapacitors. Fuel Cell 2018;18:299–305.
[39] Shimoi R, Ono Y. Fuel cell system. Japan Patent; 2005.
[40] Wu B, Parkes MA, Yufit V, De Benedetti L, Veismann S, Wirsching C, et al. Design and testing of a 9.5 kWe proton exchange membrane fuel cell–supercapacitor passive hybrid system. Int J Hydrogen Energy 2014;39:7885–96.
[41] Phadermrod B, Crowder RM, Wills GB. Importance-Performance Analysis based SWOT analysis. Int J Inf Manag 2019;44:194–203. 2019/02/01/.
[42] Cox BL, Mutel CL. The environmental and cost performance of current and future motorcycles. Appl Energy 2018;212:1013–24. 2018/02/15/.
[43] Macías A, Kandidayeni M, Boulon L, Trovão J. Passive and active coupling comparison of fuel cell and supercapacitor for a three-wheel electric vehicle. Fuel cells. 2019. 2019/10/29.
[44] J. P. Trovao, M. R. Dubois, M. Roux, E. Menard, and A. Desrochers, "Battery and SuperCapacitor hybridization for a pure electric three-wheel roadster," in 2015 IEEE vehicle power and propulsion conference (VPPC), 2015, pp. 1-6.
[45] Trovão JPF, Roux M, É M, Dubois MR. Energy- and power-split management of dual energy storage system for a three-wheel electric vehicle. IEEE Trans Veh Technol 2017;66:5540–50.
[46] Bouscayrol A, Hautier J-P, Lemaire-Semail B. Graphic formalisms for the control of multi-physical energetic systems: COG and EMR. In: Wiley Ia, editor. Systemic design methodologies for electrical energy systems; 2012. p. 89–124.
[47] Kandidayeni M, Macias A, Amamou AA, Boulon L, Kelouwani S, Chaoui H. Overview and benchmark analysis of fuel cell parameters estimation for energy management purposes. J Power Sources 2018;380:92–104.
[48] Kandidayeni M, Macias A, Amamou AA, Boulon L, Kelouwani S. Comparative analysis of two online identification algorithms in a fuel cell system. Fuel cells, vol. 18; 2018. p. 347–58.
[49] Kravos A, Ritzberger D, Tavcar G, Hametner C, Jakubek S, Katrasnik T. Thermodynamically consistent reduced dimensionality electrochemical model for proton exchange membrane fuel cell performance modelling and control. J Power Sources 2020;454:227930. 2020/04/01/.
[50] Inc BPS. FCvelocity-9SSL V4.3 Product manual and integration Guide. 2017.
[51] Zhao X, Li Y, Liu Z, Li Q, Chen W. Thermal management system modeling of a water-cooled proton exchange membrane fuel cell. Int J Hydrogen Energy 2015;40:3048–56. 2015/02/23/.
[52] Oruganti PS, Ahmed Q, Jung D. Effects of thermal and auxiliary dynamics on a fuel cell based range extender. SAE Technical Paper; 2018.
[53] San Martín I, Ursúa A, Sanchis P. Modelling of PEM fuel cell performance: steady-state and dynamic experimental validation. Energies 2014;7.
[54] Campbell JM. Gas conditioning and processing Volume 2. In: The Equipment modules. ninth ed. PetroSkills: U.S.A.; 2014.
[55] Dicks A, Rand DAJ. Fuel cell systems explained. Wiley Online Library; 2018.
[56] Wang C, He H, Zhang Y, Mu H. A comparative study on the applicability of ultracapacitor models for electric vehicles under different temperatures. Appl Energy 2017;196:268–78. 2017/06/15/.
[57] M. Technologies, "Maxwell Ultracapacitor cells Product comparison matrix," ed, 2020.
[58] Wang Y, Liu C, Pan R, Chen Z. Modeling and state-of-charge prediction of lithium-ion battery and ultracapacitor hybrids with a co-estimator. Energy 2017;121:739–50. 2017/02/15/.
[59] Wang J, Zhang L, Mao J, Zhou J, Xu D. Fractional order equivalent circuit model and SOC estimation of supercapacitors for use in HESS. IEEE Access 2019;7:52565–72.
[60] Lohse-Busch H, Stutenberg K, Duoba M, Iliev S. Technology assessment of A fuel cell vehicle: 2017 Toyota Mirai. Argonne, IL (United States): Argonne National Lab.(ANL); 2018.
[61] Choi CH, Yu S, Han I-S, Kho B-K, Kang D-G, Lee HY, et al. Development and demonstration of PEM fuel-cell-battery hybrid system for propulsion of tourist boat. Int J Hydrogen Energy 2016;41:3591–9. 2016/02/09/.
[62] Das HS, Tan CW, Yatim AHM, Li S. Fuel cell and ultracapacitor energy system control using linear quadratic regulator proportional integral controller. Electr Eng July 08 2019;101(2):559–73.
[63] Silvas E, Hofman T, Murgovski N, Etman LFP, Steinbuch M. Review of optimization strategies for system-level design in hybrid electric vehicles. IEEE Trans Veh Technol 2017;66:57–70.
[64] Huang Y, Wang H, Khajepour A, Li B, Ji J, Zhao K, et al. A review of power management strategies and component sizing methods for hybrid vehicles. Renew Sustain Energy Rev 2018;96:132–44. 2018/11/01/.
[65] Li T, Liu H, Wang H, Yao Y. Multiobjective optimal predictive energy management for fuel cell/battery hybrid construction vehicles. IEEE Access 2020;8:25927–37.
[66] Jiang H, Xu L, Li J, Hu Z, Ouyang M. Energy management and component sizing for a fuel cell/battery/supercapacitor hybrid powertrain based on two-dimensional optimization algorithms. Energy 2019;177:386–96. 2019/06/15/.
[67] Hou S, Gao J, Zhang Y, Chen M, Shi J, Chen H. A comparison study of battery size optimization and an energy management strategy for FCHEVs based on dynamic programming and convex programming. Int J Hydrogen Energy 2020;45(41):21858–72. 2020/07/01/.
[68] Soumeur MA, Gasbaoui B, Abdelkhalek O, Ghouili J, Toumi T, Chakar A. Comparative study of energy management strategies for hybrid proton exchange membrane fuel cell four wheel drive electric vehicle. J Power Sources 2020;462:228167. 2020/06/30/.
[69] Lü X, Wu Y, Lian J, Zhang Y, Chen C, Wang P, et al. Energy management of hybrid electric vehicles: a review of energy optimization of fuel cell hybrid power system based on genetic algorithm. Energy Convers Manag 2020;205:112474. 2020/02/01/.
[70] Zhou Y, Ravey A, Péra M-C. Multi-objective energy management for fuel cell electric vehicles using online-learning enhanced Markov speed predictor. Energy Convers Manag 2020;213:112821. 2020/06/01/.
[71] Song K, Wang X, Li F, Sorrentino M, Zheng B. Pontryagin's minimum principle-based real-time energy management strategy for fuel cell hybrid electric vehicle considering both fuel economy and power source durability. Energy 2020;205:118064. 2020/08/15/.
[72] Meng X, Li Q, Zhang G, Wang T, Chen W, Cao T. A dual-mode energy management strategy considering fuel cell degradation for energy consumption and fuel cell efficiency comprehensive optimization of hybrid vehicle. IEEE Access 2019;7:134475–87.
[73] Deb K, Deb K. Multi-objective optimization. In: Burke EK, Kendall G, editors. Search methodologies: introductory tutorials in optimization and decision support techniques. Boston, MA: Springer US; 2014. p. 403–49.
[74] U. S. D. o. Energy. Fuel cells. Multi-Year Research, Development, and Demonstration Plan; 2017.
[75] Song Z, Li J, Hou J, Hofmann H, Ouyang M, Du J. The battery-supercapacitor hybrid energy storage system in electric vehicle applications: a case study. Energy 2018;154:433–41. 2018/07/01/.
[76] DRIVE U. Electrical and Electronics Technical Team Roadmap. 2017.
[77] U. S. D. o. Energy. Hydrogen production. Multi-Year Research, Development, and Demonstration Plan; 2015.
[78] Galla S, Szewczyk A, Smulko J, Przygocki P. Methods of assessing degradation of supercapacitors by using various measurement techniques. Appl Sci 2019;9.
[79] Chen H, Pei P, Song M. Lifetime prediction and the economic lifetime of Proton Exchange Membrane fuel cells. Appl Energy 2015;142:154–63. 2015/03/15/.
[80] Song K, Chen H, Wen P, Zhang T, Zhang B, Zhang T. A comprehensive evaluation framework to evaluate energy management strategies of fuel cell electric vehicles. Electrochim Acta 2018;292:960–73. 2018/12/01/.
[81] Zhou W, Yang L, Cai Y, Ying T. Dynamic programming for new energy vehicles based on their work modes Part II: fuel cell electric vehicles. J Power Sources 2018;407:92–104. 2018/12/15/.
[82] Zhou W, Yang L, Cai Y, Ying T. Dynamic programming for new energy vehicles based on their work modes part I: electric vehicles and hybrid electric vehicles. J Power Sources 2018;406:151–66. 2018/12/01/.
[83] Zhang R, Tao J. GA-based fuzzy energy management system for FC/SC-powered HEV considering H2Consumption and load variation. IEEE Trans Fuzzy Syst 2018;26:1833–43.

[84] Li T, Liu H, Ding D. Predictive energy management of fuel cell supercapacitor hybrid construction equipment. Energy 2018;149:718–29. 2018/04/15/.
[85] Luta DN, Raji AK. Optimal sizing of hybrid fuel cell-supercapacitor storage system for off-grid renewable applications. Energy 2019;166:530–40. 2019/01/01/.
[86] Ettihir K, Boulon L, Agbossou K. Optimization-based energy management strategy for a fuel cell/battery hybrid power system. Appl Energy 2016;163:142–53.
[87] Parvini Y, Vahidi A, Fayazi SA. Heuristic versus optimal charging of supercapacitors, lithium-ion, and lead-acid batteries: an efficiency point of view. IEEE Trans Contr Syst Technol 2018;26:167–80.
[88] Álvarez Fernández R, Corbera Caraballo S, Beltrán Cilleruelo F, Lozano JA. Fuel optimization strategy for hydrogen fuel cell range extender vehicles applying genetic algorithms. Renew Sustain Energy Rev 2018;81:655–68. 2018/01/01/.
[89] Tao J, Zhang R, Zhu Y. DNA computing based genetic algorithm: applications in Industrial process modeling and control. Springer Nature; 2020.
[90] Giakoumis EG. Motorcycles. In: Giakoumis EG, editor. Driving and engine cycles. Cham: Springer International Publishing; 2017. p. 167–91.
[91] Brady J, O'Mahony M. Development of a driving cycle to evaluate the energy economy of electric vehicles in urban areas. Appl Energy 2016;177:165–78. 2016/09/01/.

Chapter 4 - New perspective of fuel cell passive hybridization for electric vehicles

4.1 Introduction

The conducted benchmark problem in Chapter 3 revealed that the passive configuration suits recreational vehicles better due to its low weight, cost, and energy conversion losses. However, the main drawback of the presented FC-SC passive coupling is the requirement of a pre-charging strategy to balance the electric potential of FC and SC, which limits the drawn current from the FC by increasing the start-up time and energy losses [63]. As mentioned in Chapter 1, an alternative method to the simple pre-charging resistor is the use of hybrid lithium-ion capacitors (LIC) instead of porous polymer electrodes as present in the EDLC. The LIC has a positive activated carbon electrode, a negative carbon lithium pre-doped electrode, and a lithium salt electrolyte [52]. This composition acquiesces good electrochemical properties with a relatively high-energy density, high-power density, and stable operating voltage that avoids a pre-charging strategy. In addition, owing to the different impedance of the components, the system is self-management. FC supplies the average power component and LIC operates as a low-pass filter avoiding abrupt changes in the FC current. Therefore, this chapter evaluates the integration of a LIC in the three-wheel electric vehicle platform to reach a more compact, efficient, and simple to implement power source.

The proposed assessment is presented in an article entitled "Passive Fuel Cell/Lithium-ion Capacitor Hybridization for Vehicular Applications". The utilized methodology and the summary of the results are discussed first. Afterwards, the paper is presented.

4.2 Article 3: Passive Fuel Cell/Lithium-ion Capacitor Hybridization for Vehicular Applications

Authors: A. Macias, N. El Ghossein, J. Trovão, A. Sari, P. Venet, L. Boulon

Journal: International Journal of Hydrogen Energy, Elsevier

Publication date: 13 August 2021

DOI: https://doi.org/10.1016/j.ijhydene.2021.06.126

4.2.1 Methodology

The last stage of the Ph.D. project was to evaluate the possibility of replacing the SC of the proposed architecture with a LIC. With this objective in mind, a collaboration has been set up between two Canadian laboratories; the Hydrogen Research Institute from the UQTR, the e-TESC laboratory from the University of Sherbrooke, and the Ampère laboratory from the University of Lyon in France. First a literature review of the leading energy storage systems (ESS) for electric vehicles reveals that the LICs are suitable for regenerative braking systems, high-requested power with deep discharging demand, and high cyclability applications [53, 54]. To the best of the author's knowledge, this is the first attempt to integrate a LIC into a hybrid fuel cell electric vehicle. The selected case study is the e-TESC-3W motorcycle platform that is exposed to high requested power peaks, and it is limited in physical dimensions. In this respect, the already proven passive configuration is chosen due to its low system weight and volume, enhanced FC system performance, and absorption of intermittent power fluctuations by the ESS. Then, the FC, LIC, and Spyder powertrain models were developed. These virtual simulators are constructed based on experimental data.

The data collection is carried out from the well-equipped Ampère Lab in Lyon under the supervision of Prof. Ali Sari and Prof. Pascal Venet, who are experts in the research subject of LIC and SC. The hybrid system's performance is analyzed in the MATLAB/Simulink environment at different stages of the life of the FC system under three motorcycle driving cycles. In this regard, the LIC bank of the studied system is rated for a higher value than the FC open-circuit voltage at different system stages of life, as shown in Figure 4.1. Moreover, the DC bus voltage is within the motor drive range (80V – 120V), and most of the FC power under the three stages of life fall in the same range. Due to the parallel connection of the FC system and LIC bank, they will share the same voltage, which means a high FC power will result in a low SOC_{LIC} and a low FC power will result in a high SOC_{LIC}. It is expected that the system will operate in a range of 20% - 70% of the SOC_{LIC}.

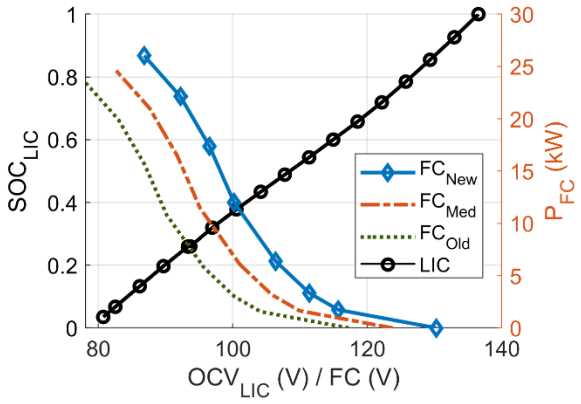

Figure 4.1 Correlation of LIC voltage with SOC and FC voltage with output power.

4.2.2 Outcomes

After designing the semi-empirical models for the traction sub-system, multi-physic FC system, and LIC storage, the vehicle performance is evaluated under three standard driving cycles. The selected driving profiles are NEDC, FTP-72 and WMTC, built from a collection

of daily and real motorcycle driving behavior from different countries. Contrary to most of the works found in the literature, the presented work of this chapter integrates the degradation decay (Δ_{FC}) as a complementary metric to the fuel consumption performance evaluation, as reported in Figure 4.2. The LIC degradation is neglected due to its long-life and low degradation rate [93]. The systems with older FCs consume the most hydrogen because it operates in higher currents to deliver the same requested power from the powertrain. In the case of NEDC profile, the variation in the Δ_{FC} are very small because most of the degradation comes from the initial start-up event and natural decay, which are similar for all the states. However, for the FTP-72 case, there is a notorious change in the FC degradation caused by the increment of load changes in the FC. Furthermore, for the case of the WMTC profile, which has the highest average speed and duration, it is more evident that the new FC operates at lower currents than the degraded FC systems, as reflected in its hydrogen consumption and FC degradation.

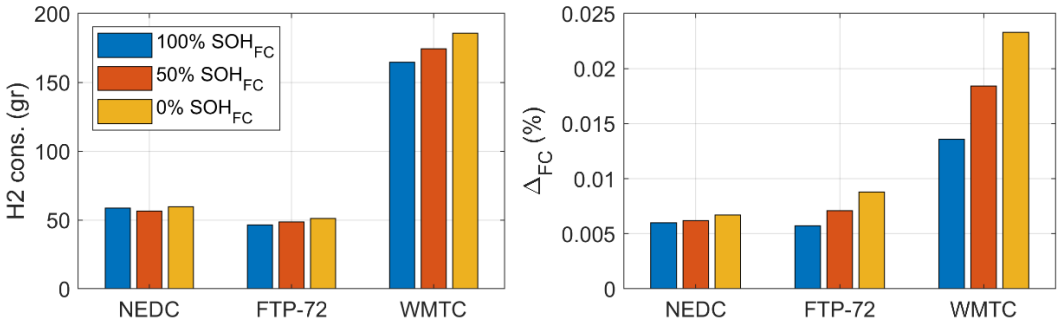

Figure 4.2 Breakdown analysis, a) hydrogen consumption, b) FC degradation

The previous test shows that the FC-LIC passive hybrid system supplies the requested power completely and operates within the motor driver voltage range in all the conditions. However, due to self-energy management, the system finishes in different SOC levels, which makes the performance comparison difficult. In this sense, Figure 4.3 plots the hydrogen

consumption for different initial SOC_{LIC} levels; 0.2, 0.3, 0.4, 0.5, 0.6, 0.7 and 0.8. Based on these results, it demonstrates that a system with an old FC will have a higher hydrogen consumption with any initial SOC_{LIC}. On average, compared to the FC_{New} condition, the increment in hydrogen consumption is by 12% for the FC_{Old} and 6% for the FC_{Med}.

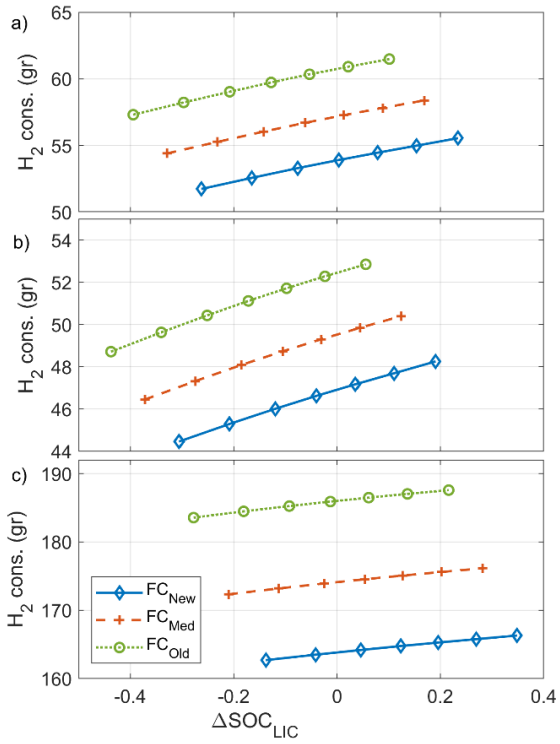

Figure 4.3 Hydrogen consumption versus ΔSOC_{LIC} for the driving cycles: a) NEDC, b) FTP-72, and c) WMTC

The combination of the FC system with the explained merits of LIC is expected to decrease the hydrogen consumption and capital cost of the whole power supply system compared to other ESS. Furthermore, an industrial interest of this work is that the proposed architecture increases the portability of the system, which is highly useful in many industrial applications. It should be noted that although the LIC shows better results compared to the SC as an ESS, the price of the SC is much lower and more commercially available due to the level of maturity of the technology.

Available online at www.sciencedirect.com

ScienceDirect

journal homepage: www.elsevier.com/locate/he

Passive fuel cell/lithium-ion capacitor hybridization for vehicular applications

Alvaro Macias [a,b,c,*], *Nagham El Ghossein* [e], *João Trovão* [c,d], *Ali Sari* [e], *Pascal Venet* [e], *Loïc Boulon* [a,b]

[a] *Université Du Québec à Trois-Rivières, Trois-Rivières, QC, G8Z 4M3, Canada*

[b] *Institut de Recherche Sur L'Hydrogène, UQTR, Trois-Rivières, QC, G9A 5H7, Canada*

[c] *e-TESC Laboratory, Dept. Electrical & Computer Engineering, University of Sherbrooke, Sherbrooke, QC, J1K 2R1, Canada*

[d] *Canada Research Chair in Efficient Electric Vehicles with Hybridized Energy Storage Systems, University of Sherbrooke, Sherbrooke, QC, J1K 2R1, Canada*

[e] *Univ Lyon, Univ. Claude Bernard Lyon 1, Ecole Centrale de Lyon, INSA Lyon, CNRS, Ampère, 69130, France*

HIGHLIGHTS

- Integration of LIC technology with a fuel cell system for a recreational vehicle.
- Development of a hybrid FC-LIC vehicle simulator based on experimental data.
- The system is tested under standard driving cycles at different FC lifespan stages.
- The proposed passive design supplies the requested power under all the conditions.
- The passive FC-LIC topology is lighter, simpler to implement and self-management.

GRAPHICAL ABSTRACT

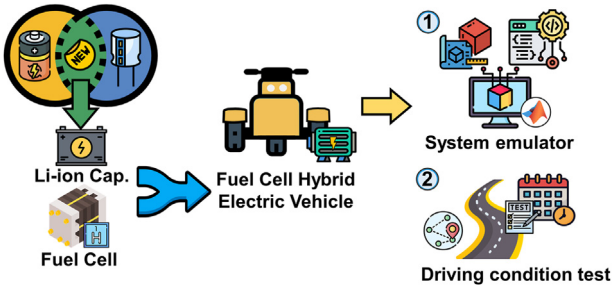

ARTICLE INFO

Article history:
Received 14 April 2021
Received in revised form
14 June 2021
Accepted 15 June 2021
Available online xxx

Keywords:
Electric motorcycle
Hybrid electric vehicle

ABSTRACT

Electric recreational vehicles represent a new challenge in terms of power supply systems compared to the current light-duty electric vehicles, which achieve high performance and long-range. The recreational vehicles need to heed the limited dimension requirements while assuring the high requested power. This paper proposes an integration of Lithium-Ion Capacitor (LIC) with Fuel Cell (FC) without any power electronic device for a three-wheel electric motorcycle. Unlike other hybrid power supply systems, the proposed FC-LIC passive configuration is lighter, compact, more efficient, and simpler to implement. Due to the different impedance of the components the system is self-management, in which FC supplies the average power component and LIC operates as a low-pass filter. In this respect, a simulator is built based on experimental tests to study the system

* *Corresponding author*. Université Du Québec à Trois-Rivières, Trois-Rivières, QC, G8Z 4M3, Canada.
E-mail address: alvaro.omar.macias.fernandez@uqtr.ca (A. Macias).

https://doi.org/10.1016/j.ijhydene.2021.06.126

Lithium-ion capacitor
Passive configuration
PEMFC
Recreational vehicle

performance in terms of hydrogen consumption and FC degradation. Subsequently, the system is tested under three standard motorcycle driving cycles at three different FC system lifespan stages. The obtained results demonstrate that a passive topology can supply the requested power along different FC stages of life and reported just an increment of 12% of hydrogen consumption at the oldest condition compared to the new condition.

Introduction

Electric vehicles are proposed to reduce greenhouse gas emissions from the transportation sector, mainly relying on non-renewable resources. Nowadays, electric vehicles can be powered by batteries or Fuel Cell (FC) systems. FC vehicles benefit from a higher driving range, zero-local emissions, and faster refueling than battery vehicles [1]. Even though FC vehicles are now available, their worldwide deployment is yet to come as they require more cost reduction and durability improvement. One of the FC systems durability vulnerabilities is their exposure to sudden power variations in vehicle applications, which leads to the deterioration of the internal electrolyte membrane [2]. In this respect, the high variations cause a decrement in the oxygen concentration of the FC and, consequently, a sudden power drop occurs [3]. The Fuel Cell Hybrid Electric Vehicles (FCHEV) couple a FC stack with an Energy Storage System (ESS) to cope with this issue. Through this, the vehicle can store regenerative energy, supplies high peaks of current, has higher range autonomy and obtains less capital and running cost [4]. Also, avoiding harsh changes in the FC current density is one of the low-cost water management method [5]. The coupling of the FC and the ESS to the DC bus is conducted in active and passive ways [6]. In the active topology, the components are connected to the DC bus via a DC-DC converter. The researchers prefer the active topology due to its high degree of freedom to control the power split between the sources. Through an Energy Management Strategy (EMS), the DC converter maintains a constant voltage level in the DC bus and splits the requested power among the components to enhance the performance and the lifespan of the system [7]. In this regard, it can be found in the literature that the multi-objective cost functions are able to reduce the hydrogen consumption while taking care of the FC stack and ESS [8,9]. Contrary to the active configuration, the passive one is a direct connection and self-management of the FC and the ESS to the DC bus, reducing the complexity, cost, and weight of the system [10]. In addition, the implementation of passive topology is simple and benefits from self-management due to the different impedance of the components.

The battery and the Supercapacitor (SC) have been broadly employed in the literature and industry as secondary ESS for vehicular applications [11]. The most common rechargeable battery used in vehicles is the lithium-ion battery because of its high energy density and high efficiency. However, its main disadvantages are the low power density, the reduced life cycle, and the long charging time. Regarding the SC, it is the most suitable device to provide rapid peaks of current due to the fast formation of the electric double layer at the interface between the electrodes and the electrolyte. Furthermore, the SC has higher specific power, a longer lifespan, and better resilience to different operation temperatures than the batteries. Nevertheless, SCs suffer from a low energy density and a high self-discharge, which can generate a high-power peak request if both systems do not have the same electric potential. In order to prevent this high inrush peak, a precharging strategy is needed, causing an increment in the startup time [12].

The Lithium-Ion Capacitor (LIC) is a novel hybrid device that may have a SC positive electrode (activated carbon), a battery kind negative electrode (carbon material pre-doped with lithium), and an electrolyte containing a lithium salt [13]. This composition yields good electrochemical properties with a relatively high-energy density and a high-power density, as illustrated in Fig. 1. Also, LIC operates in a voltage range of 2 V and 3.8 V, compared to SC cell that operates between 0 V and its rated voltage (between 2.7 V and 3 V). Fig. 1 shows a comparison of the performance of the mentioned ESSs and FC, in which the specific energy (Wh/kg) is plotted versus the specific power (W/kg).

Table 1 summarizes the main characteristics of three main ESS for electric vehicles [14,15]. Owing to the mentioned characteristics, LICs are suitable for regenerative braking systems, high-requested power with deep discharging demand, and high cyclability applications. In this respect, it can be found in the literature that some of the works integrate the LIC into battery-based electric vehicles [16,17].

Based on the reviewed papers, some efforts have already been made concerning different ESSs with active and passive topologies for vehicular applications. However, so far, the hybrid systems with a secondary ESS are heavier, complex, and limited to provide either high peak currents or high autonomy. To the best knowledge of the authors, no efforts have been made to integrate a LIC into an electric recreational

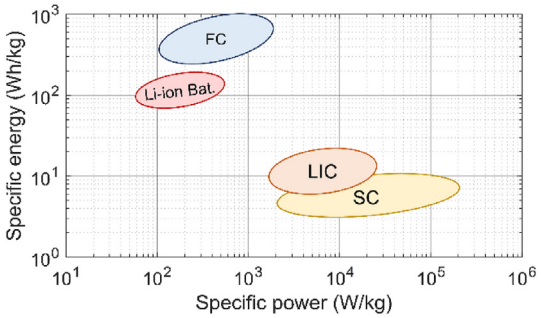

Fig. 1 – Ragone plot of FCs, Li-ion batteries, SCs and LICs.

Please cite this article as: Macias A et al., Passive fuel cell/lithium-ion capacitor hybridization for vehicular applications, International Journal of Hydrogen Energy, https://doi.org/10.1016/j.ijhydene.2021.06.126

Table 1 – Comparison of ESSs.

Characteristics	Lithium-ion capacitor	Supercapacitor	Lithium-ion battery
Energy density	Low to medium	Low	High
Power density	High	Very high	Low
Charging time	In terms of tens of second or minutes	In terms of seconds or tens of tens of second	In terms of hours or tens of minutes
Internal resistance	Low	Very low	High
Self-discharge	Medium	High	Low
Lifetime (cycles)	Long (~ 100,000)	Long (~ 1,000,000)	Relatively short (~ 5000)

vehicle with a passive hybrid architecture. This type of vehicle is usually exposed to high requested power peaks and is limited in physical dimensions. In this respect, the selected passive configuration will reduce the weight and the volume of the system, enhance the FC system performance, and induce the absorption of the intermittent power fluctuations by the LIC. Moreover, the performance of the hybrid system is analyzed in the MATLAB/Simulink environment at different stages of the life of the FC system under three motorcycle driving cycles. The rest of this paper is organized as follows. The vehicle modeling is detailed in Section Vehicle modeling. Section Case study presents the case study conditions and the utilized evaluation metrics. In Section Results analysis, the performance analysis at different stages of the FC life is performed and discussed. Finally, the conclusion is given in Section Conclusions.

Vehicle modeling

The principal objective of the manuscript is to analyze the performance of the new proposed FC-LIC hybrid system, shown in Fig. 2a, to power up a three-wheel electric vehicle (e-TESC-3W platform). The motorcycle studied in this manuscript, shown in Fig. 2b, is a recreational electric motorcycle utilized as an experimental test bench in e-TESC laboratory at the University of Sherbrooke [18].

Table 2 presents the main characteristics of this vehicle [19]. The e-TESC-3W platform powertrain has a permanent magnet synchronous machine (28 kW and 96 V) directly connected to the rear wheel. More details of the vehicle model are explained in Ref. [18]. The developed study in this article

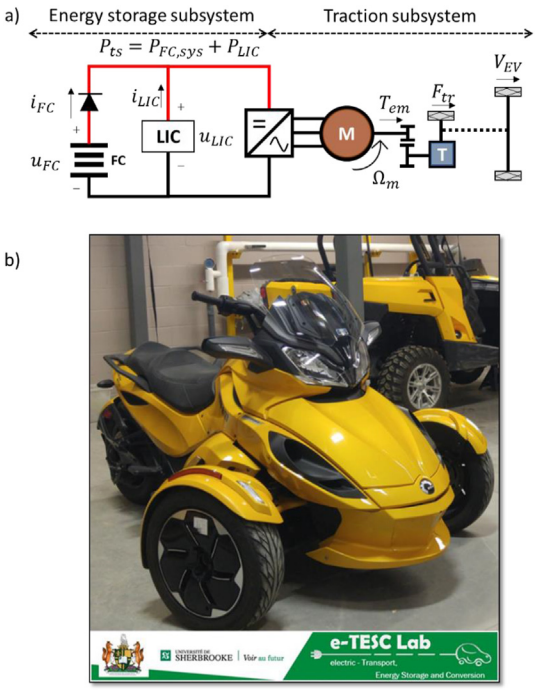

Fig. 2 – e-TESC 3 W electric vehicle platform, a) architecture powertrain, b) picture.

Please cite this article as: Macias A et al., Passive fuel cell/lithium-ion capacitor hybridization for vehicular applications, International Journal of Hydrogen Energy, https://doi.org/10.1016/j.ijhydene.2021.06.126

Table 2 – Vehicle specifications.

Variable	Symbol	Value	Units
Vehicle mass (w/o power source)	m_{eq}	350	kg
Typical rolling resistance coefficient	μ_{fr}	0.02	–
Typical aerodynamic drag coefficient	C_d	0.75	–
Vehicle front area	A_{aero}	1.25	m^2
Wheel radius	r	0.305	m
Belt transmission drive ratio	G_{gb}	5.033 (30:151)	–
Belt transmission drive efficiency	η_{gb}	95	%
Maximum vehicle speed	$V_{EV,max}$	140	km/h
Acceleration time (0–70 km/h)		8	s

focuses on the performance of the FC-LIC power supply system at different stages of the life of the system.

Usually, recreational vehicles are characterized by their high acceleration behavior, lightweight, and compactness. Following the mentioned requirements, the component size that supplies the demanded energy is first defined by considering the weight and the volume of the system. Based on the electric machine specifications, a 27.3 kW (135 cells) air-breathing FC is selected to supply the maximum stable power for a long time, imposed by the high-speed driving condition. The LICs operate as a low-pass filter, absorbing all the high-frequency components. Due to the direct coupling of the LIC bank and FC stack to the DC bus, they will share the same voltage value. To avoid any reverse current inside the FC, a diode is placed in series, as shown in Fig. 2a. Consequently, the current splitting depends on the natural behavior of each component, and is defined as follows:

$$i_{FC} = \frac{(u_{FC} - u_{LIC})}{R_D} \tag{1}$$

where R_D is the dynamic diode resistance (with diode threshold voltage neglected), and the requested current is equal to the sum of FC and LIC currents. Therefore, the FC system can be turned-off, when the LIC voltage becomes higher than the Open Circuit Voltage (OCV) of the FC. In this regard, the studied system uses 36 LICs, ULTIMO prismatic cells developed by JM Energy and JSR Micro, connected in series to assure a higher voltage at different system stages of life. Moreover, the DC bus voltage needs to be within a range of 80 V–120 V that corresponds to the input voltage of the electric motor drive. As shown in Fig. 3, the LIC bank operational voltage is within the motor drive range, and most of the FC power under the three stages of life fall in the same range. Due to the parallel connection of the FC system and LIC bank they will share the same voltage, that means a high FC power will result in a low SOC_{LIC}. It is expected that the system will operate in a range of 20%–70% of the SOC_{LIC}.

In addition, only one branch of LIC is selected in order to minimize the dimensions of the system. The LIC pack has a total energy of 157 Wh, which is enough to buffer the high dynamics. For comparison purpose, to reach the same storage of energy capacity, the mass of a SC bank is almost the double. Also, the selected LIC banks operates as a low-pass filter with a cut-off frequency of 69 mHz based on the capacitance of 91.6F and the equivalent series resistance of 25.2$m\Omega$ of the LIC pack.

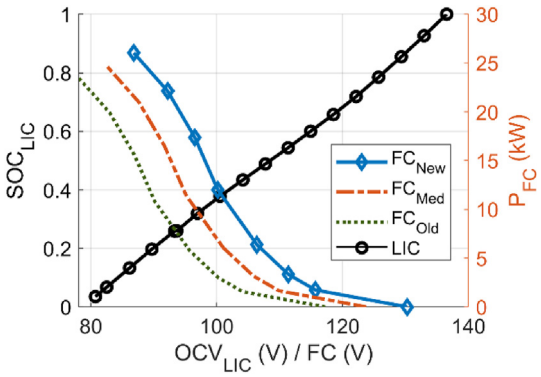

Fig. 3 – Correlation of LIC voltage with SOC and FC voltage with output power.

Traction subsystem

The traction subsystem part of the vehicle model is assumed as a static model of the electric machine and its drive, and Newton's second law is used to explain the motion interaction with the road. It is considered that an internal control loop regulates the motor torque to achieve the desired speed, considering the motor efficiency map [18]. The fundamental vehicle model equations are represented as follows:

$$\frac{dV_{EV}}{dt} = \frac{(F_{tr} - F_{env})}{m_{eq}} \tag{2}$$

$$F_{tr} = (G_{gb}/r)T_{em}\eta_{gb}^{\beta} \tag{3}$$

$$F_{env} = F_{roll} + F_{grade} + F_{air} \tag{4}$$

$$F_{roll} = m_{eq} g \mu_{fr} \cos\theta \tag{5}$$

$$F_{air} = 0.5\rho_{air} A_{aero} C_d V_{EV}^2 \tag{6}$$

$$F_{grade} = m_{eq} g \sin\theta \tag{7}$$

$$\Omega_m = (G_{gb}/r)V_{EV} \tag{8}$$

where F_{tr} is the traction force (N), F_{env} is the vehicle traction force resistance (N), m_{eq} is the vehicle mass (kg), G_{gb} is the gearbox transmission ratio, r is the wheel radius (m), T_{em} is the electric machine torque (N m), η_{gb} is the gearbox transmission efficiency, β is a discrete value that takes the value of -1 when the vehicle is in the braking mode and the value of 1 otherwise, g represents the gravity constant and θ is the slope of the road. The studied vehicle integrates a hybrid braking system in the rear wheel to recover a portion of the braking force into an electric energy. This system can recover an average of 10% from the total braking force that is distributed between the front and rear wheels, and a maximum recovered power of 10 kW. Considering that the reference torque is achieved with a drive efficiency (η_m) that considers the inverter and motor efficiency, the required power in watts into the machine to reach the desired speed, Ω_m (rad/s), is then calculated by:

$$P_{ts} = T_{em}\Omega_m\eta_m^{\beta} \tag{9}$$

Please cite this article as: Macias A et al., Passive fuel cell/lithium-ion capacitor hybridization for vehicular applications, International Journal of Hydrogen Energy, https://doi.org/10.1016/j.ijhydene.2021.06.126

The mathematical model of the vehicle was validated with an on-road driving test carried out in the e-TESC laboratory [18]. A comparison of the recorded data by the precision eDAQ acquisition system and the model estimation are shown in Fig. 4. The acquisition system is directly connected to the CAN bus and battery-management system and record the data with a frequency rate of 10 Hz. The Root Mean Square Error (RMSE) of the estimated speed is 0.42 and 1.7 for the simulated traction system power. The error value in the simulated traction power is due to the fast variations on the speed profile, resulting in rapid dynamic changes in the traction system power. This difference is also attributed to the simplified model used in the motor drive module and the used typical rolling and drag coefficients. However, for the performance assessment purpose of this paper by comparison, this model is considered adequate.

Fuel cell system

The FC system is a multiphysics element in which the voltage is influenced by external and internal factors such as current, temperature, hydrogen, and oxygen pressure. In the literature, the FC models are divided based on their physical insight and granularity in: mechanistic, black box, and semi-empirical [20]. The mechanistic models, which rely on thermodynamics, electrochemistry, and fluid mechanics differential equations, have a high computational cost. On the other hand, the black box models are straight forward but they require a big dataset to reduce the uncertainties under new operating conditions. The semi-empirical models reach an acceptable compromise between complexity and accuracy by using experimental data and electrochemical based equations. Based on the mentioned characteristics, it has been opted, in this study to use an electrochemical based Proton Exchange Membrane Fuel Cell (PEMFC) model proposed by Amphlett et al. [21]. This model considers the reversible potential E_{Nernst} (V), which is the maximum FC voltage, and the irreversible voltage losses which are: activation u_{act} (V), ohmic u_{ohmic} (V), and concentration u_{con} (V). It is assumed that all the cells (N_{FC}) in the stack have the same behavior. The PEMFC voltage u_{FC} (V) is calculated by:

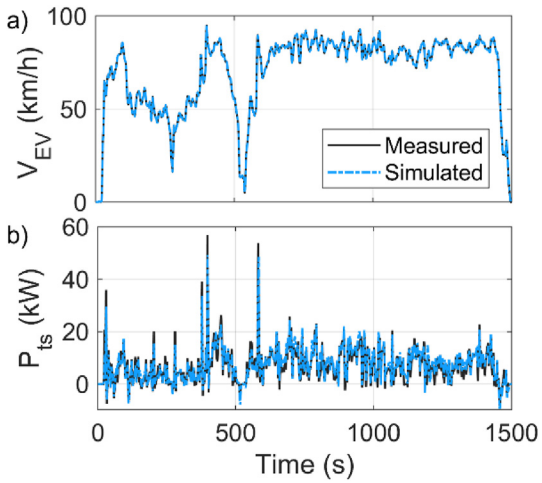

Fig. 4 – Experimental and simulation results for the three-wheel EV prototype, a) vehicle speed V_{EV} and b) requested machine power P_{ts}.

$$u_{FC} = N_{FC}(E_{Nernst} + u_{ohmic} + u_{con}) \tag{10}$$

$$E_{Nernst} = 1.229 - 0.85 \times 10^{-3}(T_{FC} - 298.15) + 4.3085 \times 10^{-5} T_{FC}\left[\ln(p_{H2}) + 0.5\ln(p_{O2})\right] \tag{11}$$

$$\begin{cases} u_{act} = \xi_1 + \xi_2 T_{FC} + \xi_3 T_{FC}\ln(CO_2) + \xi_4 T_{FC}\ln(i_{FC}) \\ C^*_{O_2} = \dfrac{p_{O2}}{5.08 \times 10^6 \exp(-498/T_{FC})} \end{cases} \tag{12}$$

$$u_{ohmic} = -i_{FC} R_{internal} = -i_{FC}(\zeta_1 + \zeta_2 T_{FC} + \zeta_3 i_{FC}) \tag{13}$$

$$u_{con} = \alpha ln(1 - i_{FC} / i_{FC,max}) \tag{14}$$

where the temperature of the stack T_{FC} is assumed to be uniform (K), p_{H2} is the hydrogen partial input pressure (Pa), p_{O2} is the oxygen partial input pressure (Pa), ξ_n (n = 1, …, 4) are empirical coefficients, $C^*_{O_2}$ is the oxygen concentration (mol/cm^3), i_{FC} is the FC operating current (A), $R_{internal}$ is the internal resistor (Ω) defined by the three empirical coefficients ζ_n (n = 1, …, 3), α is a semi-empirical parameter related to the diffusion mechanism ($0.3 \leq \alpha \leq 1.8$), and $i_{FC,max}$ is the maximum current (A). As this FC model is air-breathing, the oxygen partial pressure is approximated to 21% of the cathode pressure, which is the oxygen content of the air. Regarding the hydrogen partial pressure, it is approached to 99% of the anode pressure. The cathode pressure is computed by an empirical equation in terms of FC current, on which the airflow mainly depends. The current flow, is then calculated by:

$$p_{ca} = a_1 + a_2 i_{FC} + a_3 {i_{FC}}^2 + a_4 {i_{FC}}^3 \tag{15}$$

Where the anode inlet pressure p_{an} has been maintained at 0.2 bar above the cathode pressure p_{ca} [22]. This is to reduce the nitrogen crossover, enhance the cell stability, and purge the formed water through the cathode.

The empirical parameters of the electrochemical model are extracted offline with a metaheuristic algorithm based on the experimental dataset reported in Ref. [22]. This kind of approach has been implemented in previous works, due to their robustness, flexibility, and capabilities to compute the linear and nonlinear parameters of a PEMFC model [23]. The tuned semi-empirical model performance is compared with the single cell dataset found in the FCvelocity-9SSL Ballard datasheet, as shown in Fig. 5, and reported a RMSE of 0.0052. The polarization curve is chosen because it is one of the most common methods of testing a FC, which displays the voltage output for a given current load.

The FC thermal behavior is modeled by the conservation of energy law, which is comprehensively explained in Ref. [24]. The energy balance of the FC system temperature dynamic is calculated by:

$$\frac{dT_{FC}}{dt} = \frac{Q_{heat} - Q_{conv}}{MC_{FC}} \tag{16}$$

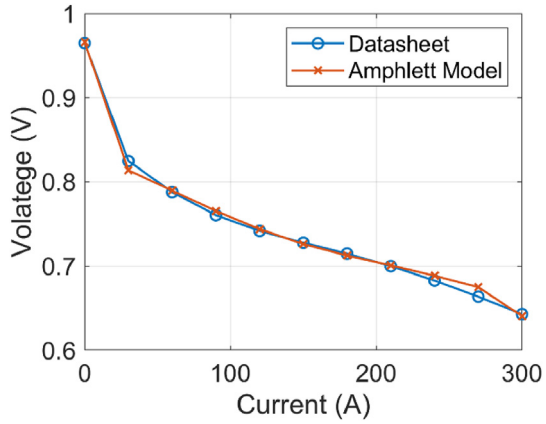

Fig. 5 – Comparison of the Amphlett model and the manufacturer polarization curve for a single cell.

$$Q_{heat} = N_{FC} i_{FC} (1.254 - u_{FC}) \quad (17)$$

$$Q_{conv} = H_{FC} (T_{FC} - T_{amb}) \quad (18)$$

where the change in the FC temperature T_{FC} (K) is generated by Q_{heat} the difference of heat in the FC (W) and Q_{conv} the heat dissipated due to convection (W). The thermal capacity of the FC MC_{FC} (J/K) and heat transfer coefficient H_{FC} (W/K) are in-depth discussed in Ref. [24].

The total FC system power $P_{FC,sys}$ (W) is obtained by subtracting the losses from the hydrogen electrochemical reaction, as shown in Eq. (13). The losses consist of fan power P_{fan} (W), which is considered as constant (200 W), and the power of the compressor P_{comp} (W).

$$P_{FC,sys} = P_{FC} - P_{comp} - P_{fan} \quad (19)$$

Based on the datasheet of the FC, the hydrogen consumption W_{H_2} (Standard Liter Per Minute), is approximated by a linear function in terms of the number of cells and the current [25].

$$W_{H_2}(t) = 0.00696 i_{FC} N_{FC} \quad (20)$$

The efficiency of the FC system is calculated considering the consumed energy by the liquid and air-cooling auxiliaries systems.

$$\eta_{FC,sys} = P_{FC,sys} / (W_{H_2} \times HHV) \quad (21)$$

where *HHV* represents the hydrogen high heating value.

Lithium-ion capacitor

A LIC is a hybrid ESS that combines the energy storage mechanisms of lithium-ion batteries and SC. This hybrid system is usually composed of a lithium-ion battery negative electrode and a SC positive electrode [14]. It can supply a relatively high energy value and high peaks of power over long cycle a life. These advantages make it suitable for hybrid electric vehicles to support the primary power supply system under high-dynamic and fast-transmit load current profiles [26]. The electrochemical process inside the LIC cell occurs within a voltage range of 2.2–3.8 V. The neutral state is considered at 3 V when no ions are absorbed at the positive electrode. In the charging process from 3 V to 3.8 V, the electrolyte salt breaks down, the Li^+ cations are intercalated in the carbon material anode, and the negative ions are adsorbed at the surface of the activated carbon electrode. The discharge from 3 V to 2.2 V generates an exchange of ions between both electrodes. The positive Li^+ ions are deintercalated from the negative electrode and adsorbed at the surface of the positive one [27].

It was previously proved that LIC technology can operate in a wide range of temperatures (−10 °C–60 °C), and its electric characteristics; capacity and equivalent resistance, presents minimal changes when it operates in a range of 25 °C–50 °C [28]. From this perspective, it is assumed that the selected LIC will operate within this temperature range and their electric properties will remain constant. Following this assumption, LIC is represented by a classical equivalent circuit model in this paper, and no thermal model is included. The classical RC model includes a capacitance element and an equivalent series resistance (ESR), as shown in Fig. 6 [29]. The self-discharge, represented as a parallel resistance with the capacitor, is omitted in this work due to the low impact in the short-term and constant operation. This self-discharge rate varies depending on the SOC level, and is approximated to be less than 1% per day [30].

During charge of the LIC, the electrical behavior is calculated as follow:

$$u_{LIC}(t) = R_{LIC} * i_{LIC}(t) + \int \frac{i_{LIC}(t)dt}{C_{LIC}} + u_C(t-1) \quad (22)$$

where at the initial state $u_c(t_0)$ is equal to the OCV of the LIC (V), i_{LIC} is the current across the LIC (A), C_{LIC} is the equivalent capacitance value of the LIC (F) and R_{LIC} is the ESR of the LIC (Ω). The equivalent constant parameters, $R_{LIC} = 1m\Omega$ and $C_{LIC} = 3300F$, are obtained from the JM Energy manufacturer datasheet. The main electric parameters of the selected LIC are presented in Table 3.

The performance of the RC model has been tested on the presented test bench in Fig. 7a. A square current signal, which charges completely the LIC up to 3.8 V with a current of 100 A and then discharge it completely until 2.2 V with a current of −100 A, was imposed as shown in Fig. 7b. The mentioned test was carried out in a climatic chamber at 40 °C in the AMPERE

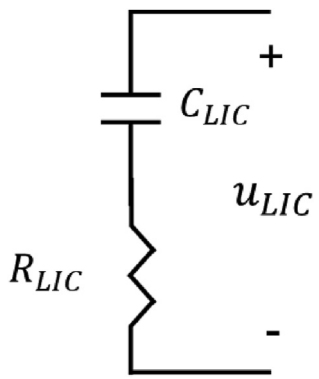

Fig. 6 – LIC equivalent circuit model.

Please cite this article as: Macias A et al., Passive fuel cell/lithium-ion capacitor hybridization for vehicular applications, International Journal of Hydrogen Energy, https://doi.org/10.1016/j.ijhydene.2021.06.126

Table 3 – 3300F ULTIMO LIC specifications.

Variable	Value	Units
Voltage range	2.2–3.8	V
Max. charging current	125	A
Max discharging current	360	A
Nominal capacitance	3300	F
Energy density	13	Wh/kg
Power density	10	kW/kg

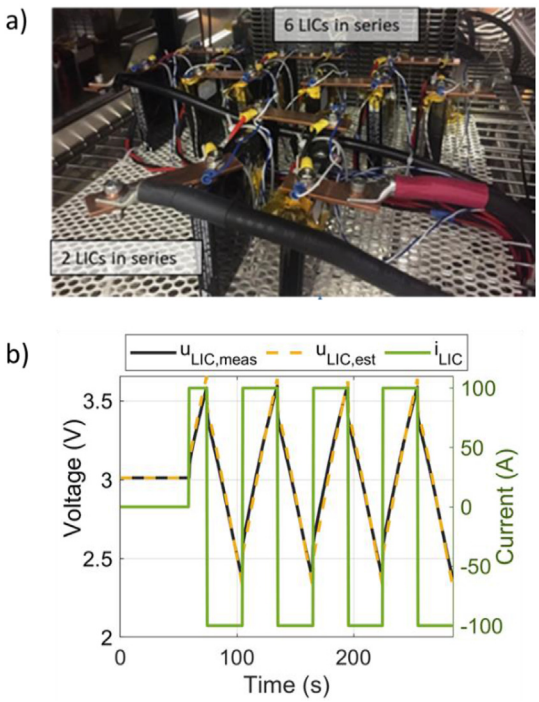

Fig. 7 – LIC test bench setup in a climatic chamber, and voltage comparison during continuous cycling of the LIC prismatic cells.

Laboratory of Lyon 1 University. The estimated output voltage of the RC model is compared with the real LIC voltage in Fig. 7b, in which the estimation reported a RMSE of 0.04. For the sake of this paper the estimation of the utilized RC model reaches an acceptable voltage approximation.

The coulomb counting method is used to calculate the LIC state of charge (SOC) due to its low computational effort and easy implementation in the simulation.

$$SOC_{LIC}(t) = SOC_{LIC}(t_0) + \frac{1}{3600C}\int i_{LIC}\,dt \tag{23}$$

where $SOC_{LIC}(t_0)$ represents the initial value of state of charge, and C is the LIC's ideal capacity (Ah). In Ref. [31], a LIC has been characterized at different ambient temperature conditions from −20 °C to 60 °C. It is observed that at 25 °C, the relationship between SOC and OCV can be represented as a linear function. Based on experimental data, a first-order function is fitted, as shown in Fig. 8, resulting in the next equation:

$$OCV_{LIC}(t) = [1.655 * SOC_{LIC}(t)] + 2.178 \tag{24}$$

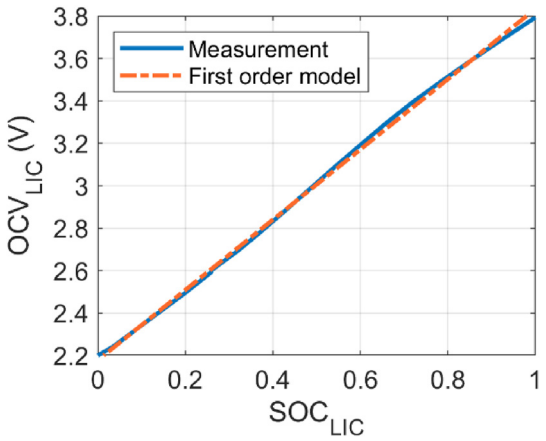

Fig. 8 – OCV-SOC correlation.

Case study

Standard driving cycles ease the evaluation of the performance and lifecycle costs of emerging vehicular technologies. They avoid bias in the performance results compared to on-drive conditions, because they represent a more distributed and richer signal built from a collection of daily and real motorcycle driving behavior from different countries. In this respect, some of the driving cycles used for the certification of motorcycles, which are all chassis-dynamometer type, are the NEDC profile by the European Union, the Class III FTP-72 profile by the United States Environmental Protection Agency (US EPA), and the Worldwide Motorcycle Test Cycle (WMTC) Class3-1 that represents an on-road worldwide vehicle operation [32]. Table 4 summarizes the main characteristics of the selected driving cycles.

Although the component size is the same in all the driving conditions, the hybridization ratio (HR) is calculated to give a clearer idea of the contribution of the LIC into the delivered power. The HR is defined as the percentage of the maximum power component of the LIC ($P_{LIC,max}$) to the maximum requested power of the traction submodule ($P_{ts,max}$).

$$HR = \frac{P_{LIC,max}}{P_{ts,max}} \tag{25}$$

System durability analysis

Most of the existing papers have merely focused on fuel consumption minimization. However, FC cost and durability are critical obstacles to speed up the FCHEV commercialization [33]. In this respect, the degradation rate is a comple-

Table 4 – Motorcycle driving cycle characteristics.

Variable	NEDC	FTP-72	WMTC
Relative positive acceleration	0.11m/s^2	0.16m/s^2	0.14m/s^2
Cycle Average Driving Speed	32.4km/h	30.6km/h	53.1km/h
Maximum speed	117km/h	88.7km/h	108.1km/h
Duration	1178s	1369s	1820s
Distance	10.62km	11.65km	26.84km

Please cite this article as: Macias A et al., Passive fuel cell/lithium-ion capacitor hybridization for vehicular applications, International Journal of Hydrogen Energy, https://doi.org/10.1016/j.ijhydene.2021.06.126

mentary metric to evaluate vehicle performance with the proposed passive configuration. Based on the US Department of Energy (DOE) objectives for vehicle application, the End of Life (EOL) of a FC is defined as a 10% drop in the maximum power, and it should be reached after 5000 h and 5000 startup/shutdown cycles. It was validated that the commercial FCs are capable of operating for 5000 h with stable current steps, but they can just perform 1300 start/stop cycles [34]. In this context, start/stop cycling and load changing conditions are responsible for more than 80% of the FC degradation. Table 5 summarizes the degradation conditions and their corresponding FC performance losses [35].

The percentage of FC degradation, Δ_{FC}, is calculated as the sum of FC degradation under each condition.

$$\Delta_{FC} = k_1 t_1 + k_2 n_1 + k_3 n_2 + k_4 t_3 + k_5 t_{FC_{ON}} \quad (26)$$

where k_1 is the low power coefficient (less than 5% of maximum power), k_2 represents one start-stop coefficient, k_3 is the fast-dynamics coefficient (absolute value of power variations more significant than 10% of maximum power per second), k_4 is the high power coefficient (more than 90% of maximum power), k_5 is the natural decay rate (the time that FC is under operation), n_j (j = 1,2) is the number of cycles, t_i ($i = 1, 2, FC_{ON}$) is the operational time in its corresponding condition. The State of Health (SOH) indicator tracks the performance evolution of the FC, due to degradation, by comparing it with the beginning of life state [36]. This degradation represents the loss of power that the FC can provide for a specific current value. Consequently, to provide the same power level with a lower SOH, the system output current needs to increase. The SOH is calculated as follows:

$$SOH_{FC} = SOH_{FC,init} - \frac{\Delta_{FC}}{\Delta_{FC,max}} \quad (27)$$

where $SOH_{FC,init}$ is the initial SOH that corresponds to the new condition (100%), and $\Delta_{FC,max}$ represents the maximum percentage of FC degradation defined by the DOE (10%).

Concerning the LIC degradation, it was proved that the LICs are a long-life energy storage system. In Ref. [13], calendar aging of the cells was assessed. When the cells were stored at a SOC of 50%, a negligible decrease of the capacitance was noticed after 20 months of aging. Moreover, when the cells were continuously cycled over the complete potential window, they were far from reaching the EOL criterion even after 450,000 cycles. These results were confirm in a second study, where a LIC has been cycled continuously with a dynamic power profile at a variable temperature for more than two years and reported just a 4% capacity loss [37]. As a result, it can be assumed that the degradation of the LIC is negligible in comparison with the FC one.

Table 5 – Coefficients of FC performance degradation.

Variable	Coefficient
k_1	0.00126 (%/h)
k_2	0.00196 (%/cycle)
k_3	5.93×10^{-5} (%/cycle)
k_4	0.00147 (%/h)
k_5	0.002 (%/h)

Results analysis

The vehicle performance using the proposed passive hybrid system is evaluated under three driving cycles considering the degradation of the FC system. This study is carried out with the e-TESC-3W platform, explained in section Vehicle modeling. As discussed in Section Case study, the LIC suffers from a small percentage of degradation compared to the FC system. In this respect, each driving cycle is implemented into an arrangement at three different stages of the FC life, namely New (SOH 100%), Med (SOH 50%) and Old (SOH 0%).

Fig. 9a shows the speed profile of the NEDC driving cycle. In this profile, the vehicle operates for almost 1000s with a speed level of less than 50 km/h, and it has several full-stop conditions. These characteristics make the FC works at low current region, as shown in Fig. 9b. Due to the series diode connected to the FC, the requested power is supplied only by the LIC bank at the beginning until its voltage level reaches the same value as the FC OCV. However, the OCV level decreases depending on the stage of health, and this makes the newer FC work sooner than the older ones, as seen in Fig. 9b. As shown in the zoom on Fig. 9b, the older FCs operate in higher currents to deliver the same requested power from the powertrain. In Fig. 9c, the LIC SOC fluctuates around different values depending on the FC SOH. Moreover, the LIC bank operates for a longer period in low power when the FC system is newer, as observed in Fig. 9d. Also, from Fig. 9a and d, it can be deduced that the hybridization ratio is about 12%.

Table 5 summarizes the performance metrics for the complete driving cycle. The system presents a lower hydrogen consumption in newer FCs due to their smaller current operation. However, the variation in the Δ_{FC} values are very small because most of the degradation comes from the initial

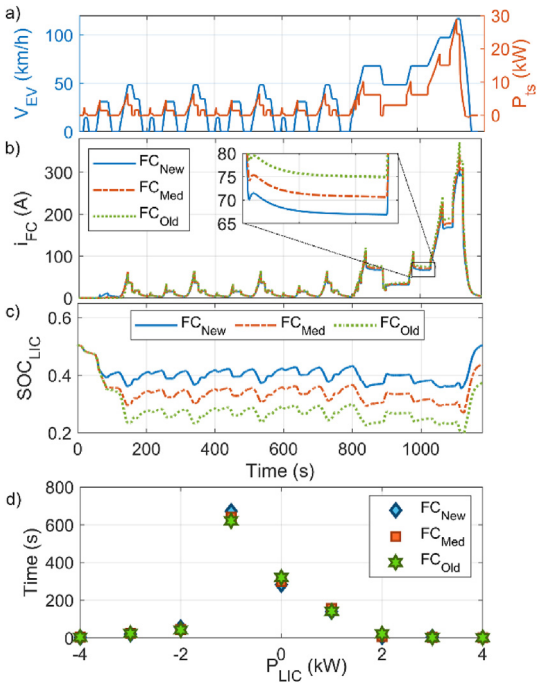

Fig. 9 – NEDC results from the Simulink model.

Please cite this article as: Macias A et al., Passive fuel cell/lithium-ion capacitor hybridization for vehicular applications, International Journal of Hydrogen Energy, https://doi.org/10.1016/j.ijhydene.2021.06.126

startup event and natural decay, which are the same for all the cases. As it is observed in Fig. 9c, the three cases have different final SOCs. The last column of Table 6 (ΔSOC_{LIC}) represents the difference between the final and initial LIC SOC. A negative ΔSOC_{LIC} implies that the LIC finishes with less energy than the initial one.

The same analysis has been followed for all the driving cycles. The second driving cycle, FTP-72, presents a high relative positive acceleration due to the consecutive high-power demand accelerations. However, it has a low average speed that makes the FC and LIC operate in low currents, as shown in Fig. 9b. It is observed that although the SOC_{LIC} drop up to a 20%, the corresponding u_{LIC} is always within the operating motor driver voltage. As shown in Fig. 10d, the LIC will operate most of the time in negative power. That means the LIC is absorbing the surplus power while the FC power is adjusted. Although the average and maximum requested power from this profile are lower compared to the previous NEDC cycle, the HR is about 30%. This results from the higher acceleration rate that requires the LIC to contribute more to the requested power peaks.

The system performance and FC degradation are summarized in Table 7. It is observed that there is a higher fuel usage in the older FC system because the old system operates at higher current values. On average, the increment of Δ_{FC} is consistent with the high relative positive acceleration of this profile. Moreover, by the time the FC gets degraded, it increases the load changes and reduces the low-power phases of the FC current trend. The FC degradation caused by load changing has a much more significant effect than low-power, as explained in Ref. [38], occasioning an increment in Δ_{FC} with older FC systems.

Table 6 – Breakdown analysis for NEDC profile.

FC	SOH_{FC}	W_{H_2} (gr)	Δ_{FC} (%)	ΔSOC_{LIC} (%)
FC_{New}	100%	58.8	0.0060	−0.1
FC_{Med}	50%	56.6	0.0062	−6.6
FC_{Old}	0%	59.6	0.0067	−13.2

Table 7 – Breakdown analysis for FTP-72 profile.

FC	SOH_{FC}	W_{H_2} (gr)	Δ_{FC} (%)	ΔSOC_{LIC} (%)
FC_{New}	100%	46.5	0.0057	−4.4
FC_{Med}	50%	48.6	0.0071	−11
FC_{Old}	0%	51.1	0.0088	−17.3

The WMTC driving cycle, shown in Fig. 11, has the highest average speed and duration. It is composed of 3 parts. The first part consists of eight micro-trips, the second part represents secondary rural roads, and the third part is a micro-trip on a highway. In the last part of the profile, as shown in Fig. 11b, it is more evident that the new FC operates at lower currents compared to the degraded FC systems. As observed in Fig. 11c, the last seconds of the driving cycle presents a low speed which allow the FC system to recharge the LIC and, in the new condition, to finish at the same initial SOC_{LIC}. From Fig. 11d, it can be noted that the LIC, as the FC, operate in higher power due to the higher average driving speed and result in a 34% of HR.

The summary of the performance analysis of the WMTC driving cycle is reported in Table 8. As expected, due to the long duration and high average speed of WMTC, the hydrogen consumption and FC degradation values are higher than the other driving cycles. The high current operation is mostly located in the third part of the driving cycle, which has an

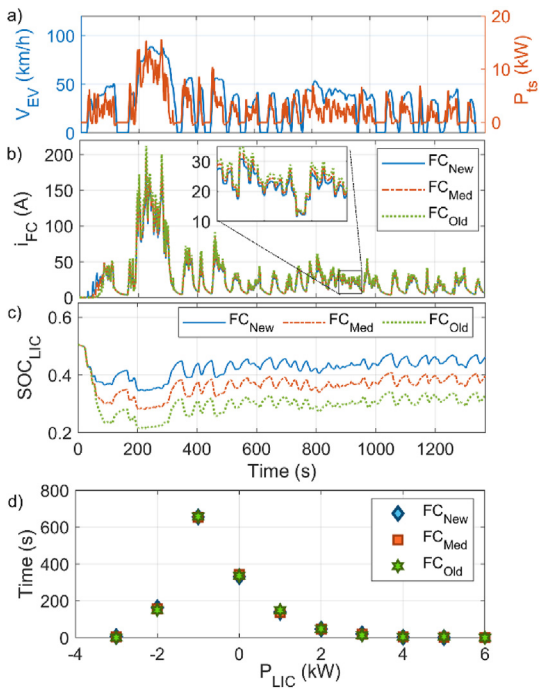

Fig. 10 – FTP-72 results from the Simulink model.

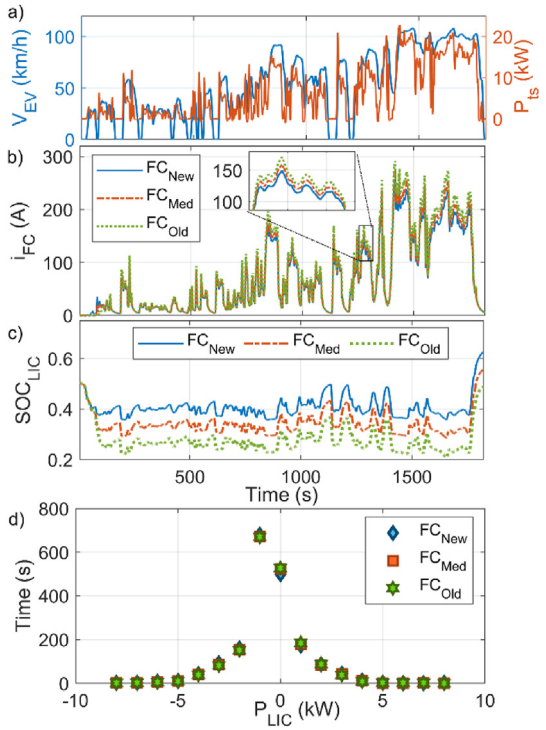

Fig. 11 – WMTC results from the Simulink model.

Please cite this article as: Macias A et al., Passive fuel cell/lithium-ion capacitor hybridization for vehicular applications, International Journal of Hydrogen Energy, https://doi.org/10.1016/j.ijhydene.2021.06.126

Table 8 – Breakdown analysis for WMTC profile.

FC	SOH_{FC}	W_{H_2} (gr)	Δ_{FC} (%)	ΔSOC_{LIC} (%)
FC_{New}	100%	164.7	0.0136	11.8
FC_{Med}	50%	174.5	0.0184	4.9
FC_{Old}	0%	185.8	0.0233	−1.7

84 km/h and a top speed of 110 km/h, and it has a long-time presence in the older systems.

In the three studied driving cycles, the FC-LIC passive hybrid system can supply the requested power and operate within the motor driver voltage range. However, the SOC_{LIC} reaches very low values in the FC_{Old} condition, that can lead to low performance of the LIC. Besides, it is difficult to compare the three life stages as there is no guarantee that they will finish in the same final SOC. In this sense, the driving profiles have been tested under different initial SOC_{LIC} levels; 0.2, 0.3, 0.4, 0.5, 0.6, 0.7 and 0.8. Fig. 12 gives a better point of comparison; it plots the hydrogen consumption for a given ΔSOC_{LIC}. The ΔSOC_{LIC} will vary depending on the performance of the FC system and the requested power behavior. It demonstrates that a system with an old FC will have a higher hydrogen consumption with any initial SOC_{LIC}. On average, compared to the FC_{New} condition, the increment in hydrogen consumption is by 12% for the FC_{Old} and 6% for the FC_{Med}. As shown in Fig. 12c, the highest hydrogen consumption in the WMTC driving cycle is in linked to the higher ΔSOC_{LIC} values.

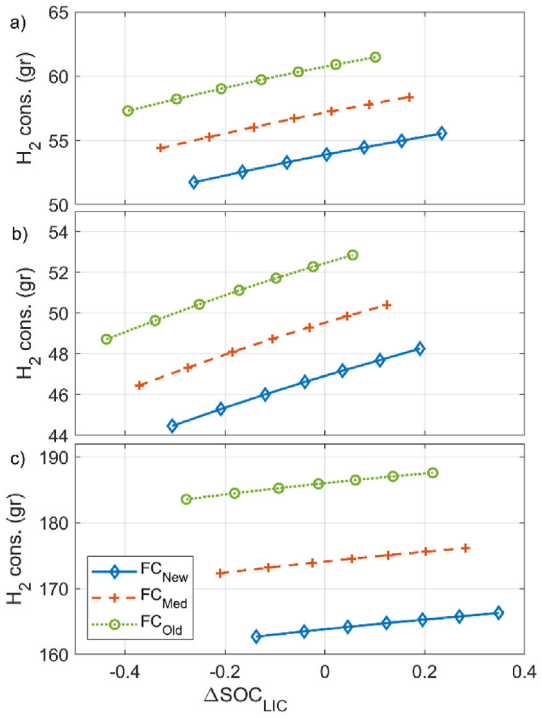

Fig. 12 – Hydrogen cons. versus ΔSOC_{LIC} for the driving cycles: a) NEDC, b) FTP-72, and c) WMTC.

Conclusions

This paper investigates vehicle performance using a new hybrid power supply system for automotive applications. The proposed system integrates a FC stack and a LIC bank in a passive configuration to furnish the requested power of a three-wheel electric motorcycle. In this respect, the power splitting is done without an energy management strategy due to the different impedance of the components connected in the DC bus. The performance assessment is done under three stages of the FC stack life, 100%, 50%, and 0% SOH. The results show that the system can supply the requested power, and the selected LIC size has enough energy to operate the DC bus between the desired voltage levels (80 V–120 V). In addition, the reported HR has a direct link to the relative positive acceleration of the driving cycle. However, the SOC_{LIC} operates at lower values by the time that the FC gets degraded.

In terms of hydrogen consumption, on average, there is an increment of 12% for the FC_{Old} and 6% for the FC_{Med} compared to the FC_{New} condition. Regarding the FC degradation, an increment in Δ_{FC} is observed in the FTP-72 and WMTC driving cycles, which has a high relative positive acceleration and more stops along with the profile. Also, according to the reported information of both profiles, it appears that the Δ_{FC} of an old FC is almost two times more than the one at the beginning of life. Based on this, it can be concluded that in the more dynamic profiles, there will be an increment of Δ_{FC} while the FC deteriorates.

Future works can consider evaluating the passive configuration in more driving conditions, as the FC hybrid system is highly nonlinear, and its performance is heavily relying on the driving conditions. While this study shows the potential of a FC-LIC passive configuration, the implementation of this hybrid system on a real test bench should be practiced in upcoming studies. In this respect, first a small-scale test will be carried out to validate the proposed architecture and then the passive FC-LIC power supply system will be implemented in the e-TESC-3W platform. It should be noted that this implementation will be the first in its class, therefore different studies are needed to make sure about its safety and system integrity. Looking forward, one of the remaining challenges to reach more affordable FC vehicles is the component sizing that is directly related to the cooperation of the hybrid system components. Therefore, future works should focus on the integration of optimized sizing methodologies that consider the hydrogen consumption and power supply system degradation into the design phase. In addition, a sensitivity analysis of the component price is recommended due to their fluctuation that vary depending on the retail, acquisition volume, and technology readiness level.

Declaration of competing interest

The authors declare that they have no known competing financial interests or personal relationships that could have appeared to influence the work reported in this paper.

Please cite this article as: Macias A et al., Passive fuel cell/lithium-ion capacitor hybridization for vehicular applications, International Journal of Hydrogen Energy, https://doi.org/10.1016/j.ijhydene.2021.06.126

Acknowledgments

This work was supported in part by the Fonds de Recherche du Québec Nature et Technologies (283370), Réseau Québécois sur l'Énergie Intelligente (3rd cycle scholarship), Grant 950-230863 and 950-230672 from Canada Research Chairs Program, and in part by Grant RGPIN-2018-06527 and RGPIN-2017-05924 from the Natural Sciences and Engineering Research Council of Canada.

Nomenclatures

Acronyms

DOE	US Department of Energy
EMS	Energy Management Strategy
EOL	End of Life
ESS	Energy Storage System
FC	Fuel Cell
FCHEV	Fuel Cell Hybrid Electric Vehicles
LIC	Lithium-Ion Capacitor
OCV	Open Circuit Voltage
RMSE	Root Mean Square Error
SC	Supercapacitor
SOH	State of Health
US EPA	United States Environmental Protection Agency
WMTC	Worldwide Motorcycle Test Cycle

REFERENCES

[1] Acar C, Dincer I. The potential role of hydrogen as a sustainable transportation fuel to combat global warming. Int J Hydrogen Energy 2018;45:3396–406. https://doi.org/10.1016/j.ijhydene.2018.10.149.

[2] Ao Y, Laghrouche S, Depernet D, Chen K. Lifetime prediction for proton exchange membrane fuel cell under real driving cycles based on platinum particle dissolve model. Int J Hydrogen Energy 2020;45:32388–401. https://doi.org/10.1016/j.ijhydene.2020.08.188.

[3] Wang J. System integration, durability and reliability of fuel cells: challenges and solutions. Appl Energy 2017;189:460–79. https://doi.org/10.1016/j.apenergy.2016.12.083.

[4] Bendjedia B, Rizoug N, Boukhnifer M, Bouchafaa F, Benbouzid M. Influence of secondary source technologies and energy management strategies on Energy Storage System sizing for fuel cell electric vehicles. Int J Hydrogen Energy 2018;43:11614–28. https://doi.org/10.1016/j.ijhydene.2017.03.166.

[5] Wang XR, Ma Y, Gao J, Li T, Jiang GZ, Sun ZY. Review on water management methods for proton exchange membrane fuel cells. Int J Hydrogen Energy 2020;46:12206–29. https://doi.org/10.1016/j.ijhydene.2020.06.211.

[6] Das HS, Tan CW, Yatim AHM. Fuel cell hybrid electric vehicles: a review on power conditioning units and topologies. Renew Sustain Energy Rev 2017;76:268–91. https://doi.org/10.1016/j.rser.2017.03.056.

[7] Yue M, Jemei S, Gouriveau R, Zerhouni N. Review on health-conscious energy management strategies for fuel cell hybrid electric vehicles: degradation models and strategies. Int J Hydrogen Energy 2019;44:6844–61. https://doi.org/10.1016/j.ijhydene.2019.01.190.

[8] Hu X, Zou C, Tang X, Liu T, Hu L. Cost-optimal energy management of hybrid electric vehicles using fuel cell/battery health-aware predictive control. IEEE Trans Power Electron 2019;35:382–92. https://doi.org/10.1109/TPEL.2019.2915675.

[9] Wu X, Hu X, Yin X, Li L, Zeng Z, Pickert V. Convex programming energy management and components sizing of a plug-in fuel cell urban logistics vehicle. J Power Sources 2019;423:358–66. https://doi.org/10.1016/j.jpowsour.2019.03.044.

[10] Arora D, Bonnet C, Mukherjee M, Raël S, Lapicque F. Direct hybridization of PEMFC and supercapacitors: effect of excess hydrogen on a single cell fuel cell durability and its feasibility on fuel cell stack. Electrochim Acta 2019;310:213–20. https://doi.org/10.1016/j.electacta.2019.04.073.

[11] Lü X, Qu Y, Wang Y, Qin C, Liu G. A comprehensive review on hybrid power system for PEMFC-HEV: issues and strategies. Energy Convers Manag 2018;171:1273–91. https://doi.org/10.1016/j.enconman.2018.06.065.

[12] Dépature C, Macías A, Jácome A, Boulon L, Solano J, Trovão JP. Fuel cell/supercapacitor passive configuration sizing approach for vehicular applications. Int J Hydrogen Energy 2020;45:26501–12. https://doi.org/10.1016/j.ijhydene.2020.05.040.

[13] Ghossein NE, Sari A, Venet P. Effects of the hybrid composition of commercial lithium-ion capacitors on their floating aging. IEEE Trans Power Electron 2019;34:2292–9. https://doi.org/10.1109/TPEL.2018.2838678.

[14] Lamb JJ, Burheim OS. Lithium-ion capacitors: a review of design and active materials. Energies 2021;14:979. https://doi.org/10.3390/en14040979.

[15] Nadeem F, Hussain SMS, Tiwari PK, Goswami AK, Ustun TS. Comparative review of energy storage systems, their roles, and impacts on future power systems. IEEE Access 2019;7:4555–85. https://doi.org/10.1109/ACCESS.2018.2888497.

[16] Soltani M, Ronsmans J, Kakihara S, Jaguemont J, Van den Bossche P, van Mierlo J, Noshim O. Hybrid battery/lithium-ion capacitor energy storage system for a pure electric bus for an urban transportation application. Appl Sci 2018;8:1176. https://doi.org/10.3390/app8071176.

[17] Goussian A, LeBel F-A, Trovão JP, Boulon L. Passive hybrid energy storage system based on lithium-ion capacitor for an electric motorcycle. J Energy Storage 2019;25:100884. https://doi.org/10.1016/j.est.2019.100884.

[18] Trovão JPF, Roux M, É M, Dubois MR. Energy- and power-split management of dual energy storage system for a three-wheel electric vehicle. IEEE Trans Veh Technol 2017;66:5540–50. https://doi.org/10.1109/TVT.2016.2636282.

[19] Macías A, Kandidayeni M, Boulon L, Trovão J. Passive and active coupling comparison of fuel cell and supercapacitor for a three-wheel electric vehicle. Fuel Cell 2019;20:351–61. https://doi.org/10.1002/fuce.201900089.

[20] Kandidayeni M, Macias A, Amamou AA, Boulon L, Kelouwani S, Chaoui H. Overview and benchmark analysis of fuel cell parameters estimation for energy management purposes. J Power Sources 2018;380:92–104. https://doi.org/10.1016/j.jpowsour.2018.01.075.

[21] Mann RF, Amphlett JC, Hooper MAI, Jensen HM, Peppley BA, Roberge PR. Development and application of a generalised steady-state electrochemical model for a PEM fuel cell. J Power Sources 2000;86:173–80. https://doi.org/10.1016/S0378-7753(99)00484-X.

[22] Zhao X, Li Y, Liu Z, Li Q, Chen W. Thermal management system modeling of a water-cooled proton exchange membrane fuel cell. Int J Hydrogen Energy 2015;40:3048–56. https://doi.org/10.1016/j.ijhydene.2014.12.026.

[23] Kandidayeni M, Macias A, Khalatbarisoltani A, Boulon L, Kelouwani S. Benchmark of proton exchange membrane fuel

cell parameters extraction with metaheuristic optimization algorithms. Energy 2019;183:912–25. https://doi.org/10.1016/j.energy.2019.06.152.
[24] Oruganti PS, Ahmed Q, Jung D. Effects of thermal and auxiliary dynamics on a fuel cell based range extender. SAE Technical Paper; 2018. https://doi.org/10.4271/2018-01-1311.
[25] Ballard Power Systems. FCvelocity-9SSL V4 product manual and integration guide. 2017. https://www.ballard.com/docs/default-source/spec-sheets/fcvelocity9ssl.pdf?sfvrsn=4aebc380_4. [Accessed 14 June 2021].
[26] Zhang L, Wilkinson DP, Chen Z, Zhang J. Lithium-ion supercapacitors: fundamentals and energy applications. 1st ed. Boca Raton: CRC Press/Taylor & Francis; 2018.
[27] Ghossein NE, Sari A, Venet P. Nonlinear capacitance evolution of lithium-ion capacitors based on frequency- and time-domain measurements. IEEE Trans Power Electron 2018;33:5909–16. https://doi.org/10.1109/TPEL.2017.2745716.
[28] Barcellona S, Piegari L. A lithium-ion capacitor model working on a wide temperature range. J Power Sources 2017;342:241–51. https://doi.org/10.1016/j.jpowsour.2016.12.055.
[29] Soltani M, Beheshti SH. A comprehensive review of lithium ion capacitor: development, modelling, thermal management and applications. J Energy Storage 2020;34:102019. https://doi.org/10.1016/j.est.2020.102019.
[30] Li X, Huang Z, Tian Y, Tian J. Modeling and comparative analysis of a lithium-ion hybrid capacitor under different temperature conditions. Int J Energy Res 2020;44:3801–20. https://doi.org/10.1002/er.5168.
[31] Soltani M, De Sutter L, Ronsmans J, van Mierlo J. A high current electro-thermal model for lithium-ion capacitor technology in a wide temperature range. J Energy Storage 2020;31:101624. https://doi.org/10.1016/j.est.2020.101624.
[32] Giakoumis EG. Motorcycles. In: Giakoumis Evangelos G, editor. Driving and engine cycles, giakoumis EG. Switzerland: Springer International Publishing; 2017. p. 167–91.
[33] Kurnia JC, Sasmito AP. Hydrogen fuel cell in vehicle propulsion: performance, efficiency, and challenge. In: Sulaiman SA, editor. Energy efficiency in mobility systems. Singapore: Springer; 2020. p. 9–26.
[34] Vichard L, Petrone R, Harel F, Ravey A, Venet P, Hissel D. Long term durability test of open-cathode fuel cell system under actual operating conditions. Energy Convers Manag 2020;212:112813. https://doi.org/10.1016/j.enconman.2020.112813.
[35] Song K, Chen H, Wen P, Zhang T, Zhang B, Zhang T. A comprehensive evaluation framework to evaluate energy management strategies of fuel cell electric vehicles. Electrochim Acta 2018;292:960–73. https://doi.org/10.1016/j.electacta.2018.09.166.
[36] Vichard L, Harel F, Ravey A, Venet P, Hissel D. Degradation prediction of PEM fuel cell based on artificial intelligence. Int J Hydrogen Energy 2020;45:14953–63. https://doi.org/10.1016/j.ijhydene.2020.03.209.
[37] Soltani M, Ronsmans J, Van Mierlo J. Cycle life and calendar life model for lithium-ion capacitor technology in a wide temperature range. J Energy Storage 2020;31:101659. https://doi.org/10.1016/j.est.2020.101659.
[38] Zhang T, Wang P, Chen H, Pei P. A review of automotive proton exchange membrane fuel cell degradation under start-stop operating condition. Appl Energy 2018;223:249–62. https://doi.org/10.1016/j.apenergy.2018.04.049.

Please cite this article as: Macias A et al., Passive fuel cell/lithium-ion capacitor hybridization for vehicular applications, International Journal of Hydrogen Energy, https://doi.org/10.1016/j.ijhydene.2021.06.126

Chapter 5 - Conclusion

As one of the power source options for the transition to electric vehicles, there have been considerable breakthroughs in the last years on implementing hydrogen FC systems in vehicular applications. However, there is a lack of research on FC systems for recreational vehicle applications, which represent a new challenge due to their dimensions constraints and aggressive power profiles. In this regard, this thesis focuses on defining the most suitable power source system configuration and energy management strategies for an electric motorcycle. Driven by this motivation, an experimental-based simulator for the Can-Am Spyder electric vehicle as to the case study and a two-step optimization sizing method are developed, as illustrated in chapter 2 of this dissertation. In addition, a sensitivity analysis is carried out for a multi-objective cost function that considers the hydrogen consumption, the system's cost, and the lifetime of the system. This study shows that EMS leads to a 5% reduction in the trip cost when proper sizing is utilized for each set of weights. Hence, special attention needs to be paid to selecting the component prices to avoid negative impacts on the sizing and EMS performance.

After defining the two-step optimization method, chapter 3 presents a benchmark study of three optimized FC-SC configurations: full-active, semi-active, and passive. It is observed that the trip cost of the proposed passive connection is 14.8% less than the full-active configuration and 6.4% less than the semi-active configuration for a WMTC standard driving profile. Furthermore, the passive configuration presents 6.3% less cost in the on-road case than the other configurations. The results of this chapter provide concrete proof of the potential of the passive topology in the Spyder recreational vehicle. The above benchmark

methodology proposed can serve as a general way to dimension the power components of a vehicle and as a basis to study the effect of different cost functions.

After defining that passive configuration is the most suitable configuration for the motorcycle, this thesis aims at proposing the integration of LIC and FC in a passive hybrid configuration. To do so, chapter 4 put forward a proof-of-concept simulation based on LIC semi-empirical model that can represent the different electric behavior phases. According to this study, the passive topology can supply the requested power along different FC stages of life and reported an increment of 12% of hydrogen consumption at the oldest condition compared to the new condition. Moreover, the LIC operates as a low-pass filter leaving the FC with a more stable power profile. As a result of the presented prelaminar test, it has been observed that the FC-LIC configuration results in a lighter, more compact, more efficient, and more straightforward configuration. This study opens up the way to new research works to implement the FC-LIC configuration as a power supply system.

5.1 Future works

Accordingly, the above conclusions show a promising electric configuration for FC hydrogen vehicles, that can result in a simple implementation, self-management, low asset cost, compact and light power supply system. Despite all the propositions, the future of this concept is highly dependent on the manufacturing trends and costs. Nonetheless, the essence of the proposed approaches should be considered in future architecture that present hard dimensional constraints and high-power profiles. Looking forward to this thesis work, the following attempts should be made to improve the proposed system architecture:

5.1.1 Improvement on the fuel cell/supercapacitor passive configuration implementation

As discussed throughout this thesis, the passive configuration refers to the directly connection of the power source to the DC bus in the FCHEV. This configuration benefits from less weight, cost, and energy losses than the active one. Throughout this thesis work, it has been identified that the FC-SC coupling is a good candidate due to its low-pass filter nature, higher specific power, longer lifespan, and broader operating temperature range than batteries. However, the downside of passive configuration is that the power split between the FC system and SC is based on the natural characteristics of each source.

One solution to this problem is to indirectly control the FC power with a water management, humidity regulation, temperature control, and/or hydrogen pressure. These FC local controls have a significant impact on the energetic efficiency of the stack and are intrinsic correlated between each other [94]. In fact, a water overflow or dehydration in the FC affects its performance and the lifetime [95, 96]. The appearance of water in the anode or cathode will affect the service life of the catalyst, reduce the flow rate of the hydrogen, and might cause the sack to stop working. On the other hand, if the moisture in the membrane is insufficient, the transmission efficiency of hydrogen ions will be greatly reduced, the catalyst layer micropores on the cathode side will be blocked and the stack will be flooded. Proper water management can prolong the FC service life, while ensuring a stable performance of the system, and increasing the hydrogen utilization rate that will improve the efficiency of FC. Hence, the water content of the membrane can be managed, to boost the efficiency, with different means, such as anode/cathode purge, hydrogen recirculation system, cooling system and gas humidifier [97]. Operating the FC at the right high temperature can improve the FC

performance because of higher gas diffusivity and membrane conductivity [98, 99]. But, if temperature becomes too high the saturated vapor pressure will increase, the water content in the membrane will decrease and its internal resistance will increase too, resulting in low FC performance. And, operating at low values will result in a decrement of the electrochemical reaction rate and vapor pressure saturation, that will result in accumulation of water in the cathode. In [100], it is shown that if the FC follows the right reference temperature will lead to provide the requested power with the minimum current level, that minimize the hydrogen consumption. Finally, a suitable air stoichiometric ratio and a fueling regulator can improve the generated power, fuel economy, system performance and reduce the internal reactant gas starvation [101, 102]. In the case that the anode of the FC lacks hydrogen, it will cause severe carbon corrosion in the outlet region of the anode with an increment of temperature at the inlet region, which will result in an uneven current density distribution inside the FC [103].

5.1.2 Benchmark study of hybrid-electric configurations for Fuel cell/Lithium-ion capacitor

While this thesis provides the basis for FC-LIC passive configurations for vehicular applications, looking forward, future work should focus on benchmarking the different hybrid configurations for a FC-LIC power supply. In this respect, a two-step optimization method with a nested structure to obtain a system-level economic-based optimal solution, presented in Chapter 2 -, can perform a fair performance comparison of the system configurations. Furthermore, the proposed cost function attempts to compromise the system degradation and fuel consumption defined goals using a weighted sum approach, which is widely practiced in the literature. Also, additional work should be made to verify the

conclusions of this work by a real-time implementation of the FC-LIC configuration. In this respect, it should be evaluated the complete balance of plant of the FC system; that includes the air compressor, cooling system, and hydrogen tank for the recreational vehicle case study.

Another variable in the sizing problem to take into account is the utilized driving cycle, since it can generate specific system sizing, that can mislead the performance results. Robust optimization has become a method of choice for optimization to incorporate uncertainty into mathematical programming models. An implementation of a two-stage robust optimization has been implemented in a mobile facility fleet sizing, and reported optimal solutions for varying degrees of uncertainty in demand [104]. The implementation of a robust optimization method can improve the benchmark results of the FC and ESS sizing.

Although the integration of LIC technology in a hybrid FC system has been discussed in very few works, numerous sizing methods have been successfully implemented in different hybrid systems [65, 105]. Based on the works mentioned above, a new sizing strategy for FC hybrid configurations could be put forward to choose the optimal FC frequency operation based on degradation, performance, or efficiency criteria. This approach has been put in place in [106], where a power splitting is based on the load power frequency decomposition. The presented results show that a frequency separation rule-based method enabled supplying sources to be close to their nominal operating points while increasing their lifetime. Another work that has proven the effectiveness of this method is [107], where a power control strategy with an adjustable cut-off frequency is developed to split the load current between a FC and SC adaptively. The objective is to let the low-frequency portion of the load to the FC, and the SC handles the higher frequency ones. The cut-off frequency in the low-pass filter is adaptively controlled by the load frequency spectrum area ratio that changes based on the SC

SOC. In this respect, a more precise FC degradation model is required to operate under dynamic profiles as presented in the automotive application.

5.1.3 Improvement of online parameter identification for lithium-ion capacitor models

The new trend of vehicles focuses on electric powertrains, which has made the energy storage systems (ESS) a critical piece for their development. In this respect, the safety and management systems of ESSs require improvement. Therefore, significant research attention is focused on battery management systems, parameters identification, and state of charge estimation for batteries and SCs [108-110]. However, few works have investigated these parameters for the lithium-ion capacitor (LIC) [51]. Since the LIC is a hybrid technology composed of a battery and SC pole, it faces similar challenges, such as non-linearity, degradation effects, and influence of external environmental conditions. Therefore, further advancement is required to have higher accuracy in state of power (SOP) and SOC estimation for LICs. The SOP and SOC estimation will enhance EVs' system lifetime and driving safety. Particular attention should be paid to some of the foremost implementation factors of the data-driven algorithms in terms of data preprocessing, hyperparameter adjustment, evaluation criteria, computational cost, and robustness. In this context, a recursive filter-based parameter identification model of the LIC has been developed to improve its state of charge estimation [111]. A dual-estimators algorithm combines an adaptive square root cubature Kalman filter to estimate the state variable and the variable forgetting factor recursive least square to update model parameters that improve state estimation accuracy. However, this method has been evaluated in a simple equivalent circuit model. Another aspect of the thesis that can be further developed is implementing and testing an already

proved data-driven; novel multi-model fusion equivalent circuit, model, and state estimation algorithm; forgetting factor recursive extended least squares, under different temperatures conditions and stages of health [112]. A further idea to extend the prospects of this thesis in this direction is the capacity estimation by using the state of charge and transferred charge.

References

[1] A. Méjean, C. Guivarch, J. Lefèvre, and M. Hamdi-Cherif, "The transition in energy demand sectors to limit global warming to 1.5 °C," *Energy Efficiency,* vol. 12, pp. 441-462, February 01 2019.

[2] Z. Li, A. Khajepour, and J. Song, "A comprehensive review of the key technologies for pure electric vehicles," *Energy,* vol. 182, pp. 824-839, 2019/09/01/ 2019.

[3] Z. P. Cano, D. Banham, S. Ye, A. Hintennach, J. Lu, M. Fowler*, et al.*, "Batteries and fuel cells for emerging electric vehicle markets," *Nature Energy,* vol. 3, pp. 279-289, 2018/04/01 2018.

[4] Y. Wang, B. Seo, B. Wang, N. Zamel, K. Jiao, and X. C. Adroher, "Fundamentals, Materials, and Machine Learning of Polymer Electrolyte Membrane Fuel Cell Technology," *Energy and AI,* p. 100014, 2020/06/29/ 2020.

[5] M. A. Hannan, M. M. Hoque, A. Mohamed, and A. Ayob, "Review of energy storage systems for electric vehicle applications: Issues and challenges," *Renewable and Sustainable Energy Reviews,* vol. 69, pp. 771-789, 2017.

[6] B. Bendjedia, N. Rizoug, M. Boukhnifer, F. Bouchafaa, and M. Benbouzid, "Influence of secondary source technologies and energy management strategies on Energy Storage System sizing for fuel cell electric vehicles," *International Journal of Hydrogen Energy,* vol. 43, pp. 11614-11628, 2018/06/21/ 2018.

[7] Q. Xun, Y. Liu, and E. Holmberg, "A Comparative Study of Fuel Cell Electric Vehicles Hybridization with Battery or Supercapacitor," in *2018 International Symposium on Power Electronics, Electrical Drives, Automation and Motion (SPEEDAM)*, 2018, pp. 389-394.

[8] C. Raga, A. Barrado, H. Miniguano, A. Lazaro, I. Quesada, and A. Martin-Lozano, "Analysis and Sizing of Power Distribution Architectures Applied to Fuel Cell Based Vehicles," *Energies,* vol. 11, p. 2597, 2018.

[9] V. K. Kasimalla, N. S. G., and V. Velisala, "A review on energy allocation of fuel cell/battery/ultracapacitor for hybrid electric vehicles," *International Journal of Energy Research,* vol. 42, pp. 4263-4283, 2018.

[10] H. S. Das, C. W. Tan, and A. H. M. Yatim, "Fuel cell hybrid electric vehicles: A review on power conditioning units and topologies," *Renewable and Sustainable Energy Reviews,* vol. 76, pp. 268-291, 2017.

[11] R. C. Samsun, C. Krupp, S. Baltzer, B. Gnörich, R. Peters, and D. Stolten, "A battery-fuel cell hybrid auxiliary power unit for trucks: Analysis of direct and indirect hybrid configurations," *Energy Conversion and Management,* vol. 127, pp. 312-323, 2016.

[12] R. Á. Fernández, F. B. Cilleruelo, and I. V. Martínez, "A new approach to battery powered electric vehicles: A hydrogen fuel-cell-based range extender system," *International Journal of Hydrogen Energy,* vol. 41, pp. 4808-4819, 2016/03/02/ 2016.

[13] S. Hardman and G. Tal, "Who are the early adopters of fuel cell vehicles?," *International Journal of Hydrogen Energy,* vol. 43, pp. 17857-17866, 2018/09/13/ 2018.

[14] P. Zhang, F. Yan, and C. Du, "A comprehensive analysis of energy management strategies for hybrid electric vehicles based on bibliometrics," *Renewable and Sustainable Energy Reviews,* vol. 48, pp. 88-104, 2015/08/01/ 2015.

[15] T. Eguchi and K. Hirota, "Scooter type motorcycle equipped with fuel cell system ", 2014.

[16] Y. Makuta, Y. Horii, and K. Ikui, "Motor cycle with fuel cell and stack structure of fuel cell ", 2010.

[17] R. E. Silva Sanchez, "Contribution au pronostic de durée de vie des systèmes pile à combustible de type PEMFC," Université du Québec à Trois-Rivières, 2016.

[18] C. Dépature, "Commandes par inversion d'un véhicule à pile à combustible et supercondensateurs ", Université du Québec à Trois-Rivières, 2017.

[19] K. Ettihir, "Gestion de l'énergie intégrant les variations de comportement non modélisées dans un véhicule électrique à pile à combustible," Université du Québec à Trois-Rivières, 2017.

[20] M. Kandidayeni, "Integrating various operating conditions into real-time identification and energy management of a fuel cell vehicle," Université du Québec à Trois-Rivières, 2020.

[21] P. Micheau and M. Boisvert, "Développement et expérimentation d'une stratégie optimale de freinage régénératif pour les véhicules électriques basée sur la commande avancée du glissement de la roue," Université de Sherbrooke, 2015.

[22] J. Nadeau, "Commande prédictive nonlinéaire d'un système de freinage hybride électro-hydraulique régénératif," PhD, Université de Sherbrooke, 2017.

[23] J. P. Fernandes Trovao, A. Bouscayrol, and B. H. Nguyen, "Energy management strategies of electric and hybrid vehicles supplied by hybrid energy storage systems," Université de Sherbrooke, 2019.

[24] J. P. Fernandes Trovao, A. Khoumsi, and C. Hannachi, "Réalisation d'un banc de test échelle réduite pour l'émulation des véhicules électriques et de leurs composants," Université de Sherbrooke, 2019.

[25] I. Alvarez-Meaza, E. Zarrabeitia-Bilbao, R. M. Rio-Belver, and G. Garechana-Anacabe, "Fuel-Cell Electric Vehicles: Plotting a Scientific and Technological Knowledge Map," *Sustainability,* vol. 12, p. 2334, 2020.

[26] R. E. Yonoff, G. V. Ochoa, Y. Cardenas-Escorcia, J. I. Silva-Ortega, and L. Meriño-Stand, "Research trends in proton exchange membrane fuel cells during 2008–2018: A bibliometric analysis," *Heliyon,* vol. 5, p. e01724, 2019/05/01/ 2019.

[27] M. S. Raboaca, N. Bizon, and O. V. Grosu, "Optimal energy management strategies for the electric vehicles compiling bibliometric maps," *International Journal of Energy Research,* vol. 45, pp. 10129-10172, 2021.

[28] N. Sulaiman, M. A. Hannan, A. Mohamed, P. J. Ker, E. H. Majlan, and W. R. Wan Daud, "Optimization of energy management system for fuel-cell hybrid electric vehicles: Issues and recommendations," *Applied Energy,* vol. 228, pp. 2061-2079, 2018/10/15/ 2018.

[29] Y. Han, Q. Li, T. Wang, W. Chen, and L. Ma, "Multisource Coordination Energy Management Strategy Based on SOC Consensus for a PEMFC–Battery–Supercapacitor Hybrid Tramway," *IEEE Transactions on Vehicular Technology,* vol. 67, pp. 296-305, 2018.

[30] S. Cheng, L. Xu, K. Wu, C. Fang, J. Hu, J. Li*, et al.*, "Optimal warm-up control strategy of the PEMFC system on a city bus aimed at improving efficiency," *International Journal of Hydrogen Energy,* vol. 42, pp. 11632-11643, 2017/04/20/ 2017.

[31] P. Wu, J. Partridge, and R. Bucknall, "Cost-effective reinforcement learning energy management for plug-in hybrid fuel cell and battery ships," *Applied Energy,* vol. 275, p. 115258, 2020/10/01/ 2020.

[32] H. V. Truong, H. V. Dao, T. C. Do, C. M. Ho, X. D. To, T. D. Dang*, et al.*, "Mapping Fuzzy Energy Management Strategy for PEM Fuel Cell–Battery–Supercapacitor Hybrid Excavator," *Energies,* vol. 13, 2020.

[33] H. Lohse-Busch, K. Stutenberg, M. Duoba, X. Liu, A. Elgowainy, M. Wang*, et al.*, "Automotive fuel cell stack and system efficiency and fuel consumption based on vehicle testing on a chassis dynamometer at minus 18 °C to positive 35 °C temperatures," *International Journal of Hydrogen Energy,* vol. 45, pp. 861-872, 2020/01/01/ 2020.

[34] K. Gérardin, S. Raël, C. Bonnet, D. Arora, and F. Lapicque, "Direct Coupling of PEM Fuel Cell to Supercapacitors for Higher Durability and Better Energy Management," *Fuel Cells,* vol. 18, pp. 315-325, 2018.

[35] D. Arora, C. Bonnet, M. Mukherjee, S. Raël, and F. Lapicque, "Direct hybridization of PEMFC and supercapacitors: Effect of excess hydrogen on a single cell fuel cell durability and its feasibility on fuel cell stack," *Electrochimica Acta,* vol. 310, pp. 213-220, 2019/07/01/ 2019.

[36] Q. Xun and Y. Liu, "Evaluation of fluctuating voltage topology with fuel cells and supercapacitors for automotive applications," *International Journal of Energy Research,* vol. 0, 2019/06/07 2019.

[37] A. Macías, M. Kandidayeni, L. Boulon, and J. Trovão, "Passive and Active Coupling Comparison of Fuel Cell and Supercapacitor for a Three-Wheel Electric Vehicle," *Fuel Cells,* 2019/10/29 2019.

[38] Y. Maiket, R. Yeetsorn, W. Kaewmanee, and D. Hissel, "INVESTIGATING PERFORMANCE AND VOLTAGE DEGRADATION OF PEMFC/SUPERCAPACITOR DIRECT-HYBRIDIZATION SYSTEM," *Grand Renewable Energy proceedings,* vol. 1, p. 220, 2018.

[39] D. Arora, K. Gérardin, S. Raël, C. Bonnet, and F. Lapicque, "Effect of supercapacitors directly hybridized with PEMFC on the component contribution and the performance of the system," *Journal of Applied Electrochemistry,* 2018.

[40] B. Wu, M. A. Parkes, V. Yufit, L. De Benedetti, S. Veismann, C. Wirsching*, et al.*, "Design and testing of a 9.5 kWe proton exchange membrane fuel cell–supercapacitor passive hybrid system," *International Journal of Hydrogen Energy,* vol. 39, pp. 7885-7896, 2014.

[41] B. Morin, D. Van Laethem, C. Turpin, O. Rallières, S. Astier, A. Jaafar*, et al.*, "Direct Hybridization Fuel Cell - Ultracapacitors," *Fuel Cells,* vol. 14, pp. 500-507, 2014.

[42] B. Wu, V. Yufit, J. Campbell, G. J. Offer, R. F. Martinez-Botas, and N. P. Brandon, "Simulated and experimental validation of a fuel cell-supercapacitor passive hybrid system for electric vehicles," in *IET Hybrid and Electric Vehicles Conference 2013 (HEVC 2013)*, 2013, pp. 1-6.

[43] O. Hegazy and J. V. Mierlo, "Particle Swarm Optimization for optimal powertrain component sizing and design of fuel cell hybrid electric vehicle," in *2010 12th International Conference on Optimization of Electrical and Electronic Equipment*, 2010, pp. 601-609.

[44] R. Shimoi and Y. Ono, "Fuel cell system," Japan Patent, 2005.

[45] H. Wang, A. Gaillard, and D. Hissel, "A review of DC/DC converter-based electrochemical impedance spectroscopy for fuel cell electric vehicles," *Renewable Energy,* vol. 141, pp. 124-138, 2019/10/01/ 2019.

[46] S. Reddi Khasim and C. Dhanamjayulu, "Selection parameters and synthesis of multi-input converters for electric vehicles: An overview," *Renewable and Sustainable Energy Reviews,* vol. 141, p. 110804, 2021/05/01/ 2021.

[47] Y. Zhang, H. Liu, J. Li, M. Sumner, and C. Xia, "DC–DC Boost Converter With a Wide Input Range and High Voltage Gain for Fuel Cell Vehicles," *IEEE Transactions on Power Electronics,* vol. 34, pp. 4100-4111, 2019.

[48] A. M. A. Malkawi, A. Al-Quraan, and L. A. C. Lopes, "Extending DC Bus Signaling and Droop Control for Hybrid Storage Units to Improve the Energy Management and Voltage Regulation," *Inventions,* vol. 7, p. 55, 2022.

[49] L. Zhang, X. Hu, Z. Wang, F. Sun, and D. G. Dorrell, "A review of supercapacitor modeling, estimation, and applications: A control/management perspective," *Renewable and Sustainable Energy Reviews,* vol. 81, pp. 1868-1878, 2018.

[50] X. Lü, Y. Qu, Y. Wang, C. Qin, and G. Liu, "A comprehensive review on hybrid power system for PEMFC-HEV: Issues and strategies," *Energy Conversion and Management,* vol. 171, pp. 1273-1291, 2018/09/01/ 2018.

[51] M. Soltani and S. H. Beheshti, "A comprehensive review of lithium ion capacitor: development, modelling, thermal management and applications," *Journal of Energy Storage,* p. 102019, 2020/10/29/ 2020.

[52] N. E. Ghossein, A. Sari, and P. Venet, "Effects of the Hybrid Composition of Commercial Lithium-Ion Capacitors on Their Floating Aging," *IEEE Transactions on Power Electronics,* vol. 34, pp. 2292-2299, 2019.

[53] J. J. Lamb and O. S. Burheim, "Lithium-Ion Capacitors: A Review of Design and Active Materials," *Energies,* vol. 14, p. 979, 2021.

[54] F. Nadeem, S. M. S. Hussain, P. K. Tiwari, A. K. Goswami, and T. S. Ustun, "Comparative Review of Energy Storage Systems, Their Roles, and Impacts on Future Power Systems," *IEEE Access,* vol. 7, pp. 4555-4585, 2019.

[55] T. Li, L. Huang, and H. Liu, "Energy management and economic analysis for a fuel cell supercapacitor excavator," *Energy,* vol. 172, pp. 840-851, 2019/04/01/ 2019.

[56] R. Koubaa, S. Bacha, M. Smaoui, and k. Lotfi, "Robust optimization based energy management of a fuel cell/ultra-capacitor hybrid electric vehicle under uncertainty," *Energy,* p. 117530, 2020/04/11/ 2020.

[57] M. G. Carignano, R. Costa-Castelló, V. Roda, N. M. Nigro, S. Junco, and D. Feroldi, "Energy management strategy for fuel cell-supercapacitor hybrid vehicles based on prediction of energy demand," *Journal of Power Sources,* vol. 360, pp. 419-433, 2017/08/31/ 2017.

[58] Z. Sun, Y. Wang, Z. Chen, and X. Li, "Min-max game based energy management strategy for fuel cell/supercapacitor hybrid electric vehicles," *Applied Energy,* vol. 267, p. 115086, 2020/06/01/ 2020.

[59] C. Turpin, D. Van Laethem, B. Morin, O. Rallières, X. Roboam, O. Verdu*, et al.*, "Modelling and analysis of an original direct hybridization of fuel cells and ultracapacitors," *Mathematics and Computers in Simulation,* vol. 131, pp. 76-87, 2017.

[60] S. Ait Hammou Taleb, D. Brown, J. Dillet, P. Guillemet, J. Mainka, O. Crosnier*, et al.*, "Direct Hybridization of Polymer Exchange Membrane Surface Fuel Cell with Small Aqueous Supercapacitors," *Fuel Cells,* vol. 18, pp. 299-305, 2018.

[61] R. E. Silva, F. Harel, S. Jemeï, R. Gouriveau, D. Hissel, L. Boulon*, et al.*, "Proton Exchange Membrane Fuel Cell Operation and Degradation in Short-Circuit," *Fuel Cells,* vol. 14, pp. 894-905, 2014.

[62] M. Kaus, J. Kowal, and D. U. Sauer, "Modelling the effects of charge redistribution during self-discharge of supercapacitors," *Electrochimica Acta,* vol. 55, pp. 7516-7523, 2010/10/30/ 2010.

[63] C. Dépature, A. Macías, A. Jácome, L. Boulon, J. Solano, and J. P. Trovão, "Fuel cell/supercapacitor passive configuration sizing approach for vehicular applications," *International Journal of Hydrogen Energy,* 2020/05/30/ 2020.

[64] M. Hinaje, S. Raël, J. P. Caron, and B. Davat, "An innovating application of PEM fuel cell: Current source controlled by hydrogen supply," *International Journal of Hydrogen Energy,* vol. 37, pp. 12481-12488, 2012/09/01/ 2012.

[65] Y. Huang, H. Wang, A. Khajepour, B. Li, J. Ji, K. Zhao, *et al.*, "A review of power management strategies and component sizing methods for hybrid vehicles," *Renewable and Sustainable Energy Reviews,* vol. 96, pp. 132-144, 2018/11/01/ 2018.

[66] S. D. Gaikwad and P. C. Ghosh, "Sizing of a fuel cell electric vehicle: A pinch analysis-based approach," *International Journal of Hydrogen Energy,* vol. 45, pp. 8985-8993, 2020/03/18/ 2020.

[67] S. Palani, S. C. Subramanian, and R. Chetty, "Component Sizing Based on Multi-Objective Optimization for a Fuel Cell Hybrid Vehicle," in *2019 6th International Conference on Control, Decision and Information Technologies (CoDIT)*, 2019, pp. 434-439.

[68] T. H. Kwan, X. Wu, and Q. Yao, "Parameter sizing and stability analysis of a highway fuel cell electric bus power system using a multi-objective optimization approach," *International Journal of Hydrogen Energy,* vol. 43, pp. 20976-20992, 2018/11/08/ 2018.

[69] T. Li, H. Liu, H. Wang, and Y. Yao, "Multiobjective Optimal Predictive Energy Management for Fuel Cell/Battery Hybrid Construction Vehicles," *IEEE Access,* vol. 8, pp. 25927-25937, 2020.

[70] J. L. Sampietro, V. Puig, and R. Costa-Castelló, "Optimal Sizing of Storage Elements for a Vehicle Based on Fuel Cells, Supercapacitors, and Batteries," *Energies,* vol. 12, p. 925, 2019.

[71] H. Sadek, R. Chedid, and D. Fares, "Power sources sizing for a fuel cell hybrid vehicle," *Energy Storage,* vol. n/a, p. e124, 2019/12/30 2019.

[72] H. Jiang, L. Xu, J. Li, Z. Hu, and M. Ouyang, "Energy management and component sizing for a fuel cell/battery/supercapacitor hybrid powertrain based on two-dimensional optimization algorithms," *Energy,* vol. 177, pp. 386-396, 2019/06/15/ 2019.

[73] L. Xu, C. D. Mueller, J. Li, M. Ouyang, and Z. Hu, "Multi-objective component sizing based on optimal energy management strategy of fuel cell electric vehicles," *Applied Energy,* vol. 157, pp. 664-674, 2015/11/01/ 2015.

[74] M. Kandidayeni, J. P. Trovão, M. Soleymani, and L. Boulon, "Towards health-aware energy management strategies in fuel cell hybrid electric vehicles: A review," *International Journal of Hydrogen Energy,* vol. 47, pp. 10021-10043, 2022/02/26/ 2022.

[75] M. Yue, S. Jemei, R. Gouriveau, and N. Zerhouni, "Review on health-conscious energy management strategies for fuel cell hybrid electric vehicles: Degradation models and strategies," *International Journal of Hydrogen Energy,* vol. 44, pp. 6844-6861, 2019/02/18/ 2019.

[76] Z. Hua, Z. Zheng, E. Pahon, M.-C. Péra, and F. Gao, "Remaining useful life prediction of PEMFC systems under dynamic operating conditions," *Energy Conversion and Management,* vol. 231, p. 113825, 2021/03/01/ 2021.

[77] H. Chen, P. Pei, and M. Song, "Lifetime prediction and the economic lifetime of Proton Exchange Membrane fuel cells," *Applied Energy,* vol. 142, pp. 154-163, 2015/03/15/ 2015.

[78] K. Song, H. Chen, P. Wen, T. Zhang, B. Zhang, and T. Zhang, "A comprehensive evaluation framework to evaluate energy management strategies of fuel cell electric vehicles," *Electrochimica Acta,* vol. 292, pp. 960-973, 2018/12/01/ 2018.

[79] Y. Zhou, A. Ravey, and M.-C. Péra, "Real-time cost-minimization power-allocating strategy via model predictive control for fuel cell hybrid electric vehicles," *Energy Conversion and Management,* vol. 229, p. 113721, 2021/02/01/ 2021.

[80] A. Ceschia, T. Azib, O. Bethoux, and F. Alves, "Optimal Sizing of Fuel Cell Hybrid Power Sources with Reliability Consideration," *Energies,* vol. 13, 2020.

[81] A. Biswas and A. Emadi, "Energy Management Systems for Electrified Powertrains: State-of-the-Art Review and Future Trends," *IEEE Transactions on Vehicular Technology,* vol. 68, pp. 6453-6467, 2019.

[82] B.-H. Nguyễn, T. Vo-Duy, C. Henggeler Antunes, and J. P. F. Trovão, "Multi-objective benchmark for energy management of dual-source electric vehicles: An optimal control approach," *Energy,* vol. 223, p. 119857, 2021/05/15/ 2021.

[83] X. Meng, Q. Li, G. Zhang, and W. Chen, "Efficient Multidimensional Dynamic Programming-based Energy Management Strategy for Global Composite Operating Cost Minimization for Fuel Cell Trams," *IEEE Transactions on Transportation Electrification,* pp. 1-1, 2021.

[84] A. Macias, M. Kandidayeni, L. Boulon, and J. P. Trovão, "Fuel cell-supercapacitor topologies benchmark for a three-wheel electric vehicle powertrain," *Energy,* vol. 224, p. 120234, 2021/06/01/ 2021.

[85] G. Morrison, J. Stevens, and F. Joseck, "Relative economic competitiveness of light-duty battery electric and fuel cell electric vehicles," *Transportation Research Part C: Emerging Technologies,* vol. 87, pp. 183-196, 2018/02/01/ 2018.

[86] E. Silvas, T. Hofman, N. Murgovski, L. F. P. Etman, and M. Steinbuch, "Review of Optimization Strategies for System-Level Design in Hybrid Electric Vehicles," *IEEE Transactions on Vehicular Technology,* vol. 66, pp. 57-70, 2017.

[87] J. P. F. Trovão, M. Roux, M. É, and M. R. Dubois, "Energy- and Power-Split Management of Dual Energy Storage System for a Three-Wheel Electric Vehicle," *IEEE Transactions on Vehicular Technology,* vol. 66, pp. 5540-5550, 2017.

[88] A. Saltelli, K. Aleksankina, W. Becker, P. Fennell, F. Ferretti, N. Holst*, et al.*, "Why so many published sensitivity analyses are false: A systematic review of sensitivity analysis practices," *Environmental Modelling & Software,* vol. 114, pp. 29-39, 2019/04/01/ 2019.

[89] A. Saltelli, M. Ratto, T. Andres, F. Campolongo, J. Cariboni, D. Gatelli*, et al.*, *Global sensitivity analysis: the primer*: John Wiley & Sons, 2008.

[90] N. Andrei, "Sequential Quadratic Programming (SQP)," in *Continuous Nonlinear Optimization for Engineering Applications in GAMS Technology*, N. Andrei, Ed., ed Cham: Springer International Publishing, 2017, pp. 269-288.

[91] B. Phadermrod, R. M. Crowder, and G. B. Wills, "Importance-Performance Analysis based SWOT analysis," *International Journal of Information Management,* vol. 44, pp. 194-203, 2019/02/01/ 2019.

[92] E. G. Giakoumis, "Motorcycles," in *Driving and Engine Cycles*, E. G. Giakoumis, Ed., ed Cham: Springer International Publishing, 2017, pp. 167-191.

[93] M. Soltani, J. Ronsmans, and J. Van Mierlo, "Cycle life and calendar life model for lithium-ion capacitor technology in a wide temperature range," *Journal of Energy Storage,* vol. 31, p. 101659, 2020/10/01/ 2020.

[94] J. C. Gómez, M. Serra, and A. Husar, "Controller design for polymer electrolyte membrane fuel cell systems for automotive applications," *International Journal of Hydrogen Energy,* vol. 46, pp. 23263-23278, 2021/07/01/ 2021.

[95] X. R. Wang, Y. Ma, J. Gao, T. Li, G. Z. Jiang, and Z. Y. Sun, "Review on water management methods for proton exchange membrane fuel cells," *International Journal of Hydrogen Energy,* 2020/07/22/ 2020.

[96] Z. Liu, J. Chen, H. Liu, C. Yan, Y. Hou, Q. He*, et al.*, "Anode purge management for hydrogen utilization and stack durability improvement of PEM fuel cell systems," *Applied Energy,* vol. 275, p. 115110, 2020/10/01/ 2020.

[97] K. Ou, W.-W. Yuan, M. Choi, S. Yang, and Y.-B. Kim, "Performance increase for an open-cathode PEM fuel cell with humidity and temperature control," *International Journal of Hydrogen Energy,* vol. 42, pp. 29852-29862, 2017.

[98] Z. Song, Y. Pan, H. Chen, and T. Zhang, "Effects of temperature on the performance of fuel cell hybrid electric vehicles: A review," *Applied Energy,* vol. 302, p. 117572, 2021/11/15/ 2021.

[99] M. Kandidayeni, A. Macias, L. Boulon, and S. Kelouwani, "Investigating the impact of ageing and thermal management of a fuel cell system on energy management strategies," *Applied Energy,* vol. 274, p. 115293, 2020/09/15/ 2020.

[100] M. Kandidayeni, A. Macias, L. Boulon, and S. Kelouwani, "Efficiency Enhancement of an Open Cathode Fuel Cell through a Systemic Management," *IEEE Transactions on Vehicular Technology,* vol. 68, pp. 11462-11472, 2019.

[101] N. Bizon and P. Thounthong, "A Simple and Safe Strategy for Improving the Fuel Economy of a Fuel Cell Vehicle," *Mathematics,* vol. 9, p. 604, 2021.

[102] H. Chen, B. Liu, R. Liu, Q. Weng, T. Zhang, and P. Pei, "Optimal interval of air stoichiometry under different operating parameters and electrical load conditions of proton exchange membrane fuel cell," *Energy Conversion and Management,* vol. 205, p. 112398, 2020/02/01/ 2020.

[103] R. Lin, H. Yu, D. Zhong, L. Han, Y. Lu, S. Tang*, et al.*, "Investigation of real-time changes and recovery of proton exchange membrane fuel cell in voltage reversal," *Energy Conversion and Management,* vol. 236, p. 114037, 2021/05/15/ 2021.

[104] C. Lei, W.-H. Lin, and L. Miao, "A two-stage robust optimization approach for the mobile facility fleet sizing and routing problem under uncertainty," *Computers & Operations Research,* vol. 67, pp. 75-89, 2016/03/01/ 2016.

[105] X. Hu, J. Han, X. Tang, and X. Lin, "Powertrain Design and Control in Electrified Vehicles: A Critical Review," *IEEE Transactions on Transportation Electrification,* vol. 7, pp. 1990-2009, 2021.

[106] M. N. Boukoberine, M. F. Zia, M. Benbouzid, Z. Zhou, and T. Donateo, "Hybrid fuel cell powered drones energy management strategy improvement and hydrogen saving using real flight test data," *Energy Conversion and Management,* vol. 236, p. 113987, 2021/05/15/ 2021.

[107] Q. Xun, V. Roda, Y. Liu, X. Huang, and R. Costa-Castelló, "An adaptive power split strategy with a load disturbance compensator for fuel cell/supercapacitor powertrains," *Journal of Energy Storage,* vol. 44, p. 103341, 2021/12/01/ 2021.

[108] I. B. Espedal, A. Jinasena, O. S. Burheim, and J. J. Lamb, "Current Trends for State-of-Charge (SoC) Estimation in Lithium-Ion Battery Electric Vehicles," *Energies,* vol. 14, p. 3284, 2021.

[109] Y. Wang, J. Tian, Z. Sun, L. Wang, R. Xu, M. Li*, et al.*, "A comprehensive review of battery modeling and state estimation approaches for advanced battery management systems," *Renewable and Sustainable Energy Reviews,* vol. 131, p. 110015, 2020/10/01/ 2020.

[110] M. S. Hossain Lipu, M. A. Hannan, A. Hussain, A. Ayob, M. H. M. Saad, T. F. Karim*, et al.*, "Data-driven state of charge estimation of lithium-ion batteries: Algorithms, implementation factors, limitations and future trends," *Journal of Cleaner Production,* vol. 277, p. 124110, 2020/12/20/ 2020.

[111] H. Yang, X. Sun, Y. An, X. Zhang, T. Wei, and Y. Ma, "Online parameters identification and state of charge estimation for lithium-ion capacitor based on improved Cubature Kalman filter," *Journal of Energy Storage,* vol. 24, p. 100810, 2019/08/01/ 2019.

[112] W. Chen, C. Xu, M. Chen, K. Jiang, and K. Wang, "A novel fusion model based online state of power estimation method for lithium-ion capacitor," *Journal of Energy Storage,* vol. 36, p. 102387, 2021/04/01/ 2021.

[113] J. P. Trovao, M. R. Dubois, M. Roux, E. Menard, and A. Desrochers, "Battery and SuperCapacitor Hybridization for a Pure Electric Three-Wheel Roadster," in *2015 IEEE Vehicle Power and Propulsion Conference (VPPC)*, 2015, pp. 1-6.

[114] G. Chiappori, P. L. Moigne, P. Delarue, and M. Chemin, "Voltage Stabilization System for Stop - Start Vehicles: Systemic Approach," in *2014 IEEE Vehicle Power and Propulsion Conference (VPPC)*, 2014, pp. 1-6.

[115] Y. Wang, J. Chen, J. Liu, K. Liu, Y. Zhang, J. Wu*, et al.*, "Research and implementation of key technology of braking energy recovery system for off-highway dump truck," in *IECON 2017 - 43rd Annual Conference of the IEEE Industrial Electronics Society*, 2017, pp. 3912-3917.

Appendix A - Résumé

A.1 Introduction

L'électrification du secteur des transports fait désormais partie de l'agenda de plusieurs pays afin de réduire sa dépendance aux combustibles fossiles, car ce secteur est l'un des principaux responsables des émissions de gaz à effet de serre (37 % selon l'AIE) et d'autres polluants [1]. À cet égard, les chercheurs et les fabricants ont travaillé au développement de véhicules électriques hybrides (VEH), de véhicules électriques à batterie (VEB) et de véhicules à pile à combustible (PAC) [2]. Le VEH génère moins de pollution, mais présente toujours une dépendance aux combustibles fossiles. D'autre part, les VEB sont alimentés uniquement par les batteries internes, ce qui en fait des véhicules à émissions locales nulles. Cependant, leur temps de recharge est long et leur autonomie limitée. Et enfin, les véhicules à PAC, qui offre une solution avec des avantages intéressants à long terme: émission locale nulle, niveau élevé d'autonomie de conduite et temps de recharge rapide [3]. Néanmoins, à court terme, cette technologie est confrontée à un coût d'acquisition élevé et à une réponse dynamique lente [4]. Pour répondre à ces préoccupations, il a été prouvé que l'hybridation d'un système de PAC avec un système de stockage d'énergie (SSE), tel qu'une batterie, un supercondensateur (SC) ou un condensateur lithium-ion (LIC), peut donner lieu à un système moins cher, plus résilient et plus efficace. En outre, cette hybridation permet également au système de stocker l'énergie régénérative du mécanisme de freinage, de fournir la puissance dynamique élevée des applications des véhicules et de gérer les conditions de démarrage à froid [5]. Dans ce type de système hybride, connu sous le nom de véhicule électrique hybride à PAC, la PAC fournira la puissance basse fréquence demandée tandis que le SSE prendra

en charge les variations haute fréquence [6]. Dans la littérature, certains travaux ont déjà examiné les caractéristiques du couplage d'une PAC et d'un SSE dans les applications de véhicules [7-11]. Cependant, la plupart des études utilisent la même taille de composants pour les configurations actives et passives, alors qu'un dimensionnement précis est nécessaire pour chacun d'eux afin d'exploiter leurs forces individuelles et d'avoir une comparaison équitable.

À ce jour, l'utilisation de la technologie de l'hydrogène dans le secteur automobile a été limitée car l'infrastructure nécessaire n'a pas été suffisamment développée. Toutefois, leur commercialisation commence à décoller, puisque plus de 50 000 véhicules sont actuellement en circulation dans le monde. Les différents constructeurs automobiles ont concentré leurs efforts sur les véhicules légers pour passagers, qui représentaient les trois quarts du marché, les bus avec 15% et 10% le reste des véhicules. Parmi les véhicules commerciaux à PAC qui ont déjà été construits et testés dans des conditions routières réelles, citons le Toyota Mirai, le Hyundai Tucson et le Honda FCX Clarity 2014 [12, 13].

Suivant l'objectif de réduire l'impact environnemental du secteur des transports, ce travail de thèse se concentre sur les véhicules de loisirs, qui représentent un nouveau défi en termes de systèmes d'alimentation électrique par rapport aux véhicules électriques légers actuels. Ces types de véhicules doivent tenir compte des exigences de dimensions limitées tout en garantissant une puissance élevée, une dynamique agressive et des déplacements sur de longues distances. Par conséquent, l'intégration d'un système de PAC comme source d'alimentation réduira leur masse, le temps de remplissage/charge et augmentera leur autonomie par rapport à une configuration de batterie pure. Mais pour parvenir à des véhicules plus abordables, une attention particulière est requise au stade de la conception, ce

qui implique le choix de la technologie de le SSE, le dimensionnement des composants et la définition de la stratégie de gestion de l'énergie (SGE) [14]. À cet égard, quelques chercheurs des chez Toyota et Suzuki ont déjà commencé à travailler sur des véhicules de loisirs à pile à combustible, mais aucun véhicule commercial n'a encore été produit [15, 16].

A.2 Énoncé du problème et cadre conceptuel de la thèse

En raison de la diversité des axes de recherche dans le sujet des véhicules à PAC, une analyse documentaire spécifique approfondie est présentée ci-après. Tout d'abord, les avantages et les inconvénients de chaque topologie et la situation actuelle sont discutés. Ensuite, les méthodes les plus pertinentes de dimensionnement des sources d'énergie et de répartition de l'énergie, qui influencent considérablement les performances et le coût du système d'alimentation du véhicule, sont analysées.

Les topologies d’alimentation électrique d'un véhicule électrique hybride à PAC sont discutées dans différents travaux de la littérature et peuvent être classées en six catégories [7-11], comme le montre la Figure A.1 [10]. Les architectures totalement actives, T1 et T2, sont caractérisées par la connexion de toutes les sources d'énergie au bus continu par l'intermédiaire d'un convertisseur CC-CC, tandis que les structures semi-actives, T3, T4 et T5, ont au moins une des sources connectées directement au bus CC. Contrairement aux connexions actives, la configuration passive présentée dans T6 connecte directement le FC et l'SSE au bus CC. La principale force d'une connexion active est sa flexibilité pour ajuster la répartition de la puissance entre la PAC et l'SSE par la formulation d'un SGE, ce qui en a fait le choix habituel pour améliorer la durée de vie du système [28]. À cet égard, la topologie entièrement active a été davantage appliquée dans les applications à forte charge telles que les tramways, les bus hybrides, les navires et les excavateurs [29-32]. Dans ces applications,

la tension au niveau du bus CC doit être stable et se situer dans une plage spécifique car le variateur de moteur triphasé et les systèmes auxiliaires sont généralement couplés directement au bus CC. Cependant, un contrôle strict du convertisseur CC est nécessaire dans la structure pleinement active pour atteindre un niveau de tension stable pendant les profils de puissance à forte impulsion. La structure semi-active a été largement utilisée car le composant passif absorbe l'énergie excédentaire dans le bus, facilitant ainsi le contrôle de la répartition de puissance sur le CC. Sa principale application est dans les véhicules légers tels que Toyota Mirai, Honda Clarity, entre autres. D'autre part, le couplage passif bénéficie d'une mise en œuvre simple, d'une autogestion, d'un faible coût des actifs et d'un système léger [34, 35]. Cependant, seuls quelques travaux en dehors de cette thèse ont proposé la configuration passive pour les applications de véhicules [34-44]. Du point de vue des contraintes d'aménagement des véhicules de tourisme, les topologies T1 et T3 sont écartées de l'étude en raison de leur poids et de leurs volumes élevés, qui ne sont pas une limitation dans les véhicules à haut rendement avec plus d'espace pour placer les composants.

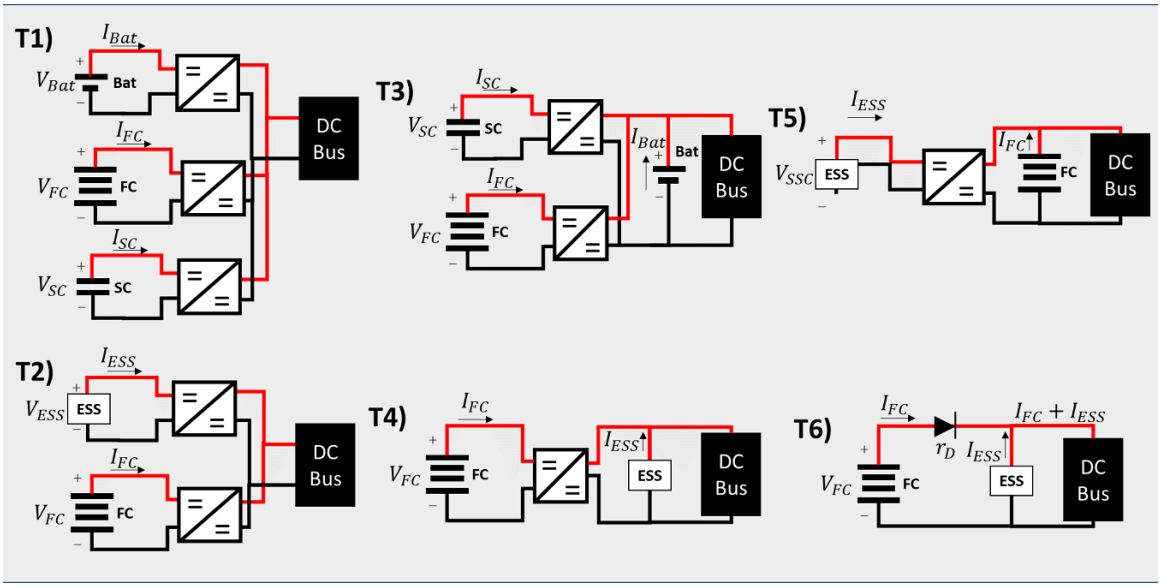

Figure A.1 Topologies d’alimentation électrique d'un véhicule électrique hybride à PAC

En se basant sur les travaux mentionnés, la batterie et le SC ont été largement utilisés dans la littérature et dans l'industrie comme SSE secondaires pour les applications embarquées [50]. La batterie rechargeable la plus couramment utilisée dans les véhicules est la batterie lithium-ion en raison de sa haute densité énergétique et de son efficacité. Cependant, ses principaux inconvénients sont sa faible densité de puissance, son cycle de vie réduit et son long temps de charge. Cependant le SC est le dispositif le plus approprié pour fournir des pics de courant rapides en raison de la formation rapide de la double couche électrique à l'interface entre les électrodes et l'électrolyte. En outre, la SC a une puissance spécifique plus élevée, une durée de vie plus longue et une meilleure résistance aux différentes températures de fonctionnement que les batteries. Néanmoins, les SCs souffrent d'une faible densité d'énergie et d'une autodécharge élevée, ce qui peut générer une demande de pic de puissance élevée si les deux systèmes n'ont pas le même potentiel électrique. Le LIC est un nouveau condensateur hybride qui présente des résultats prometteurs dans d'autres systèmes électriques, tels que les bus électriques, les tramways, les énergies renouvelables, les engins spatiaux et la connexion au réseau. Cette condensateur est composé d'une électrode positive comme le SC (charbon actif), d'une électrode négative comme la batterie (matériau en carbone pré-dopé au lithium) et d'un électrolyte contenant un sel de lithium [52]. Cette structure hybride permet d'obtenir une densité énergétique supérieure à celle d'une SC tout en conservant sa densité de puissance élevée et sa longue durée de vie. Cependant, la configuration FC-LIC n'a jamais été intégrée, ni testée dans un d'un véhicule électrique hybride à PAC pour des applications de loisirs. Les principales caractéristiques électriques des SSE susmentionnés sont illustrées à la Figure A.2 [53, 54].

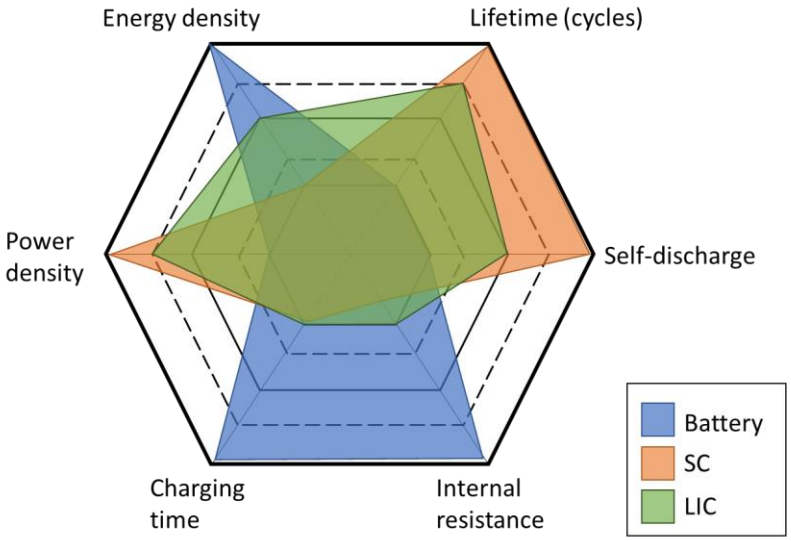

Figure A.2 Comparaison des SSE dans une carte radar

Une attention particulière doit être accordée à la sélection de l'SGE et à la méthode de dimensionnement pour éviter des conclusions trompeuses. Car, la performance d'un SGE dépend de la taille du système et cette taille va définir la plage de fonctionnement et les combinaisons possibles des états du système [65]. Un dimensionnement approprié des composants permet de réduire le coût global d'un véhicule électrique hybride à PAC tout en maintenant les performances attendues. L'utilisation d'un SGE est également nécessaire car les sources d'énergie impliquées ont des caractéristiques énergétiques différentes dans ce groupe motopropulseur hybride. Cependant, la plupart des travaux sur le véhicule électrique hybride à PAC n'analysent qu'une topologie spécifique et/ou n'utilisent pas le meilleur dimensionnement de système. Aussi, il est nécessaire d'analyser le coût des différentes tailles avec des SGE basés sur l'optimisation, comme une méthode en deux étapes qui atteint le minimum global et qui est principalement utilisée comme référence pour évaluer les nouvelles SGE et les méthodologies de dimensionnement. De plus, les quelques articles

concernant les méthodes de dimensionnement basées sur l'optimisation ne sont mis en œuvre que pour une configuration électrique hybride à PAC.

A.3 Objectifs et contributions

Comme indiqué précédemment, le choix de le SSE est une tâche importante qui est intérieurement liée au comportement du PAC et au taux de dégradation des composants. À cet égard, les conditions qui influent sur les performances et la durée de vie du PAC sont les cycles de charge, les cycles de démarrage et d'arrêt, les charges de faible puissance et les charges de forte puissance [78]. Bien que la plupart des véhicules commerciaux utilisent une batterie comme source d'énergie secondaire, le couplage d'une PAC avec un SC est plus répandu car les caractéristiques du PAC sont plus appropriées pour faire face au comportement intermittent d'un véhicule électrique hybride à PAC de loisir. En d'autres termes, le SC fonctionnera comme un filtre passe-bas qui laisse les principaux composants de la puissance demandée au système PAC. De plus, le SC rend la puissance tirée du PAC plus régulière, réduisant les changements de charge de forte puissance et permettant de faire fonctionner le PAC plus longtemps, ce qui conduit à un meilleur rendement énergétique et à une plus longue durée de vie du PAC. En outre, la SC bénéficie d'une densité de puissance élevée, d'un rendement élevé (dans la région de haute tension), d'une charge rapide, d'une large gamme de températures de fonctionnement et d'une excellente recyclabilité [49].

À cet égard, cette thèse vise à étudier l'applicabilité d'une configuration hybride de PAC pour les véhicules de loisirs. Pour combler les lacunes qui sont mises en évidence, trois objectifs principaux sont fixés.

1. Définir une méthode de dimensionnement optimal des composants qui intègre la gestion de l'énergie et une fonction de coût multi-objectif.
2. Comparer de manière exhaustive les performances de trois configurations personnalisées de systèmes énergétiques hybrides PAC-SC : active, semi-active et passive.
3. Évaluer la pertinence de l'utilisation du condensateur lithium-ion au lieu du SC comme deuxième source d'alimentation à côté du PAC dans une configuration passive.

En tant que tel, les contributions de cette thèse seront :

1. Développer un émulateur de système d'alimentation hybride PAC-SC pour un véhicule électrique de loisir à trois roues qui intègre les phénomènes de consommation d'hydrogène et de dégradation du PAC. Par rapport aux études existantes qui utilisent un pack de batteries pour alimenter un véhicule de loisirs, ce travail est le premier de sa catégorie à proposer l'utilisation de la PAC comme système d'alimentation électrique. En outre, ce système hybride peut réduire les émissions de CO_2 par rapport à un système à moteur à combustion interne et augmenter l'autonomie par rapport à un système à batterie.
2. Conception d'une méthodologie d'optimisation en deux étapes pour déterminer la taille optimale des composants du système. Il existe une variété de méthodes de dimensionnement pour les systèmes hybrides dans la littérature, mais les plus appropriées pour une étude de référence sont les méthodes séquentielles et en deux étapes basées sur l'optimisation. Cependant, ces méthodes ont tendance à utiliser une fonction de coût simple ou en temps réel pour coordonner la

répartition de la puissance du système tout en réduisant le temps de traitement. À cet égard, la fonction objective de la méthode proposée tient compte d'un coût de voyage composé de la consommation d'hydrogène, de la dégradation de la PAC, du coût opérationnel du SSE et des convertisseurs CC. En outre, elle réduit le temps de calcul et résout la non-linéarité de la fonction de coût multi-objectif en utilisant une nouvelle méthode de solution unifiée pour DP et GA. Cette méthodologie s'applique à tout véhicule électrique hybride dans lequel une PAC est couplé à un SSE secondaire.

3. Mise en œuvre d'une architecture passive PAC-SC comme système d'alimentation en énergie d'un véhicule électrique. L'architecture passive pour un système d'alimentation en énergie hybride n'a pas été largement étudiée par les chercheurs car il manque d’un contrôle direct sur les performances des composants. Cependant, cette configuration est plus légère, plus compacte et plus simple à intégrer que les autres architectures hybrides. De plus, ce système peut fournir la puissance irrégulière demandée tout en prenant soin des composants grâce à la fonction de filtrage passe-bas de SC et au rôle d'alimentation en énergie élevée de PAC.
4. Intégration du condensateur Lithium-Ion comme deuxième système d'alimentation dans une configuration passive PAC. Le LIC est un nouvel SSE qui n'a jamais été utilisé dans les systèmes PAC hybrides. Cependant, il garantit le bon fonctionnement du système PAC grâce à sa densité d'énergie et de puissance élevée

A.4 Méthodologie

Une méthodologie en six étapes a été suivie pour mener à bien cette thèse. La première étape consiste à passer en revue la littérature afin de fournir des informations sur l'état de l'art concernant le sujet proposé. A cet égard, les travaux récents relatifs aux véhicules hybrides à PAC sont étudiés et regroupés en systèmes d'alimentation et de stockage d'énergie, en méthodes de dimensionnement et en stratégies de division de puissance. Il en ressort une lacune dans la comparaison des architectures hybrides des véhicules électriques, ce qui a donné lieu à l'étude de référence développée dans ce travail de thèse. A cet égard, pour réaliser l'analyse mentionnée, la deuxième étape de ce travail consiste à développer un émulateur de la chaîne cinématique complète et des systèmes d'alimentation du véhicule étudié. Cet émulateur est conçu à partir de données expérimentales dans l'environnement MATLAB/™Simulink pour étudier les performances du système. Par rapport l'essai sur véhicule réel, un simulateur offre un gain de temps, un environnement plus sécurité, une procédure rentable et des conditions de répétabilité pour tester les systèmes électroniques de forte puissance avant une implémentation matérielle [81]. Ensuite, la troisième étape de ce projet utilise l'environnement virtuel en place pour définir une méthode de dimensionnement optimal qui permet une comparaison équitable des performances des systèmes hybrides. L'approche proposée est basée sur l'utilisation d'un algorithme d'optimisation métaheuristique et sur un partage optimal du flux de puissance entre les sources pour satisfaire la puissance demandée tout en diminuant la consommation de carburant et en améliorant la durée de vie du système. En plus de la consommation d'hydrogène qui est une préoccupation commune, le coût et la durée de vie du système sont pris en compte dans une fonction de coût multi-objectif pour laquelle une analyse de sensibilité est effectuée en

quatrième étape. À cet égard, cette analyse de sensibilité donne un aperçu de l'influence des incertitudes des paramètres d'entrée et de la fluctuation des prix sur les avantages économiques et les performances du système. Compte tenu des configurations discutées, certaines tentatives ont déjà été faites pour coupler la PAC et un SSE dans des applications embarquées. Cependant, il manque une étude de référence de la configuration de couplage pour les véhicules hybrides, ce qui donne lieu à la cinquième étape de cette thèse. Elle compare les performances du véhicule sous deux cycles de conduite standard et une condition réelle de trois architectures de taille optimale, à savoir full-active, semi-active et passive. La dernière étape de ce travail porte sur une étude de compatibilité sur l'intégration du LIC et du PAC dans une configuration hybride passive. Le choix de ce nouveau composant pour un couplage passif avec la PAC réside dans ses propriétés électriques, telles qu'une puissance et une densité d'énergie élevées. Une revue des modèles semi-empiriques qui peuvent représenter les différentes phases du comportement électrique du LIC, est effectuée pour étudier la viabilité de cette nouvelle configuration dans un environnement virtuel. En outre, sur la base de données expérimentales, le modèle sélectionné est ajusté et validé. Les performances du système sont évaluées en termes de dégradation de la PAC et de consommation d'hydrogène dans trois phases de vie différentes.

A.5 Description des résultats publiés

Une description générale des publications réalisées dans le cadre de cette thèse est présentée dans cette section. Pour chaque publication, nous détaillons les contributions, l'approche proposée et la technique adoptée de chaque sujet étudié. De la même façon, nous décrivons les aspects importants des formulations, leurs procédures et leurs résultats.

Le chapitre 2 présente qu'une méthodologie d'analyse de sensibilité est nécessaire pour mieux comprendre l'impact de la fluctuation des prix sur la taille des composants et la SGE d'un véhicule électrique hybride à PAC. Tout d'abord, une approche d'optimisation en deux étapes qui tient compte de la consommation d'hydrogène, de la dégradation du système et du coût du voyage est utilisée pour minimiser un coûts multi-objectifs. Afin d'atteindre un compromis entre les objectifs définis, on utilise une approche de somme pondérée [84]. Cependant, ces pondérations sont normalement spécifiées sur la base des prix des composants, qui varient en fonction des différentes politiques et avancées technologiques [85]. À cet égard, la méthode d'optimisation en deux étapes avec une structure emboîtée permet de trouver un compromis entre la taille des composants et les performances du système. Pour cela, l'algorithme génétique (GA) définit un dimensionnement quasi-optimal et la programmation dynamique (DP) trouve la répartition optimale de la puissance. Les pondérations utilisées décrivent l'importance de la fonction objective et sont généralement définies sur la base des prix de chaque composant qui varient en fonction des différentes politiques et de la maturité technologique.

En tant qu'étude de cas, la plateforme du véhicule Can-Am Spyder e-TESC-3W de l'Université de Sherbrooke est d'abord modélisée à l'aide du formalisme de la représentation énergétique macroscopique (REM) [87]. Cette méthode organise et montre graphiquement toutes les interactions des éléments des modèles de systèmes multiphysiques complexes. Ensuite, la méthode des boucles d'optimisation deux niveaux est mise en œuvre. Dans le contexte de ce travail, la méthode de Morris ou méthode des effets élémentaires (EE) est sélectionnée comme l'une des techniques de sélection globale convenant à l'analyse

systémique des véhicules électrique hybride à PAC, principalement en raison de sa capacité à gérer des systèmes complexes à critères multiples avec une faible complexité de calcul [89].

Les résultats de l'analyse de sensibilité des effets sur les prix des composants dans le cadre du cycle d'essai mondial des motocyclettes (WMTC) et des cycles de conduite sur route sont présentés à la Figure A.3.

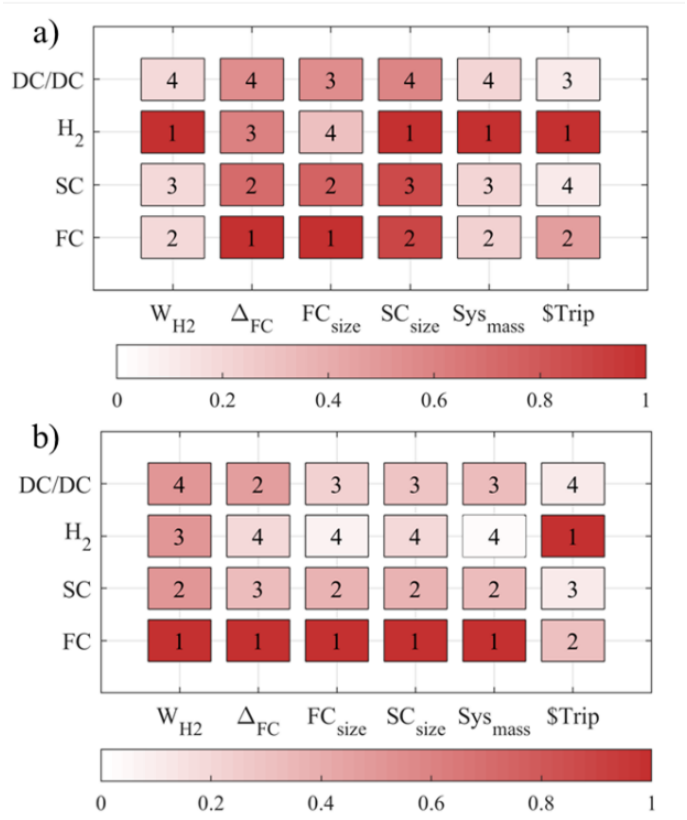

Figure A.3 Effets élémentaires de la variation du prix des composants sur les performances du système dans le cadre (a) du cycle de conduite WMTC et (b) du cycle de conduite sur route.

Le rang de chaque paramètre se trouve au centre du sous-carré, qui est défini en utilisant la moyenne des valeurs absolues des EE des prix des composants concernant les performances du système en termes de consommation d'hydrogène (W_{H_2}), de dégradation du système PAC (Δ_{FC}), de taille du PAC ($P_{FC,max}$), de taille du SC (c_{sc}), de masse du système

(m_{pow_sys}) et de coût total du voyage ($\$Trip$). On peut voir sur cette figure que les prix de l'hydrogène et du PAC sont les paramètres les plus influents dans les deux cas. En d'autres termes, cela signifie qu'une légère variation de ce paramètre aura un effet significatif sur le comportement du fractionnement et du dimensionnement de la puissance. Ces simulations indiquent que chacun d'entre eux peut donner lieu à des tailles de système et des compromis SGE différents. Ensuite, un SGE d'optimisation en ligne basé sur la programmation quadratique séquentielle est utilisé sur une configuration avec matérielle dans la boucle (HIL) à échelle réduite pour évaluer les résultats de simulation avec des poids variés. Dans cette le SC est un modèle mathématique, et le système de la PAC est le composant réel. La puissance de sortie du système PAC est mise à l'échelle après le convertisseur CC-CC pour satisfaire la puissance demandée. Le SGE a été codé dans l'environnement LabVIEW et mis en œuvre dans le module temps réel de Compact-RIO au moyen du bloc "Constrained Nonlinear Optimization virtual instrument VI". La taille du système, le coût du voyage, la consommation totale d'hydrogène et la dégradation de la PAC de trois cas de base sont comparés à deux tailles optimales et présentés dans le Tableau A-1.

Table A-1 Comparaison des performances des fonctions de coût multi-objectifs

Poids des fonctions de coût	Coût des voyages	Cons. de H2	Deg. de la PAC
Prix le plus élevé$_{référence}$	\$8.091	6.72 gr	%0.0039
PAC à bax prix$_{référence}$	\$7.065	6.73 gr	%0.0040
H2 à bax prix$_{référence}$	\$5.008	6.63 gr	%0.0055
PAC à bax prix$_{optimal}$	\$6.668	6.65 gr	%0.0040
H2 à bax prix$_{optimal}$	\$4.809	6.62 gr	%0.0055

Les résultats obtenus montrent que la modification des poids des prix dans un système des véhicules électrique hybride à PAC peut entraîner une dégradation et une consommation de combustible plus importantes tout en utilisant la même taille. Cependant, trouver un dimensionnement optimal pour chaque changement de prix dans le système peut améliorer leur performance jusqu'à 6 %. Cette recherche démontre l'impact de la variation du prix dans le véhicule électrique hybride à PAC, ce qui pourrait aider à guider le développement futur de l'industrie automobile et sa stratégie de marché. À plus détaille analyse sur le processus de dimensionnement du système et l'analyse de sensibilité sont expliquées dans l'article intitulé " Price Range Variation Impact on Optimal Sizing and Energy Management of a Hybrid Fuel Cell Vehicle ".

Le chapitre 3 présente une comparaison de trois configurations de systèmes énergétiques hybrides PAC-SC optimaux, à savoir : active, semi-active et passive, pour l'étude de cas des véhicules de loisirs. Car, dans la littérature, on constate que la plupart des travaux concentrent leurs efforts sur une seule configuration électrique, des méthodes de dimensionnement ou des stratégies de gestion de l'énergie. À cet égard, la méthode de dimensionnement en deux étapes et la fonction de coût multi-objectif présentées dans le chapitre précédent sont utilisées pour définir une taille personnalisée qui exploite les points forts de la configuration et réalise une comparaison équitable. En outre que les intérêts communs concernant le coût, la consommation d'hydrogène et la durée de vie du système, la légèreté et la compacité sont également des considérations nécessaires à la conception de ce type de véhicule. Ce chapitre examine d'abord les caractéristiques, les avantages et les inconvénients des trois configurations électriques hybrides PAC-SC. Dans un premier temps, une analyse SWOT est réalisée afin de reconnaître la configuration la plus appropriée pour le véhicule récréatif

hybride à PAC. Cette matrice est habituellement utilisée pour positionner et évaluer les ressources et l'environnement d'une organisation/système en quatre régions : Forces, Faiblesses, Opportunités et Menaces [91]. Il en ressort que les configurations actives bénéficient d'un meilleur contrôle des sources d'énergie qui se traduit par une consommation d'hydrogène et un taux de dégradation plus faibles. D'autre part, la configuration passive présente des pertes de masse et de conversion d'énergie plus faibles. À cet égard, le chapitre présenté vise à évaluer les configurations hybrides afin de définir la solution la plus avantageuse pour les véhicules de loisirs en termes de performances du système. En identifiant ces facteurs, il est possible de reconnaître ses principaux avantages pour une prise de décision, une planification et des stratégies de construction. Ensuite, un simulateur d'étude de cas est développé, dans lequel un modèle basé sur l'expérimentation pour chaque composant du véhicule électrique Can-Am Spyder est utilisé. Ensuite, la taille optimale de chaque topologie est déterminée par l'approche d'optimisation en deux étapes pour le cycle de conduite WMTC, comme le montre l'organigramme de la Figure A.4. Enfin, la taille optimale de chaque architecture est comparée en termes de coût d'investissement, de poids du système et de coût du trajet. Le coût du voyage est composé de la consommation d'hydrogène, de la dégradation de la PAC et d'un coût d'utilisation équivalent pour la SC et le convertisseur.

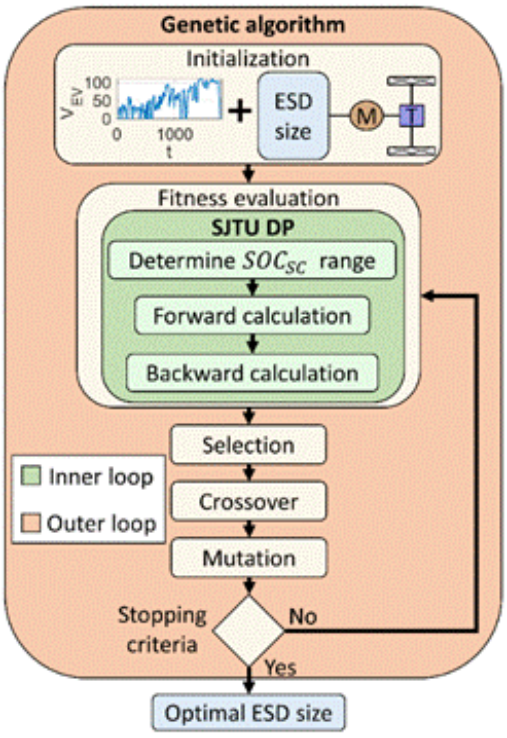

Figure A.4 Le cadre de l'optimisation en deux étapes pour le dimensionnement et le SME

Les résultats du processus d'optimisation sont résumés dans le Tableau 3 1, où sont indiqués la taille, la masse et le coût du PAC et du SC. La masse et le volume du système sont approximatifs, basés sur les fiches techniques, et le coût d'investissement est basé sur les valeurs cibles proposées par le département américain de l'énergie (DoE).

Table A-2 Résultats obtenus par la méthode d'optimisation en deux étapes

Configuration	$C_{SC,u}$	$R_{SC,u}$	Q_{max}	$N_{SC,s}$	$N_{SC,p}$	$P_{FC,max}$	Masse	Coût
Active	310 F	2.2 mΩ	202 Wh	43	15	22.2 kW	77.9 kg	$ 6424
Semi-active	310 F	2.2 mΩ	230 Wh	49	15	22.2 kW	72.3 kg	$ 5598
Passive	450 F	2.8 mΩ	241 Wh	59	9	27.3 kW	59.3 kg	$ 4721

On peut observer que la configuration active est celle qui présente la plus petite valeur de capacité, suivie par la configuration semi-active. Et la configuration passive est celle qui présente la plus grande taille de PAC et la plus grande capacité de SC. D'autre part, la configuration passive, qui n'utilise aucun convertisseur CC-CC, bénéficie d'une masse légère

et d'un faible volume. En outre, le coût d'investissement déclaré du système est plus faible dans la configuration passive que dans les autres architectures. Les coûts de déplacement détaillés de la meilleure fonction d'adaptation pour le profil WMTC et un cycle de conduite réel sont présentés à la Figure A.5. Comme les résultats du dimensionnement des composants dépendent fortement du cycle de conduite sélectionné, ils sont évalués avec un profil de conduite réel. On observe que la configuration passive a obtenu la valeur la plus faible en termes de coût de déplacement par rapport aux autres configurations. Cette performance supérieure de la configuration passive est obtenue principalement grâce à l'absence de convertisseur CC-CC. Cela réduit le coût et les pertes d'énergie et génère une consommation d'hydrogène plus faible. Cependant, les configurations actives opèrent la PAC de manière à minimiser sa dégradation.

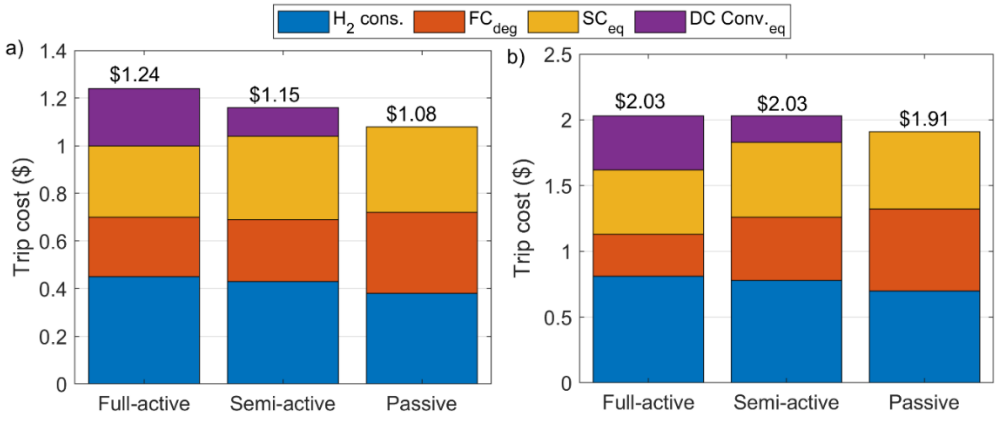

Figure A.5 Décomposition du coût du voyage, a) WMTC, b) profil de conduite réel

Le processus d'évaluation comparative des topologies des véhicules électriques est expliqué en plus détail dans un article intitulé "Fuel cell-supercapacitor topologies benchmark for a three-wheel electric vehicle powertrain". Il convient de noter qu'un article intitulé "Passive and Active Coupling Comparison of Fuel Cell and Supercapacitor for a Three-Wheel Electric Vehicle" est ajouté à l'annexe B. Cet article présente une première

tentative d'évaluation des performances des configurations passives et actives et n'a pas été placé dans cette section afin de garder ce chapitre cohérent et concis.

Le problème de référence mené dans le chapitre 3 a révélé que la configuration passive convient mieux aux véhicules de loisirs en raison de son faible poids, de son coût et de ses pertes de conversion d'énergie. Cependant, le principal inconvénient du couplage passif PAC-SC présenté est la nécessité d'une stratégie de précharge pour équilibrer le potentiel électrique de la PAC et du SC, ce qui limite le courant tiré de la PAC en augmentant le temps de démarrage et les pertes d'énergie [63]. Comme mentionné au chapitre 1, une méthode alternative à la simple résistance de précharge est l'utilisation de condensateurs hybrides lithium-ion (LIC) au lieu d'électrodes polymères poreuses comme celles présentes dans le condensateur électrique à double couche. A cet égard, le chapitre 4 présente la dernière étape du projet de doctorat que consistait à évaluer la possibilité de remplacer le SC de l'architecture proposée par un LIC. Avec cet objectif en tête, une collaboration a été mise en place entre deux laboratoires canadiens : l'Institut de recherche sur l'hydrogène de l'UQTR, le laboratoire e-TESC de l'Université de Sherbrooke et le laboratoire Ampère de l'Université de Lyon en France. À la connaissance de l'auteur, il s'agit de la première tentative d'intégration d'un LIC dans un véhicule électrique à PAC hybride. L'étude de cas choisie est la plateforme de moto e-TESC-3W avec une configuration passive qui est exposée à des pics de puissance élevés et dont les dimensions physiques sont limitées. La performance du système hybride est analysée dans l'environnement MATLAB/Simulink à différents stades de la vie du système PAC sous trois cycles de conduite de moto. À cet égard, la banque du LIC est prévue pour une valeur supérieure à la tension en circuit ouvert du système PAC à différents stades de vie du système, comme le montre la Figure A.6. De plus, la tension du bus CC se situe dans la plage

d'entraînement du moteur (80V - 120V), et la plupart de la puissance de la PAC aux trois étapes de la vie du système se situe dans la même plage. En raison de la connexion parallèle du système PAC et du LIC, ils partageront la même tension, ce qui signifie qu'une puissance FC élevée entraînera un SOC_{LIC} faible et une puissance FC faible entraînera un SOC_{LIC} élevé. On s'attend à ce que le système fonctionne dans une plage de 20 à 70 % du SOC_{LIC}.

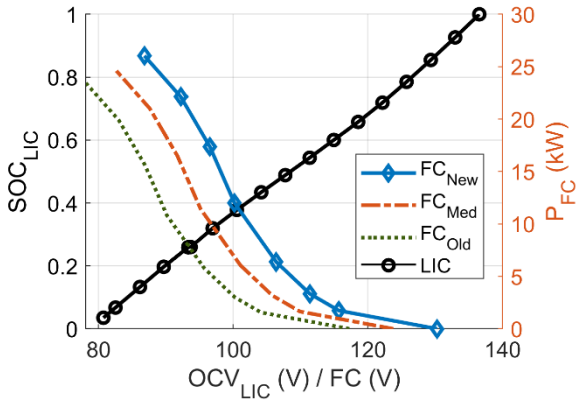

Figure A.6 Corrélation de la tension LIC avec le SOC et de la tension PAC avec la puissance de sortie.

Après avoir conçu les modèles semi-empiriques pour le sous-système de traction, le système PAC multi-physique et le stockage LIC, la performance du véhicule est évaluée sous trois cycles de conduite standard. Les profils de conduite sélectionnés sont NEDC, FTP-72 et WMTC, lesquelles sont construits à partir d'une collection de comportements de conduite quotidiens et réels de motos de différents pays. Contrairement à la plupart des travaux trouvés dans la littérature, le travail présenté dans ce chapitre intègre la décroissance de la dégradation (Δ_{FC}) comme une métrique complémentaire à l'évaluation de la performance de la consommation de combustible, comme indiqué dans la Figure A.7. La dégradation du LIC est négligée en raison de sa longue durée de vie et de son faible taux de dégradation [93]. Les systèmes dotés de PAC plus anciens consomment le plus d'hydrogène car ils fonctionnent

avec des courants plus élevés pour fournir la même puissance demandée par le groupe motopropulseur. Dans le cas du profil NEDC, les variations des Δ_{FC} sont très faibles car la plupart de la dégradation provient de l'événement initial de démarrage et de la décroissance naturelle, qui sont similaires pour tous les états. Cependant, pour le cas FTP-72, il y a un changement notoire dans la dégradation du PAC causé par l'incrément des changements de charge dans la PAC. En outre, pour le cas du profil WMTC, qui présente la vitesse moyenne et la durée les plus élevées, il est plus évident que le nouveau PAC fonctionne à des courants plus faibles que les systèmes à PAC dégradés, comme le reflète sa consommation d'hydrogène et la dégradation du PAC.

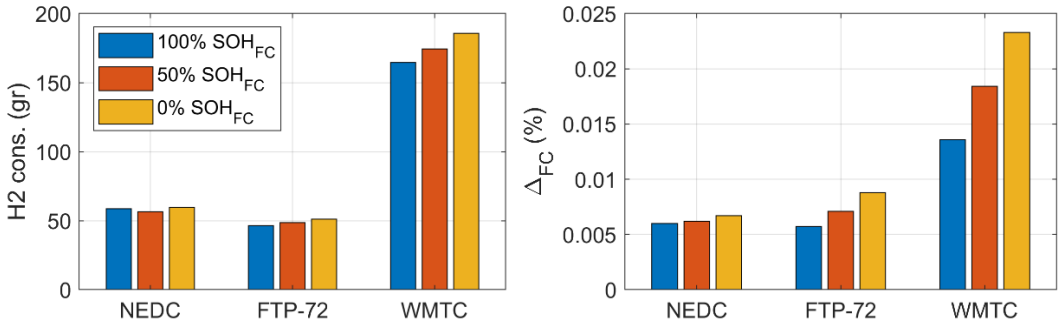

Figure A.7 Analyse de la a) consommation d'hydrogène, et b) de la dégradation de la PAC

Le test précédent montre que le système hybride passif PAC-LIC fournit complètement la puissance demandée et opère dans la plage de tension du moteur dans toutes les conditions. Cependant, en raison de l'autogestion de l'énergie, le système se termine à différents niveaux du SOC, ce qui rend la comparaison des performances difficile. Dans ce sens, la Figure A.8 montre la consommation d'hydrogène pour différents niveaux initiaux de SOC_{LIC}; 0,2, 0,3, 0,4, 0,5, 0,6, 0,7 et 0,8. Sur la base de ces résultats, il est démontré qu'un système avec un vieux FC aura une consommation d'hydrogène plus élevée avec n'importe quel SOC_{LIC} initial.

En moyenne, par rapport à la condition FC_{New}, l'augmentation de la consommation d'hydrogène est de 12 % pour le FC_{Old} et de 6 % pour le FC_{Med}.

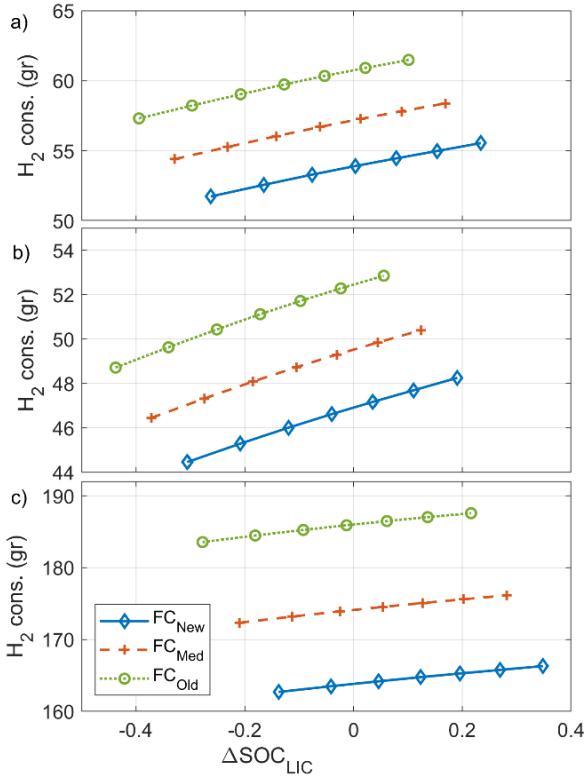

Figure A.8 Consommation d'hydrogène en fonction de ΔSOC_{LIC} pour les cycles de conduite: a) NEDC, b) FTP-72, et c) WMTC.

La combinaison du système PAC avec les mérites expliqués du LIC devrait permettre de réduire la consommation d'hydrogène et le coût d'investissement de l'ensemble du système d'alimentation électrique par rapport aux autres ESS. En outre, un intérêt industriel de ce travail est que l'architecture proposée augmente la portabilité du système, ce qui est très utile dans de nombreuses applications industrielles. L'évaluation proposée est présentée avec plus de détaille dans un article intitulé "Passive Fuel Cell/Lithium-ion Capacitor Hybridization for Vehicular Applications".

A.6 Conclusion

Des progrès considérables ont été réalisés ces dernières années dans la mise en œuvre de systèmes à base d'hydrogène pour les véhicules. Cependant, il y a un manque de recherche sur les systèmes PAC pour les applications de véhicules de loisirs, qui représentent un nouveau défi en raison de leurs contraintes de dimensions et de leurs profils de puissance agressifs. À cet égard, cette thèse se concentre sur la définition de la configuration du système de source d'énergie et des stratégies de gestion de l'énergie les plus appropriées pour une moto électrique. Poussé par cette motivation, un simulateur basé sur l'expérience pour le véhicule électrique Can-Am Spyder, qui constitue l'étude de cas de cette thèse, est développé. Pour cela, une méthodologie d'optimisation en deux étapes est conçue pour obtenir une solution optimale au niveau du système en faisant un compromis entre la taille des composants et la performance du système, comme illustré dans le chapitre 2 de cette thèse. En outre, une analyse de sensibilité est réalisée pour une fonction de coût multi-objectif qui prend en compte la consommation d'hydrogène, le coût du système et la durée de vie du système. Cette étude montre que le SGE conduit à une réduction de 5% du coût du voyage lorsque le dimensionnement approprié est utilisé pour chaque ensemble de poids. Par conséquent, une attention particulière doit être accordée à la sélection des prix des composants pour éviter les impacts négatifs sur le dimensionnement et les performances du SGE. Après avoir défini la méthode d'optimisation en deux étapes, le chapitre 3 présente une étude de référence de trois configurations FC-SC optimisées : active, semi-active et passive. On observe que le coût du trajet de la connexion passive proposée est inférieur de 14,8 % à celui de la configuration entièrement active et de 6,4 % à celui de la configuration semi-active pour un profil de conduite standard WMTC. En outre, la configuration passive présente

un coût inférieur de 6,3 % dans le cas de la route par rapport aux autres configurations. Les résultats de ce chapitre fournissent une preuve concrète du potentiel de la topologie passive dans le véhicule de loisirs Spyder. La méthodologie de référence proposée ci-dessus peut servir de moyen général pour dimensionner les composants de puissance d'un véhicule et de base pour étudier l'effet de différentes fonctions de coût. Après avoir défini que la configuration passive est la plus adaptée au véhicule étudié, cette thèse a pour objectif de proposer l'intégration du LIC et du PAC dans une configuration hybride passive. Pour ce faire, le chapitre 4 présente une simulation de preuve de concept basée sur le modèle semi-empirique du LIC qui peut représenter les différentes phases du comportement électrique. D'après cette étude, la topologie passive peut fournir la puissance demandée au cours des différentes phases de vie du véhicule et indique une augmentation de 12 % de la consommation d'hydrogène dans les conditions les plus anciennes par rapport aux nouvelles conditions. De plus, le LIC fonctionne comme un filtre passe-bas, ce qui donne au PAC un profil de puissance plus stable. Cette configuration PAC-LIC est plus légère, plus compacte, plus efficace et plus simple mettre en œuvre.

Bien que cette thèse fournisse la base des configurations passives de la PAC pour les applications embarquées, il est possible d'améliorer la mise en œuvre de la configuration passive PAC-SC en contrôlant indirectement la puissance par la gestion de l'eau, la régulation de l'humidité, le contrôle de la température et/ou la pression de l'hydrogène. Un autre point à prendre en compte dans les travaux futurs est la mise en œuvre en temps réel de la configuration passive PAC-LIC afin de vérifier les conclusions de cette thèse. En outre, une étude comparative des configurations hybrides-électriques pour la PAC-LIC pourrait apporter une meilleure compréhension de cette nouvelle configuration. Enfin, une autre idée

pour étendre les perspectives de cette thèse dans cette direction est l'estimation de la capacité en utilisant l'état de charge et la charge transférée.

Appendix B - Passive and Active Coupling Comparison of Fuel Cell and Supercapacitor for a Three-Wheel Electric Vehicle

Authors: A. Macias, M. Kandidayeni, J. Trovão, L. Boulon

Journal: Fuel Cells, John Wiley & Sons, Ltd

Publication date: 29 October 2019

DOI: https://doi.org/10.1002/fuce.201900089

B.1 Methodology

This paper proposes a proof-of-concept study for semi-active and passive configurations of a three-wheel platform (e-TESC 3W), currently used as a test bench at e-TESC laboratory of the University of Sherbrooke [113]. In this first attempt to hybridize a recreational vehicle with a FC-SC power supply system, the size of each component has been defined based on the minimum required size to provide the vehicle requested power under on-road conditions. In this manuscript, a graphical method, energetic macroscopic representation (EMR), is used to organize the complex multiphysics systems model of the e-TESC 3W platform, as shown in Figure B.1.

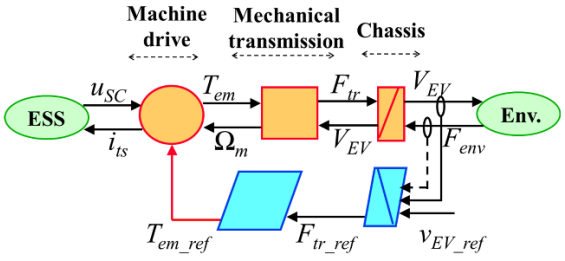

Figure B.1 Traction system of the e-TESC3W platform vehicle

The performance of the three-wheel electric vehicle is assessed by using the same component selection in both passive and active configurations. In addition, a cost function based on the system capital and trip cost was defined to evaluate both systems' performance. Passive configuration benefits from self-management and does not require the design of an EMS. However, an optimized fuzzy logic controller (FLC) is designed to deal with energy management in the active configuration. Since the comparative analysis of this work is based on a known driving cycle, the tuning parameters (membership functions and rules) of the FLC have been adjusted by a genetic algorithm to improve its performance as much as possible. The designed FLC has two inputs, requested power and SC voltage, and one output, which is the required power from the FC. The optimized reasoning rules of the FLC are presented in Figure B.2. From this figure, it is clear that the optimized EMS avoids unnecessary on-off cycles. Indeed, FLC keeps the FC stack in a very low (VL) power mode when the requested power is low, and the voltage of the SC is high. Moreover, the FC stack maintains the SC voltage at high levels to support any sudden power peaks. As a result of the optimization, the first input (P_{ts}) and output (I_{FC}) membership functions were defined with a quasi-equal distribution. On the contrary, in the second input (U_{SC}), the low level covers up to 40% of the value range, which keeps the SC within a high energy level to deal with the profile's high dynamics behavior.

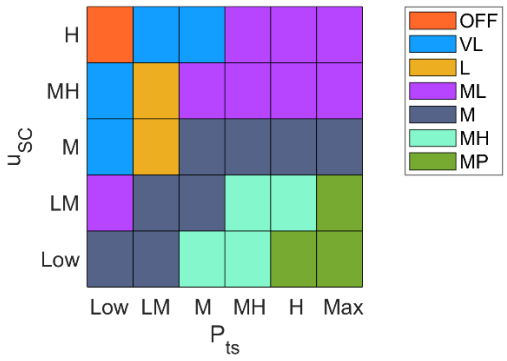

Figure B.2 Optimized rules of FLC.

B.2 Outcomes

The power distribution comparison of the semi-active and passive configurations, shown in Figure B.3, indicates that the FC stack operates mainly in a high-efficiency region in an active configuration. Furthermore, regarding the passive coupling, it is clear that the extracted power from the FC stack follows a smoother path since the SC bank functions as a low-pass filter, but this leads to operating the FC system in the low-efficiency zone.

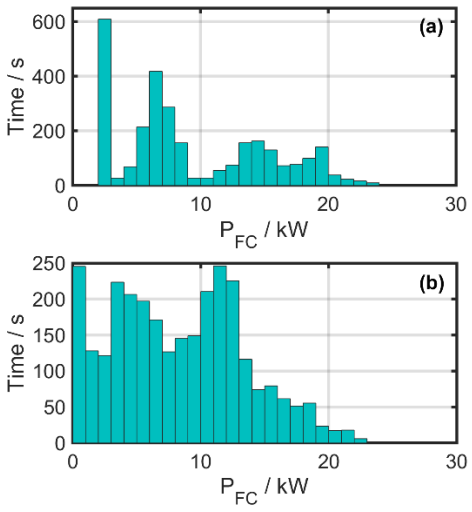

Figure B.3 FC power distribution for a) active and b) passive coupling.

FC degradation costs are $0.1825 and $0.1961, and the hydrogen consumption costs are $0.78 and $0.68, respectively, for semi-active and passive configurations. This result shows that active coupling has a 7% less FC degradation system due to managing the power between the sources. On the other hand, the passive connection consumes less hydrogen by 12% due to not having the DC-DC converter electrical losses in the system. To scrutinize the pros and cons of having a passive coupling compared to the active one, a more detailed analysis of the hourly trip cost shows that the proposed passive connection is 17% less than the studied semi-active configuration. In conclusion, although the utilized optimized EMS of semi-active configuration can diminish the FC degradation, the passive configuration reduces the capital cost and total fuel consumption resulting in 8% less trip cost. However, this conclusion is limited to combining the specific system size and the applied EMS.

DOI: 10.1002/fuce.201900089

Fuel Cells

ORIGINAL RESEARCH PAPER

Passive and Active Coupling Comparison of Fuel Cell and Supercapacitor for a Three-Wheel Electric Vehicle▲

A. Macías[1]*, M. Kandidayeni[1], L. Boulon[1,2], J. Trovão[3,4]

[1] Université du Québec à Trois-Rivières, Hydrogen Research Institute, Trois-Rivières, QC, G8Z 4M3, Canada
[2] Canada Research Chair in Energy Sources for the Vehicles of the Future, Université du Québec à Trois-Rivières,Trois-Rivières, G8Z 4M3, QC, Canada
[3] e-TESC Laboratory, Dept. Electrical & Computer Engineering, University of Sherbrooke, Sherbrooke, QC, J1K 2R1, Canada
[4] Canada Research Chair in Efficient Electric Vehicles with Hybridized Energy Storage Systems, University of Sherbrooke, QC, J1K 2R1, Canada

Received May 18, 2019; accepted September 20, 2019; published online ■■■

Abstract

The desire to reduce the power electronics related issues has turned the attentions to passive coupling of powertrain components in fuel cell hybrid electric vehicles (FCHEVs). In the passive coupling, the fuel cell (FC) stack is directly connected to an energy storage system on the DC bus as opposed to the active configuration where a DC-DC converter couples the FC stack to the DC bus. This paper compares the use of passive and active couplings in a three-wheel FCHEV to reveal their strengths and weaknesses. In this respect, a passive configuration, using a FC stack and a supercapacitor, is suggested first through formulating a sizing problem. Subsequently, the components are connected in an active configuration where an optimized fuzzy energy management strategy is used to split the power between the components. The performance of the vehicle is compared at each case in terms of capital cost and trip cost, which is composed of FC degradation and hydrogen consumption, and total cost of the system per hour. The obtained results show the superior performance of the passive configuration by 17% in terms of total hourly cost, while the active one only results in less degradation rate in the FC system.

Keywords: Active Configuration, Electric Vehicles, Fuel Cell, Hybridization, Hydrogen Car, Passive Coupling, Supercapacitor, Ultracapacitor

1 Introduction

Conventional vehicles powered by fossil fuels are considered as major contributors to air pollution and have made transportation one of the main responsible sectors for CO_2 emissions [1]. While the air pollution poses considerable risks for human health and environment, its harmful effects can be mitigated through electrification of transport systems [2]. Among the existing technologies, such as electric vehicles, hybrid electric vehicles etc., FC vehicle is one of the most auspicious due to zero-local emissions, high level of driving autonomy, and fast refueling time [3]. However, FC systems cannot tolerate sudden and significant fluctuations in the load which are normal in vehicular applications [4]. The load peaks can cause air/fuel starvation in the FC system resulting in serious power drop [5,6]. Furthermore, abrupt changes in the load have detrimental effects on the lifetime of the FC stack since it accelerates the degradation rate of the system [7,8]. Hybridization of a FC system with other sources, such as batteries and supercapacitors (SCs), has been widely used in the literature to alleviate the problems regarding the slow dynamic essence of a FC system [9]. The main goal of this hybridization is to supply the power peaks with an energy storage device and benefit from the regenerative braking mechanism. Different hybridization configurations can be found in literature [10–13]. In Ref. [12], a review of six topologies, which can be mainly fallen into two categories of active and passive, for a FCHEV is presented. Active configuration

▲ *Paper presented at the 8th International Conference on Fundamentals and Development of Fuel Cells (FDFC2019), held 12–14.02.2019 in Nantes, France.*

[*] *Corresponding author, alvaro.omar.macias.fernandez@uqtr.ca*

refers to the connection of the power source to the DC bus via a converter. In active configurations, normally, an energy management strategy (EMS) is required to perform the power split among the components while satisfying the requested power. Several EMSs from rule based and optimization based to intelligent based strategies have been proposed for such configuration [14]. Among them, fuzzy logic control (FLC) is one of the most commonly used due to the flexibility, robustness, and convenient implementation [15]. FLCs provide strategic rules by using linguistic labels. Several grounds, such as inaccurate model of a vehicle's components, nonlinearity, and unknown aspects, like traffic, weather, etc., can be mentioned for appropriateness of employing a FLC in FCHEV application. Contrary to the active configuration, passive coupling refers to the connection of the component directly to the DC bus. This kind of architecture is independent of an EMS and has self-management due to the characteristics (different impedance) of the components. The passive configuration provides similar benefits as the active architecture while it does not require any DC-DC converter saving of weight, cost, and energy losses linked with an extra level of power conversion. However, the drawback of the passive hybrid system is that the FC stack is the main responsible for supplying the requested traction power as there is no control over power regulation among the power sources. The power split between the FC system and the SCs depends on the natural behavior of each source (internal resistor and open circuit voltage for instance). Therefore, several authors refer to it as "natural energy management" [16, 17]. This can lead to the presence of higher power ripples at the FC side and consequently increase the degradation rate of the stack. In [10], the comparison of active and passive hybrid configurations of FC and battery, as an auxiliary power unit of trucks, reveals that the direct coupling of FC and battery has a better performance as long as the demanded power does not have substantial variations. However, marked fluctuations of the demanded power can make the FC operate in low-efficiency regions. The selection of active and passive configurations has been considered in a FCHEV, using a SC bank and a battery pack as the secondary power source units [11]. This study demonstrates that the active coupling of the battery with the FC stack leads to high power variations in the stack while the passive connection of FC-SC makes the requested power from the FC smoother and has a higher energetic efficiency. Although active configuration provides a better management of the components, several researchers have opted to use passive connections to reduce the complexity, cost, and weight of the system [18]. In this among, the direct connection of FC with SC, as an energy storage system, is more prevalent, compared to the battery, due to the capability of a SC in coping with intermittency of behavior in FCHEV applications. In [19–21], the main focus is on the direct hybridization of SC to a single FC. The obtained experimental results indicate that the passive connection avoids negative voltage, provides self-protection against sudden power changes, increases the dynamic of the system, and enhances the electrical performance as patented by NISSAN company [22]. In Ref. [23], the performed study takes the arrangement of SCs into consideration in the passive configuration and concludes that increasing the number of SCs reduces the power supplied by the FC as well as the hydrogen consumption, while escalating the capital cos of the system. In [24, 25], the FC-SC passive coupling is specifically used for the vehicular application. In [26], the simulation results show that direct hybridization of FC-SC benefits from high fuel economy and recovers more regenerative energy than battery due to its low internal resistance. In [27], the experimental results of a 9.5-kW proton exchange membrane FC (PEMFC) passively coupled with a SC array illustrate a reduction in dynamic load, idling time, and rapid load changes in the FC without using a DC/DC converter.

In the light of discussed manuscripts, it is obvious that some attempts have been already done regarding the direct coupling of FC and SC in vehicular applications. However, such a coupling has never been used for a recreational three-wheel electric vehicle so far. These types of vehicles are normally exposed to high dynamics and need to be light and compact. The thing that makes the choice of passive couplings interesting here is that these configurations provide low mass and compactness through elimination of power electronics. Moreover, SC, which is a prevalent component in this kind of configuration, is highly capable of dealing with high dynamics. In this regard, a comparative analysis of FC-SC passive and active configurations for a three-wheel vehicle, which has more power demand variation than conventional vehicles, is put forward in this manuscript. To do so, firstly, the minimum required size of the main components is determined in order to meet the requested power since this type of vehicle is expected to have low mass and volume. Afterwards, the performance of the three-wheel electric vehicle is assessed by using the selected components in both of passive and active configurations. Passive configuration benefits from self-management and does not require the design of an EMS. However, in the active configuration, the power split is performed by using an optimized fuzzy strategy. As opposed to other similar works which only use the hydrogen consumption as a means of comparison, a detailed performance index based on capital cost and trip cost of the system is defined in this work. Moreover, a real driving cycle from the three-wheel electric vehicle is utilized to carry out the simulation.

The remainder of this paper is organized as follows. The vehicle modeling with passive and active configurations is described in Section 2. The designed EMS for the active configuration is presented in Section 3. The obtained results of the comparative analysis are discussed in Section 4. Finally, the conclusion is given in Section 5.

2 Modeling

2.1 Components Sizing

The studied vehicle in this paper (e-TESC-3W platform shown in Figure 1) is a three-wheel electric vehicle used essentially for leisure purposes. This prototype is currently used as

Fig. 1 The studied e-TESC 3W vehicle.

a test bench at e-TESC laboratory of University of Sherbrooke [28]. The e-TESC-3W platform has a 28-kW (96 V) permanent magnet synchronous motor (PMSM) directly connected to the rear wheel. The main specifications of this vehicle are listed in Table 1 and explained thoroughly in [28]. This vehicle can reach a maximum speed of 120 km h^{-1}.

Originally, e-TESC-3W platform has been a pure battery electric vehicle (BEV). In [29], a coupling of battery, as the main power source, and the SC, as the energy storage system, is proposed for this vehicle where battery supplies the average power while the SC is held responsible for the high dynamic phase. The authors in [29] indicate that their proposed hybrid configuration can enhance the lifetime of the e-TESC 3W platform powertrain components compared to the pure BEV. The principal objective of the current manuscript is to provide a comparison of passive and active FC-SC powertrain configurations for the e-TESC 3W platform. To do so, initially, performing a component sizing to figure out the rated power of the FC and SC in relation to the requirements of the vehicle is necessary. Leisure activity vehicles are typically characterized as being light and compact, but with a high acceleration and speed capabilities. In this regard, sizing problem should ascertain the minimum required component dimensions to satisfy the requested power for all the constraints specified in Table 2 [30]. Based on the specifications, the FC needs to be sized in a way to supply the maximum power for a long distance, continuous, and high-speed driving. Otherwise the SC will get discharged quickly [31]. The FC supplies the base power (P_e) in the maximum speed condition premised on the hybrid vehicle traction force resistance (F_{env}) as:

$$P_e = F_{env} V_{EV} / (1000 \eta_t \eta_{em}) \quad (1)$$

$$F_{env} = F_{roll} + F_{grade} + F_{air} \quad (2)$$

$$F_{roll} = M_{eq}\, g\, \mu_{fr}\, cos(\theta) \quad (3)$$

$$F_{air} = 0.5 \rho_a\, A_f\, C_d\, V_{EV}^2 \quad (4)$$

$$F_{grade} = M_{eq} g\, sin(\theta) \quad (6)$$

where F_{roll} is the rolling resistance force, F_{grade} is the grade related force, F_{air} is the resistance force against the air, M_{eq} is the mass of the vehicle, g is gravity, μ_{fr} is the rolling resistance coefficient, ρ_a is the air density, C_d is the aerodynamic drag coefficient, A_f is the frontal area, V_{EV} is the vehicle speed, θ is the road grade, η_t is the transmission efficiency, and η_{em} is the motor average efficiency [32]. Solving Eq. (1) leads to the value of 26.5 kW for P_e under maximum speed condition (120 km h^{-1}) on a flat road. This value defines the size of the FC for steady conditions. Moreover, the maximum electric power for the vehicle acceleration from 0 to 120 km h^{-1} in 7 s comes to 88 kW on a flat road, obtained by:

$$P_{tot} = \left(F_{roll} + F_{grade} + F_{air} + F_{acc}\right) V_{EV} / (1,000\, \eta_t \eta_{em}) \quad (7)$$

$$F_{acc} = M_{eq} \delta d\, V_{EV} / dt \quad (8)$$

where F_{acc} is the accelerating force, and δ is the mass factor related to the rotational inertia. δ is assumed to be 1.035 for a one-speed gear-box [33].

With respect to the calculated P_{tot}, the minimum SC size should be 60.7 kW while the selected FC size is 27.3 kW (FCvelocity-9SSL) from Ballard [34, 35]. The utilized SC in this work is K2 Series from Maxwell Technologies [24]. The characteristics of the selected components are listed in Table 2.

It is worth reminding that due to the direct connection of the SC bank and FC stack in passive configuration, the SC nominal voltage needs to be higher than the open circuit voltage of the FC. In this respect, the studied system requires 50 SCs connected in series. Regarding the active configuration, a 30-kW DC/DC converter (non-isolated) with a mass around 11 kg is used [36].

The tank size selection is done by assuming a similar autonomy as the pure electric

Table 1 Vehicle specifications.

Variable	Symbol	Value	Units
Vehicle mass (w/o power source)	M_{eq}	350	kg
Typical rolling resistance coefficient	μ_{fr}	0.02	–
Typical aerodynamic drag coefficient	C_D	0.75	–
Vehicle front area	A_f	1.25	m^2
Wheel radius	r	0.305	m
Belt transmission drive ratio	G_{gb}	5.033 (30:151)	–
Belt transmission drive efficiency	η_{gb}	95	%
Maximum speed	V_{max}	120	km h^{-1}
Acceleration speed	V_{acc}	100	km h^{-1}
Acceleration time	t_{acc}	7	s
Grade slope at 100 km/h	θ	0.03	%

ORIGINAL RESEARCH PAPER

Table 2 FC stack and SC characteristics.

Component	Parameter	Variable	Value	Units
FC	No. cells	N_{cell}	135	Cells
	Max power	$P_{FC,max}$	27.3	kW
	Max current	$i_{FC,max}$	300	A
	OCV voltage	$V_{FC,OCV}$	130.2	V
	Max temperature	$T_{FC,max}$	70	°C
	Thermal capacity	MC_{fc}	140	kJ K^{-1}
	Power of fan	P_{fan}	200	W
	Stack mass	FC_{mass}	19.5	kg
	Current slew rate	FC_{SR}	20	As^{-1}
SC	No. SC in series	SC_{serie}	50	
	SC mass	SC_{mass}	510	gr
	Equivalent series resistance (ESR)	SC_{ESR}	0.29	mΩ
	Capacitance	SC_c	3,000	F
	Rated voltage	$SC_{v,rated}$	2.7	V
	Max current	$SC_{Max,i}$	1,900	A
	Cut-off frequency	$SC_{cut-off}$	26	mHz

e-TESC 3W platform, which is around 150 km for a full charge. Taking into account this autonomy and the performance of the FC system in the lowest efficient zone, which is at the maximum speed of 120 km h^{-1}, the required hydrogen would be 1.77 kg. Based on the targets of light-duty fuel cell vehicles of US Department of Energy (DOE), the system volumetric capacity of the tank in 2020 should be 0.040 kg H_2 L^{-1} [37]. Therefore, the weight of the high-pressure tank in this manuscript comes to 32.2 kg.

2.2 Energetic Macroscopic Representation

In this manuscript, energetic macroscopic representation (EMR), which is a graphical method to organize the model of complex multiphysics systems, is used to model the e-TESC-3W platform in both active and passive configurations [38, 39]. The traction system of e-TESC 3W platform vehicle is shown in Figure 2. Passive and active energy source subsystems (ESSs) are presented in Figures 3 and 4, respectively. According to Figure 2, the hybrid vehicle velocity can be derived from the traction force and traction force resistance as [28]:

$$M_{eq} dV_{EV}/dt = F_{tr} - F_{env} \quad (9)$$

$$F_{tr} = \left(G_{gb}/r\right) T_{em} \eta_{gb}^{\xi} \quad (10)$$

$$\Omega_m = \left(G_{gb}/r\right) V_{EV} \quad (11)$$

$$\zeta = 1, \quad \text{for } T_{em} \geq 0 \quad (12)$$

$$\zeta = -1, \quad \text{for } T_{em} < 0 \quad (13)$$

$$T_{em} = T_{em\_r} \quad (14)$$

where F_{tr} is the traction force, G_{gb} is the gearbox transmission ratio, r is the wheel radius, T_{em} is the electric machine torque, η_{gb} is the Gearbox transmission efficiency, Ω_m is the rotor rotation speed, and T_{em_r} is reference torque to control the electric machine.

The requested current of the vehicle from the electric motor side (i_{ts}) is then formulated as:

$$i_{ts} = \left(T_{em}\, \Omega_m\, \eta_m^{\beta}\right)/U_{SC} \quad (15)$$

where U_{SC} is the SC voltage. In the passive configuration, as it can be seen in Figure 3, there is no DC-DC converter and a diode is used in series with the PEMFC stack to prevent the reversed current.The equivalent resistor of the diode (r_D) along with the voltage difference of the FC (U_{fc}) and SC (U_{SC}) determine the current of the FC system ($i_{FC\text{-}sys}$).

$$i_{FC\text{-}sys} = (U_{fc} - U_{SC})/r_D \quad (16)$$

$$i_{ts} = i_{FC\text{-}sys} + i_{SC} \quad (17)$$

where i_{SC} is the current of the SC. On the other hand, in the active configuration, as shown in Figure 4, the current goes through a converter as [36]:

$$i_{FC\text{-}sys} V_{fc} = i_{dc/dc}\, U_{SC}\, \eta_{dc/dc} \quad (18)$$

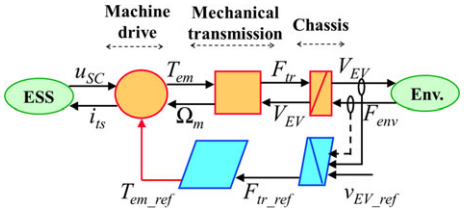

Fig. 2 Traction system of the e-TESC 3W platform vehicle.

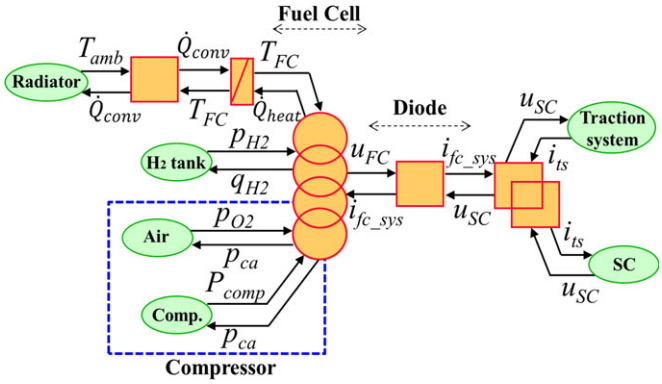

Fig. 3 The proposed passive ESS for the e-TESC 3W platform vehicle.

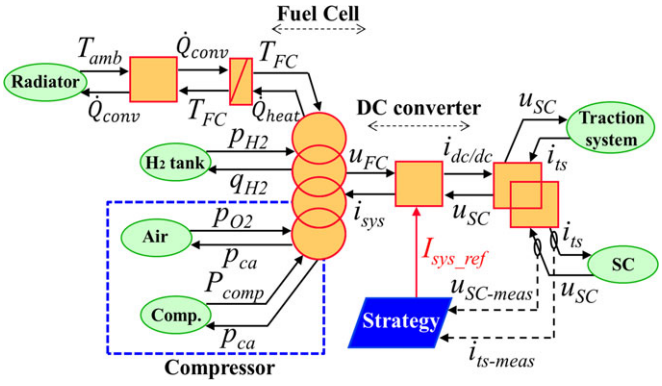

Fig. 4 The utilized active ESS of e-TESC 3W platform vehicle.

$$i_{ts} = i_{dc/dc} + i_{SC} \tag{19}$$

where $i_{dc/dc}$ is the converter current and $\eta_{dc/dc}$ is the converter efficiency.

The PEMFC voltage (U_{fc}) is calculated by using the semi-empirical model suggested in [40].

$$U_{fc} = N_{cell} \times (E_{Nernst} + U_{act} + U_{ohmic} + U_{con}) \tag{20}$$

$$E_{Nernst} = 1.229 - 0.85 \times 10^{-3}(T_{fc} - 298.15) + 4.3085 \times 10^{-5} T_{fc}\left[\ln(p_{H_2}) + 0.5\ln(p_{O_2})\right] \tag{21}$$

$$U_{act} = \Upsilon_1 + \Upsilon_2\, T_{fc} + \Upsilon_3\, T_{fc} \ln(CO_2) + \Upsilon_4\, T_{fc} \ln(i_{FC}) \tag{22}$$

$$CO_2 = p_{O_2}/5.08 \times 10^6 e^{-(498/Tfc)} \tag{23}$$

$$U_{ohmic} = -i_{FC} R_{internal} = -i_{FC}(\xi_1 + \xi_2\, T_{fc} + \xi_3\, i_{FC}) \tag{24}$$

$$U_{con} = \alpha i_{FC}^{G} \ln(1 - \beta i_{FC}) \tag{25}$$

where E_{Nernst} is the reversible voltage, U_{act} is the activation loss, U_{ohmic} is the ohmic loss, U_{con} is the concentration loss, T_{fc} is the stack temperature, p_{H_2} is the hydrogen partial pressure, p_{O_2} is the oxygen partial pressure, Υ_n ($n = 1 \ldots 4$) is the empirical coefficients, CO_2 is the oxygen concentration, i_{fc} is the the FC operating current, $R_{internal}$ is the internal resistor defined by the three parametric coefficients ξ_n ($n = 1 \ldots 3$), α is a semi-empirical parameter related to the diffusion mechanism ($0.3 \le \alpha \le 1.8$), G is a dimensionless number related to the water flooding phenomena ($1 \le G \le 4$), and β is the inverse of the limiting current.

The thermal behavior of the stack is modeled by using the energy conservation law. The energy balance for describing the temperature dynamic of the PEMFC can be given by [41]:

$$Q_{heat} = N_{fc}\, i_{fc}(1.254 - U_{fc}) \tag{26}$$

$$H_{fc} = (N_{fc}/36)(2,700\, k_{t_1} + k_{t_2}) \tag{27}$$

$$Q_{conv} = H_{fc}(T_{fc} - T_{amb}) \tag{28}$$

$$dT_{fc}/dt = (Q_{heat} - Q_{conv})/MC_{fc} \tag{29}$$

where Q_{heat} is the generated heat in the FC, N_{fc} is the number of cells, H_{fc} is the heat transfer coefficient, k_{t1} and k_{t2} are the coefficiencts obtained experimentally in [41], T_{amb} is the ambient temperature, T_{fc} is the stack temperature, Q_{conv} is the convection heat transfer, and MC_{fc} is the thermal capacity of the FC.

The current of the PEMFC system ($i_{FC\text{-}sys}$) is obtained by considering the losses from the balance of plant as [41, 42]:

$$i_{FC\text{-}sys} = \left(P_{fc} - P_{comp} - P_{fan}\right)/U_{fc} \tag{30}$$

$$P_{comp} = \eta_{comp}^{-1}\, W_{air}\, c_p\, T_{amb}\left((p_{ca}/p_{amb})((\gamma - 1)/\gamma) - 1\right) \tag{31}$$

$$P_{fc} = U_{fc}\, i_{fc} \tag{32}$$

$$W_{air} = \lambda W_{O_2}/\chi_{O_2} \tag{33}$$

$$W_{O_2} = M_{O_2}\, N_{fc}\, i_{fc}/2F \tag{34}$$

$$p_{O_2} = 0.21 p_{ca} \tag{35}$$

$$p_{H_2} = 0.99 p_{an} \tag{36}$$

$$p_{ca} = a_1 + a_2\, i_{fc} + a_3\, i_{fc}^2 + a_3\, i_{fc}^3 \tag{37}$$

$$p_{an} = p_{ca} + 20{,}000 \tag{38}$$

where P_{comp} is the consumed power by the compressor, p_{ca} is the pressure in the cathode, P_{fan} is the consumed power by the FC fan (200 W), η_{comp} is considered as the average compressor efficiency (0.70) [43], W_{air} is the rate of used air, c_p is the air specific heat capacity (1,005 J K^{-1}), p_{amb} is the ambient pressure, γ is the ratio of specific heats of air (1.4), λ is the oxygen excess ratio which is two, W_{O_2} is the oxygen consumption rate, χ_{O_2} is the oxygen mass fraction (0.233), M_{O_2} is oxygen molar mass, F is the Faraday constant, p_{an} is the pressure in the anode, and a_i ($i = 1 \ldots 3$) is the experimentally obtained coefficient.

The hydrogen flow (q_{H_2}) is calculated based on an experimental formula as [34]:

$$q_{H_2} = 0.00696 i_{fc}\, N_{fc} \tag{39}$$

Based on the mentioned models, the efficiency of the FC system is calculated considering the power losses of the auxiliaries:

$$\eta_{sys} = \left(P_{fc} - P_{comp} - P_{fan}\right)/\left(q_{H_2} HHV\right) \tag{40}$$

where the generated hydrogen power is the product of hydrogen flow and the high heating value of hydrogen (HHV = 286 kJ mol^{-1}). In the active coupling, the converter efficiency is multiplied by the FC system efficiency to know the efficiency in the DC bus.

Finally, the SC is modeled based on the equivalent circuit proposed in [44].

$$U_{SC} = r_{SC} i_{SC} + (1/C_{SC}) \int i_{sc} dt \quad (41)$$

where r_{SC} is the SC bank resistance and C_{SC} is the SC bank capacitance.

2.3 Degradation

One of the most significant factors while using a FC system as the main power source of a vehicle is durability consideration. This is mainly due to the fact that FC is really damage prone although it is one of the costly components of the powertrain. In automotive applications, the end of life (EOL) of a FC stack is defined when a 10% voltage loss is reached [45]. For this reason, it is vital to include the degradation of the FC stack in the analysis of the system performance. According to [25, 46, 47], the causes of FC degradation fit into five cases of load changing, startup and shutdown, low power load (idle condition), high power load, and natural decay. An empirical model for determining the voltage degradation of the FC stack can be formulated as [46]:

$$\Delta FC_{deg} = \Delta FC_{nat} + \Delta FC_{add} \quad (42)$$

where ΔFC_{deg} denotes the degradation of the FC in percentage, ΔFC_{nat} is the natural decay rate related to the expected lifetime of the FC in normal operation conditions, and ΔFC_{add} is the degradations rooted from unfavorable operations.

The influence of each factor on the degradation of the FC can be defined as:

$$\Delta FC_{deg} = k_1\, t_1 + k_2\, n_1 + k_3\, t_2 + k_4\, t_3 + \beta_{nat}\, t_{FC\_ON} \quad (43)$$

where t_1 is the idle time, n_1 is the number of start-stops, t_2 is the duration of heavy loading, and t_3 is the time in high power condition. The idle condition is described as the output power which is less than 5% of maximum power (P_{Low}), the heavy loading is an absolute variation more than 10% of maximum power per second, and high power is delimited as higher than 90% of maximum power (P_{High}). Based on the 2020 FC lifetime target of DOE (5,000 h), the natural decay rate β_{nat} is set to reach a voltage loss of 10% in 5,000 h [48]. Table 3 represents all the degradation rates for all the phenomena based on experimental data [25].

In addition to the FC stack, a calendar degradation model has been considered for the SC based on the datasheet of the manufacturer. According to this datasheet, the expected lifetime of this device is 10 years. Moreover, the EOL of the SOC is defined as an increment of 100% in SC_{ESR} and a decrement of 20% in SC_C [24].

3 Energy Management Strategy for Active Coupling

As explained earlier, the main purpose of this work is to compare the use of FC-SC passive and active couplings for the e-TESC 3W platform vehicle. Passive configuration does not need an EMS as the operating current harmonics are chiefly provided by the component with the lowest impedance, SC herein, in such configuration. However, to bring into attention the strengths of the utilized passive architecture, its performance is compared with an active configuration where the same selected FC stack is connected to the DC bus through a DC-DC converter and the SC is directly connected to the bus. Such active configuration needs an EMS to split the power between the FC and SC. In this respect, a FLC based EMS is designed and optimized by genetic algorithm (GA) for the purpose of this paper. FLC uses some if-then rules to integrate the knowledge of an expert into the design procedure and does not require a precise model of the system. Since the comparative analysis of this work is mainly based on a specific real deriving cycle, the parameters of the FLC has been adjusted by GA to improve its performance as much as possible for this known driving cycle.

The designed FLC for the purpose of power splitting in the active powertrain of this work has two inputs, requested power and SC voltage, and one output, which is the required power from the FC. The input and output membership functions (MFs) of the FLC as well as the fuzzy reasoning rules are tuned by GA. Since the optimization of FLC is a common approach in the literature [49, 50], its explanation has been considered unnecessary in this manuscript. The proposed cost function for optimizing the performance of the FLC is as follows.

$$C_{Trip} = FC_{cost}\, \Delta_{FC} + H_{2,cost}\, H_{cons} \quad (44)$$

where FC_{cost} is the cost of the FC, specified in Table 4, Δ_{FC} is the degradation percentage of the FC, obtained by Eq. (43),

Table 3 FC degradation coefficients.

Coefficient	Value	Units
k_1	0.00126	% h^{-1}
k_2	0.00196	% per cycle
k_3	0.0000593	% h^{-1}
k_4	0.00147	% h^{-1}
β	0.002	% h^{-1}

Table 4 Coefficient for FC degradation model.

Component	Cost	Reference
Storage system	$ 589.5	[37]
FC_{cost}	$ 1092	[48]
$H_{2,cost}$	$ 2.3 per kg	[51]
SC	$ 1965	[52]
DC/DC converter	$ 1500	[53]

$H_{2,cost}$ is the cost per kilogram of hydrogen, and H_{cons} is the hydrogen consumed during the trip. Table 4 shows the cost breakdown of the complete power source system.

Figure 5 shows the comparison of the FC system efficiency between active and passive configurations. According to this figure, the overall efficiency of the passive system is higher than the active system due to the exclusion of the power electronic related losses. Figure 5 also delimits the low power (P_{Low}) zone, which is 5% of the maximum power, and high power (P_{High}) zone, which is 90% of the maximum power. For both cases of passive and active configurations, the maximum efficiency is located near to P_{Low}.

The optimization process has been carried out for a real driving cycle recorded from e-TESC 3W platform shown in Figure 6. The optimized reasoning rules of the FLC are presented in Figure 7. From this figure, it is clear that the optimized EMS avoids unnecessary on-off cycles. Indeed, it keeps the FC stack in a very low (VL) power mode when the requested power is low, and the voltage of the SC is high. Moreover, the FC stack tries to maintain the SC voltage in high levels in order to embrace any sudden peaks of power.

Figure 8 shows the initial and optimized MFs of the two inputs and one output. Regarding the MFs of the first input (P_{ts}) and the output (I_{FC}), it can be seen that they have almost

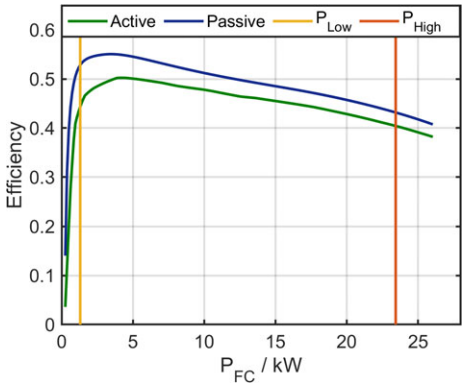

Fig. 5 FC system efficiency comparison of active and passive couplings.

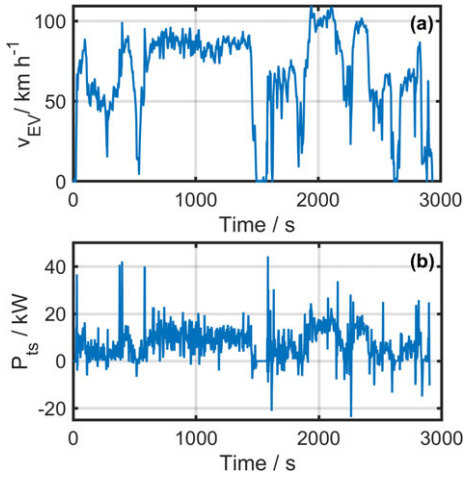

Fig. 6 The real driving cycle of e-TESC 3W platform vehicle.

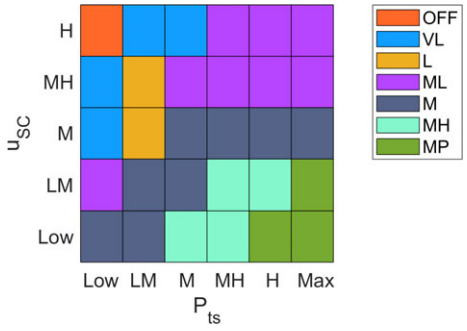

Fig. 7 Optimized rules of FLC.

formed an equal distribution over the universe of discourse. On the contrary, in the second input (U_{SC}), the low level covers up to 40% of the range of value. This range implies that the optimization algorithm has opted to keep the SC within a high level of energy to deal with the high dynamics behavior of the profile. In order to clarify the obtained shape in the MFs of the optimized fuzzy, it should be reminded that a trapezoidal MF can be defined as Trapezoidal (x; a, b, c, d, while a < b < c < d):

$$0 \; x < a \tag{45}$$

$$m_1 = x\text{-}a/b\text{-}a \quad a \le x \le b \tag{46}$$

$$1 \; b \le x \le c \tag{47}$$

$$m_2 = d\text{-}x/d\text{-}c \quad c \le x \le d \tag{48}$$

$$0 \; d \le x \tag{49}$$

where x represents real value (Crisp Value) within the universe of discourse while a, b, c, d represent a *x*-coordinates of the four heads of the trapezoidal. During the optimization process of this work, the two constructing slopes of each trapezoidal MF (m_1 and m_2) has been forced to reach the same value.

4 Results and Discussion

The achieved results of the carried out comparative study is presented in this section. Primarily, the results related to the distribution of power among the power sources are investigated. Secondly, the cost of FC degradation and hydrogen consumption are compared for each of the configurations. Finally, other aspects, such as trip cost, total cost of the system, and hourly system cost, are compared for each case study.

Figure 9 shows the power split between the FC stack and SC bank in each configuration. Comparison of the active and passive configurations shows that in the active coupling, the SC operates in a wider range which leads to more efficient performance of the FC stack. Regarding the passive coupling, it is clear that the extracted power from the FC stack follows a smoother path since the SC bank functions as a low-pass filter in such configurations. It is worth mentioning, that both of the

ORIGINAL RESEARCH PAPER

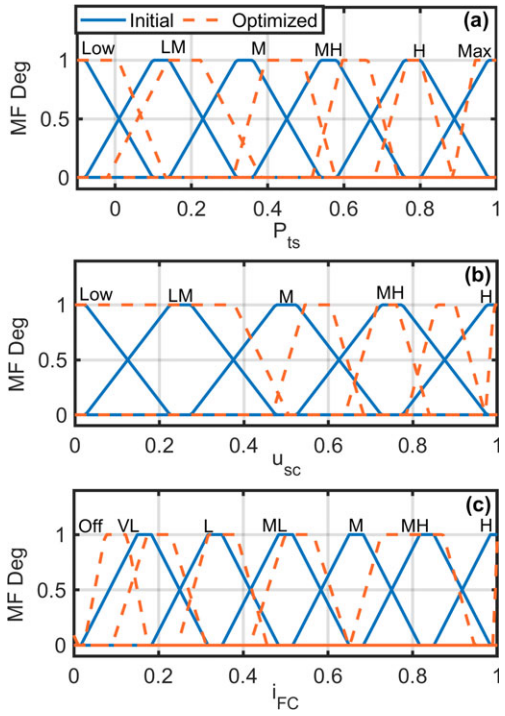

Fig. 8 Optimized FLC MFs, a) requested power (input 1), b) voltage of SC (input 2), and c) required current from the FC (output).

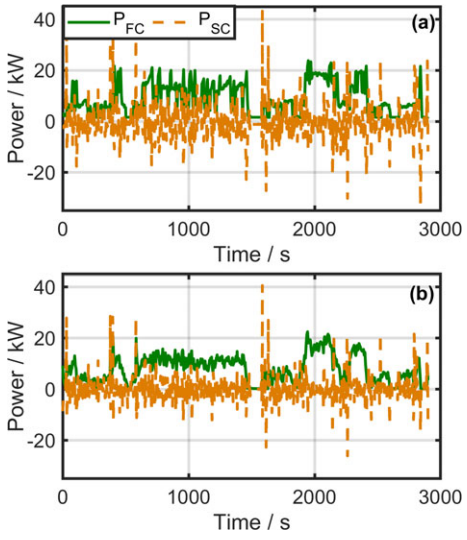

Fig. 9 Power split signals for a) active and b) passive configuration.

passive and active configurations respect the current slew rate of the FC specified in Table 2.

From Figure 10, it can be seen that active configuration manages to run the FC stack between P_{Low} and P_{High} regions. Operating the FC stack within this region results in higher efficiency and less degradation of the system. Figure 10b shows that the passive configuration provides a homogeneous power distribution while it sometimes leads to the operation of the FC system in the low efficiency zone.

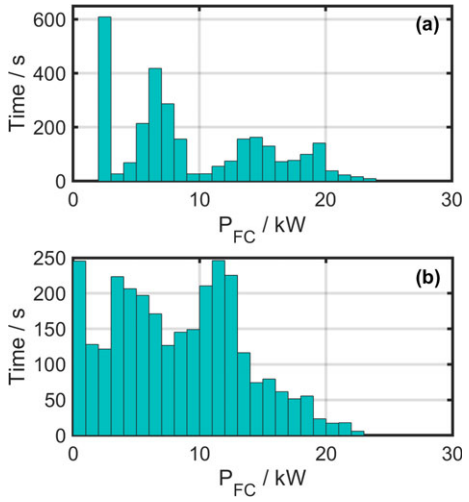

Fig. 10 FC power distribution for a) active and b) passive coupling.

Figure 11 compares the cost of FC stack caused by the degradation as well as the hydrogen consumption for each considered case under the real driving profile condition. As explained earlier, the degradation cost of the FC stack is due to the idle time, number of start-stops, duration of heavy loading, and the operation time in high power condition. On the one hand, Figure 11 indicates that the FC degradation cost is \$0.1825 and \$0.1961 in active and passive configurations, respectively. This result discloses the superior performance of the active coupling by almost seven percent in terms of wear and tear in the FC system due to the management of the power between the sources while respecting their defined restrictions. On the other hand, form Figure 11, it can be seen that the passive connection consumes less hydrogen than the active coupling by virtually 12%. This is essentially the result of not having the DC-DC converter electrical losses in the system.

To scrutinize deeper the pros and cons of having a passive coupling compared to the active one, a more detailed analysis from different perspectives is presented in Table 5.

According to this table, the trip cost, which is the sum of FC degradation and utilized hydrogen, is less in passive configuration by 8%. Furthermore, the possible number of trips by one tank of hydrogen, calculated by using the total storage capacity of the tank and the hydrogen consumption, is higher in the passive coupling by almost 13.5%. However, the possible number of trips before reaching the EOL of the FC stack is

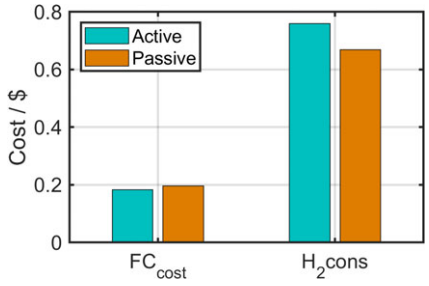

Fig. 11 Cost breakdown comparison of active and passive configuration.

Table 5 The cost comparison of FC-SC passive and active couplings.

Type	Active	Passive
Trip cost	$ 0.9420	$ 0.8650
No. Trips per tank	5.36	6.08
No. trips up to EOL of FC	5,983	5,569
Trip cost up to EOL	$ 5,636	$ 4,817
Capital cost	$ 3,929	$ 2,564
Total cost of the system	$ 9,565	$ 7,381
Total system cost per hour	$ 1.957	$ 1.623

higher in the active coupling by practically 7%, which refers to the faster degradation of the stack in the passive configuration. This table also shows that the total cost of the system, which is composed of capital cost and trip cost up to EOL of the FC stack, is lower in the passive configuration by 22.8%. The last presented result in the table is related to the total cost of operating a passive or active configuration per hour, which is less in the passive coupling by 17%. This cost per hour has been obtained by the division of total cost by the number of hours the FC is able to operate before reaching its EOL. To sum up, Table 5 reveals that a passive coupling, despite of having a shorter operational time in the FC system, leads to a less expensive hourly total cost of the system.

5 Conclusions

This paper performs a comparative study of active and passive FC-SC couplings for the powertrain configuration of e-TESC 3W platform vehicle. In this respect, the size of the components is determined in relation to the requirements of the vehicle in the first place. Afterwards, the performance of the passive configuration is compared with a commonly used active one to spotlight the assets and liabilities of each case. An optimized FLC based on a real driving cycle of the e-TESC 3W platform is used to split the power between the FC stack and SC bank in the active configuration while the passive coupling does not require an EMS for power distribution. In order to investigate the performance of each configuration, an hourly total system cost for the operation of each case is calculated. This cost mainly contains the trip cost, which is composed of the FC degradation and consumed hydrogen costs, and the capital cost of the components. The performed analysis indicates that the hourly cost of the proposed passive connection is 17% less than the studied active configuration. It is worth reminding that the passive configuration causes higher rate of degradation in the FC system compared to the active one. However, this cost is compensated by the other aspects such as lower hydrogen consumption and the capital cost of the system.

Acknowledgements

This work was supported in part by Grant 950-230863 and 950-230672 from Canada Research Chairs Program, and in part by Grant RGPIN-2018-06527 and RGPIN-2017-05924 from the Natural Sciences and Engineering Research Council of Canada.

List of Symbols

c_p	Air specific heat capacity / J K^{-1}
C_{SC}	SC bank capacitance / F
C_{Trip}	Cost function / $
CO_2	Oxygen concentration / mol cm^{-3}
E_{Nernst}	Cell reversible voltage / V
F	Faraday constant / s A mol^{-1}
F_{air}	Resistance force against the air / N
F_{acc}	Accelerating force / N
F_{env}	Traction force resistance / N
F_{grade}	Grade related force / N
F_{roll}	Rolling resistance force / N
F_{tr}	Traction force / N
g	Gravity / m s^{-2}
G_{gb}	Gearbox transmission ratio
H_{cons}	Consumed Hydrogen / kg
H_{fc}	Heat transfer coefficient / W K^{-1}
$i_{dc/dc}$	Converter current / A
I_{FC}	Current of the FC / A
$i_{FC\text{-}sys}$	Current of the FC system / A
i_{SC}	SC current / A
i_{ts}	Electric motor current / A
k_n	Degradation coefficient
k_{tn}	Empirical coefficient
MC_{fc}	Thermal capacity of the FC / kJ K^{-1}
M_{O2}	Oxygen molar mass kg mol^{-1}
N_{cell}	Number of cells
p_{amb}	Ambient pressure / Pa
p_{an}	Pressure in the anode / Pa
p_{ca}	Pressure in the cathode / Pa
P_{comp}	Consumed power by the compressor / W
P_e	Power at maximum speed condition / kW
P_{fan}	Consumed power by the FC fan / W
P_{fc}	Generated power by the FC / W
p_{H_2}	Hydrogen partial pressure / Pa
P_{High}	FC high power limit / W
P_{Low}	FC low power limit / W
p_{O_2}	Oxygen partial pressure / Pa
P_{tot}	Power at maximum acceleration / kW
P_{ts}	Transmission power / W
Q_{conv}	Convection heat transfer / W
q_{H_2}	Hydrogen flow / SLPM
Q_{heat}	Generated heat in the FC / W
r_D	Diode resistance / Ω
r_{SC}	SC bank resistance / Ω
T_{amb}	Ambient temperatue / K

T_{em}	Electric machine torque / N m
T_{em_r}	Reference torque for electric machine / N m
T_{fc}	Stack temperature / K
t_n	FC operational time / s
U_{act}	Activation voltage drop / V
U_{con}	Concentration voltage drop / V
U_{fc}	FC voltage / V
U_{ohmic}	Ohmic voltage drop / V
U_{SC}	SC voltage / V
V_{EV}	vehicle speed / m s^{-1}
W_{air}	Rate of used air
W_{O_2}	Oxygen consumption rate
β	Inverse of the limiting current / A^{-1}
γ	Ratio of specific heats of air
δ	Mass factor
ΔFC_{deg}	Voltage degradation of the FC stack / %
ΔFC_{add}	Additional degradation of the FC / %
ΔFC_{nat}	Natural degradation of the FC / %
η_{comp}	Average compressor efficiency
$\eta_{dc/dc}$	Converter efficiency
η_{em}	Motor average efficiency / %
η_{gb}	Gearbox transmission efficiency / %
η_{sys}	Efficiency of the FC system
η_t	Transmission efficiency / %
λ	Oxygen excess ratio
ξ_n	Parametric coefficients related to ohmic resistance
ρ_a	Air density / kg m^{-3}
Υ_n	Experiential coefficients related to activation loss
χ_{O_2}	Oxygen mass fraction
Ω_m	Rotor rotation speed / rad s^{-1}

References

[1] US DOE Energy Information Administration (EI), Office of Energy Analysis, Washington, DC, USA, **2019**.

[2] Y. Wu, L. Zhang, *Transportation Research Part D: Transport and Environment* **2017**, *51*, 129.

[3] Z. P. Cano, D. Banham, S. Ye, A. Hintennach, J. Lu, M. Fowler, Z. Chen, *Nature Energy* **2018**, *3*, 279.

[4] B. Hollweck, M. Moullion, M. Christ, G. Kolls, J. Wind, *Fuel Cells* **2018**, *18*, 669.

[5] M. Bodner, A. Schenk, D. Salaberger, M. Rami, C. Hochenauer, V. Hacker, *Fuel Cells* **2017**, *17*, 18.

[6] F. X. Chen, Y. Yu, J. X. Chen, *Fuel Cells* **2017**, *17*, 671.

[7] D. Zhang, C. Cadet, N. Yousfi-Steiner, F. Druart, C. Bérenguer, *Fuel Cells* **2017**, *17*, 268.

[8] X. Zhang, Y. Yang, X. Zhang, L. Guo, H. Liu, *Fuel Cells* **2019**, *19*, 160.

[9] T. Zimmermann, P. Keil, M. Hofmann, M. F. Horsche, S. Pichlmaier, A. Jossen, *Journal of Energy Storage* **2016**, *8*, 78.

[10] R. C. Samsun, C. Krupp, S. Baltzer, B. Gnörich, R. Peters, D. Stolten, *Energy Conversion and Management* **2016**, *127*, 312.

[11] Q. Xun, Y. Liu, E. Holmberg, *Proc. 2018 International Symposium on Power Electronics, Electrical Drives, Automation and Motion (SPEEDAM 2018)*, (Eds.: A. Binder, A. Del Pizzo, I. Miki), Amalfi, Italy **2018**, pp. 389.

[12] H. S. Das, C. W. Tan, A. H. M. Yatim, *Renewable and Sustainable Energy Reviews* **2017**, *76*, 268.

[13] J. P. Trovão, M. A. Silva, C. H. Antunes, M. R. Dubois, *Applied Energy* **2017**, *205*, 244.

[14] V. K. Kasimalla, N. S. G. V. Velisala, *International Journal of Energy Research* **2018**, *42*, 4263.

[15] M. Kandi Dayeni, M. Soleymani, *Clean Technologies and Environmental Policy* **2016**, *18*, 1945.

[16] R. E. Silva, F. Harel, S. Jemeï, R. Gouriveau, D. Hissel, L. Boulon, K. Agbossou, *Fuel Cells* **2014**, *14*, 894.

[17] C. Turpin, D. Van Laethem, B. Morin, O. Rallières, X. Roboam, O. Verdu, V. Chaudron, *Mathematics and Computers in Simulation* **2017**, *131*, 76.

[18] H. Wang, A. Gaillard, D. Hissel, *Renewable Energy* **2019**, *141*, 124.

[19] S. Ait Hammou Taleb, D. Brown, J. Dillet, P. Guillemet, J. Mainka, O. Crosnier, C. Douard, L. Athouël, T. Brousse, O. Lottin, *Fuel Cells* **2018**, *18*, 299.

[20] K. Gérardin, S. Raël, C. Bonnet, D. Arora, F. Lapicque, *Fuel Cells* **2018**, *18*, 315.

[21] B. Morin, D. Van Laethem, C. Turpin, O. Rallières, S. Astier, A. Jaafar, O. Verdu, M. Plantevin, V. Chaudron, *Fuel Cells* **2014**, *14*, 500.

[22] R. Shimoi, Y. Ono, *International Patent No. PCT/IB2005/001260*, **2005**, can be found under https://patentscope.wipo.int/search/en/detail.jsf?docId=WO2005107360&tab=PCTBIBLIO

[23] D. Arora, K. Gérardin, S. Raël, C. Bonnet, F. Lapicque, *Journal of Applied Electrochemistry* **2018**, *48*, 691–699.

[24] 2.7V 650-3000F ultracapacitor, can be found under https://www.maxwell.com, **2013**.

[25] P. Pei, Q. Chang, T. Tang, *International Journal of Hydrogen Energy* **2008**, *33*, 3829.

[26] H. Zhao, A. F. Burke, *Fuel Cells* **2010**, *10*, 879.

[27] B. Wu, M. A. Parkes, V. Yufit, L. De Benedetti, S. Veismann, C. Wirsching, F. Vesper, R. F. Martinez-Botas, A. J. Marquis, G. J. Offer, N. P. Brandon, *International Journal of Hydrogen Energy* **2014**, *39*, 7885.

[28] J. P. F. Trovão, M. R. Dubois, M. Roux, E. Menard, A. Desrochers, *Proc. 2015 IEEE Vehicle Power and Propulsion Conference (VPPC 2015)*, Montreal, Quebec, Canada, **2015**, pp. 1–6.

[29] J. P. F. Trovão, M. Roux, É. Ménard, M. R. Dubois, *IEEE Transactions on Vehicular Technology* **2017**, *66*, 5540.

[30] A. S. Mohammadi, J. P. Trovão, M. R. Dubois, *IET Electrical Systems in Transportation* **2018**, *8*, 12.

[31] G. Wenzhong, *IEEE Transactions on Vehicular Technology* **2005**, *54*, 846.

[32] R. Abousleiman, O. Rawashdeh, *Proc. 2015 IEEE Transportation Electrification Conference and Expo (ITEC 2015)*, Metro Detroit, MI, USA, **2015**, pp. 1–5.

[33] C. Mi, M. A. Masrur, *Hybrid Electric Vehicles: Principles and Applications with Practical Perspectives*, John Wiley & Sons, Ltd., Chichester, West Sussex, United Kingdom, **2017**.
[34] FCvelocity®-9SSL Product Manual and Integration Guide, can be found under www.ballard.com, **2017**.
[35] V. Liso, M. P. Nielsen, S. K. Kær, H. H. Mortensen, *International Journal of Hydrogen Energy* **2014**, *39*, 8410.
[36] C. H. Choi, S. Yu, I.-S. Han, B.-K. Kho, D.-G. Kang, H. Y. Lee, M.-S. Seo, J.-W. Kong, G. Kim, J.-W. Ahn, S.-K. Park, D.-W. Jang, J. H. Lee, M. Kim, *International Journal of Hydrogen Energy* **2016**, *41*, 3591.
[37] Fuel Cell Technologies Office Multi-Year Research, Development, and Demonstration Plan – Hydrogen Storage, can be found under www.energy.gov, **2015**.
[38] A. Bouscayrol, in *Systemic Design Methodologies for Electrical Energy Systems* (Ed. X. Roboam), ISTE, Croydon, **2012**, pp. 89.
[39] L. Boulon, D. Hissel, A. Bouscayrol, M. Pera, *IEEE Transactions on Industrial Electronics* **2010**, *57*, 1882.
[40] M. Kandidayeni, A. Macias, A. A. Amamou, L. Boulon, S. Kelouwani, *Fuel Cells* **2018**, *18*, 347.
[41] P. S. Oruganti, Q. Ahmed, D. Jung, *Proc. WCX World Congress Experience 2018*, Detroit, MI, USA., **2018**.
[42] X. Zhao, Y. Li, Z. Liu, Q. Li, W. Chen, *International Journal of Hydrogen Energy* **2015**, *40*, 3048.
[43] J. M. Campbell, *Gas Conditioning and Processing, Volume 2: The Equipment Modules*, PetroSkills, J. M. Campbell & Co., Tulsa, OH, USA, **2014**, pp. 197.
[44] L. Zubieta, R. Bonert, *IEEE Transactions on Industry Applications* **2000**, *36*, 199.
[45] Y. Wang, S. J. Moura, S. G. Advani, A. K. Prasad, *International Journal of Hydrogen Energy* **2019**, *44*, 8479–8492.
[46] Z. Hu, J. Li, L. Xu, Z. Song, C. Fang, M. Ouyang, G. Dou, G. Kou, *Energy Conversion and Management* **2016**, *129*, 108.
[47] K. Song, H. Chen, P. Wen, T. Zhang, B. Zhang, T. Zhang, *Electrochimica Acta* **2018**, *292*, 960.
[48] Fuel Cell Technologies Office Multi-Year Research, Development, and Demonstration Plan – Fuel Cells, can be found under www.energy.gov, **2015**.
[49] R. Zhang, J. Tao, *IEEE Transactions on Fuzzy Systems* **2018**, *26*, 1833.
[50] R. Zhang, J. Tao, H. Zhou, *IEEE Transactions on Fuzzy Systems* **2019**, *27*, 45.
[51] Fuel Cell Technologies Office Multi-Year Research, Development, and Demonstration Plan – Hydrogen Production, can be found under www.energy.gov, **2015**.
[52] Z. Song, J. Li, J. Hou, H. Hofmann, M. Ouyang, J. Du, *Energy* **2018**, *154*, 433.
[53] Electrical and Electronics Technical Team Roadmap, can be found under www.energy.gov, **2017**.

Appendix C - Fuel cell/supercapacitor passive configuration sizing approach for vehicular applications

Authors: Clément Dépature, Alvaro Macías, Andres Jácome, Loïc Boulon, Javier Solano, João P. Trovão

Journal: International Journal of Hydrogen Energy, Elsevier

Publication date: 9 October 2020

DOI: https://doi.org/10.1016/j.ijhydene.2020.05.040

C.1 Methodology

This paper proposes a three-criteria sizing method and a pre-charging strategy for a FC-SC hybrid power supply system. The considered criteria are the storage capacity, maximum voltage, and FC operating current dynamics. The electric diagram connection of the testbench, shown in Figure C.1, is composed of the FC system, the pre-charge resistor, the SC system, and the programmable load. In this case study, the components are connected employing four 40 A contactors K_{fc}, K_r, K_{sc} and K_{load}. The contactors K_{fc}, and K_{load} are implemented as safe contactors to stop the test in case of failure. Moreover, a fixed pre-charged resistor (R) of 1 Ω is used to limit the FC current.

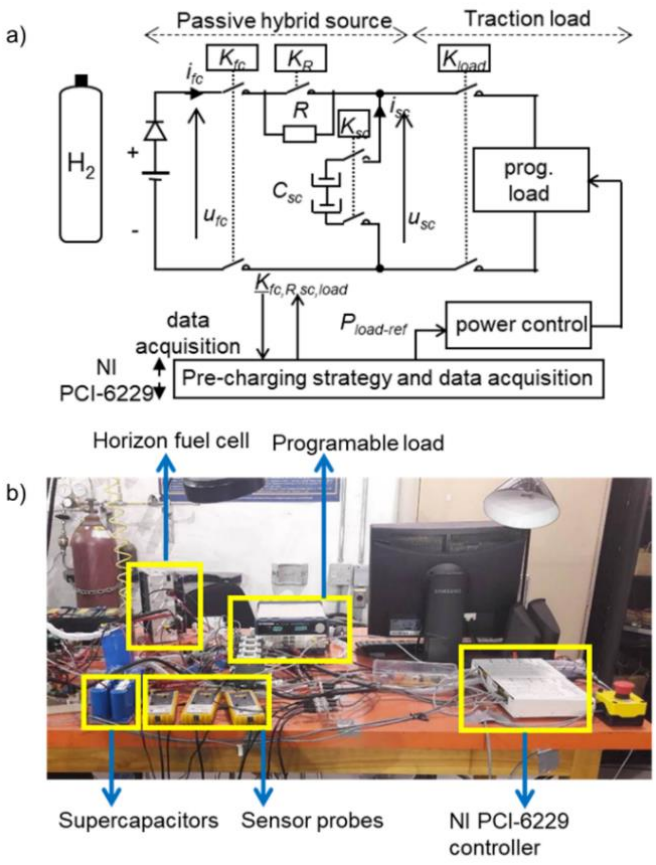

Figure C.1 Test bench, a) diagram, b) experimental platform

The developed pre-charging strategy is built and implemented in a National Instrument NI PCI-6229 controller. The management of the contactors allows two operation modes:

Mode 1: SC pre-charging. K_{fc} and K_{sc} are closed. K_r and K_{load} are opened. The system becomes a closed circuit with the FC, diode, pre-charging resistor, and SC connected in series. The FC charges the SC up to its OCV. Moreover, the pre-charged resistor limits the inrush current i_{fc}.

Mode 2: Vehicle operation. K_{fc}, K_{sc}, K_r and K_{load} are closed. The emulated traction load is connected in parallel to the SC of the system. Therefore, the system becomes a circuit

with three branches in parallel: FC and diode, SC, and load. The FC operation frequency depends on the SC characteristics.

In the case that the SC is discharged, it is necessary to balance both components at the same electric potential; this process is shown in Figure C.2. When the FC is turned on, it is on OCV. Then the FC is connected to the SC by closing the contactor K_{fc} and K_{sc} at $t = 10s$, its voltage drops instantly to around 20 V. The pre-charged resistor limits the load current to 20 A. The charging current decreases with a time constant of about 38 s, and then an operating frequency of 4.2 mHz is below the defined operation frequency limit. The stabilization time is about 190 s.

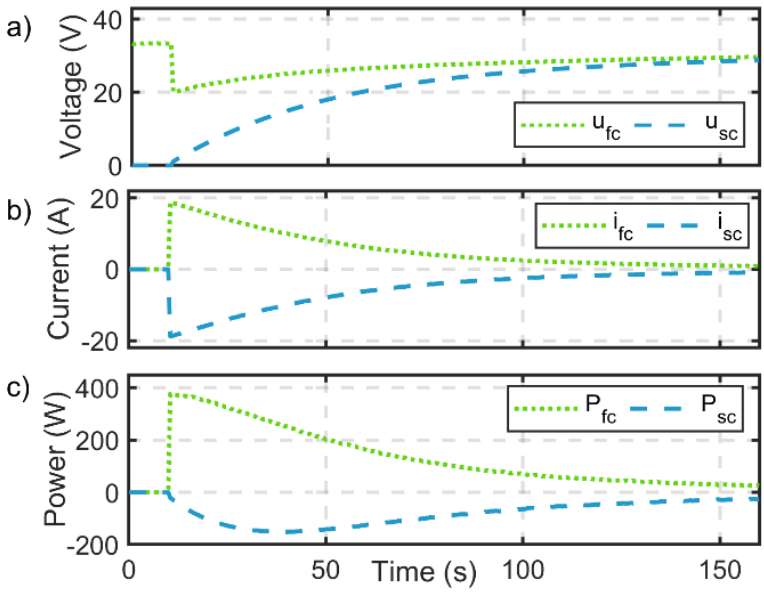

Figure C.2 Supercapacitor pre-charge sequence, a) voltage profile, b) current profile, and c) power profile

C.2 Outcomes

The advantage of the chosen pre-charging method is that it limits the charging current, which avoids component stress during the FC/SC passive connection. However, SC charging

time is relatively long. Note that for this pre-charging test, the SC was fully discharged. This is the worst operation case that should not often happen because the SC self-discharge time constant is relatively long [62]. Nevertheless, experimental results reveal a reduction in the FC degradation and improvement in the global system. The SCs support the FC to meet the requirements of the load while guarantying the system stability and less stress over the FC system. Moreover, advanced pre-charging strategies could be implemented, including short-circuit or progressive FC/SC connection [61], using a Voltage Stabilization System (VSS) [114], or a control system to regulate the connection of a pre-charging resistance before starting the vehicle [115].

Available online at www.sciencedirect.com

ScienceDirect

journal homepage: www.elsevier.com/locate/he

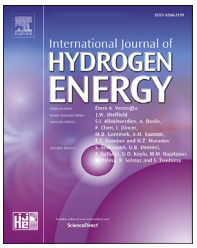

Fuel cell/supercapacitor passive configuration sizing approach for vehicular applications

Clément Dépature [a], Alvaro Macías [a,c,*], Andres Jácome [b], Loïc Boulon [a], Javier Solano [b], João P. Trovão [c]

[a] Université du Québec à Trois-Rivières, Hydrogen Research Institute, Trois-Rivières, Quebec, Canada
[b] Universidad Industrial de Santander – Escuela de Ingenierías Eléctrica, Electrónica y de Telecomunicaciones, Bucaramanga, Colombia
[c] e-TESC Laboratory, Dept. Electrical & Computer Engineering, University of Sherbrooke, Sherbrooke, Quebec, Canada

HIGHLIGHTS

- Low-cost passive configuration between fuel cell and supercapacitor is employed.
- A frequency-based sizing methodology is proposed for the fuel cell system.
- Higher global performance and less stress to the fuel cell system are achieved.

ARTICLE INFO

Article history:
Received 27 January 2020
Received in revised form
4 May 2020
Accepted 5 May 2020
Available online xxx

Keywords:
Energy management
Fuel cell
Passive configuration
Multi-source sizing
Supercapacitor
Vehicular applications

ABSTRACT

Active configuration i.e., source coupling via a power converter, is the most common configuration for fuel cell/supercapacitor (FC/SC) vehicles. Passive connection of the FC with the SCs without any converters is an original and less expensive solution to distribute the power among the sources. This passive configuration does not require an energy management strategy. In fact, the power distribution only depends on the FC and SC impedance characteristics. Conventional methods to size the SC follow two criteria: storage capacity and maximum voltage. In this paper, a third criterion is added which is the FC operating current dynamics. This novel sizing methodology reduces the FC degradation and improves the global system efficiency. Experimental results provide validation to the proposed sizing approach. The SCs boost the FC to meet the requirements of the load with a guarantee of system stability reaching higher global performances and less stress to the FC.

Introduction

In the last decade, there has been a growing interest in fuel cell (FC) vehicles [1,2]. By using hydrogen (H_2), FC vehicles are considered as a promising solution to reduce greenhouse gases for long-range vehicles [3,4]. However, FC systems offer a limited dynamic. Fast power transients can lead to a gas starvation, which can permanently damage the FC [5,6].

* Corresponding author. Université Du Québec à Trois-Rivières, Hydrogen Research Institute, Trois-Rivières, Quebec, Canada.
E-mail address: alvaro.omar.macias.fernandez@uqtr.ca (A. Macías).

https://doi.org/10.1016/j.ijhydene.2020.05.040

Furthermore, the energy flow of FC systems is unidirectional, which does not allow recovering braking energy. The literature review of energy storage systems (ESS) presented in Ref. [7], shows that the hybridization of ESSs with complementary features copes with the harsh working environment that a single ESS cannot achieve. Thus the coupling of FC with other ESS devices can improve the vehicle performances by handling the power transients, recovering braking energy, extending its lifetime and reducing its cost [8]. The hybrid configurations are classified in mainly in active and passive connection, based on the way that the components are connected to the DC bus [9]. Active configurations use at least one converter to combine the sources. Like the case of Toyota Mirai and Hyundai Tucson that have an active FC/battery configuration, using Ni-Mh and Li-Poly battery packs, respectively [10]. Honda has chosen an active fuel cell/supercapacitor (FC/SC) configuration to supply fast power dynamic of the vehicle in its 2002 FCX. However, the new 2014 FCX Clarity uses a FC/battery in active configuration. Active configurations require designing and performing a stable control associated to an energy management strategy and an additional DC/DC converter, where its size is a function of the power demand [11]. In Ref. [12], Blackwelder et al. proposed hybrid power source that allows the interconnection of a FC and a battery having dissimilar operating voltages, and supply high current peaks by an energy management strategy. In this respect, different criteria to design an energy management strategy can be found in the literature; minimization of fuel consumption or cost, and maximal efficiency, power identification or degradation [13,14]. However, the converters utilized in the active configuration increase the energy losses, the volume, the weight, the cost and the failure probabilities of the hybrid system [15].

Contrary to active configuration, passive configurations avoid the use of power electronics converter. Passive configurations provide a natural power split by directly connecting the FC and an ESS in parallel. In such architecture, the current distribution between the FC and the ESS is not controlled. In this respect, a previous study explores an indirect power control in a FC/battery passive configuration by regulating the FC pressure [16]. However, this method operates the FC at pressure lower that its nominal value that makes complicated the purging. In Ref. [17], a comparative study shows that the passive configuration of FC/SC reduce the hydrogen consumption due to the elimination of the energy conversion losses of the converter. In this regard, Arora et al. present that the hydrogen stoichiometry can be reduced for a passive configuration of FC/SC to reduce the fuel overconsumption and avoid flooding inside the FC [18]. Another study shows that the passive hybridization of FC/SC improves the FC performance due to the SC removes the peaks from the demanded power [19]. Macias et al. compare the active and passive FC/SC configuration for a vehicular application [20]. Simulation results show that passive configuration increases the global efficiency due to the elimination of power electronics and makes the drawn power from the FC smoother that leads to longer lifetime of the FC. It should be noted that simulation has been used in the majority of studies and experimental validations considering driving operations are limited to a few studies [21,22]. In another perspective, recent papers study the response of a passive FC/SC configuration at the scale of each FC cell under different situations [23,24]. The configuration of a FC with SC as energy/power buffer represents an interesting solution, because their high specific power and power density as compared to batteries, SC can assist a FC to meet the transients and high-power requirements peaks [25].

However, the parallel connection can result in a high inrush current if both systems do not have the same electric potential. Recently, some efforts have been made in the initial voltage conditions of the FC/SC passive configuration mainly focusing on the SC pre-charging and the passive system operation. In the commonly used SCs, the terminals voltage decay can vary from 5 to 15% within 48 h, due to auto-discharge phenomenon [26]. Therefore, in case that the SC is completely discharged or has a lower voltage than the FC in the startup phase of the passive hybrid energy system, the demanded load can produce a high inrush current and lead to the degradation of the FC system. Wu et al. use a pre-charging fixed resistor to charge the SC just below the FC open circuit voltage (OCV). This avoids inrush current at the time of connecting the sources but increases the startup time [22]. The instantaneous high input current can also be limited without a resistor, by controlling the initial H_2 flow [27]. Silva et al. propose to turn on the FC after connecting the SC in order to increase progressively the voltage and reduce the high peak of current [28]. The presented principles are experimentally validated using a current pulse load. Silva et al. study FC/SC passive configuration by simulation and implement an experimental setup to study the effect of high current on FC degradation.

Another important aspect is the sizing of the hybrid system, i.e. the selection of the FC and ESS characteristics, this stage is crucial to obtain a functional passive power split. Compare to active configuration where a DC/DC converter adapts the voltage of the components to the bus voltage. In this respect, Arora et al. analyze the FC and SC characteristics to split the power based on the traction power frequency distribution, and concluded that the SC has to store enough energy to assist the FC [29]. In Ref. [30], a study of a passive SC/battery configuration presents a method to calculate the SC size by using a supercapacitor energy controller in a PV power smoothing application. This method determines the required energy storage size of the SC while assuring the defined smoothness of the battery power.

In view of the reviewed works, some efforts have already been made concerning the sizing of passive FC/SC configuration in vehicular applications. However, so far, these methods just consider the energetic behavior of the SC along the utilized profiles. In addition to common concerns regarding the voltage and SOC levels of the SC, the current dynamics operational limits of the FC are necessary to be considered along the different operation phases of the system. These requirements have made the formulation of this sizing method of a passive FC/SC hybrid energy system for a vehicle application. Prior to this paper, no sizing approach for FC vehicles considers the storage capacity, maximum voltage, and current dynamics of the FC at the same time. Experimental tests are performed to assess the performance of the proposed sizing approach. Three tests are carried out: SC pre-charging, load current step, and on-road operation. The remainder of

Please cite this article as: Dépature C et al., Fuel cell/supercapacitor passive configuration sizing approach for vehicular applications, International Journal of Hydrogen Energy, https://doi.org/10.1016/j.ijhydene.2020.05.040

the paper is organized as follows. Vehicle modeling and representation describes the studied FC/SC system along with the explanation of the model and the pre-charging strategy. Fuel cell and supercapacitor design describes the FC and SC designs. Real-time validation copes with the real-time validation and the discussion of the experimental results.

Vehicle modeling and representation

Studied vehicle

The studied FC/SC architecture is based on the traction characteristics of low speed Nemo battery electric truck of the Hydrogen Research Institute of *Université du Québec à Trois-Rivières* (UQTR), shown in Fig. 1a. The studied traction subsystem is composed of a voltage-source inverter (VSI), a three-phase machine, a gearbox, a differential, and two driven wheels shown in Fig. 1b. The powertrain is built on an ACX-2043, 3 A C/4.8 kW induction machine which is operated by an AC induction motor controller to set the motor speed. The speed and torque control of 3-phase AC motors has a wide input voltage range of 40 V–80 V. The main characteristics of the FC hybrid electric vehicle are detailed in Ref. [31]. The vehicle was instrumented with current and voltage sensors as well as a satellite global positioning system (GPS) antenna which provides speed and altitude information. An on-road urban driving cycle test has been carried out by the Nemo vehicle at the campus of the UQTR [32]. From this on-road test, the studied driving cycle is composed of a repetitive sequence of constant speed (20 km/h), acceleration and braking phases. In addition, during this test, the vehicle has not been on a flat road. The maximum speed of Nemo is 40 km/h, and it reaches a maximum acceleration of 1.7 m/s^2.

This results in a full-scale traction power profile P_{ts} which is used as a reference for this paper in order to subject the sizing approach to the real operation of a specific vehicle shown in Fig. 2.

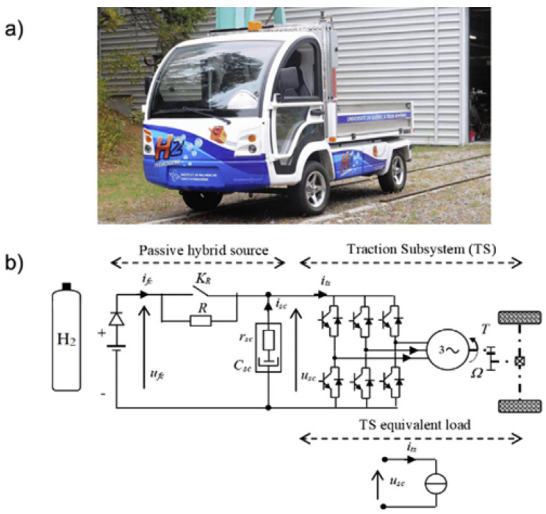

Fig. 1 – Nemo electric vehicle, a) picture, b) studied FC/SC vehicle architecture.

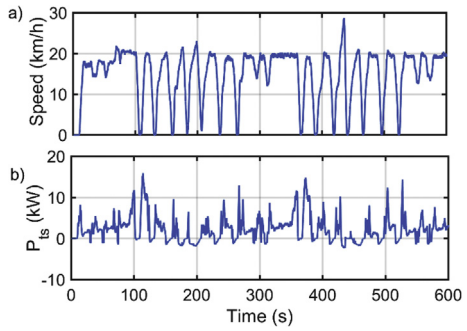

Fig. 2 – Full-scale Nemo vehicle speed and power from an on-road test drive.

In a pure electric mode with two passengers, the Nemo vehicle has an autonomy of 60 km. This autonomy can be increased by replacing the original battery pack with a passive FC/SC energy system. Fig. 1b shows the used passive configuration in which the FC is associated with a diode and the SC are directly connected in parallel. The traction is represented as an electric load connected to the DC bus voltage. As in a conventional capacitor, SC terminals voltage (u_{sc}) depends on the energy stored in its electric field. When the SC are charged or discharged, the terminals voltage respectively increases or decreases in a rate which depends on the size of the SC. In this respect, the current in a SC can instantaneously change its value while the SC voltage can be considered continuous with a limited change rate. As the FC and the SC are connected in parallel, the voltage and the FC current are continuous and with a limited change rate which mainly depends on the SC capacitance. Depending on the SC characteristics, this configuration allows to filter the FC current (i_{fc}), reducing stack faults, and degradation [33]. Fig. 3 illustrates the natural current distribution response of the utilized passive FC/SC energy system. The SC acts as a low-pass filter, that supply the requested current while the FC increase gradually its voltage. In this example, it is assumed that the FC and the SC starts at the same potential and the load current step maintains a constant value. This current step can be interpreted as the hardest load required to the FC/SC energy system, where the current is represented as per-unit (pu) current.

When the passive system is turned on, the FC delivers a positive voltage. In this case, if the SC is initially discharged, a direct connection between the FC and the SC happens which is comparable to a short circuit of the FC resulting in a high peak inrush current i_{fc}. In Ref. [34], a study shows that the short circuit operation reduced the mass transfer performance that is reflected as a higher voltage drop at high current levels. To avoid this phenomenon a SC pre-charging system is implemented, as patented by NISSAN in 2005 [35]. The pre-charging system consists of a fixed resistor R and a switch K_R, as shown in Fig. 1b. The current will flow through the resistor Rif the state of the switch K_R is open. That means the resistor $R$is placed in series with the FC and SC. The function of this resistor is to limit the inrush current during power-up phase, this high peak of current reduces the lifetime of the FC due to the starvation phenomena. This is the most classical method defined in the literature for DC bus capacitors initialization. When the voltage level of the FC is like the one of the SC, the state of the

Please cite this article as: Dépature C et al., Fuel cell/supercapacitor passive configuration sizing approach for vehicular applications, International Journal of Hydrogen Energy, https://doi.org/10.1016/j.ijhydene.2020.05.040

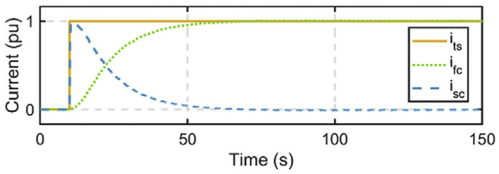

Fig. 3 – FC/SC current distribution principle for a load current step.

switch is changed to close. When the switch K_R is close the resistor R is bypassed, this means the current flows through the short-circuit generated by the contactor of the switch.

Modeling

The passive ESS is composed of a FC, a diode, a pre-charged resistor, a switch, and finally a SC pack. The FC operation depends on many phenomena such as the gas and liquid transport, heat exchanges, and electrochemical reactions. In this regard, there are two important approaches of mechanistic and semi-empirical modeling in FC domain. The former goes through these phenomena in details and the latter adopts a macroscopic approach to mask certain internal phenomena. Here, the FC model is represented in an energetic way as detailed in Ref. [36]. The u_{fc} output voltage is then a non-linear function of the current i_{fc}, which depends on the double-layer and quasi-static capacity voltages of the cells [37]. The capacitive behavior of the cells changes in gas pressure (Nernst law), and electrical losses govern this function, which can be statically presented by a polarization curve [38]. In a passive configuration the current i_{fc} imposed to the FC depends on the states of the switch K_R, the diode, and the pre-charged resistor as:

$$\frac{u_{fc}-u_{sc}}{r_D+K_R R}=i_{fc}, with\ K_R=\{0,1\} \quad (1)$$

where r_D is the diode resistance, R represents the pre-charged resistor, u_{sc} is the SC voltage, and the state of the switch K_R becomes 1 when it is open and the current flow through the resistor, and 0 when it is closed and pre-charging resistor is bypassed. As shown in Fig. 1b, the FC is connected in series with a diode to prevent reverse current into the FC and this circuit is connected in parallel with the SC. The diode represented as a resistor element causes a voltage drop, triggering a current flow from the FC to the system. This difference is the one that regulates the current of the FC.

The FC/SC electric parallel connection distributes the power of the FC and SC subsystems to the traction system load. The FC and traction subsystem current, i_{fc} and i_{ts}, are added together to generate the SC currents i_{sc}, which is modeled by the Kirchhoff's current law Eq. (2).

$$i_{sc}=i_{ts}-i_{fc} \quad (2)$$

Regarding the SCs, a series *RC* model is used to only consider their fast dynamics Eq. (3). The resistor r_{sc} models the voltage drops during the charging and discharging phases, and the constant capacitance C_{sc} characterizes the capacitive behavior of the SC. The linear dependence of the capacitance with respect to the voltage across the capacitor u_{sc}, the leakage resistance which induces losses when the SCs are not used, and the charge distributions phenomenon are not taken into account due to the fact that their time constants are very large compared with the dynamics of the considered application (from a few hundreds of seconds to several hours) [39].

$$u_{sc}=r_{sc}i_{sc}+\frac{1}{C_{sc}}\int i_{sc}dt \quad (3)$$

The traction subsystem is considered as an electric load (Fig. 1b). The current of traction subsystem, i_{ts}, is then expressed by the electrical traction power, P_{ts} (depending on the considered driving cycle) and the DC bus voltage, u_{sc} (see Fig. 2):

$$i_{ts}=P_{ts}/u_{sc} \quad (4)$$

Energetic Macroscopic Representation and pre-charged strategy

The Energetic Macroscopic Representation (EMR) of the studied vehicle is deduced from the relationships presented in Modeling (Fig. 4). The components are connected respecting the physical interaction principle of action-reaction [40]. One of the main advantages of this graphical description is to represent the interaction of different physical phenomena in the same diagram.

The FC system, the SC, and the traction system are considered as electrical sources which impose the FC voltage u_{fc}, the SC voltage u_{sc}, and the traction subsystem current i_{ts}, respectively. The diode, the pre-charged resistor, and the switch are considered as a mono-domain conversion element with the voltages of $u_{fc}$and u_{sc} as the inputs, the current i_{fc}as the output, and the reference switch state $K_R$as the tuning input. The parallel connection is represented as a coupling element.

A strategy-level output needs to be defined, which will be the pre-charging strategy block of Fig. 4. The pre-charged switch K_R state depends on the SC voltage u_{sc}. K_R is switched on when the SC voltage u_{sc} reaches a value close to the FC OCV by the pre-charging strategy.

Fuel cell and supercapacitor design

Hybrid system design

In this paper, the studied hybrid power source is based on a Horizon 500-W FC (H-500 FC). The rated power of the selected

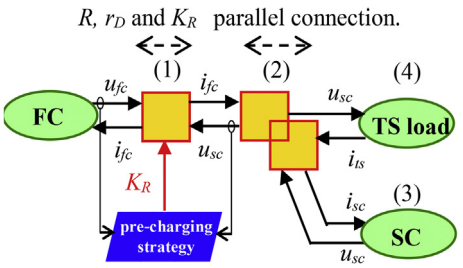

Fig. 4 – Energetic Macroscopic Representation of the studied vehicle.

Please cite this article as: Dépature C et al., Fuel cell/supercapacitor passive configuration sizing approach for vehicular applications, International Journal of Hydrogen Energy, https://doi.org/10.1016/j.ijhydene.2020.05.040

FC can supply the requested power of the 1/25th scale electrical traction power during the maximum speed and high acceleration rates. In order to preserve and reduce the FC degradation, frequency decomposition of traction power is often performed for active FC/SC configurations with power electronics [41,42]. If the system is well designed, the passive coupling of the FC with SC naturally preserves the FC from excessively fast dynamic power demands. If the FC is expose to sudden peak currents, its lifetime is reduced, and the output voltage will not get a steady value at the requested moment. This effect is due to the phenomenon of starvation, which means there is an insufficient supply of reactant gas [43]. Thus, to avoid starvation some authors considered that the power gradient value should be between 2% and 20% of the FC maximum power per second, or 4–50 A/s as the FC dynamic limitation [44]. In addition, other studies indicate that the FC suffers a percentage of power reduction when there is a load variation rate higher than 10% of the maximum FC power per second [45,46]. These limitations generally result in a current slope which should not be exceeded in order to reduce the stress in the FC system. Considering typical values on the literature, it has been assumed that a limitation of 2 A/s allows to avoid degradation and gas starvation. That means the system can reach its maximum current in 15 s, while respecting the slow dynamics of the FC.

In order to select the adequate value, a comparison of several cut-off frequencies responses to a step traction current is shown in Fig. 5. In the figure the FC current is plotted in per-unit, and the maximum corresponding current slope is also indicated. Assuming a current step of 30 A, which correspond to the nominal current of the Horizon FC, the maximum current slope varies from 18.9 A/s for a cut-off frequency of 100 mHz to 1.8 A/s for a cut-off frequency of 10 mHz. The selected cut-off frequency is $f_c = 10$ mHz, which corresponds to a maximum current slope of 1.8 A/s. The resulted current slope respects the specified current limitation of 2 A/s. However, the selected cut-off frequency has a stabilization time of about 80 s as shown in Fig. 5. Operating at this frequency has two main advantages. First, the FC does not suffer from any significant current transients (1.8 A/s), preventing it from gas starvation and its degradation effects [47]. Secondly, the FC rarely operates at its OCV since the stabilization time is very short. A frequency of 10 mHz therefore preserves the FC membrane and catalyst, since operation at the OCV accelerates the generation of peroxide and hydroperoxide radicals, which attack the membrane and catalyst [48,49]. Finally, if the FC and the SC have the same initial potential, the startup time to achieve 50% of the rated current for the FC system is 10 s. Regarding the United States Department of Energy (DOE) targets for light-duty FC vehicles, the ultimate target for FC startup time to full-flow is between 5 and 15 s, depending on the ambient temperature [50]. The chosen cut-off frequency of 10 mHz is thus a compromise between performance and degradation minimization. However, the SC sizing should be done taking into consideration the maximum current peak of the system that corresponds to maximum acceleration.

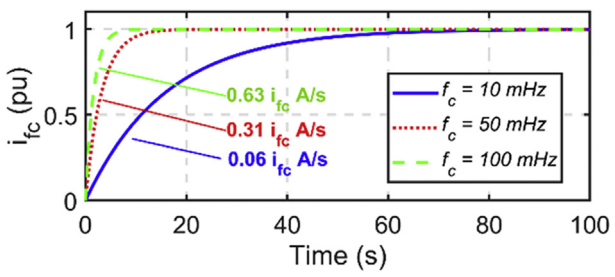

Fig. 5 – Frequency decomposition and current slopes considering a traction current step.

Supercapacitor design

By comparison, FC/SC passive configurations are less expensive and simpler to operate than active configurations, nevertheless, the performance depends on the sizing of the energy systems [51]. Conventional methods size SC according to two criteria: storage capacity and maximum voltage [22,29,33,51]. However, in this work, a third criterion has been added which is the current dynamic range of the FC. This section first explains the two common criteria found in the literature, then how SC parameters affect the FC operating frequency, and finally based on the desired FC current dynamic this analysis is used to size the SC.

Concerning the storage capacity criterion, the SC must assist the FC regardless of the load stress imposed by the traction. In this respect, SC need to be designed according to their storage capacity (Wh) since their energy density is relatively low (5–10 Wh/kg) compared to their power density (1–5 kW/kg) [52]. Hence, if the energy requirements are met, the power requirements will be met too. This requires knowing the maximal vehicle operation requirements by a frequency decomposition. The frequency decomposition at 10 mHz of the 1/25th scale electrical traction power during the road test of Fig. 2b, is divided in low frequency and compensation power. The low frequency power (P_{LF}) is the power expected to be delivered by the FC, and the compensation power is the power that should be supplied by the SC. In order to identify the maximum requested energy during the driving cycle the compensation power component is integrated through the time and represented in terms of energy in Fig. 6. From this analysis, the energy that SC needs to store is less than 1.05 Wh.

Regarding the maximum voltage criterion, the maximum voltage of the SC must be higher than the FC's OCV. As the FC and diode are connected in parallel to the SC, the two circuits share the same voltage. For safety purposes, SC should not be overloaded. The right size of the SC arrangement avoids exceeding their maximum permissible voltage [22,53]. Apropos the third criteria, a signal flow graphs, and Mason's

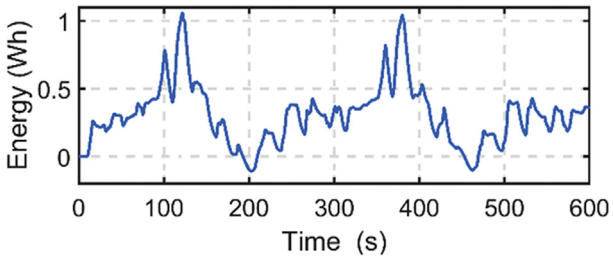

Fig. 6 – Compensation power in terms of energy evolution.

Please cite this article as: Dépature C et al., Fuel cell/supercapacitor passive configuration sizing approach for vehicular applications, International Journal of Hydrogen Energy, https://doi.org/10.1016/j.ijhydene.2020.05.040

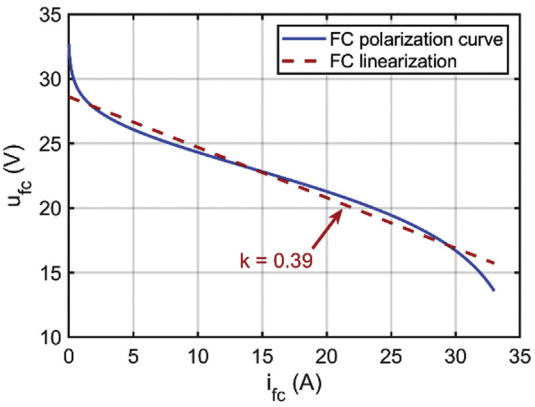

Fig. 7 – H-500 FC polarization curve.

gain formula are useful to complex system analysis. In this paper, these methods are used to analyze the passive hybrid design. Mason's gain formula allows defining the transfer function of a complex system in an efficient way. It is often applied from signal flow graphs [54]. A signal flow graph consists of a diagram composed of a set of nodes connected by paths, representing a set of linear equations.

In the literature semi-empirical models are utilized to describe the behavior of the FC, which is represented in a graphical way as the polarization curve [55]. Fig. 7 presents the H-500 FC static model experimentally validated. The FC polarization curve is composed of the reversible voltage; which is the maximum possible voltage of the FC, and irreversible voltage losses; which are the activation, ohmic and concentration losses. The activation loss represents the energy needed to start the reaction. The ohmic losses are caused by ionic, electronic, and contact resistances, which in most of the models is assumed as a linear function. The concentration losses happen at high currents and represents the mass transport, which is caused by the concentration reduction of hydrogen and oxygen gases in electrodes. In this work it is assume that the FC will operate mostly in the ohmic region. Therefore, the proposed SC design method assumes that the used models are linear. If the FC does not operate at OCV and high currents, this polarization curve can be linearized to provide the linear model of the studied FC:

$$u_{fc} = u_{fc0} - k i_{fc} \tag{5}$$

where the linear FC OCV (u_{fc0}) is 28.61 V and $k = 0.39$ is a linear coefficient.

The FC current i_{fc} versus the traction system current i_{ts} signal flow chart is presented in Fig. 8a. It has been obtained by using the model equations presented in Vehicle modeling and representation B, assuming a Laplace domain representation and the FC linear model.

The Mason's gain formula determines the linear transfer function $T(s)$ between an independent input (the traction system current i_{ts}) and a dependent output (the FC current i_{fc}) as follows:

$$T(s) = \frac{\sum_n P_n \Delta_n}{\Delta} \tag{6}$$

where P_n is the nth path gain of the input variable to the output variable, Δ is the determinant of the graph, and Δ_n is the P_n path cofactor. The determinant Δ is calculated as follows:

$$\Delta = 1 - \sum_o L_o + \sum_{m,q} L_m L_q - \sum_{r,s,t} L_r L_s L_t + \ldots \tag{7}$$

where $\sum L_o$ is the sum of all individual loop gains.

From the signal flow graph described in Fig. 8a, there are two forward paths P_1 and P_2 that link i_{ts} to i_{fc} (yellow and red paths presented in Fig. 8b, respectively) and 3 loops L_1, L_2 and L_3 (green, light blue and dark blue paths in Fig. 8b). Note that P_1 and P_2 touch all the loops so $\Delta_1 = 1$ and $\Delta_2 = 1$. L_1, L_2 and L_3 touch each other leading to $\Delta = 1 - L_1 - L_2 - L_3$ Eq. (8). $T(s)$ is finally defined in Eq. (9).

$$\begin{cases} P_1 = \dfrac{R}{r_D} & L_1 = \dfrac{R}{r_D} & \Delta_1 = 1 \\ P_2 = \dfrac{1}{C r_D s} & L_2 = \dfrac{1}{C r_D s} & \Delta_2 = 1 \\ & L_1 = \dfrac{k}{r_D} & \Delta = 1 - L_1 - L_2 - L_3 \end{cases} \tag{8}$$

$$T(s) = \frac{i_{fc}}{i_{ts}} = \frac{P_1\Delta_1 + P_2\Delta_2}{\Delta} = \frac{1 + RC_s}{1 + C(r_D + R + k)s} \tag{9}$$

The stabilization of the obtained $T(s)$ is studied in the complex plane as shown in Fig. 9. The pole, represented by a cross, is the root of the denominator of $T(s)$. The zero, represented as a circle, is the root of the numerator. The system is exponentially stable since the pole is in the left half of the complex plane. It is also possible to compare $T(s)$ with the second order transfer function $T_{2d}(s)$:

$$T_{2d}(s) = \frac{\omega_n^2}{s^2 + 2\xi\omega_n s + \omega_n^2} \tag{10}$$

where ξ represents the damping coefficient and ω_n the natural

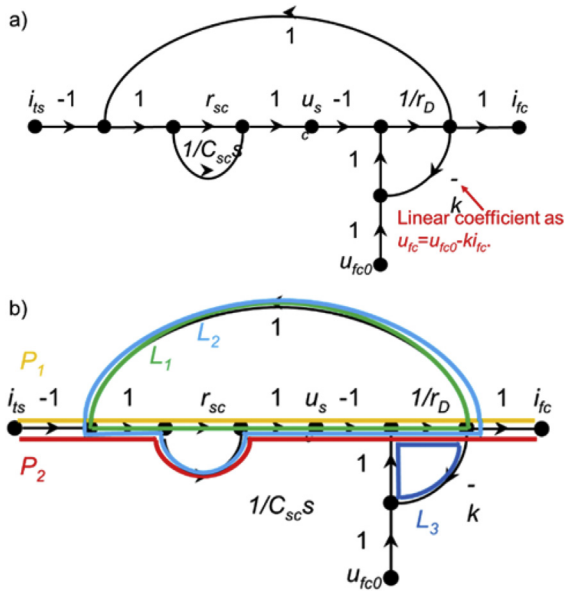

Fig. 8 – Fuel cell current i_{fc} versus traction system current i_{ts}, a) signal flow graph, b) Mason's gain formula application.

Please cite this article as: Dépature C et al., Fuel cell/supercapacitor passive configuration sizing approach for vehicular applications, International Journal of Hydrogen Energy, https://doi.org/10.1016/j.ijhydene.2020.05.040

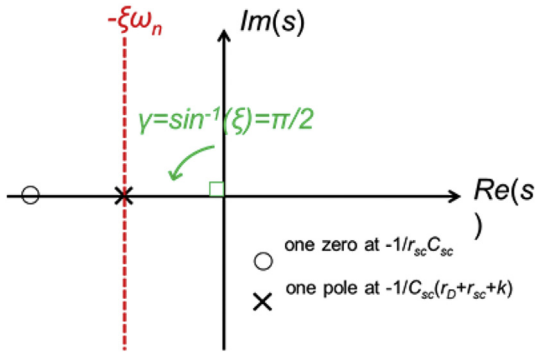

Fig. 9 – Complex plan of the studied transfer function T(s).

pulsation of the second order system. Considering that $T(s)$ and $T_{2d}(s)$ poles have the same real values (red dashes in Fig. 9) and assuming that the zero of $1/C_{sc}r_{sc}$ is higher than the pole of $1/C_{sc}(r_D + r_{sc} + k)$, it is possible to identify that:

$$\xi\omega_n = \frac{1}{C_{sc}(r_D + r_{sc} + k)} \tag{11}$$

with $\xi = 1$ (see the green part in Fig. 9), and $\omega_n t_s = 4.744$ from the settling time chart. The FC current stabilization time at 1% of the final value in steady state t_s can be defined as:

$$t_s(1\%) = 4.744C_{sc}(r_D + r_{sc} + k) = 5\tau \tag{12}$$

where τ is the time constant of the FC operation. Finally, the FC current cut-off frequency can be calculated as:

$$f_c = \frac{1}{2\pi\tau} = \frac{5}{2\pi t_s(1\%)} = \frac{5}{2\pi 4.744 C_{sc}(r_D + r_{sc} + k)} \tag{13}$$

Study case

Based on the three criteria of the proposed sizing method the standard electrolytic capacitor value that satisfy the constrains is a pack of two 16.2 V–58 F SC (BMOD0058 Maxwell SC) connected in series. This arrangement has a higher voltage than the H-500 FC OCV, enough energy to assist the FC, and a cut-off frequency of 13 mHz. The main characteristic of the FC/SC testbench are summarized in Table 1. The useful energy of the 2 SC Maxwell modules E_u is computed from the nominal voltage u_{sc0} up to the 50% of maximum voltage by Eq. (14), which is sufficient to operate in a good efficiency operation range and to avoid physical instability due to a low FC voltage [53,56].

Table 1 – Reduced-scale FC/SC passive vehicle.

Component	Variable	Value
Fuel Cell	u_{fc}	15–32 V
	$P_{fc,max}$	500 W
	u_{fc0}	28.6 V
	k	0.39
Supercapacitors	u_{sc0}	32.4 V
	C_{sc}	29 F
	r_{sc}	44 mΩ
Diode	r_D	2 mΩ
Pre-charge resistor	R	1 Ω
Power load	$P_{load,max}$	1.2 kW

$$E_u = \frac{1}{2}C_{sc}u_{sc0}^2\left(1 - \left(\frac{50}{100}\right)^2\right) = 11360J\frac{1h}{3600s} = 3.15Wh \tag{14}$$

As the SCs have been selected according to the FC desired operating current dynamic and the FC OCV, it is not surprising that the SCs seem energetically oversized (3.15 Wh compared to the 1.05 Wh required). The energy supplied by the SC do not exceed its limits, this ensures the physical stability and high SC efficiency.

Real-time validation

Experimental setup

Based on the traction characteristics of the low speed Nemo (Fig. 1a), a reduced scale validation is performed on an experimental platform as shown in Fig. 10. The set-up is composed of a 500-W Horizon PEM FC, a pack of 2 Maxwell SCs, a diode, a 1 Ω pre-charged resistor and a 1.2 kW programmable DC load to emulate the traction subsystem. The programmable DC load is used as a load drive with a power reduction of 25 compared to the full-scale studied vehicle. For the validation purpose, only mechanical braking is considered. Furthermore, the components with the selected sizes are cable of supplying the requested power during a constant phase of maximum speed. Voltages and currents are measured with classical LEM transducers and voltage probes. As shown in Fig. 10a electric diagram of the test-bench is composed of the FC system, the pre-charged resistor, the SC system, and the programmable load. These components are connected together by means of four 40 A contactors K_{fc}, K_R, K_{sc} and K_{load}. The contactor K_{fc}, and K_{load} are implemented as safe contactors to stop the test in case of a failure.

A test is proposed to validate the design of the FC/SC passive configuration system under the conditions of the maximum FC current. Fig. 11 shows the response of the system alongside a 30 A step current. When $t = 0$ s, the values of u_{fc} and u_{sc} are 29.7 V and 29.3 V, respectively. The voltage difference is linked to the voltage drop in the diode, and so the SCs are correctly loaded. A pulse current step ($i_{ts} = 0$–30 A) at $t = 10$ s is imposed on the passive FC/SC system. From the proposed method, the objective FC operating frequency is 10 mHz. However, the SC sizes are limited in commercial standard values. Consequently, the FC current i_{fc} has a stabilization time of 74 s, which corresponds to an operating frequency of 13 mHz. The results show that the SC responds correspond to the calculated theoretical cut-off frequency of Eq. (13), although the FC polarization curve has been defined as a linear model. Indeed, the polarization curve characterization assumes voltage, current, and temperature steady state, thus neglecting the transient states. During this test, the minimum voltage of the SC is 18.8 V. This voltage is higher than $u_{sc0}/2$. Consequently, the selected SCs allow to maintain an enough SC state of charge, which limits the currents and the efficiency of the SC. Finally, the configuration allows the system to respond to the traction demands in a passive way. Peak power demands are

Please cite this article as: Dépature C et al., Fuel cell/supercapacitor passive configuration sizing approach for vehicular applications, International Journal of Hydrogen Energy, https://doi.org/10.1016/j.ijhydene.2020.05.040

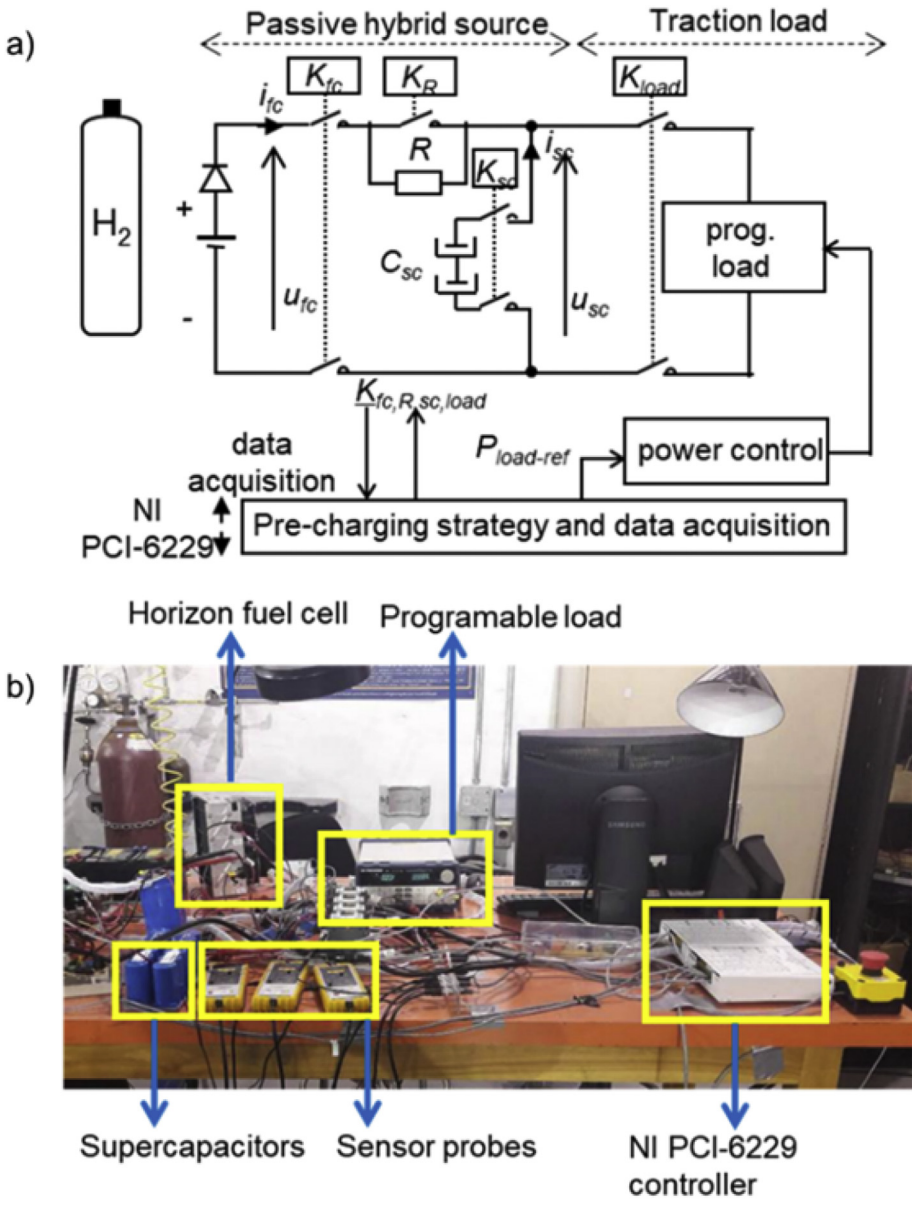

Fig. 10 – Test bench, a) diagram, b) experimental platform.

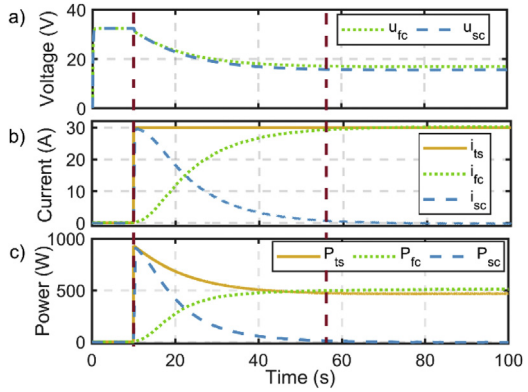

Fig. 11 – Passive hybrid source current step validation, a) voltage profile, b) current profile, and c) power profile.

provided by the SC and the FC provides an average traction power. For example, the 440 W power demand at $t = 10$ s is exclusively provided by the SC. The FC then progressively increase its power component and takeover of the SC contribution.

Supercapacitors pre-charging

The developed pre-charging strategy is built and implemented in a National Instrument NI PCI-6229 controller. The management of the contactors allows two operation modes:

1) Mode 1: SC pre-charging. K_{fc} and K_{sc} are closed. K_R and K_{load} are opened. The system becomes a closed circuit with the FC, diode, pre-charging resistor and SC connected in series.

Please cite this article as: Dépature C et al., Fuel cell/supercapacitor passive configuration sizing approach for vehicular applications, International Journal of Hydrogen Energy, https://doi.org/10.1016/j.ijhydene.2020.05.040

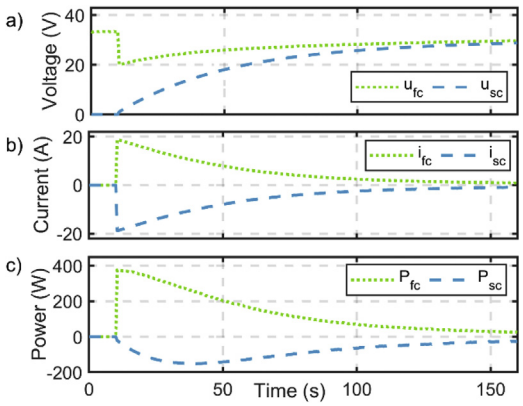

Fig. 12 – Supercapacitors pre-charge, a) voltage profile, b) current profile, and c) power profile.

The FC charges the SC up to its OCV. And the pre-charged resistor limits the inrush current i_{fc}.

2) Mode 2: Vehicle operation. K_{fc}, K_{sc}, K_R and K_{load} are closed. The emulated traction load is connected in parallel to the SC of the system. Therefore, the system becomes a circuit with three branches in parallels: the FC and the diode, the SC, and the load. The FC operation frequency depends on the SC characteristics.

The first pre-charging step is necessary to balance the FC and the SC at the same electric potential, this process is shown in Fig. 12. When the FC is turned on, it is on OCV. Then the FC is connected to the SC by closing the contactor K_{fc} and K_{sc} at $t = 10$ s, its voltage drops instantly to around 20 V. The pre-charged resistor limits the load current to 20 A. The charging current decreases with a time constant about 38 s, and then an operating frequency of 4.2 mHz. This corresponds to the frequency defined by Eq. (13), but considering the additional fixed pre-charged resistor of 1 Ω. The stabilization time is about 190 s. The advantage of the chosen pre-charging method is that it limits the charging current, which avoids component stress during the FC/SC passive connection, however the SC charging time is relatively long. Note that for this pre-charging test, the SC was fully discharged. This is the worst operation case that should not happen often because the SC self-discharge time constant is relatively long [26]. More advanced pre-charging strategies could be used in further studies, including short-circuit or progressive FC/SC connection [28], using a Voltage Stabilization System (VSS) [57], or a control system to regulate the connection of a pre-charging resistance before starting the vehicle [58].

On-road operation

The 1.2 kW programmable load reproduces the on-road power profile with a scale reduction of 25. And the studied hybrid power source is based on a Horizon 500-W FC (H-500 FC) connected in parallel with a SC pack. Based on the proposed three-criteria sizing method the selected capacitor value is a pack of two 16.2 V–58 F SC (BMOD0058 Maxwell SC) connected in series. This passive configuration avoids using a power electronics converter, because the current distribution

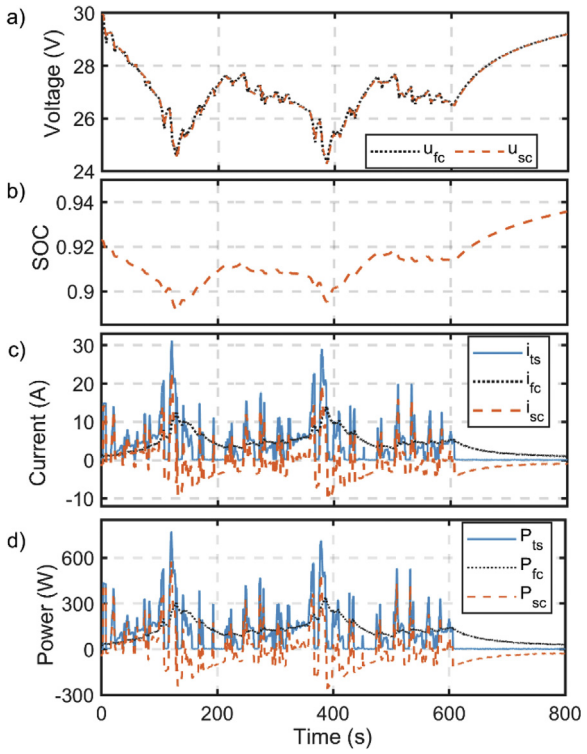

Fig. 13 – Reduced-scale vehicle operation validation, measured signals a) voltage, b) SC SOC, c) current, and d) power.

between the FC and the SC depends on the natural behavior of each component. The experimental results of implemented FC/SC passive coupling in real-time conditions; power, voltage, and current splits; are shown in Fig. 13. As with the hybrid source design validation test, the SCs are charged at $t = 0$ s. It is observed from Fig. 13a that the traction power profile has two main peaks that overpass the maximum power of the FC. However, the SC has enough energy to immediately supply the requested power without a high voltage drop as shown in the storage capacity criterion. In this respect Fig. 13b shows the SOC evolution of the SC. The lowest SOC is 89% that happens during the highest current peak of 30 A. The FC voltage evolution operates in the linear zone of the polarization curve as shown in Fig. 13c, that avoids physical instability on the FC. In addition, the SC voltage never exceeds its voltage limits. Also, the FC current distribution is filtered thru the SC avoiding high current stress by the FC, as shown in Fig. 13d. The maximum current change per second is 1.2 A/s, which is inferior to the 2 A/s design limit. As described, the FC/SC passive system respects the all the sizing constraints, and the SCs assist the FC to meet the requirements of the load with a guarantee of system stability in real-time.

Conclusion

This paper deals with the design of a passive FC/SC hybrid source based on a three-criteria sizing method. As other sizing method found in the literature, storage capacity and voltage of

Please cite this article as: Dépature C et al., Fuel cell/supercapacitor passive configuration sizing approach for vehicular applications, International Journal of Hydrogen Energy, https://doi.org/10.1016/j.ijhydene.2020.05.040

the SC must be checked for security and efficiency purposes. The additional design criterion is the FC current dynamic, defined in a heuristic way to limit the FC degradation by limiting the FC current slope. For the SC design, the FC current versus the traction system current transfer function is defined based on the Mason's gain. Assuming that the used models are linear, the FC model, the analysis of this transfer function allows selecting the SC according to the desired FC operating frequency.

The proposed sizing approach allows to 1) reduce the FC degradation rate because the current slope, OCV, and stop-start operation are limited, and 2) improve the system efficiency because the SCs operate at a voltage discharge ratio upper than 50%. The developed design method is validated in real-time on an experimental setup. Three tests are carried out: SC pre-charging, traction current step, and on-road operation. Experimental results have shown that the SC can assist the FC to meet the power requirements with a guarantee of system stability and design constrains.

In future, new strategies could be put forward to choose the optimal FC frequency operation, based on degradation, performance, or efficiency criteria. Additional work is required to model the FC degradations under a dynamic profile as presented in automotive application. Moreover, the study of a passive/active configuration, which uses an additional converter to convert the power from the SC to the traction, can be explored. This configuration could allow to start the vehicle without finishing the pre-charging phase but requires studying the minimum SC voltage to switch on the converter.

Acknowledgment

This work was supported by the Canada Research Chairs Program (grants 950–230863 and 950–230672), the National Sciences and Engineering Research Council of Canada (grants RGPIN-2018-06527 and RGPIN-2017-05924), the Emerging Leaders in the Americas Program (ELAP) and also with the support of the "*Service de Coopération et d'Action Culturelle du Consulat Général de France à Québec*" within the Samuel-De Champlain Program.

Nomenclatures

C_{sc}	Equivalent capacitance of SC [F]
E_u	SC energy [J]
f_c	Cut-off frequency [Hz]
i_{fc}	FC current [A]
i_{sc}	SC current [A]
I_{ts}	Traction current [A]
K_{fc}	FC switch
K_{load}	Load switch
K_R	Pre-charged switch
K_{sc}	SC switch
L_i	Loop gain
$P_{FC,max}$	Maximum FC power [W]
P_{LF}	Low frequency power [W]
$P_{load,max}$	Maximum load power [W]
P_n	Path cofactor
P_{ts}	Traction power [W]
r_D	Equivalent diode resistance [Ω]
r_{sc}	Equivalent resistance of SC [Ω]
$T(s)$	Linear transfer function
u_{fc}	FC voltage [V]
u_{sc}	SC voltage [V]
Δ	Determinant
ξ	Damping coefficient
τ	Time constant [s]
ω_n	Natural pulsation
R	Fixed resistor [Ω]
k	Linear FC coefficient

Abbreviations and acronyms

DOE	United States Department of Energy
FC	Fuel cell
FC/SC	Fuel cell/supercapacitor
GPS	Global positioning system
H-500 FC	Horizon 500-W FC
OCV	Open circuit voltage
SC	Supercapacitor
UQTR	Université du Québec à Trois-Rivières
VSS	Voltage Stabilization System

REFERENCES

[1] Glenk G, Reichelstein S. Economics of converting renewable power to hydrogen. Nature Energy 2019;4:216–22. 2019/03/01.
[2] Li Z, Khajepour A, Song J. A comprehensive review of the key technologies for pure electric vehicles. Energy 2019;182:824–39. 2019/09/01/.
[3] Morrison G, Stevens J, Joseck F. Relative economic competitiveness of light-duty battery electric and fuel cell electric vehicles. Transport Res C Emerg Technol 2018;87:183–96. 2018/02/01/.
[4] Acar C, Dincer I. The potential role of hydrogen as a sustainable transportation fuel to combat global warming. Int J Hydrogen Energy 2018;45(5):3396–406. 2018/11/23/.
[5] Bodner M, Schenk A, Salaberger D, Rami M, Hochenauer C, Hacker V. Air starvation induced degradation in polymer electrolyte fuel cells. Fuel Cell 2017;17:18–26.
[6] Chen FX, Yu Y, Chen JX. Control system design of power tracking for PEM fuel cell automotive application. Fuel Cell 2017;17:671–81.
[7] Nadeem F, Hussain SMS, Tiwari PK, Goswami AK, Ustun TS. Comparative review of energy storage systems, their roles, and impacts on future power systems. IEEE Access 2019;7:4555–85.
[8] Bendjedia B, Rizoug N, Boukhnifer M, Bouchafaa F, Benbouzid M. Influence of secondary source technologies and energy management strategies on Energy Storage System sizing for fuel cell electric vehicles. Int J Hydrogen Energy 2018;43:11614–28. 2018/06/21/.
[9] Das HS, Tan CW, Yatim AHM. Fuel cell hybrid electric vehicles: a review on power conditioning units and topologies. Renew Sustain Energy Rev 2017;76:268–91.
[10] Fernández RÁ, Cilleruelo FB, Martínez IV. A new approach to battery powered electric vehicles: a hydrogen fuel-cell-based range extender system. Int J Hydrogen Energy 2016;41:4808–19. 2016/03/02/.
[11] Wang H, Gaillard A, Hissel D. A review of DC/DC converter-based electrochemical impedance spectroscopy for fuel cell electric vehicles. Renew Energy 2019;141:124–38. 2019/10/01/.

Please cite this article as: Dépature C et al., Fuel cell/supercapacitor passive configuration sizing approach for vehicular applications, International Journal of Hydrogen Energy, https://doi.org/10.1016/j.ijhydene.2020.05.040

[12] Blackwelder MJ, Dougal RA. Power coordination in a fuel cell–battery hybrid power source using commercial power controller circuits. J Power Sources 2004;134:139–47. 2004/07/12/.
[13] Djerioui A, Houari A, Zeghlache S, Saim A, Benkhoris MF, Mesbahi T, et al. Energy management strategy of Supercapacitor/Fuel Cell energy storage devices for vehicle applications. Int J Hydrogen Energy 2019;44(41):23416–28. 2019/07/31/.
[14] Yue M, Jemei S, Gouriveau R, Zerhouni N. Review on health-conscious energy management strategies for fuel cell hybrid electric vehicles: degradation models and strategies. Int J Hydrogen Energy 2019;44(13):6844–61. 2019/02/18/.
[15] Perdigão MS, Trovão JPF, Alonso JM, Saraiva ES. Large-signal characterization of power inductors in EV bidirectional DC–DC converters focused on core size optimization. IEEE Trans Ind Electron 2015;62:3042–51.
[16] Bernard J, Hofer M, Hannesen U, Toth A, Tsukada A, Büchi FN, et al. Fuel cell/battery passive hybrid power source for electric powertrains. J Power Sources 2011;196:5867–72. 2011/07/15/.
[17] Zhao H, Burke AF. Fuel cell powered vehicles using supercapacitors-device characteristics, control strategies, and simulation results. Fuel Cell 2010;10:879–96.
[18] Arora D, Bonnet C, Mukherjee M, Raël S, Lapicque F. Direct hybridization of PEMFC and supercapacitors: effect of excess hydrogen on a single cell fuel cell durability and its feasibility on fuel cell stack. Electrochim Acta 2019;310:213–20. 2019/07/01.
[19] Xun Q, Liu Y, Holmberg E. A comparative study of fuel cell electric vehicles hybridization with battery or supercapacitor. In: International symposium on power electronics, electrical drives. Automation and Motion (SPEEDAM); 2018. p. 389–94. 2018.
[20] Macías A, Kandidayeni M, Boulon L, Trovão J. Passive and active coupling comparison of fuel cell and supercapacitor for a three-wheel electric vehicle. Fuel Cell 2019;n/a. 2019/10/29.
[21] Gérardin K, Raël S, Bonnet C, Arora D, Lapicque F. Direct coupling of PEM fuel cell to supercapacitors for higher durability and better energy management. Fuel Cell 2018;18:315–25.
[22] Wu B, Parkes MA, Yufit V, De Benedetti L, Veismann S, Wirsching C, et al. Design and testing of a 9.5 kWe proton exchange membrane fuel cell–supercapacitor passive hybrid system. Int J Hydrogen Energy 2014;39:7885–96.
[23] Turpin C, Van Laethem D, Morin B, Rallières O, Roboam X, Verdu O, et al. Modelling and analysis of an original direct hybridization of fuel cells and ultracapacitors. Math Comput Simulat 2017;131:76–87.
[24] Morin B, Van Laethem D, Turpin C, Rallières O, Astier S, Jaafar A, et al. Direct hybridization fuel cell - ultracapacitors. Fuel Cell 2014;14:500–7.
[25] Dépature C, Lhomme W, Sicard P, Bouscayrol A, Boulon L. Real-time backstepping control for fuel cell vehicle using supercapacitors. IEEE Trans Veh Technol 2018;67:306–14.
[26] Kaus M, Kowal J, Sauer DU. Modelling the effects of charge redistribution during self-discharge of supercapacitors. Electrochim Acta 2010;55:7516–23. 2010/10/30/.
[27] Hinaje M, Raël S, Caron JP, Davat B. An innovating application of PEM fuel cell: current source controlled by hydrogen supply. Int J Hydrogen Energy 2012;37:12481–8. 2012/09/01/.
[28] Silva RE, Harel F, Jemeï S, Gouriveau R, Hissel D, Boulon L, et al. Proton exchange membrane fuel cell operation and degradation in short-circuit. Fuel Cell 2014;14:894–905.
[29] Arora D, Hinaje M, Bonnet C, Raeel S, Lapicque F. Sizing supercapacitor for direct hybridization with polymer electrolyte membrane fuel cell. In: IEEE vehicle power and propulsion conference. VPPC); 2018. p. 1–7. 2018.
[30] Abeywardana DBW, Hredzak B, Agelidis VG, Demetriades GD. Supercapacitor sizing method for energy-controlled filter-based hybrid energy storage systems. IEEE Trans Power Electron 2017;32:1626–37.
[31] Martel F, Kelouwani S, Dubé Y, Agbossou K. Optimal economy-based battery degradation management dynamics for fuel-cell plug-in hybrid electric vehicles. J Power Sources 2015;274:367–81. 2015/01/15/.
[32] Kelouwani S, Agbossou K, Dubé Y, Boulon L. Energetic optimization of the driving speed based on geographic information system data. IEEE Vehicular Technology Conference (VTC Fall); 2012. p. 1–5. 2012.
[33] Snoussi J, Elghali SB, Benbouzid M, Mimouni MF. Optimal sizing of energy storage systems using frequency-separation-based energy management for fuel cell hybrid electric vehicles. IEEE Trans Veh Technol 2018;67:9337–46.
[34] Bonnet C, Lapicque F, Belhadj M, Gerardin K, Raël S, Hinaje M, et al. Can PEM fuel cells experience appreciable degradation at short circuit? Fuel Cell 2017;17:157–65. 2017/04/01.
[35] Nissan. Fuel cell system. 2005.
[36] Marx N, Hissel D, Toquica Cárdenas DC, Boulon L, Gustin F. Degraded mode operation of multi-stack fuel cell systems. IET Electr Syst Transp 2016;6:3–11.
[37] Saadi A, Becherif M, Hissel D, Ramadan HS. Dynamic modeling and experimental analysis of PEMFCs: a comparative study. Int J Hydrogen Energy 2017;42:1544–57. 2017/01/12/.
[38] Kandidayeni M, Macias A, Amamou AA, Boulon L, Kelouwani S, Chaoui H. Overview and benchmark analysis of fuel cell parameters estimation for energy management purposes. J Power Sources 2018;380:92–104.
[39] Zubieta L, Bonert R. Characterization of double-layer capacitors for power electronics applications. IEEE Trans Ind Appl 2000;36:199–205.
[40] Bouscayrol A, Hautier J-P, Lemaire-Semail B. Graphic formalisms for the control of multi-physical energetic systems: COG and EMR. In: Wiley Ia, editor. Systemic design methodologies for electrical energy systems; 2012. p. 89–124.
[41] Marzougui H, Kadri A, Amari M, Bacha F. Energy management of fuel cell vehicle with hybrid storage system: a frequency based distribution. In: 6th international conference on control. Decision and Information Technologies (CoDIT); 2019. p. 1853–8. 2019.
[42] Wu W, Partridge JS, Bucknall RWG. Stabilised control strategy for PEM fuel cell and supercapacitor propulsion system for a city bus. Int J Hydrogen Energy 2018;43:12302–13.
[43] Chen H, Xu S, Pei P, Qu B, Zhang T. Mechanism analysis of starvation in PEMFC based on external characteristics. Int J Hydrogen Energy 2019;44:5437–46.
[44] Carignano MG, Costa-Castelló R, Roda V, Nigro NM, Junco S, Feroldi D. Energy management strategy for fuel cell-supercapacitor hybrid vehicles based on prediction of energy demand. J Power Sources 2017;360:419–33. 2017/08/31/.
[45] Wang Y, Moura SJ, Advani SG, Prasad AK. Power management system for a fuel cell/battery hybrid vehicle incorporating fuel cell and battery degradation. Int J Hydrogen Energy 2019;44:8479–92. 2019/03/29/.
[46] Pei P, Chang Q, Tang T. A quick evaluating method for automotive fuel cell lifetime. Int J Hydrogen Energy 2008;33:3829–36. 2008/07/01/.
[47] Wang G, Huang F, Yu Y, Wen S, Tu Z. Degradation behavior of a proton exchange membrane fuel cell stack under dynamic cycles between idling and rated condition. Int J Hydrogen Energy 2018;43:4471–81. 2018/03/01/.

Please cite this article as: Dépature C et al., Fuel cell/supercapacitor passive configuration sizing approach for vehicular applications, International Journal of Hydrogen Energy, https://doi.org/10.1016/j.ijhydene.2020.05.040

[48] Chandesris M, Vincent R, Guetaz L, Roch JS, Thoby D, Quinaud M. Membrane degradation in PEM fuel cells: from experimental results to semi-empirical degradation laws. Int J Hydrogen Energy 2017;42:8139–49. 2017/03/23/.
[49] An L, Zhao T, Yan X, Zhou X, Tan P. The dual role of hydrogen peroxide in fuel cells. Sci Bull 2015;60:55–64. 2015/01/01.
[50] U. Drive, "Target explanation document: onboard hydrogen storage for light-duty fuel cell vehicles," Department of Energy2015.
[51] Bendjedia B, Bouchafaa F, Rizoug N, Boukhnifer M. Comparative study between battery and supercapacitor hybridization with fuel cells for automotive applications. In: 2017 4th international conference on control. Decision and Information Technologies (CoDIT); 2017. p. 833–8.
[52] Zhang L, Hu X, Wang Z, Sun F, Dorrell DG. A review of supercapacitor modeling, estimation, and applications: a control/management perspective. Renew Sustain Energy Rev 2018;81:1868–78.
[53] Li T, Liu H, Zhao D, Wang L. Design and analysis of a fuel cell supercapacitor hybrid construction vehicle. Int J Hydrogen Energy 2016;41:12307–19. 2016/07/27/.
[54] Ogata K, Yang Y. Mathematical modeling of dynamic systems. Modern control engineering, vol. 17. Saddle River, NJ: Pearson Upper; 2010. p. 57–129.
[55] Abdi H, Rasouli Nezhad R, Salehimaleh M. Chapter 5 - fuel cells. In: Gharehpetian GB, Mousavi Agah SM, editors. Distributed generation systems. Butterworth-Heinemann; 2017. p. 221–300.
[56] Zhang R, Tao J. GA-based fuzzy energy management system for FC/SC-powered HEV considering H2Consumption and load variation. IEEE Trans Fuzzy Syst 2018;26:1833–43.
[57] Chiappori G, Moigne PL, Delarue P, Chemin M. Voltage stabilization system for stop - start vehicles: systemic approach. In: IEEE vehicle power and propulsion conference. VPPC); 2014. p. 1–6. 2014.
[58] Wang Y, Chen J, Liu J, Liu K, Zhang Y, Wu J, et al. Research and implementation of key technology of braking energy recovery system for off-highway dump truck. In: Iecon 2017 - 43rd annual conference of the IEEE industrial electronics society; 2017. p. 3912–7.

Please cite this article as: Dépature C et al., Fuel cell/supercapacitor passive configuration sizing approach for vehicular applications, International Journal of Hydrogen Energy, https://doi.org/10.1016/j.ijhydene.2020.05.040